# $CO_2$-free Energy from Natural Gas via BrOx cycle

**Experimental and numerical study of the bromination-oxidation cycle**

Zur Erlangung des akademischen Grades eines

**Dr.-Ing.**

von der Fakultät Bio- und Chemieingenieurwesen
der Technischen Universität Dortmund
genehmigte Dissertation

vorgelegt von

**M.Sc. Jesús González Rebordinos**

aus

Valladolid, Spain

Tag der mündlichen Prüfung: 27.01.2020

1. Gutachter/-in: Prof. Dr. Agar
2. Gutachter/-in: Prof. Dr. Grünewald

**Dortmund 2020**

*"La simplicidad puede engendrar complejidad. Átomos relativamente sencillos se unen para formar estructuras tan complejas como los genes y genes se unen para dar lugar a seres vivos extremadamente complejos. Esto es cierto independientemente de que los átomos, genes o seres vivos sean conscientes del aumento en la complejidad o no."*

*"Simplicity can generate complexity. Relatively simple atoms join to form complex structures such as gens. Gens join to form extremely complex living beings. This is true regardless of whether atoms, gens or living beings are aware of the increase in complexity or not."*

# Acknowledgements

I would like to express my appreciation to my advisor Prof. Dr. David W. Agar for his advice and guidance during my research. His technical knowledge and his suggestions have been of an enormous help in the successful research shown in this thesis. I would also like to thank the meebers of the comitee, Prof. Dr. Grünewald, Prof. Dr. Vogdt, PD Dr. Kühl and PD Dr. Held for taking the time to review and evaluate my dissertation.

Special thanks to my parents, Moisés González Madrid and Ana María Rebordinos Cubero, family and friends as well as to my wife Sara Marcos Ortega for their support during my studies and during the performance of my doctoral thesis.

I am very grateful to my colleagues of the Chair for Chemical Reaction Engineering (CVT) for the interesting discussions that lead to new research ideas but mainly for making the time I spent at the TU Dortmunt a very enjoyable experience. Additionally I would like to express my thanks to the laboratory technicians Michael Schlüter and Julian Gies whose assistance has been crucial in the development of the experimental work. I am also very grateful to the workers of the workshops (glass blowery, electronics and mechanics) for their support.

My gratitude also goes to the students who contributed with their effort to the development of this thesis, Haider Mahmood, Bastian Weith, Alexander Salten, Piotr Żołyniak, Hicham Chakir, Ruozhong Tian, Jan Kampwerth, Nicole Robert, Erik Kurrat, Furkan Saki, Felix Matulla, Peter Schinckel, Mike Kuhnigk and Thomas Piontek.

# Abstract

In the present work a novel process for energy generation from natural gas without concomitant $CO_2$ emissions, namely the Bromination-Oxidation (BrOx) cycle, is proposed and studied. This process consists of two exothermic reactions and an internal bromine recycle. Methane and bromine react in the first reaction step to yield solid carbon, that is separated by means of a cyclone or a filter, and hydrogen bromide. The latter is oxidised with oxygen in a second reactor yielding water and bromine. Bromine is separated and recycled to the first reaction step so that the energy is released in the process with solid carbon and water as only by-products.

Firstly, the thermodynamics of the process were studied to assess its feasibility and simulations on both reaction steps in plug flow reactors were carried out in order to estimate suitable reaction conditions. A bench-scale plant was constructed to study experimentally methane bromination and determine temperatures and residence times that lead to complete reaction and carbon formation. Additionally, the carbon produced was characterised and its bromine content quantitatively determined.

During methane bromination carbon deposition occurs, leading to inefficient operation. Two reactor concepts were proposed in this work, a vortex reactor that avoids deposition via the hydrodynamics of the system, and a sacrificial wall reactor in which deposition is not avoided but reactor cleaning is facilitated by means of a sacrificial coating on the inner walls. CFD simulation and optimisation of the vortex reactor was performed while sacrificial walls were studied experimentally.

A catalyst for the second reaction step, hydrogen bromide oxidation, was synthesised and characterised, and experiments on both thermal and catalytic oxidation were carried out. Moreover, both operation modes were simulated and modelling was used to propose an optimal strategy for this reaction step.

Finally, the flowsheeting of the BrOx cycle, including a preliminary economical analysis of the process, was performed and convenient separation units and operation parameters were selected based on the aforementioned data and simulation result.

# Contents

# 1. Introduction

## 1.1. Motivation

Since the industrial revolution world population, standard of living and global economy have steadily increased, especially in the last decades. As a result, an escalation in global primary energy consumption has been experienced reaching values beyond 500 EJ in past years [3]. Current trends and estimations foresee a constant increase in energy demand and it is uncertain how it will be satisfied in the medium to long term future. Moreover, energy generation is nowadays intimately linked to combustion of fossil fuels which generally involves $CO_2$ emissions to the atmosphere.

$CO_2$ emissions due to human activity have led to an unprecedented increase in its atmospheric concentration which is regarded by scientific consensus to be the main cause of climate change [93, 12]. A series of international summits over the last decades have been held aiming to an agreement that prevents climate change. In the last of these summits, the 2015 United Nations Climate Change Conference (COP21) held in Paris, an agreement was achieved to limit the world average temperature increase respective to pre-industrial levels to 1.5 °C [62]. in order to achieve this objective, a drastic reduction on $CO_2$ emissions is mandatory.

Energy production accounts for more than 55% of global $CO_2$ emissions and thus mitigation strategies are likely to have the highest impact in this sector [2]. Since more than 80% of the world energy demand is satisfied by fossil fuels, decarbonisation of hydrocarbon-based energy has a high potential effectiveness to reduce overall $CO_2$ emissions [3]. Although there exist some technologies that enable $CO_2$-free energy generation from fossil fuels they are either technologically non-mature, they lack social acceptance or are not economically feasible. In this work a novel process for $CO_2$-free energy generation, the bromination-oxidation (BrOx) cycle, is proposed and studied from an experimental and simulative point of view.

## 1.2. Background

In the past fifty years world population has increased at an ever increasing rate from 3.5 billion people to the current 7.6 billion people [4]. In the same period of time the world gross domestic product (GDP), which is the most common indicators of the economic performance of a region, has gone from 2,265 trillion US$ to 75,845 US$ [5]. The combination of this growth experienced by global economy and in human

population has led to an increase in energy consumption, reaching more than 600 EJ in 2016 [3]. Figure 1.1a clearly shows the steady increase in world primary energy demand, which is expected to continue at an even higher rate in the near future [3].

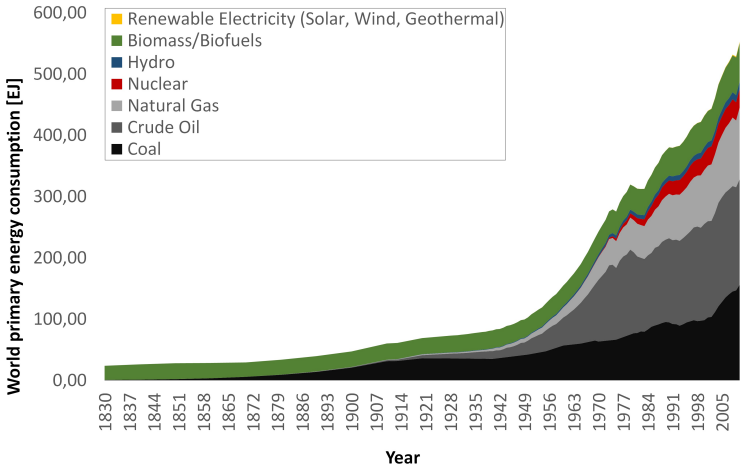


(a) World energy consumption per fuel during the last centuries

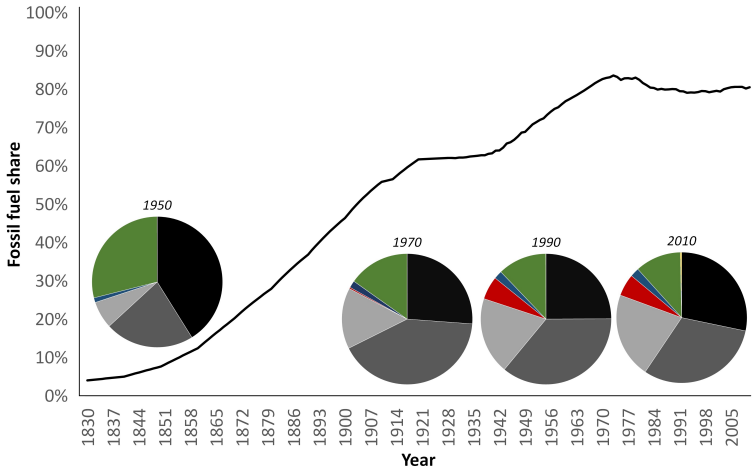


(b) Evolution of energy mix and fossil fuel share in th last centuries

Figure 1.1.: Energy production in the last centuries. Adapted [1, 6]

Currently, more than 80% of the world primary energy demand is satisfied via combustion of coal, natural gas or oil. Fossil fuels are capital to modern industry and economy and, although a small decrease in their share in the energy mix has been experienced in the last decades (figure 1.1b) their overall consumption has increased every year with a few exceptions. Estimations of future trends consider that the contribution of fossil fuels to the energy mix will decrease in the near future but will remain the dominant source of primary energy [2]. It has been argued that one of the major drawbacks of fossil fuels and modern society dependency on them is their future scarcity. A common indicator of fossil fuels availability is the amount of proven reserves which are those resources that are both technically and economically

exploitable with a probability equal or superior to 90% [7]. Contrary to popular belief and despite the ever increasing consumption of fossil fuels, their proven reserves have actually increased in the past decades. Oil and gas proven reserves have experienced increases of 64% and 59% respectively in the period going from 1992 to 2016 as shown in figure 1.2 [1, 3].

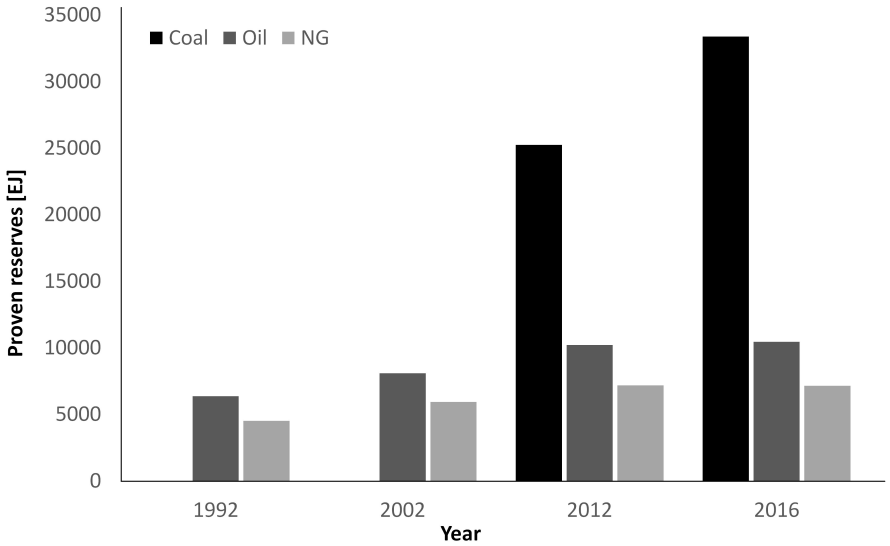


Figure 1.2.: Proven reserves of fossil fuels in the last decades. Adapted from [1, 3]

And additional source of fossil fuels are unconventional resources which currently are not technically or economically exploitable but could be in the short-medium term due to technology improvements or rising prices of fossil fuels. A good example is the boom of shale gas experienced in the last years which was driven by the development of horizontal drilling and hydraulic fracturing, and by an increase in oil prices [75, 67]. Unconventional natural gas resources mainly consist on coalbed methane, deep gas, shale gas, tight gas and methane hydrates. The estimated availability of each unconventional resource is in the same order of magnitude of current proven reserves with the exception of methane hydrates which are estimated to last hundreds to thousands of years at the current natural gas consumption rate [66]. Although profitable exploitation of methane hydrates is still far from possible, countries such as Japan, USA and China are slowly making progresses [8, 10, 9]. Although the rate of fossil fuel consumption is superior to the rate at which they replenish (which is virtually zero) and thus eventually humanity will run out of fossil fuels, their availability is not likely to be compromised in the near future.

Energy from fossil fuels is generally obtained via their combustion. This process leads to the formation of by-products, mainly steam, $CO_2$, $CO$ and $NO_x$ which are regularly discharged in the atmosphere. $CO_2$ is a greenhouse gas that contributes to heating the planet and whose concentration in the atmosphere has increased steadily in the past decades, as shown in figure 1.3. An additional cause for concern is that $CO_2$ levels in the atmosphere have increased in a very short period of time after centuries below 300 ppm, reaching a concentration superior to 400 ppm in 2013 [11]. This

increase in the atmospheric $CO_2$ and the concomitant raise in the average temperature of the planet have been determined by scientific consensus to be a result of recent human activities, being fossil fuel combustion the main contributor [12, 13, 14, 15].

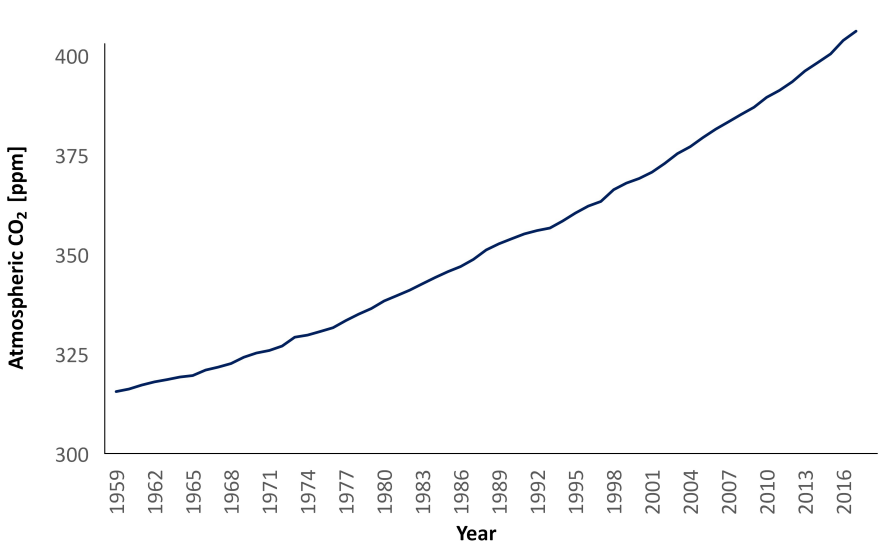


Figure 1.3.: Evolution of $CO_2$ atmospheric concentration over the last decades. Adapted from [93]

The aforementioned proves that the main limitation in the use of fossil fuels for energy production is not their availability but the $CO_2$ emissions associated to their combustion. Immediate replacement of fossil fuels in the energy sector in the short term to reduce global $CO_2$ emissions by alternatives such as renewable and nuclear energy is extremely difficult. The main challenges associated to this decarbonisation strategy are the technical problems of renewable energies (fluctuating production, problematic electricity storage and unreliability), the lack of social acceptance of nuclear energy, the absence of infrastructures for energy production and distribution and the huge economic effort involved in the creation of such infrastructures [16, 17, 18, 19, 20, 21, 22, 23]. Decarbonisation of fossil fuels is the most direct approach to reduce $CO_2$ emissions [41] and a very promising strategy since it takes advantage of the predominance of fossil fuels in the energy production mix, their relatively low cost and the presence of a worldwide infrastructure for their extraction, transportation and storage.

### 1.2.1. $CO_2$-free energy from fossil fuels

The main technologies currently available for decarbonisation of fossil fuels are carbon capture and storage (CCS) and methane pyrolysis. Carbon capture and storage refers to a series of technologies which consist on capturing $CO_2$ and sequestering it underground in order to avoid its release to the atmosphere. $CO_2$ capture can be pre-combustion or post-combustion. In pre-combustion processes the fuel is pretreated prior to its combustion. The pretreatment consists on the gasification and

subsequent enhancement via water-gas-shift reaction, followed by the separation of $CO_2$ from the $H_2/CO_2$ mixture before burning the hydrogen. In post-combustion $CO_2$ is captured after combustion, generally from a $CO_2$-concentrated stream such as flue gases of thermal power plants, steel manufacturing facilities or cement factories. Although $CO_2$ sorption is enhanced in pre-combustion CCS due to high $CO_2$ concentration post-combustion is a more mature technology because of the easiness of retrofitting already existing plants [24]. Capture of $CO_2$ can be carried out with several technologies including amine scrubbing, absorption with ionic liquids and low temperature adsorbents such as zeolites, from which the use of amines is the most extended [25]. After capture, $CO_2$ is pressurised and transported to the storage site by means of pipelines, road or rail tankers depending on the case. Finally, $CO_2$ is injected in geological features that ensure its trapping for thousands of years such as deep saline aquifers and fossil fuel reservoirs [24, 26].

At the end of year 2017 a total of 17 large-scale commercial CCS facilities operating in the world with $CO_2$ capture capacities up to 8.4 million tonnes and around 2 million tonnes per year for most of them [27]. All the plants used post-combustion separation. Despite this already existing implementation CCS long-term commercial viability is not ensured and strongly depends on the energy penalty and on the plant baseline efficiency, and is specific for each individual case [28, 29, 30].

One of the main drawbacks of CCS technology is the energy lost during the process which is mainly attributable to the $CO_2$ separation step, mainly due to sorbent regeneration, since it can account for up to 70% of the total energy losses of the process [26]. Capture of $CO_2$ involves an energy lost equivalent to the consumption of 25% to 40% of the fuel energy [31]. This situation can be aggravated by the energy required during $CO_2$ transportation, pressurisation and injection. As a result of this energy penalty together with the requirements for new and expensive equipment for the implementation of CCS in an existing plant, the price of the energy generated is substantially increased. An additional drawback of CCS technology is that the geological storage capacity, how it drive the costs associated to the process and the long-term reliability is uncertain and not fully understood [27, 32]. Finally, one big issue that may act as a barrier to CCS implementation is the lack of social acceptance, specially in countries like Germany or Poland, due to what has been named the NIMBY (not in my back yard) problem [33].

A more direct approach to reduce greenhouse gas emissions derived from energy generation is to avoid producing $CO_2$ when energy is obtained from fossil fuels instead of capturing and storing it. Methane pyrolysis is the most advanced process that uses this approach. This process consists on the thermal decomposition of methane molecule into solid carbon and hydrogen at high temperatures (equation 1.2.1).

$$CH_4 \rightleftarrows C\,(s) + 2H_2 \qquad \Delta H_{r,1000^\circ C} = 91.51 kJ/mol \tag{1.2.1}$$

Although methane pyrolysis is a mildly exothermic reaction, together with the combustion of the hydrogen produced (equation 1.2.2) after separation of the solid carbon results in a net release of energy of 480.15 $kJ/mol_{CH_4}$. The overall process results then

in energy generation at high temperatures susceptible to be used directly as primary energy for heating of industrial processes, for transportation purposes or for electricity generation. An advantage of methane pyrolysis is that its product, hydrogen, has been regarded as the future energy carrier [34, 35, 36, 37, 38, 39, 40, 41, 42, 43]. Methane thermal decomposition reaction becomes spontaneous at 550 °C but it requires temperatures superior to 800 °C to be kinetically feasible. In practice, high conversions of methane pyrolysis reaction occur at temperatures above 1200 °C [44]. Although there exist catalysts that lower the reaction temperature its application to long-term operation is still technically challenging due to the deactivation of the catalyst as a consequence of carbon fouling [45, 46].

$$H_2 + 0.5O_2 \rightarrow H_2O \qquad \Delta H_r^0 = -285.83 kJ/mol \tag{1.2.2}$$

The combination of the endothermic nature of methane pyrolysis and the high temperature requirement poses the technical challenge of introducing heat in the reaction zone. The traditional high temperature heat transfer method is the combustion but it cannot be applied to this process, being the avoidance of $CO_2$ generation one of the main motivations. Therefore, electrical heating is the main method for heating the reaction zone although it is comparatively expensive. An additional issue derived from the necessity for high temperature heat transfer is carbon deposition. Carbon is a product of methane pyrolysis that forms as a solid at the reaction zone which is located at the highest temperature zone and, since heat is transferred externally, that zone is usually the reactor walls so that carbon forms and sticks there. As a consequence carbon deposits in the reactor grow while the reaction proceeds acting as an insulating material thus increasing resistance to heat transfer and shortening the operation time of the reactor. Additionally, removal of carbon has to be carried out via mechanical methods since burning it would release $CO_2$.

Several strategies have been investigated in the last years to circumvent both the the problematic heat transfer and carbon deposition, including following reactor concepts:

- Porous-wall reactor [47]. In this a concept heat is introduced via a hot inert gas such as nitrogen through a porous ceramic wall.
- Molten-metal reactor [44]. This concept uses molten metals to transfer heat while protecting the reactor wall from carbon deposition.
- Fluidised bed reactor [48]. A nickel-based catalyst that is cyclically regenerated is used in a fluidized bed to conduct methane pyrolysis.
- Microwave-heated reactor [49]. This reactor uses microwave radiation to transfer heat to activated carbon particles that act as a catalyst.
- Plasma reactor [50]. The reaction zone is heated with gliding electric discharges generated by a pair of electrodes while reactor walls remain cold.

Despite the many strategies investigated to conduct methane bromination none of them have been able to successfully avoid technical impediments associated with a medium-to-large scale methane pyrolysis plant.

## 1.3. BrOx cycle

The challenges involved in $CO_2$-free energy generation via a combination of methane pyrolysis and hydrogen combustion are concomitant to the endothermic nature of methane pyrolysis in spite of the overall reaction being exothermic. The same net reaction can be achieved in two exothermic steps thus avoiding the challenges associated to the endothermic pyrolysis. The process to do so combines a first reaction step in which methane is oxidised with a halogen (1.3.1) and a second step consisting on the oxidation of resulting halide with oxygen (1.3.2). The result of the combination of these two reaction steps is the partial oxidation of methane with oxygen to yield energy with solid carbon and water as only by-products 1.3.3.

$$CH_4 + 2Y_2 \rightarrow C + 4HY \qquad (Y = F, Cl, Br, I) \tag{1.3.1}$$

$$4HY + O_2 \rightarrow 2Y_2 + 2H_2O \qquad (Y = F, Cl, Br, I) \tag{1.3.2}$$

$$CH_4 + O_2 \rightarrow C + 2H_2O \tag{1.3.3}$$

During methane halogenation solid carbon and the corresponding halide are produced. Naturally, if this product stream were directly fed to the second reactor and put in contact with oxygen $CO_2$ would be produced as a result of the oxidation of solid carbon. Therefore an intermediate stage in which carbon is separated from the gaseous stream by means of a cyclone, a filter or a combination of the two is necessary. By separating the production of solid carbon from the oxidation step and recycling the halogen regenerated through the oxidation reaction to the first reactor, partial oxidation of methane is achieved and thus $CO_2$-free energy released from a hydrocarbon feed.

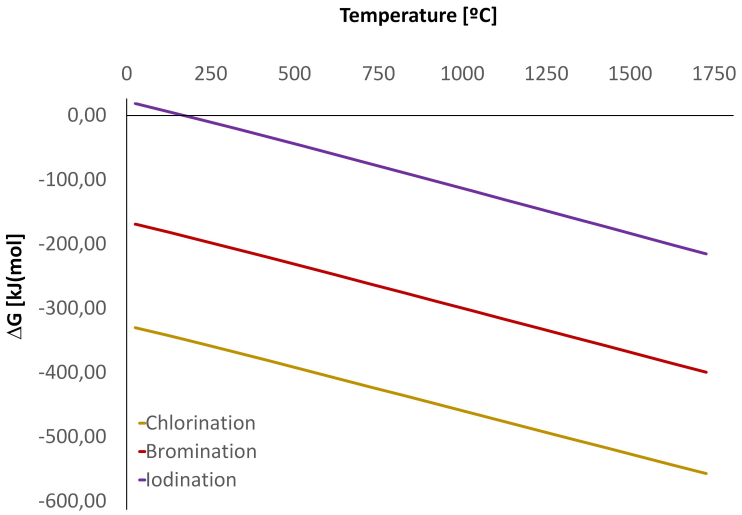


(a) ΔG for the oxidation of methane with different halogens

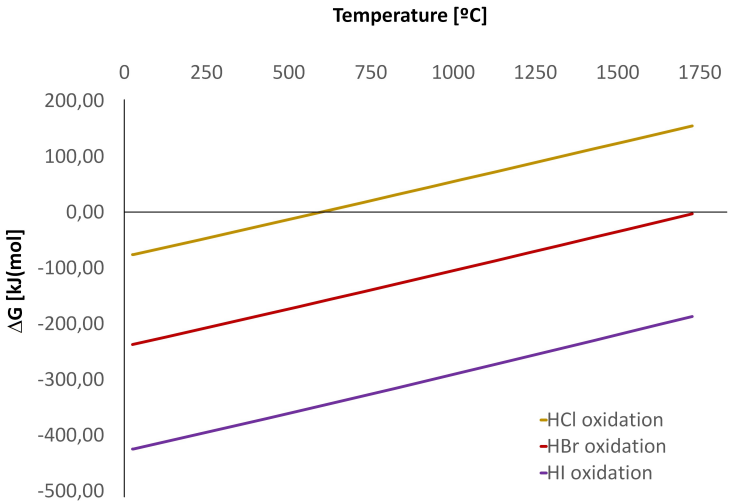


(b) ΔG for the oxidation of different halides

Figure 1.4.: Thermodynamics of different halogens in the cycle

Selection of halogen for the cyclic process is of critical importance. The halogens available are from fluorine, chlorine, bromine, iodine and astatine. From this group astatine is obviously ignored due to its high radioactivity, absence of stable isotopes [51]. Fluorine is the element in the periodic table with the highest electronegativity so it would react violently with methane during the first reaction step but the oxidation of hydrogen fluoride would be extremely difficult and thus it has not been considered for the cyclic process. In fact, methane bromination has a standard reaction enthalpy of -961.32 kJ/mol while that of hydrogen fluoride oxidation is 554.80 kJ/mol, thus indicating that the oxidation step is strongly endothermic. Figure 1.4 shows Gibbs free energies of reactions for the halogenation (figure 1.4a) and halide oxidation (figure 1.4b) steps with chlorine, bromine and iodine. Methane halogenation with either iodine, bromine or chlorine is spontaneous at temperatures above 250 °C but iodine

presents the lowest values of Gibbs free energy of reaction (actually, methane iodination is slightly endothermic for the temperature range considered). Therefore iodine has not been selected despite the fact that hydrogen iodide is easily oxidised. Halogenation of methane with both bromine and chlorine exhibit high Gibbs free energy of reaction so high equilibrium conversions are expected in this step. Nonetheless, Gibbs free energy of hydrogen chloride oxidation is positive at temperatures above 600 °C while that of hydrogen bromide oxidation is negative in the whole range considered. It can be then inferred that the equilibrium conversion of hydrogen chloride oxidation is lower than that of hydrogen bromide oxidation at any given temperature. This is proved by the numerous problems involved in the commercial implementation of Deacon process because temperatures necessary for kinetically feasible reaction (both thermal and catalytic) have low equilibrium conversion thus requiring a complex separation stage afterwards [52]. Therefore, bromine has been the halogen of choice for the cyclic process.

Literature on methane bromination is sparse and non-existing besides the work performed by the SRT (Solar Reactor Technologies) group and SANDIA National Laboratories who studied methane bromination in order to subsequently electrolyse hydrogen bromide and obtain hydrogen. The major findings are listed below:

- Steam-enhanced methane bromination results is thermodynamically more attractive than plain methane bromination, but the kinetics of the steam process are discouraging so that conducting the process without steam offers the best performance.
- Methane bromination presents high equilibrium conversion.
- If solid carbon is not formed, gaseous brominated hydrocarbons will be produced.
- Solid carbon deposited at the walls of the reactor.
- Gaseous bromocarbons were produced at some extent for all experiments (temperature up to 800 °C)
- Carbon formation occurred at residence times within 1 and 10 seconds.
- Negligible carbon formation at temperatures below 600 °C.

The experimental study on methane bromination performed by SANDIA National Laboratories was carried out in an externally-heated quartz-glass tubular reactor working at temperatures up to 800 °C. Due to the external heating carbon deposition occurred in the reactor and was removed after the experiments by burning it because the concept for hydrogen production did not aim to avoid $CO_2$ emissions. Therefore, carbon deposition avoidance were not studied and neither were carbon retrieval methods. Additionally, the main objective of methane bromination in this concept is to yield as much hydrogen bromide as possible in order to achieve a high overall hydrogen yield. Therefore all experiments with one exception were conducted with excess bromine which is not applicable to the BrOx cycle since avoiding $CO_2$ emissions requires complete conversion of methane so that it does not enter in contact

with oxygen during the second reaction step. Moreover, temperature in these studies was limited to 800 °C which is likely to be insufficient for complete conversion within reasonable times when over-stoichiometric bromine is used. Finally, carbon produced was not characterised which is of vital importance for the BrOx cycle since it is destined to be stored or sold as a potential by-product.

Literature on hydrogen bromide oxidation can be found although most of the sources are patents that do not disclose information (such as required residence times) that is important to tune reaction conditions for its application in the BrOx cycle. Moreover, most of the information available concerns the catalytic processes such as $CeO_2$, $RuO_2$ or $TiO_2$ to enable the reaction at low temperatures [100, 101, 102]. A patent suggest to carry out hydrogen bromide in a first thermal step followed by a catalytic oxidation at lower temperature with $NiO$ or $CuO$ over alumina [103]. This concept uses air to oxidise hydrogen bromide and involves isothermal operation so that overall reaction rate is reduced. Additionally, a complex nitrogen separation is necessary. A reaction mechanism and kinetic rate expression is available in the literature although the conditions at which the experimentation were done are far from those involved in the BrOx cycle and thus validation is needed [99].

## 1.4. Outline

This work is structured in five chapters which present the methodology and results of the study of the BrOx cycle. The first reaction, methane bromination, is the most challenging step due to the high temperatures involved, the presence of chemicals flammable and toxic, the formation of solid carbon during the process and the sparse literature on the topic. Therefore, three chapters have been devoted to its study.

- Chapter 1 introduces the BrOx cycle and a feasibility study of the process is carried out. Kinetic simulations of methane bromination are performed and conditions for the experimental study of the reaction are set. Finally, the experimental set-ups used are presented and the results of the experiments on bromination reaction are displayed.
- Chapter 2 deals with the challenging carbon deposition occurring during methane bromination. In this chapter a reactor concept for avoiding carbon fouling is proposed and a CFD model of the system is presented. Additionally, the results of the CFD simulations are shown and the geometry of the reactor is modified to improve its performance.
- Chapter 3 introduces the concept of sacrificial walls as an alternative method for avoiding carbon deposition, and three carbon debromination methods. In this chapter the process of coating for obtaining sacrificial walls is presented, optimal values for coating process are obtained and the performance of the reactor with sacrificial walls during methane bromination is assessed. Additionally, the effectiveness of three methods for the removal of the bromine content of the carbon produced during bromination is determined.

The second reaction step in the BrOx cycle, namely hydrogen bromide oxidation, has been more studied than bromination reaction and, more importantly, is very similar to Deacon reaction (hydrogen chloride oxidation), a widely studied process. Nonetheless, most of the existing literature on the topic is that concerning catalytic oxidation, and vital information regarding reaction kinetics and reaction times at different conditions is missing.

- Chapter 4 presents an experimental study on hydrogen bromide oxidation. The first part of the chapter shows the experimental results on thermal oxidation. Subsequently a catalyst apt for the oxidation reaction at lower temperatures is synthesised, characterised and used in catalytic oxidation experiments. Finally, the experimental data is integrated in a simulation of the oxidation process and an optimal strategy combining thermal and catalytic oxidation is presented.

Besides the two reaction steps in the BrOx cycle, the remaining operation units can be simulated and the process has been studied and optimised via a flowsheeting that incorporates the previously acquired knowledge.

- Chapter 5 explores the application of the complete BrOx cycle to a medium-size power plant. A flowsheeting of the process is carried out in this chapter together with a selection of optimal operation units and the heat integration of the plant. Additionally, a preliminary economic analysis of the process is performed.

## Funding

One funding source contributed to the development of this work:

- NRW Forschungsschule für Energieeffiziente Produktion und Logistik (NRW Graduate School for Energy Efficient Production and Logistic)

## Preamble

The following chapter has been published as:

**González Rebordinos, J., Salten, A.H.J., Agar, D.W.** (2017): "BrOx cycle: A novel process for $CO_2$-free energy production from natural gas" in *International Journal of Hydrogen Energy* 42, pp. 4710 – 4720.

This work is partly based on the experimental work performed by Mr. Salten during his Master thesis: "Experimental measurements and CFD – simulations of methane – bromination". Conceived, directed and supervised by myself and evaluated by Prof. Agar. The design and construction of the experimental plants, including the design and implementation of safety, monitoring and control procedures, the planning of experiments, initial tests and the interpretation of data was done by myself.

### 1.4.1. Table of contributions to chapter 1

Table 1.1.: Contributions to Chapter 1

| *Contributor* | *Contribution percentage* |
|---|---|
| Jesús González Rebordinos | 70 |
| Alex H. J. Salten | 25 |
| David W. Agar | 5 |

## Abstract

Currently, the combustion of fossil fuels is the major anthropogenic source of $CO_2$ and the main reason for the significant increase in its atmospheric concentration over the past decades. Despite the increase in fossil fuel consumption in recent years, the available reserves have actually increased, indicating that the use of fossil fuels is limited less by their availability than by the emissions of $CO_2$ associated with their combustion.

Energy can be generated from methane without concomitant $CO_2$ emissions by means of a bromination-oxidation (BrOx) cycle. This process comprises two exothermic reaction steps, namely methane bromination and hydrogen bromide oxidation, with a bromine recycle from the latter to the former, that result in an overall exothermic reaction in which methane and oxygen yield water and solid carbon, thus avoiding $CO_2$ production.

Thermodynamic and kinetic simulations have been performed that show the feasibility of the BrOx cycle. The influence of temperature, residence time and feed composition on methane bromination reaction was studied and indicates that carbon formation starts at temperatures as low as 500 °C for excess methane, while temperatures over 750 °C are necessary in order to achieve noticeable carbon formation when working with excess bromine. The composition of the carbon produced has been determined and the mass fraction of bromine-containing by-products has been found to decrease with increasing reaction temperatures.

# 2. BrOx cycle: a novel process for $CO_2$-free energy production from Natural Gas

Energy consumption and the standard of living are closely correlated and thus humanity needs abundant and uninterrupted energy supplies. Over the $20^{th}$ century, global energy consumption has steadily increased, reaching more than 500 EJ in year 2014 [1]. This trend is expected to continue in the coming decades due to the predicted growth in both the worldwide population and economy.

In 2014, fossil fuels represented more than 80% of the total primary energy demand of the OECD (Organisation for Economic Co-operation and Development) members [1]. This energy is primarily obtained via the combustion of coal oil and natural gas, which implies the formation of $CO_2$, a by-product that is routinely released into the atmosphere. As a consequence, its atmospheric concentration has steadily increased over the past decades [12], which scientific consensus considers to be the main cause of climate change [12]. Recently, at the 2015 United Nations Climate Change Conference (COP21) held in Paris, an agreement was achieved, that intends to limit the increase in the global average temperature to less than 2 °C above pre-industrial levels [62]. In order to do so, a dramatic reduction of $CO_2$ emissions is inescapable. Since the largest anthropogenic source of $CO_2$ is that derived from energy generation, avoiding or minimising the associated emissions is the most direct strategy.

One approach for reducing energy-derived $CO_2$ emissions is to expand the use of renewable energy. A good example of this is the energy transition (*Energiewende*) that has been adopted in Germany, which aims to reduce greenhouse gases emissions by 40% by 2020 and by 80-95% by 2050 [63]. Although the share of renewable energy in Germany's gross power supply has reached 32.5% in 2015 [64], the impact on global energy production is negligible. Additionally, several studies predict that fossil fuels will remain the predominant energy source for the next decades, still supplying at least 75% of the world energy demand in 2040 [65].

Despite the increased fossil fuel consumption over the last century and contrary to popular belief, the proven reserves of fossil fuels have not decreased in the past few decades, but actually increased as exemplified by natural gas, whose proven reserves were 117.6 $Tm^3$ in 1992 and 187,8 $Tm^3$ at the end of 2011 [1]. In addition, if natural gas from unconventional sources, such as shale gas, coal-bed methane or methane hydrates, is taken into account, the estimates of the gas supply available can be measured in centuries [66]. Naturally, not all unconventional resources are

technically or economically exploitable at the present time, but this situation may soon change as new extraction technologies are developed. The shale gas boom provides a good example of such a development in the past. Although well-known, shale gas has remained non-exploitable for decades until a combination of new technologies, namely hydraulic fracturing (fracking) together with horizontal drilling and, most importantly, high gas prices made its economic exploitation feasible [67].

The aforementioned demonstrates that the use of fossil fuels is less restricted by their availability than by the $CO_2$ emissions resulting from their combustion. In view of this and from the fact that replacing the existing infrastructure for extraction, processing, transportation and storage would be extremely expensive, and in the short term, infeasible, the decarbonisation of energy production from fossil fuels is a promising strategy to counter climate change.

CCS (Carbon Capture and Storage) has been proposed to decarbonise fossil fuels by capturing the $CO_2$ before or after combustion and sequestering it either under the ocean or subcutaneously. It is a controversial technology that lacks the acceptance of a large section of the public and entails many uncertainties regarding costs, long-term reliability and storage capacity [81]. Moreover, up to 40% of the energy being generated may be sacrificed by this process.

Another approach that enables $CO_2$-free energy production from fossil fuels is methane pyrolysis. Despite the endothermic methane pyrolysis, the hydrogen produced can react exothermically with oxygen thus leading to a net reaction in which roughly half the total energy available is released, with solid carbon and water as the only by-products. This process has been widely studied, but it still is not technically feasible, mainly due to heat exchange issues and the fact that it is only kinetically feasible at temperatures above 1200 °C [47, 44].

The BrOx cycle is a novel process that enables the use of natural gas for energy production without accompanying $CO_2$ emissions. It comprises two exothermic reactions, which result in the same net reaction as the combination of methane pyrolysis and hydrogen combustion. The BrOx cycle has thus the advantage of avoiding any heat transfer to an endothermic reaction at high temperatures.

In the BrOx cycle, methane and bromine are first fed to a reactor, where they react to yield solid carbon and hydrogen bromide (Equation 6.1.1). An excess of bromine is used to ensure that methane is completely consumed. Following subsequent separation of the solid carbon, that can be carried out with a combination of a cyclone and a filter to remove the fine particles, the remaining gaseous product stream is fed to a second reactor, in which hydrogen bromide reacts with an oxygen feed stream to regenerate bromine and form water (Equation 6.1.2). Afterwards, bromine is separated from this water and recycled to the methane bromination reactor. This process results in an overall reaction, in which methane and oxygen yield energy with solid carbon and water as the only by-products, thus circumventing $CO_2$ production (Equation 6.1.3). All the process is carried out at atmospheric pressure in order to minimise the risk of leaks. By sacrificing, at least provisionally, the energy available in the carbon, one simplifies the sequestration problem dramatically.

$$CH_4 + 2Br_2 \rightarrow C\,(s) + 4HBr \qquad \Delta H_r^o = -132.47kJ/mol \tag{2.0.1}$$

$$4HBr + O_2 \rightleftarrows 2Br_2 + 2H_2O \qquad \Delta H_r^o = -364.32kJ/mol \tag{2.0.2}$$

$$CH_4 + O_2 \rightleftarrows C\,(s) + 2H_2O \qquad \Delta H_r^o = -496.79kJ/mol \tag{2.0.3}$$

The reason for selecting bromine from the halogens lies in its high compatibility with the process. Apart from being extremely difficult to handle, fluorine would react vigorously with methane forming hydrogen fluoride, a highly stable molecule which cannot be easily oxidised. Iodine's low reactivity renders it unsuitable stripping the hydrogen off methane iodination. Chlorine would react sufficiently with methane, but hydrogen chloride oxidation (Deacon reaction) has proved to be a challenging reaction and its commercial implementation since its development in 1866 for the production of chlorine has been plagued by problems [71]. Bromine has been selected for the cycle because it ensures a good reaction with methane and a later hydrogen bromide oxidation that is more favourable thermodynamically than Deacon reaction as its equilibrium conversion is higher than that of hydrogen chloride oxidation.

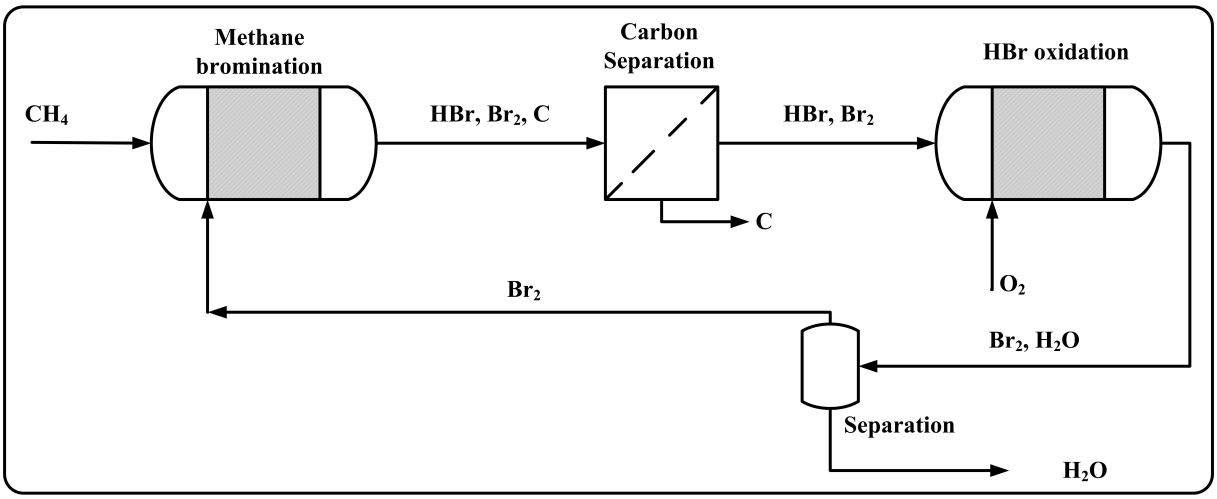


Figure 2.1.: Schematic representation of the BrOx cycle

## 2.1. Materials and methods

### 2.1.1. Thermodynamic calculations

A preliminary thermodynamic analysis of the BrOx cycle was performed in order to assess its feasibility. Thermodynamic data calculated with NASA polynomials were used for the calculation of the reaction enthalpy and the change in Gibbs free energy for methane bromination and hydrogen bromide oxidation [79].

$$\Delta H = \sum_i v_i H_i^0 \tag{2.1.1}$$

$$\Delta G = \sum_i v_i G_i^0 \tag{2.1.2}$$

First, the Gibbs energy minimisation method (Equation 2.1.3) with atomic balance constraints (Equation 2.1.4) was used only for the main reactions. The species considered were therefore $CH_4$, $Br_2$, $C(s)$, $HBr$, $O_2$ and $H_2O$. Due to the high melting point of carbon it was considered as a solid phase for the thermodynamic calculations.

$$minG = min \sum_i n_i \mu_i \tag{2.1.3}$$

$$\sum_i n_i a_{ji} = b_j \tag{2.1.4}$$

It is known that reactions of methane with halogens may lead to the production of halogenated hydrocarbons. More detailed thermodynamic calculations were therefore carried out for methane bromination using the module *RGibbs* installed in the commercial software ASPEN Plus. The most likely by-products of methane bromination, described by SANDIA Laboratories were included [55, 56].

### 2.1.2. Kinetic simulations

A reaction mechanism published in previous studies on methane bromination [55, 56] was implemented with the freeware CHEMKED-I. This reaction mechanism takes 26 chemical species into account and includes 79 elementary reactions with the corresponding values for pre-exponential factor ($k_{0_n}$), activation energy ($E_n$) and the exponential constant ($\beta$). With these parameters, the reaction rate constant can be calculated for any temperature with the modified Arrhenius expression (Equation 2.1.5).

$$k_n = k_{0_n} T^{\beta n} e^{\frac{-E_{a_n}}{RT}} \tag{2.1.5}$$

In order to numerically solve the mass balances (Equation 3.3.1) for each component and the energy balance (Equation 2.1.7) initial conditions, T and $C_{i_0}$, were supplied. CHEMKED-I can only simulate batch reactors, and therefore the results generated correspond to concentration and temperature development with time. Thermodynamic data for all chemical species was supplied to the program in the form of coefficients for NASA polynomials.

$$\frac{dC_i}{dt} = \sum_n v_{n_i} k_n \left( \prod C^{\left|v'_{n_i}\right|} - \frac{1}{K_n} \prod C^{\left|v''_{n_i}\right|} \right) \tag{2.1.6}$$

$$\frac{dT}{dt} = \frac{\sum_n \left(-\Delta_{r_n} H^0\right) k_n \left(\prod C^{\left|v'_{n_i}\right|} - \frac{1}{K_n} \prod C^{\left|v''_{n_i}\right|}\right)}{\frac{p}{RT} \sum_i C_{p_i} x_i} \tag{2.1.7}$$

### 2.1.3. Experimental study of methane bromination

An experimental set-up was constructed in order to investigate methane bromination (Figure 2.2). The reactor (R-101) and the inlet lines are made of quartz glass and heated with electric heating bands. The flow of methane (B-101) and inert gases is controlled by means of rotameters (FC-101, FC-102, FC-103). Methane can be diluted with nitrogen (B-102) prior to preheating. A saturator (S-101) is used to introduce bromine into the system. The saturator is filled with liquid bromine and argon is bubbled through it as a carrier gas, so that it leaves the system saturated in bromine. In this way, the flow of bromine can be regulated by controlling the flow of argon (B-103) and the temperature of the water bath in which the bromine saturator is located.

After the reactor, a PTFE filter (F-101) with a pore size of 2$\mu$m insures retention of the carbon particles produced. A 3-way-valve (V-106) is used to direct the product stream to a bottle containing a solution of potassium iodide (T-102). Following the experiment, the solution can be titrated and thus the conversion of bromine determined. In order to avoid the release of bromine or hydrogen bromide to the atmosphere, two bottles (T-102, T-103) containing neutralising solution (NaOH and $Na_2S_2O_3$) are installed downstream. A wash bottle containing potassium iodide solution (T-104) is used as a bromine detector for the gas stream. The plant is automatically shut down when any change in the colour of this solution is detected by the monitoring spectrophotometer.

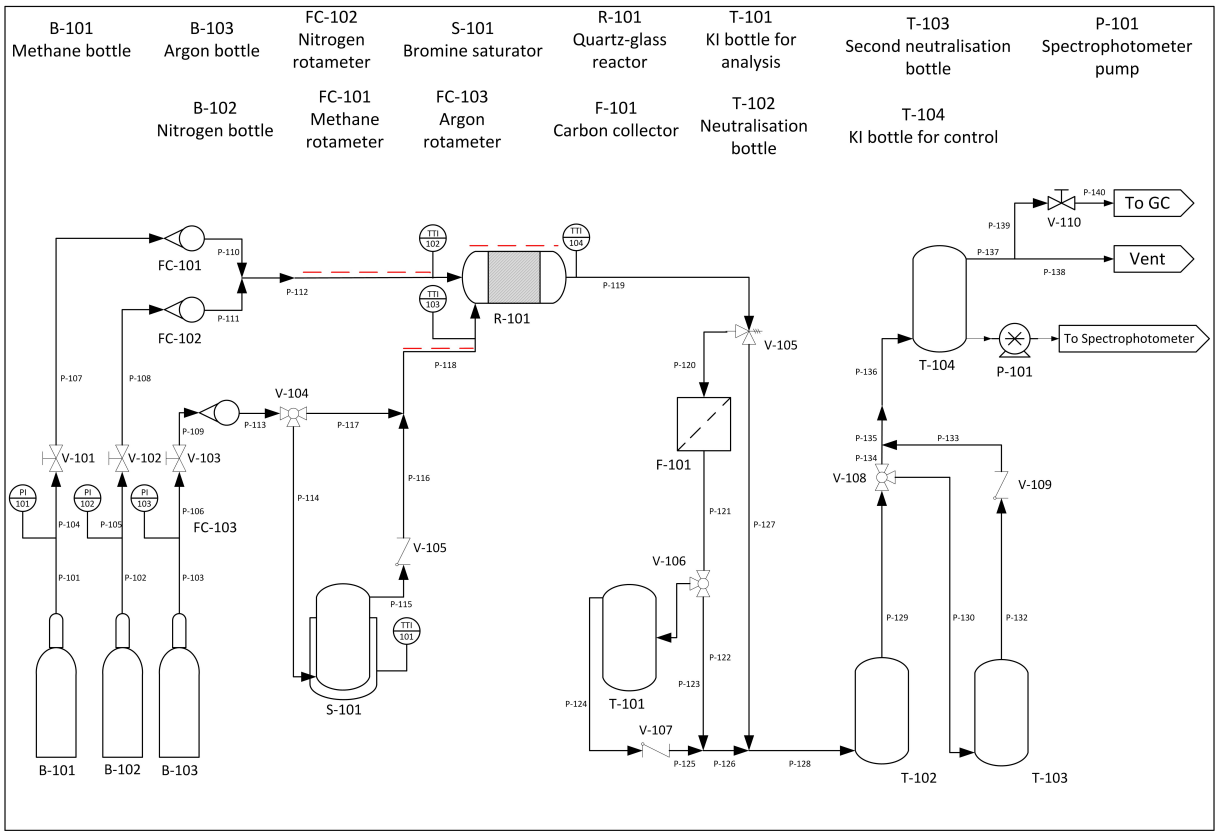


Figure 2.2.: Flowsheet of the bench-scale plant for methane bromination

A maximum temperature of 760 °C could be attained in the aforementioned laboratory bench-scale reactor. The plant was subsequently modified so that temperatures as high as 1100 °C could be achieved. The most important modification to the set-up was the substitution of an electric oven for electric heating bands and the use of a combined inlet line instead of the previous two separate ones (Figure 2.3).

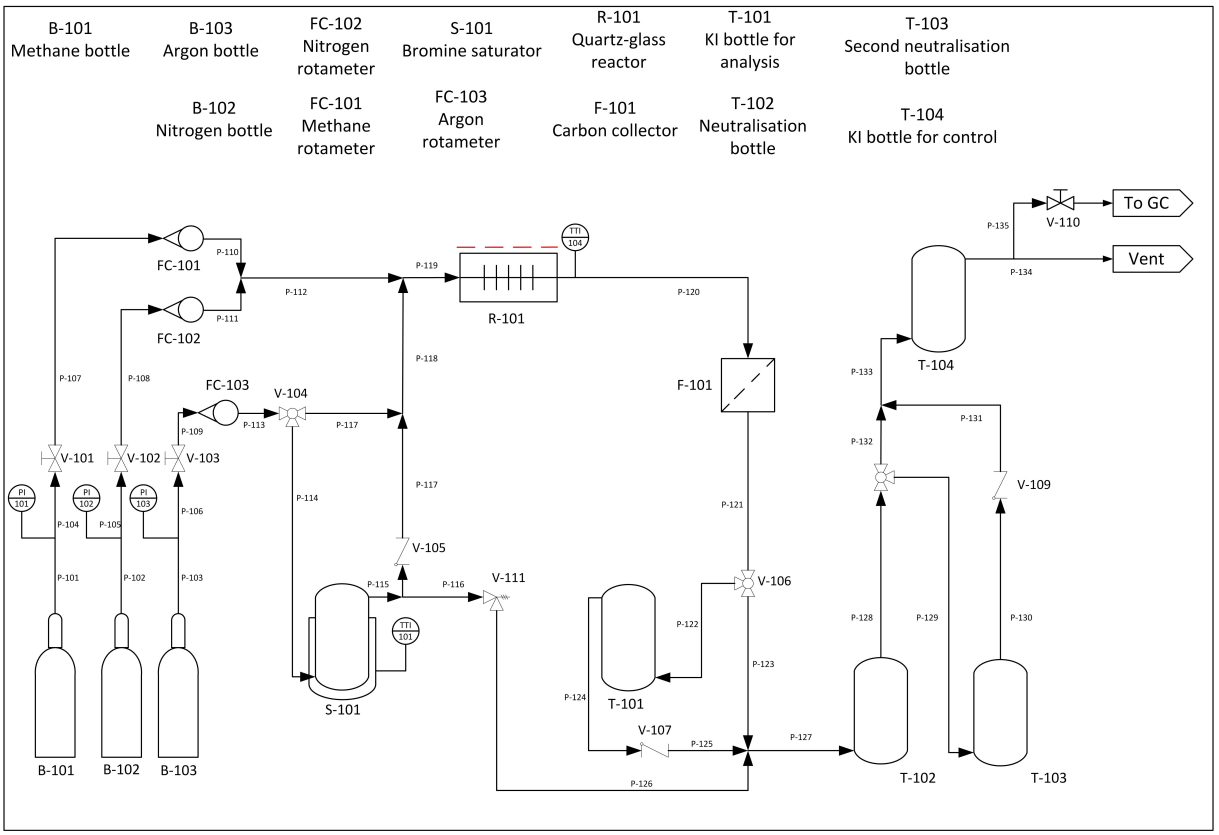


Figure 2.3.: Flowsheet of the bench-scale plant for high temperature methane bromination

Since bromine is highly corrosive, glass, quartz glass and PTFE were used as materials of construction for all pipes and equipment that was expected to come into contact with bromine. The combination of high temperatures and the presence of bromine will make necessary the use of materials such as silicon carbide or titanium (if the gas stream contains water) for industrial scale, since glass will no longer be feasible as a construction material due to its fragility.

Samples of carbon produced during high temperature methane bromination experiments were analysed with SEM (Scanning Electron Microscope) and EDX (Energy Dispersive X-Ray Spectroscopy) with the main objective of determining the chemical composition of the carbon and to determine its bromine content. Due to the method used, the residual hydrogen content of the carbon samples could not be determined and therefore it will be studied in following research.

## 2.2. Results and discussion

### 2.2.1. Thermodynamics of BrOx cycle

The results of the thermodynamic calculations (Figure 2.4) show that both methane bromination and hydrogen oxidation are exothermic reaction and that their reaction enthalpy remains virtually unchanged with temperature. The Gibbs free energy change for methane bromination remains negative over a wide range of temperatures, indicating that the reaction is highly favoured thermodynamically and therefore that high conversion of methane can be expected. The Gibbs free energy change for hydrogen bromide oxidation is also negative at temperatures up to 1700 °C although its absolute value decreases with increasing temperature, showing that the reaction is spontaneous, but that the equilibrium conversion will noticeably diminish with temperature.

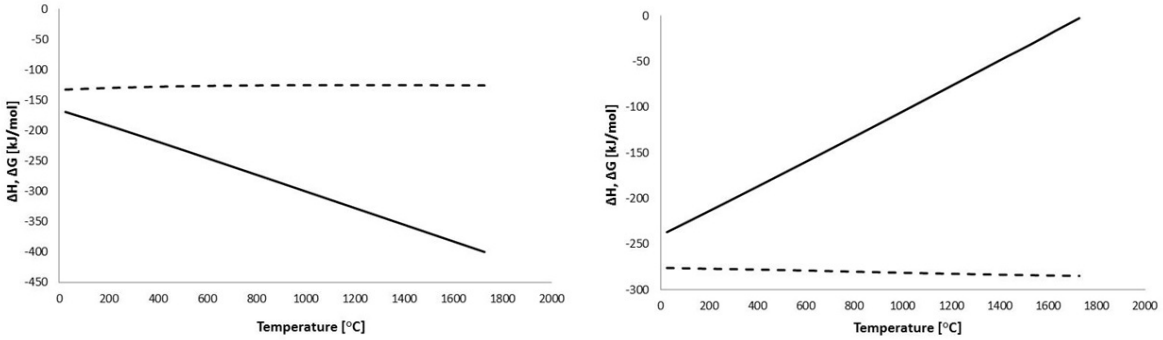


(a) Thermodynamics of methane bromination

(b) Thermodynamics of HBr oxidation

Figure 2.4.: Thermodynamic calculations of the BrOx cycle (ΔH: dotted line; ΔG: solid line)

As mentioned earlier, incomplete methane bromination may lead to the generation of brominated organic compounds. In order to assess the feasibility of the BrOx cycle, it is essential to determine whether the presence of these by-products is negligible or not. The by-products considered are the organobromine compounds $CBr_4$, $CHBr_3$, $CH_2Br_2$, $CH_3Br$, $C_2H_3Br$, $C_2H_5Br$, and the by-products of methane pyrolysis $C_2H_2$, $C_2H_4$ and $C_2H_6$, as described in a previous study by SANDIA Laboratories [55, 56].

The equilibrium composition for methane bromination over a wide range of temperatures is shown in figure 2.5a. All the species described above have been lumped together as by-products. The results of the thermodynamic calculations for stoichiometric conditions demonstrate that the main reaction products at equilibrium are solid carbon and hydrogen bromide. The amount of residual methane is close to zero, as would be expected from the analysis of the variation of the Gibbs free energy for methane bromination. The presence of by-products at equilibrium is confined to trace amounts for temperatures as high as 2000 °C and can thus be considered negligible.

Although a low level of hydrogen is observed at equilibrium due to methane pyrolysis, it is likely that at operating temperatures in the window of 1000 °C to 1400 °C, the kinetics of methane bromination can be assumed to be much faster than those of methane pyrolysis. Nevertheless, after separation of the carbon and during cooling of the reactor outlet stream the hydrogen will certainly combine with the unreacted bromine to yield hydrogen bromide.

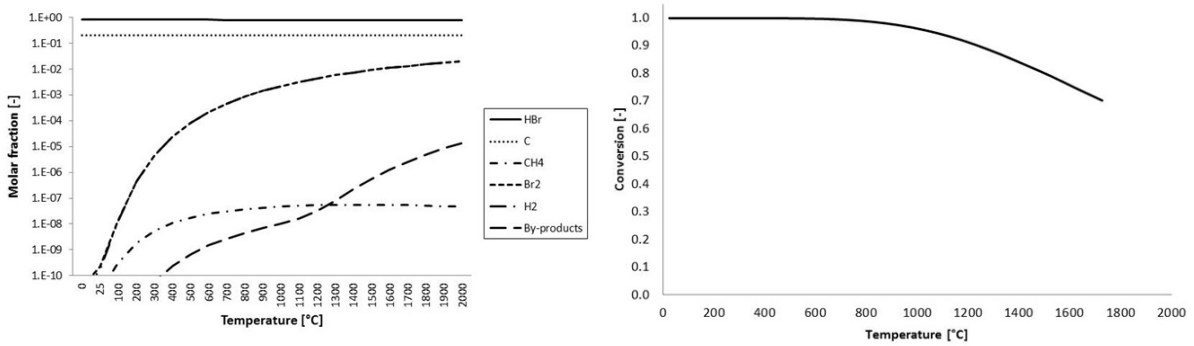


(a) Equilibrium composition of methane bromination

(b) Equilibrium composition of hydrogen bromide oxidation

Figure 2.5.: Equilibrium state of BrOx cycle for stoichiometric feed conditions

The equilibrium conversion of hydrogen bromide oxidation under stoichiometric conditions falls with increasing temperature as expected. Up to 800 °C almost complete conversion can be expected, but it drops off steadily at higher temperatures. One strategy to obtain high conversion would be to carry out the reaction in two steps, an initial adiabatic thermal oxidation step for a rapid reaction followed by a catalytic oxidation step at lower temperatures to achieve complete conversion. Several catalysts have been suggested in many publications and patents for hydrogen bromide oxidation [109, 110, 111]. From these catalysts, $CeO_2/ZrO_2$, $RuO_2/TiO_2$ and $TiO_2$ offer a high activity at temperatures that range from 150 °C to 450 °C and therefore they will be studied in future works.

The results of the thermodynamic calculations demonstrate the underlying conceptual feasibility the BrOx process. It now remains to assess which temperatures and residence times are necessary to approach these equilibria. For this purpose, kinetic simulations of methane bromination were performed.

### 2.2.2. Kinetic simulation of methane bromination

Due to the lack of reliable models describing carbon generation from the brominated intermediates, solid carbon formation was not implemented in the kinetic simulations. Thus no carbon appears in the results, and it is all effectively represented in the form of brominated compounds, even if the subsequent conversion of such compounds is almost certain.

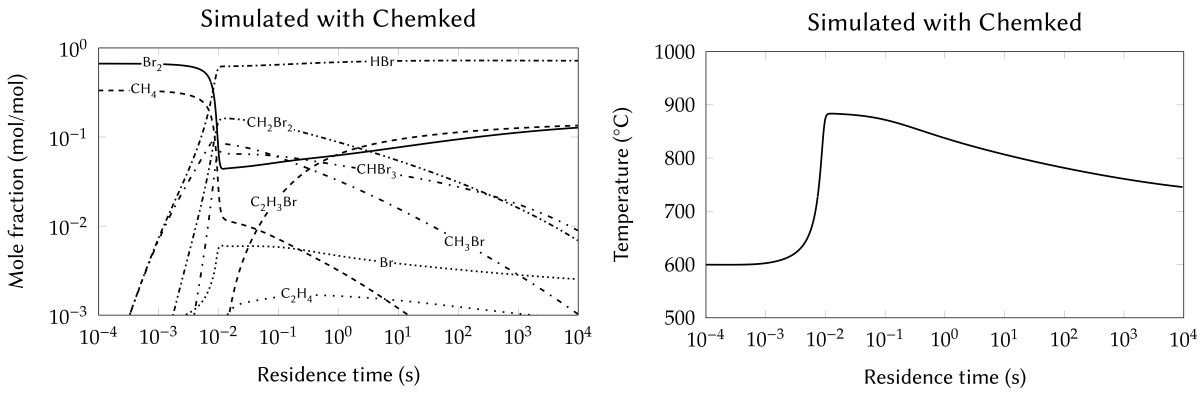


(a) Concentration profile of methane bromination

(b) Temperature profile of methane bromination

Figure 2.6.: Kinetic simulations of SANDIA mechanism for methane bromination

The initial conditions for the methane bromination simulation were stoichiometric amounts of reactants, adiabatic conditions, atmospheric pressure and an initial temperature of 600 °C. The results (Figure 2.6) illustrates that even at 600 °C methane and bromine react almost completely within the first 0.01 seconds causing a temperature rise of 300 °C. This means that the reaction of methane with bromine to the brominated precursors is very fast and hence it can be concluded that the limiting steps for complete methane bromination are those in which these brominated intermediates react to yield solid carbon and hydrogen bromide.

The kinetic simulations for methane bromination suggest that the reaction could potentially take place within residence times as low as 0.01 seconds. Although these results are promising, the final objective is to produce solid carbon and hydrogen bromide, and thus the conditions required for the intermediate compounds to progress to equilibrium conversions are of crucial importance.

### 2.2.3. Experimental results on methane bromination

An experimental study on methane bromination was performed with the main objective of determining the conditions leading to solid carbon formation and to low by-product levels (especially of organobromine compounds). The key variables that may have an influence on whether solid carbon forms or not are the bromine/methane ratio, the temperature and the residence time.

The flow rates of methane in this experimental study lay in the range of 20 ml/min to 50 ml/min while those of bromine range from 50 ml/min to 120 ml/min (all measured under ambient conditions) and the bromine/methane ratio ranged from 0.9 to 2.7. Although it was initially attempted to operate the plant under adiabatic conditions, the amount of heat generated by such flow rates was so small that the insulation of the reactor necessary was unfeasible. The experiments were therefore carried out in a quasi-isothermal regime. The temperature inside the reactor was measured by

means of a thermocouple (Ni-Cr/Ni-Al). In the first experiments, electric heating bands were used to heat up the reactor and to maintain a roughly constant temperature during the measurement.

Table 2.1.: Experimental results for methane bromination

| *No* | $Br_2/CH_4$ | *T [°C]* | $X_{Br_2}$ [-] | $X_{CH_4}$ [-] | Residence time at reaction temperature [s] | Carbon formation |
|---|---|---|---|---|---|---|
| 1 | 1.7 | 545 | 1 | — | 24 | YES |
| 2 | 0.96 | 635 | — | 1 | 27 | YES |
| 3 | 2.62 | 550 | — | 1 | 17 | NO |
| 4 | 2.13 | 755 | 0.74 | 1 | 32 | YES |

Experiments numbers 1 and 2 were performed with excess methane, while in 3 and 4 excess bromine was employed. The results (Table 2.1) show that carbon was formed when working with excess methane at both 545 °C and 635 °C. Also, as expected from the kinetic simulation, methane and bromine conversion were complete.

When the experiment was repeated at 550 °C with excess bromine, no carbon formation occurred, although methane conversion was complete. This indicates that all the methane and bromine had reacted in the reactor to give brominated compounds. Nonetheless, two black circles in the reactor were observed. These carbon spots appeared at the points where the heating band had two metallic rings. At these points, the conductivity is much higher than over the rest of the heating band and therefore so is the temperature, thus showing that higher temperatures are required in order to achieve carbon formation by decomposition of the brominated intermediates.

Experiment 4 was carried out at 755 °C, the maximum temperature achievable with the original set-up. Although some carbon was formed, it was much less than the amount generated in experiments 1 and 2 (Figure 2.7). Also, it can be seen that a brownish residue appears at the outlet, which is probably some kind of organobromine compound.

(a) Quartz glass reactor after ca. 1 hour bromination experiment 1

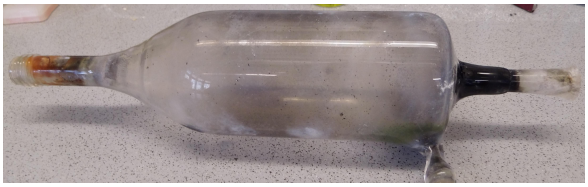

(b) Quartz glass reactor after ca. 1 hour bromination experiment 4

Figure 2.7.: Reactor following the bromination experiment

For application in the BrOx cycle, it is of interest to operate the methane bromination with excess bromine because any gaseous brominated compounds, that will

surely be produced if excess methane is used, will react with oxygen in the hydrogen bromide oxidation step thus yielding $CO_2$. Therefore, determining if carbon formation can occur with a feed containing excess bromine is of critical importance, and, for this reason, a new plant was constructed in which higher temperatures could be attained.

A tubular oven from Heraeus with a maximum operating temperature of 1100 °C was substituted for the previously used heating bands. A new quartz glass tubular reactor that could fit into the oven was fabricated. Five experiments with an approximate duration of 1 hour using excess bromine and temperatures ranging from 930 °C to 1070 °C were performed, all of which resulted in noticeable carbon formation (Figure 3.2). Most of this carbon ended up coating the inner surface of the reactor, while only a small percentage was removed in the PTFE filter downstream.

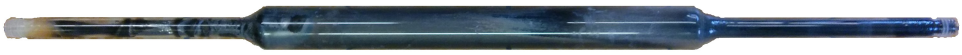

Figure 2.8.: Quartz glass reactor after 1 hour methane of the bromination experiment

In order to determine the bromine content of the carbon produced in the methane bromination experiments, samples were taken from several locations within the reactor: the inlet of the reactor, the middle, the outlet and from the filter located after the reactor. These samples were subsequently analysed using SEM (Scanning Electron Microscope) and EDX (Energy Dispersive X-Ray Spectroscopy). Table 2.2 shows the bromine content of the carbon samples from the centre of the reactor following experiments 1, 2 and 4. There is a clear decrease in the bromine content of the carbon with increasing operating temperature. This is due to the higher reaction rates achieved at higher temperatures which result in a faster decomposition of the brominated compounds to solid carbon.

Table 2.2.: Experimental results for high temperature methane bromination

| *No* | $Br_2/CH_4$ | $T$ [°C] | Residence time at reaction temperature [s] | Bromine content [% w/w] |
|---|---|---|---|---|
| 1 | 2.62 | 930 | 14 | 9.02% |
| 2 | 2.64 | 970 | 14 | 4.66% |
| 3 | 2.47 | 970 | 25 | — |
| 4 | 2.23 | 1070 | 12 | 1.95% |
| 5 | 2.16 | 1070 | 22 | — |

The bromine content of the carbon is not homogeneously distributed within the reactor. In all experiments, the carbon samples obtained from the reactor zone between 15 cm and 60 cm from the reactor inlet exhibited the lowest bromine content, while the samples collected at the inlet, the outlet and in the filter, contained higher amounts of bromine. The temperature profile of the reactor was determined experimentally using a thermocouple (60 cm long, 0.5 cm of diameter) that was connected

to the experimental set-up via a septum, so that it was possible to scan the reactor length. This process was repeated for several experiments at 1000 °C and 900 °C and always yielded a virtually identical profile.

The temperature profiles obtained can be subdivided into five different regions:

- Inlet zone (0 cm - 15 cm): In this region, the temperature increases rapidly from ambient temperature to approximately 80% the maximum temperature.
- Inlet-middle zone (15 cm - 30 cm): The slope of the temperature rise in this zone is less steep, and, at the end, reaches the maximum reactor temperature.
- Middle zone (30 cm - 60 cm): The temperature remains constant at the maximum level in this section of the reactor.
- Outlet-middle zone (60 cm - 75 cm): The temperature starts to decrease gradually down to 80% of the maximum value.
- Outlet zone (75 cm - 90 cm): The temperature decreases steeply and almost reaches ambient temperature at the outlet.
- Filter: The filter operates at ambient temperature.

When the bromine percentage at the locations from which carbon samples were taken is compared with the temperature profile (Figure 2.9) it becomes clear that a strong correlation exists between temperature and carbon purity.

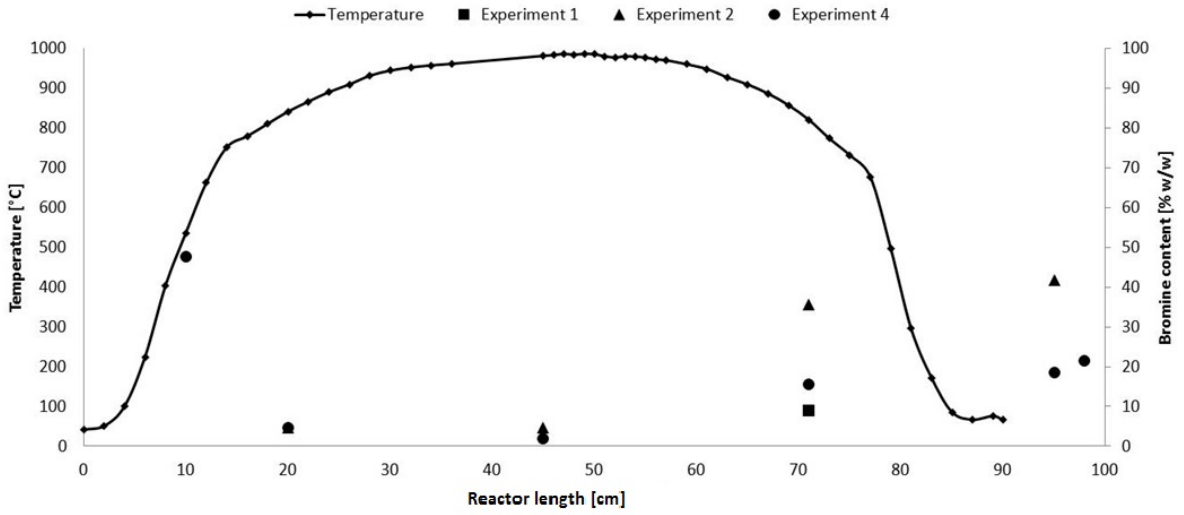


Figure 2.9.: Relationship between bromine content in carbon samples and the temperature profile of the tubular reactor

The results also show that due to the low temperature in the inlet zone, the reaction rate is not sufficient for the organobromine compounds to be converted to solid carbon and hence the high content of bromine found at this location. In the inlet-middle and middle zone, the temperatures are higher and therefore the bromine content of the carbon is minimum. Following the same logic, the high content in the outlet-middle

zone could be at first sight explained by an insufficient temperature and a too slow reaction rate. However, low reaction rate due to low temperatures cannot explain the high bromine content of the carbon found in the filter, since at ambient temperatures it is inconceivable that methane bromination reaction proceeds at all, let alone with carbon formation, suggesting that at least the carbon found in the filter has not formed there at ambient temperature.

Apart from the different carbon purity, there is another major difference that helps explain the presence of carbon with similar bromine contents in the filter and at the outlet-middle region. The carbon from the middle of the reactor was in the form of black flakes with a distinctive lustrous metallic sheen, very similar to the appearance of graphite. The carbon observed at the inlet, outlet and in the filter was a fine black matte powder. These differences are even more apparent when the samples are inspected by scanning electron microscope.

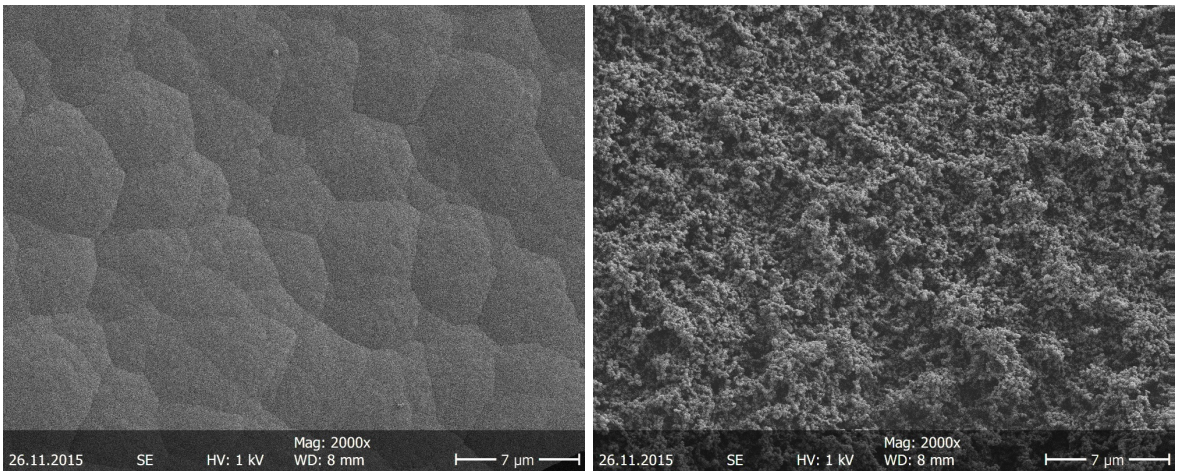


(a) Carbon sample from middle zone (b) Carbon sample from outlet-middle zone

Figure 2.10.: Carbon samples under Scanning Electron Microscope

The presence of carbon flakes firmly attached to the reactor inner surface, as well as the relatively high purity of the carbon, is explained by the high temperature causing fast formation and growth of carbon deposits at the reactor wall. The carbon formed at the low temperature inlet of the reactor, however, contains a much higher amount of bromine, because of the low reaction rate. This also implies that the carbon does not form rapidly enough to result in a graphite-like film and instead generates very small particles that either stick on the inlet wall or are carried by the flow until they deposit loosely at a surface. Consequently, the smallest carbon particles formed can make their way through the reactor and reach the filter, which is consistent with the carbon powder observed there.

## 2.3. Conclusion

A novel process enabling $CO_2$-free energy generation from natural gas in a closed bromination-oxidation cycle has been presented in this paper. This process offers the advantage against conventional technologies, such as methane combustion or chemical looping combustion, of producing zero $CO_2$ emissions although roughly half the energy contained in the methane is liberated. Additionally, the same result obtained with methane pyrolysis combined with hydrogen combustion can be achieved with the BrOx cycle while at the same time the recuperative introduction of heat required in the endothermic methane pyrolysis that leads to carbon deposition is avoided. The thermodynamics of this BrOx cycle and the kinetics of methane bromination have been examined, and an experimental study of methane bromination has been conducted with special focus on carbon formation and carbon purity.

From a thermodynamic point of view, the BrOx cycle has been found to be feasible means to access about 55 % of the energy produced through methane combustion but without $CO_2$ emissions. Methane bromination is an exothermic reaction that occurs spontaneously for a wide range of temperatures up to 2000 °C. Possible by-products, such as brominated compounds, are only present in trace amounts at equilibrium, and therefore the reaction can optimally be carried out at conditions leading to concentrations close to the equilibrium values in reasonable residence times. Hydrogen bromide oxidation is also an exothermic reaction that takes place spontaneously for temperatures up to 1800 °C. The equilibrium conversion is effectively complete at temperatures lower than 800 °C, above which it starts to drop off. The use of a catalyst for hydrogen bromide oxidation may be necessary at lower reaction temperatures.

Through the implementation and simulation of the SANDIA reaction mechanism for methane bromination at different inlet conditions, it has been determined that methane and bromine react with one another within the first 0.01 seconds. Short residence times would thus suffice to achieve conversions close to the equilibrium values. The absence of reliable models to describe the mechanism and kinetics by which brominated intermediates react to form solid carbon and hydrogen bromide means that carbon formation cannot yet be simulated and thus residence times required for minimising by-product generation cannot be ascertained theoretically.

A laboratory bench-scale plant was constructed in order to determine suitable conditions for temperature and residence time that lead to carbon formation and minimise brominated compounds. In the first experiments, it was observed that excess methane lead to carbon formation at temperatures as low as 550 °C, whilst, when working with excess bromine, moderate carbon formation commences at temperatures around 750 °C. At temperatures higher than 950 °C, carbon forms to a noticeable extent with excess bromine conditions, indicating that the rate of the reactions leading to solid carbon increases with the temperature.

The analysis of carbon samples exhibits a strong dependency of the bromine content on the reaction temperature. The comparison of the carbon composition at different locations in the reactor with its temperature profile also indicates that higher temper-

atures lead to lower bromine content. The low bromine content of the carbon entails bromine losses from the closed loop and therefore a make-up stream must be supplied. From the results of this study it is expected that higher temperatures will lead to carbon with much less than 1% and therefore it will have a small impact on the total amount of bromine being used. Nonetheless, the carbon could be treated subsequently and the bromine recovered if an economic analysis proves advantageous.

Due to the small flow rates of methane and bromine in the experimental set-up, the reactor was operated quasi-isothermally. The results obtained may be a consequence of this operating mode, since if the reaction had been carried out adiabatically, the final temperatures actually reached would have been higher than those achieved in the methane bromination experimental plant, which would therefore have led to a faster generation of solid carbon with a much lower bromine content. Future work will be devoted to increasing carbon formation rates and lowering by-product generation by using higher temperatures and employing a revamped plant with higher flow rates, so that methane bromination can be carried out in a quasi-adiabatic manner. Strategies for avoiding carbon fouling at the inner surface of the reactor and completely eliminating residual trace bromine from the carbon product formed in the reactor will also be developed.

## 2.4. Acknowledgments

Financial support from the Graduate School of Energy Efficient Production and Logistics (*Forschungsschule für Energieeffiziente Produktion und Logistik*) is gratefully acknowledged.

The authors would also like to express their appreciation for the assistance of the *Leibniz-Institut für Analytische Wissenschaften - ISAS - e.V* and of Ms. Meuris from the *Lehrstuhl für Biomaterialien und Polymerwissenschaften* in the analysis of carbon samples.

## Preamble

The following chapter will be submitted for publication as:

**González Rebordinos, Kurrat, E., Agar, D.W.**: "Numerical simulation of a vortex reactor for avoiding carbon deposition during methane bromination" in *Chemical Engineering & Processing: Process Intensification*.

This work is partly based on the calculations performed by Mr. Kurrat during his Master thesis: "CFD simulation and optimisation of a vortex reactor geometry for methane bromination". Conceived, directed and supervised by myself and evaluated by Prof. Agar. A preliminary functional CFD simulation was provided by myself.

### 2.4.1. Table of contributions to chapter 2

Table 2.3.: Contributions to Chapter 2

| *Contributor* | *Contribution percentage* |
|---|---|
| Jesús González Rebordinos | 50 |
| Erik Kurrat | 45 |
| David W. Agar | 5 |

## Abstract

Energy can be generated from natural gas without concomitant $CO_2$ emissions through the BrOx cycle, a novel process that consists of two exothermic reactions, namely methane bromination and hydrogen bromide oxidation. One of the major challenges involved in the BrOx cycle is carbon fouling during methane bromination. It has been experimentally observed that the carbon produced during the bromination step tends to deposit on the reactor walls thus rendering continuous operation unfeasible. A vortex reactor has been proposed as a strategy to avoid or minimise carbon fouling. Its working principle consists on feeding the pre-heated reactants separately to a cyclone-shaped reactor in a way that the reaction zone is constrained to the reactor centre. CFD simulations show that a 500 ml vortex reactor operating with a residence time of 2 seconds in which bromine is fed through six transversal inlets while methane is fed counter-currently through an axial inlet located at the end of the conical section is able to avoid carbon particles with diameters ranging 40-80 $\mu$m from depositing at the walls.

# 3. Numerical simulation of a vortex reactor for avoiding carbon deposition during methane bromination

## 3.1. Introduction

Since the industrial revolution human activities around the globe have led to an increase in the atmospheric concentration of $CO_2$ which is considered by scientific consensus to be the main cause of climate change [12]. The Paris agreement achieved at the 2015 United Nations Climate Change Conference (COP21) intends to limit the increase in the global average temperature to less than 2 °C above pre-industrial levels [62] thus implying the necessity of a dramatic reduction of anthropogenic $CO_2$ emissions.

Over the last century the total energy consumption of the world has increased continuously and it is expected to increase further as both world population and economy grow. In 2014 fossil fuels satisfied more than 80% of the OECD (Organisation for Economic Co-operation and Development) members total energy demand [1]. Most of this energy is obtained from fossil fuels through their combustion and the $CO_2$ obtained as a by-product of the combustion is routinely released to the atmosphere. Since energy generation is the largest anthropogenic source of $CO_2$ the reduction of the greenhouse gas emissions concomitant to energy production is the most direct strategy to achieve the objectives of the Paris agreement, especially because it is estimated that fossil fuels will remain the main energy source in the near future [65].

It is relevant to stress that the problem of the use of fossil fuels for energy generation lies on the emissions associated to their combustion. Contrary to popular belief, fossil fuel reserves have steadily increase in the last decades despite the increase in fossil fuel consumption [1]. This is due to the development of new technologies that make the exploitation of unconventional resources feasible and due to the rise of the price of fossil fuels [75]. Additionally, the estimates of fossil fuels supply reach hundreds of years when including unconventional resources such as shale gas or methane hydrates [66]. Therefore, and since fossil fuels are expected to remain the main energy source in the next decades, the decarbonisation of fossil-fuel-based energy generation is a promising strategy to reduce our footprint [47, 44].

One new concept has been presented in previous works as a feasible and promising strategy for avoiding $CO_2$ emissions concomitant to energy production is the

Bromination-Oxidation (BrOx) cycle [95]. It consists of a first exothermic reaction in which bromine and methane yield solid carbon and hydrogen bromide (6.1.1). Following carbon separation hydrogen bromide and oxygen react exothermically to yield water and bromine (6.1.2). After separation of the water, bromine is recycled to the first reaction step thus resulting in an overall process in which energy is released from methane and oxygen with solid carbon and water as only by-products (6.1.3). By resolving the net reaction (6.1.3) into two exothermic steps, the problem of high temperature heat transfer arising in simple methane pyrolysis is circumvented.

$$CH_4 + 2Br_2 \rightarrow C\,(s) + 4HBr \qquad \Delta H_r^o = -132.47kJ/mol \tag{3.1.1}$$

$$4HBr + O_2 \rightleftarrows 2Br_2 + 2H_2O \qquad \Delta H_r^o = -364.32kJ/mol \tag{3.1.2}$$

$$CH_4 + O_2 \rightleftarrows C\,(s) + 2H_2O \qquad \Delta H_r^o = -496.79kJ/mol \tag{3.1.3}$$

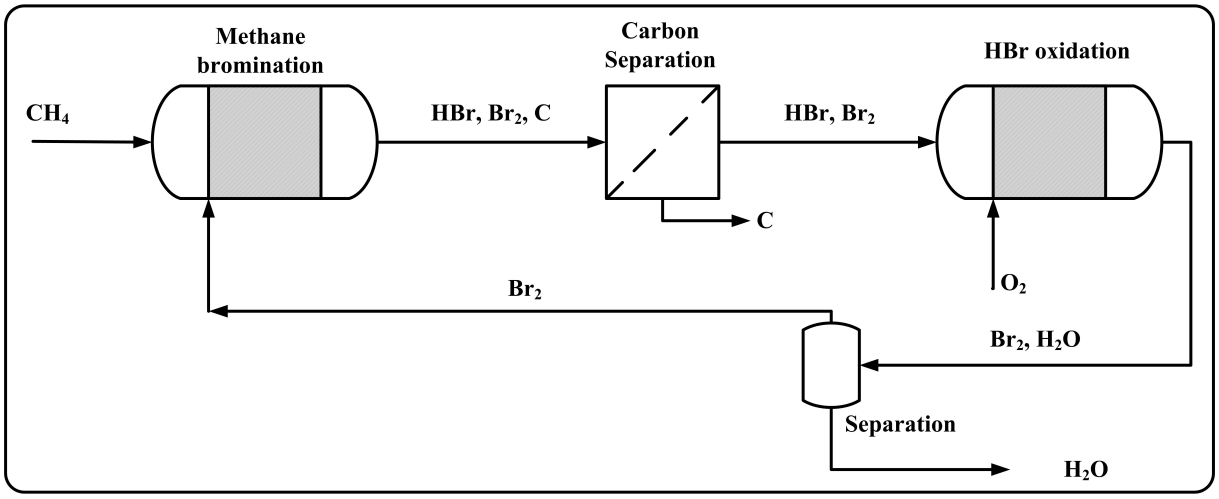


Figure 3.1.: Schematic representation of the BrOx cycle

One of the main challenges of the BrOx cycle and methane pyrolysis processes is the possibility of carbon deposition during the first reaction step. Solid carbon is produced in methane bromination that tends to deposit on the reactor walls [95, 55]. If the heat is introduced through the walls into the reaction zone as it happens in methane pyrolysis the zone of the reactor at the highest temperature and with the higher reaction rate would be the reactor walls and therefore carbon would form at the surface and deposit. In experiments with scale isothermal methane bromination the heat is also introduced via a high temperature oven resulting in carbon deposition (Figure 3.2).

Figure 3.2.: Carbon fouling in a quartz-glass reactor after methane bromination experiment

Although in normal operation of a methane bromination reactor the heat source would be the reaction itself, the possibility of carbon forming near the hot walls should be avoided since it would lead to carbon fouling. The use of a vortex reactor has been suggested as a practical way to avoiding or at least minimising carbon deposition in methane pyrolysis [90, 91] and this concept has been modified for bromination reaction. It consists of using a cyclone-like reactor with a longitudinal through which methane is fed to the reactor and a transversal inlet for the bromine feed. In this way it is intended to constrain the reaction zone to the centre of the reactor and far away from the walls so that the carbon forms at the reactor core and it is carried out of the reactor by the flow. The bromine stream should also act as a protective layer avoiding carbon particles from entering in contact with the reactor wall (Figure 3.3).

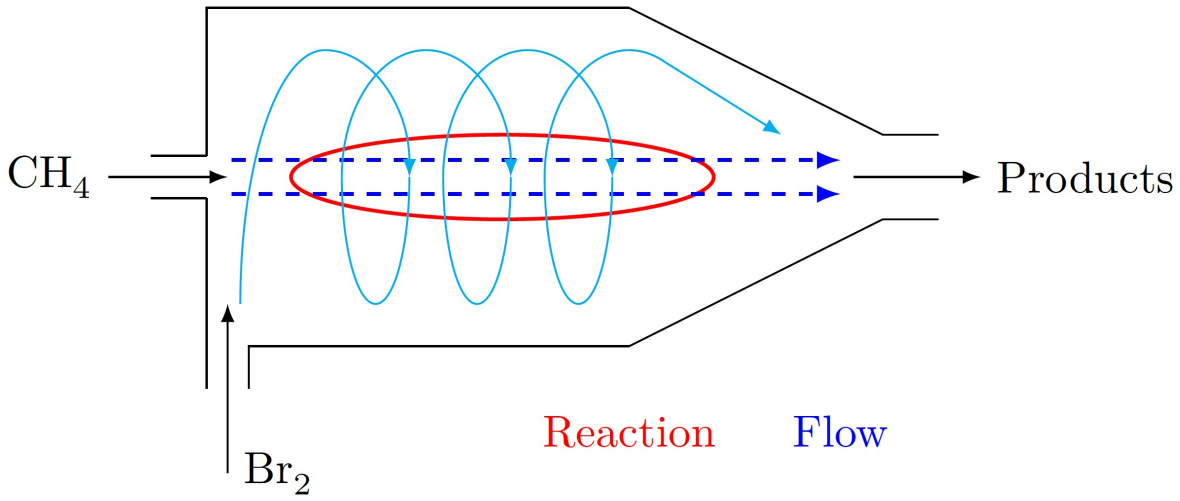


Figure 3.3.: Illustration of the vortex reactor principle

## 3.2. Computational domain, mesh, and boundary conditions

### 3.2.1. Computational domain

The computational domain used to perform the simulation consists on a cylindrical body ended in a conical part as shown in figure 3.4a. Attached to the cylindrical body are two pipes, one is connected to the reactor longitudinally at the centre while the other is connected transversely. The outlet pipe is positioned at the end of the conical section (figure 3.4a). The geometry has been modified to improve the performance of the reactor on avoiding carbon deposition. The radius and length of the cylindrical section, the length of the conical section and the diameter of the pipes have been modified in a way that the volume of the reactor remains constant at 500 ml to ensure that the results are comparable between different cases.

In order to facilitate the discretisation of the computational domain in a subsequent step, the geometry was manually divided into following substructures (figure 3.4):

1. Inlet nozzle
2. Upper cylindrical section
3. Lower cylindrical section
4. Top conical section
5. Upper conical section
6. Lower conical section
7. Bottom part
8. Reactor core

All the substructures except the inlet nozzle are revolved around the reactor axis and thus are rotationally symmetric. Two additional layers (a and b) are introduced in order to provide sufficient degrees of freedom in the meshing process.

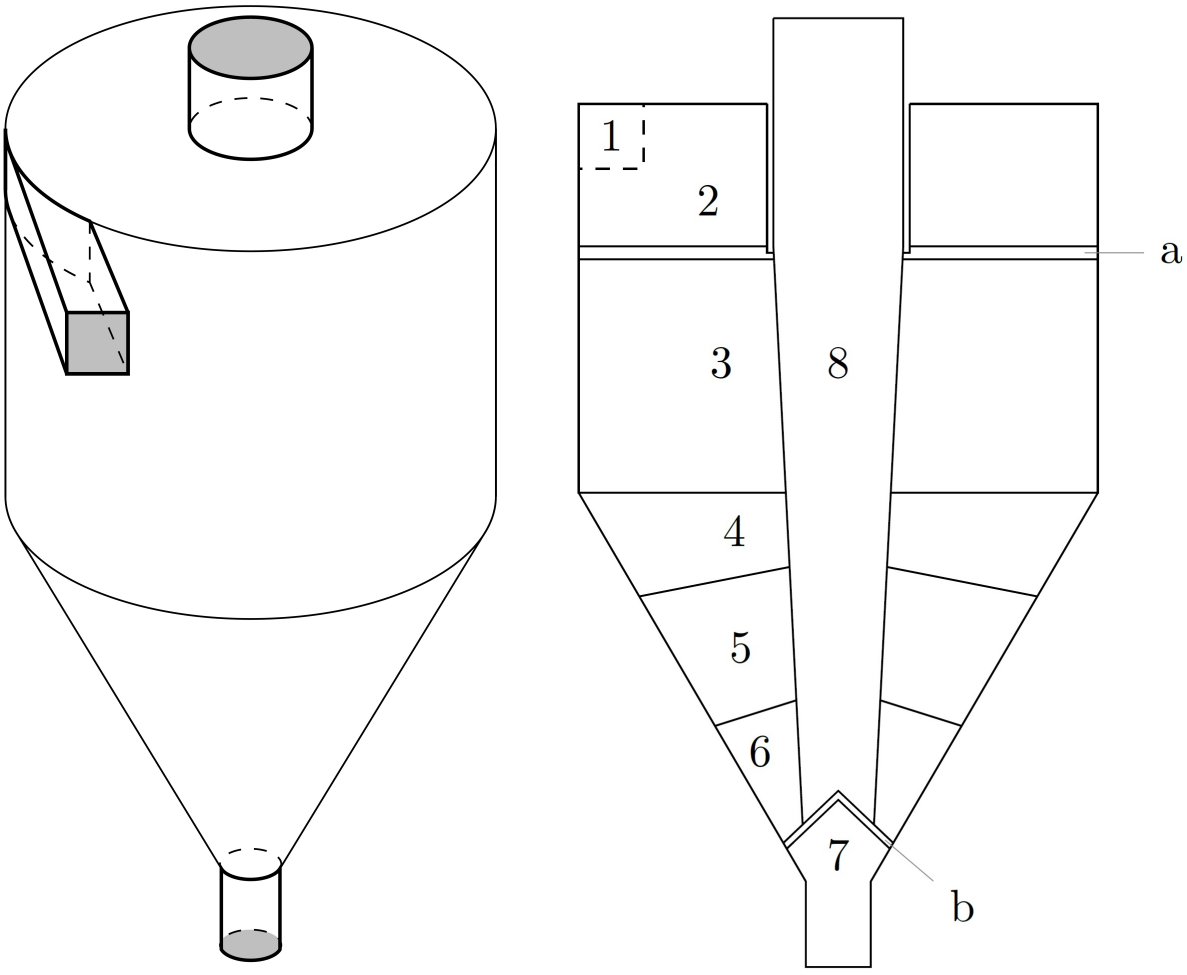


(a) Computational domain

(b) Partitioning of the computational domain

Figure 3.4.: Geometry of the vortex reactor

### 3.2.2. Discretisation of the computational domain

In order to enable the numerical solution of the system of partial differential equations, the computational domain was discretised. Three different methods of meshing have been applied to achieve a convergent solution. The first method applied (”blocking”) consists on the individual processing of the aforementioned partitions of the geometry in a sequential way. Due to the stiffness of hexaedra, parts 2, 3, 8, 4, 5, 6 and 7 were swept while part 1 was done with multizone method. The additional layers a and b were meshed using tetrahedrons. Inflation layers were used at the interface between partitions. The resulting mesh is shown in figure 3.5.

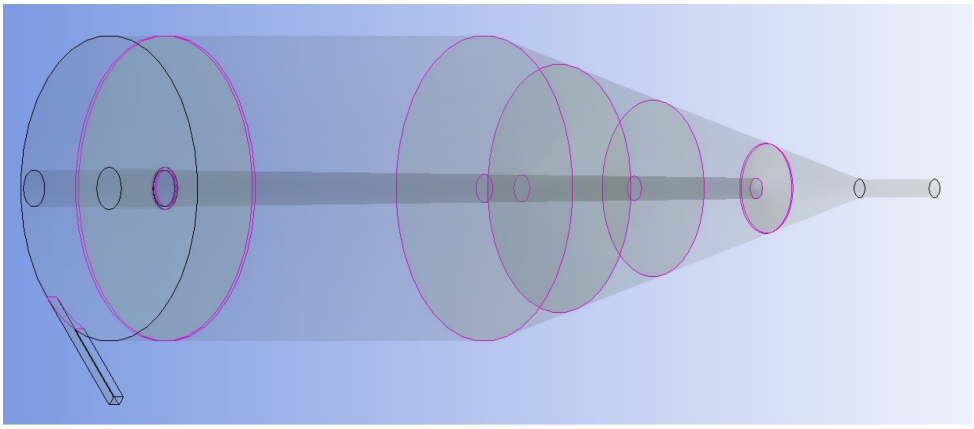

(a) Partitioning

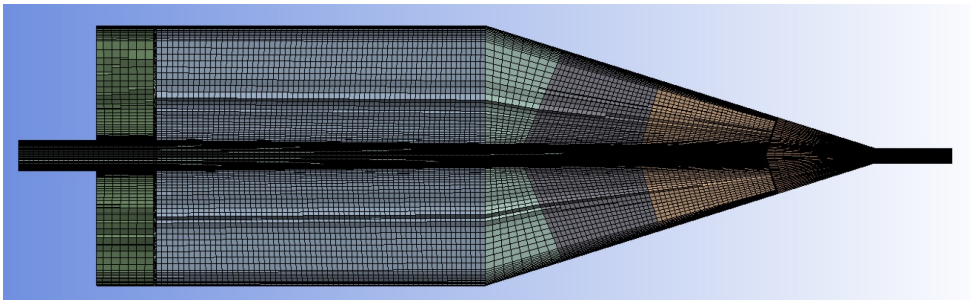

(b) Cross section

Figure 3.5.: Mesh with ”blocking” meshing

This meshing procedure resulted in a high quality mesh with more than 98% hexahedrons with respect to cell volume and an average orthogonal quality around 95%. Depending on the cell size, a total number of elements between 100,000 and 4,000,000 was obtained.

In some cases more than one inlet nozzle were used. This results in geometries that are completely rotationally symmetric so that it was possible to simulate only a portion of the computational domain with a symmetry boundary condition, thus enormously reducing the computational effort. The total size of the simulated geometry and thus the computational cost was reduced in a factor equal to the number of

transversal inlets. This method also provides a better mesh structure and the inflation layer could be applied to all surfaces that require boundary conditions (figure 3.6).

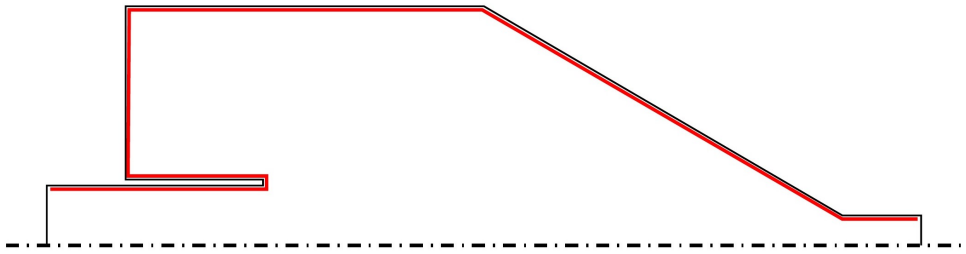

(a) Location of inflation layer

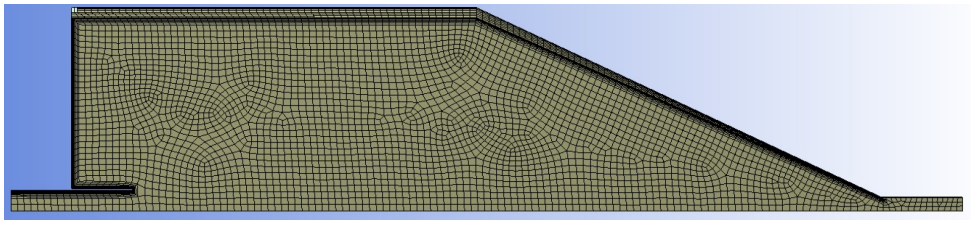

(b) Mesh example

Figure 3.6.: Mesh with procedure 2

An additional meshing method that employed the partitions described in subsection 3.2.1 was used. This method consisted on the creation of an unstructured mesh by dividing the computational domains in tetrahedral elements. An advantage of this method is that is easy to apply to different geometries and to refine locally although it comes at the cost of a higher computational cost. Inflation layers were used at the boundary surfaces and regions in which high gradients were expected were refined together with the inlets and the expected reaction zone. An example of an unstructured mesh with 430,000 cells can be seen in figure 3.7.

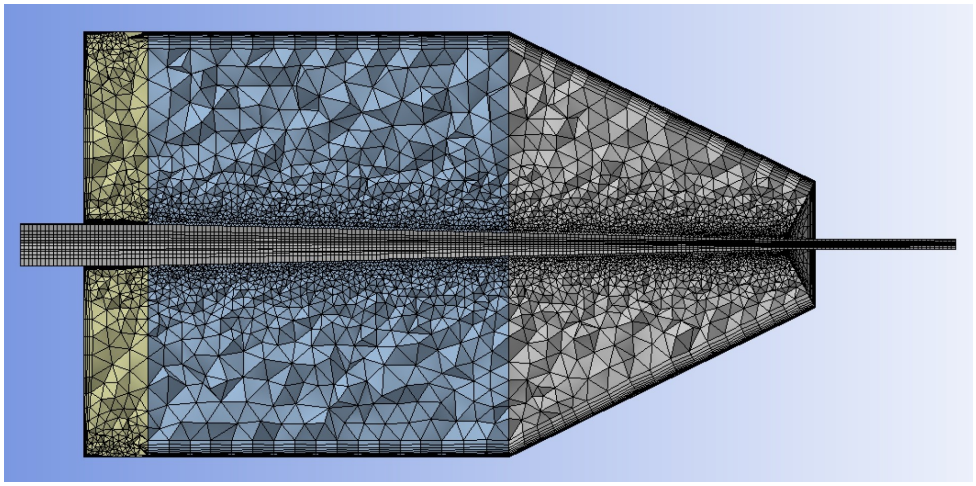

Figure 3.7.: Unstructured mesh

### 3.2.3. Boundary conditions

For the steady-state simulations of methane bromination in a vortex reactor the walls of the inlet and outlet pipes have been modeled as adiabatic without friction using the slip condition while the reactor wall has been modeled as adiabatic with friction. The outlet boundary has been set as an opening due to the instabilities that arise when set as an outlet. For the geometries with multiple transversal inlets the geometry was sliced and a symmetry condition was established at the faces of the slices.

The mass fractions at the inlets was 1, meaning that pure bromine and pure methane were fed separately to the reactor via their respective inlet pipes. The inlet velocities were always adjusted so that the average residence time in the 500 ml reactor was of 3 seconds while using a molar inlet ratio of $\frac{2.5 mol Br_2}{1 mol CH_4}$. The inlet temperature of both feeds was 1323 K.

## 3.3. Mathematical model

ANSYS CFX has been used for the steady-state simulation of methane bromination in a vortex reactor. Given the complexity of simulating the solid carbon formation as a product of methane bromination reaction, produced carbon has been described as a pseudo-gas component. Since the flow and temperature field are virtually independent of the formation of solid carbon, a good approximation can be made by introducing carbon particles with a size distribution ranging from 5 $\mu$m to 150 $\mu$m and observing how their behaviour varies with the obtained temperature and flow profiles. The biphasic solid-gas flow has been modeled with the Euler-Lagrange approach and with one way coupling. In this way, the gas is considered as a continuum while particle behaviour is solved by tracking a large number of particles through the flow field. Additionally, the particles are influenced by the gas while the latter is not influenced by the former.

### 3.3.1. Mass and momentum conservation

Since the simulations performed are time-independent the mass and momentum conservation conditions are described by equations 3.3.1 and 3.3.2.

$$\nabla \left( \rho \vec{U} \right) = 0 \tag{3.3.1}$$

$$\nabla \left( \rho \vec{U} \times \vec{U} \right) = -\nabla p + \nabla \tau \tag{3.3.2}$$

Where the shear tensor $\tau$ is calculated with equation 3.3.3

$$\tau = \mu \left( \nabla \vec{U} + \left( \nabla \vec{U} \right)^T - \frac{2}{3} \delta \nabla \vec{U} \right) \tag{3.3.3}$$

Bromine is fed transversely to a cyclone-like reactor in all simulations and thus there is always a swirling flow. A literature research showed that for problems similar to the one treated here, BSL Reynolds Stress model is a good choice as turbulence model [91].

All simulations have been pe

The substances considered in the simulations are $CH_4$, $Br_2$, $CH_2Br_2$, $HBr$ and the pseudo-gas-phase carbon. Due to the presence of several compounds a component balance has been used (3.3.4).

$$\frac{\partial\left(\rho f_{mi}\vec{U}\right)}{\partial x_y} = \frac{\partial}{\partial y}\left(\Gamma_{i_{eff}}\frac{\partial f_{mi}}{\partial x_i}\right) + v_i r \tag{3.3.4}$$

### 3.3.2. Energy conservation

All simulations have been performed with adiabatic operation and the Thermal Energy model (6.9) has been selected as heat transfer model to account for energy conservation. The only source included is the reaction enthalpy which in this case accounts for the energy released through the exothermic methane bromination reaction.

$$\nabla\left(\rho\vec{U}h\right) = \left(\lambda\vec{U}T\right) + r\Delta_r H \tag{3.3.5}$$

### 3.3.3. Thermodynamics

NASA polynomials (3.3.6,3.3.7,3.3.8) have been used to calculate the heat capacities, enthalpies and entropies of the substances used in the simulation. The coefficients have been retrieved from tables found on the literature [79].

$$\frac{c_p^0}{R} = a_1 + a_2T + a_3T^2 + a_4T^3 + a_5T^4 \tag{3.3.6}$$

$$\frac{h^0}{R} = a_1T + \frac{a_2T^2}{2} + \frac{a_3T^3}{3} + \frac{a_4T^4}{4} + \frac{a_5T^5}{5} + a_6 \tag{3.3.7}$$

$$\frac{s^0}{R} = a_1 lnT + a_2T + \frac{a_3T^2}{2} + \frac{a_4T^3}{3} + \frac{a_5T^4}{4} + a_7 \tag{3.3.8}$$

Additionally, Aungier-Redlich-Kwong model has been used as the equation of state.

### 3.3.4. Reaction kinetics

A reaction mechanism consisting of 79 elementary reactions and that considers 26 chemical species has been proposed for methane bromination [55]. This mechanism

does not consider solid carbon formation so that all atomic carbon is present in the form of brominated hydrocarbons. This mechanism has been simplified in this work with a two-step mechanism. In a first step, methane and bromine yield $CH_2Br_2$ and $HBr$ (3.3.9). Dibromomethane has been chosen to lump all intermediate brominated compounds because simulations of the original mechanism show that it is the substance predominantly produced. In a second step dibromomethane reacts to yield solid carbon and $HBr$ (3.3.10).

$$CH_4 + 2Br_2 \xrightarrow{r_1} CH_2Br_2 + 2HBr \tag{3.3.9}$$

$$CH_2Br_2 \xrightarrow{r_2} C + 2HBr \tag{3.3.10}$$

A reaction rate equation was implemented in ANSYS CFX for each reaction step to describe methane bromination. For the first step, a reaction rate of first order for both methane and bromine (equation 3.3.11) was used since it is in agreement with the results obtained from the simulation of the more complex mechanism found on the literature. A first order reaction rate expression was used for the second step (equation 3.3.12).

$$r_1 = k_1\left(T\right) c_{CH_4} c_{Br_2} \tag{3.3.11}$$

$$r_2 = k_2\left(T\right) c_{CH_2} c_{Br2} \tag{3.3.12}$$

The reaction rate constants for both equations have been calculated with an Arrhenius expression (equation 3.3.13). Values of $k_0$ and $E_a$ were obtained through fitting simulation results for the first step and experimental data for the second step.

$$k_j\left(T\right) = k_{0,j} exp\left[\frac{-E_a}{RT}\right] \tag{3.3.13}$$

### 3.3.5. Particle modeling

The particle behaviour has been simulated with a Lagrangian approach. Gravity effects have been ignored together with pressure gradient forces and the Basset-term. therefore, the force balance results in equation 3.3.14.

$$\frac{du_p}{dt} = C_D \frac{3\rho_F}{4 d_P \rho_P} u_s + \frac{\left(\rho_P - \rho_F\right) 2\omega^2}{\rho_P d_v} \tag{3.3.14}$$

A literature research showed that Brucato's model (3.3.15, 3.3.16, 3.3.17) was the most suitable model for this problem to calculate drag coefficients. Since Brucato's model is not built-in ANSYS CFX it was implemented with a FORTRAN routine.

$$\frac{C_D - C_{D_0}}{C_{D_0}} = K\left(\frac{d_P}{\lambda}\right)^3 \qquad K = 8.76.10^{-4} \tag{3.3.15}$$

$$\lambda = \left(\frac{v^3}{\epsilon}\right)^{\frac{1}{4}} \tag{3.3.16}$$

$$C_{D_0} = \alpha_1 + \frac{\alpha_2}{Re} + \frac{\alpha_3}{Re^2} \tag{3.3.17}$$

In order to assume the worst case scenario it was set that any particle that touched the reactor wall would stick there. This was implemented in the simulation by setting a value of zero for the coefficient of restitution (COR) at the walls of the body of the reactor. To avoid deposition at the inlets and outlets a COR=1 was used there.

As said before, the formation of carbon particles from the gas phase is too complex to be simulated within the span of this study and therefore carbon particles were introduced to observe how they behave in the reactor. The particles must be introduced at the reaction zone to ensure a good approximation of reality and thus a triggered model was used in which the particles behave as a gas until pseudo-gas carbon is formed (3.3.18). In this way, carbon particles are injected in the longitudinal inlet and follow the methane flow to start behaving as a solid only when carbon is produced.

$$\begin{aligned} & & D &= 1 - x_{CH_4} - x_{CH_2Br_2} \\ for \quad & D > 0.97 \Rightarrow & C_D &= f\left(Re_P, ...\right) \\ for \quad & D \leq 0.97 \Rightarrow & C_D &= 10^6 \end{aligned} \tag{3.3.18}$$

## 3.4. Results

### 3.4.1. Determination of a simplified reaction rate expression

In order to simulate methane bromination reaction a simplified mechanism consisting on two reactions has been implemented in ANSYS CFX. Results obtained from simulations of the mechanism proposed in the literature for methane bromination [95, 55] have been used to determine values for the pre-exponential factor and the activation energy of the first step of the simplified mechanism (3.3.9). Simulations at different reaction conditions have been performed and an Arrhenius plot has been used to obtain the following values for $k_0$ and $E_a$:

- $k_{0_1} = 1.13 \cdot 10^9 \frac{m^3}{mol \cdot s}$
- $E_{a_1} = 148.781 \frac{J}{mol}$

Since the mechanism proposed by SANDIA laboratories does not consider carbon formation, experimental data has been used to approximate the second reaction step

(3.3.10). From experiments performed in a bench-scale laboratory plant it is known that under excess-bromine conditions and with residence times of 10 seconds carbon formation does not occur at temperatures lower than 700 °C. At 750 °C it is possible to notice that carbon formation starts while at 930 °C carbon formation is complete with a low concentration of brominated by-products [95]. Through fitting the following parameters have been obtained:

- $k_{0_2} = 1.40 \cdot 10^{15} \frac{1}{s}$
- $E_{a_2} = 360.956 \frac{J}{mol}$

As can be seen in figure 3.8, the results of the 2-step mechanism simulation agree perfectly with both the experimental results and with the more complex 79-step mechanism. At 750 °C methane is consumed within 0.01 seconds but almost no carbon forms whereas at higher temperatures carbon formation occurs at a high extent while dibromomethane concentration is very low at a residence time of 10 seconds.

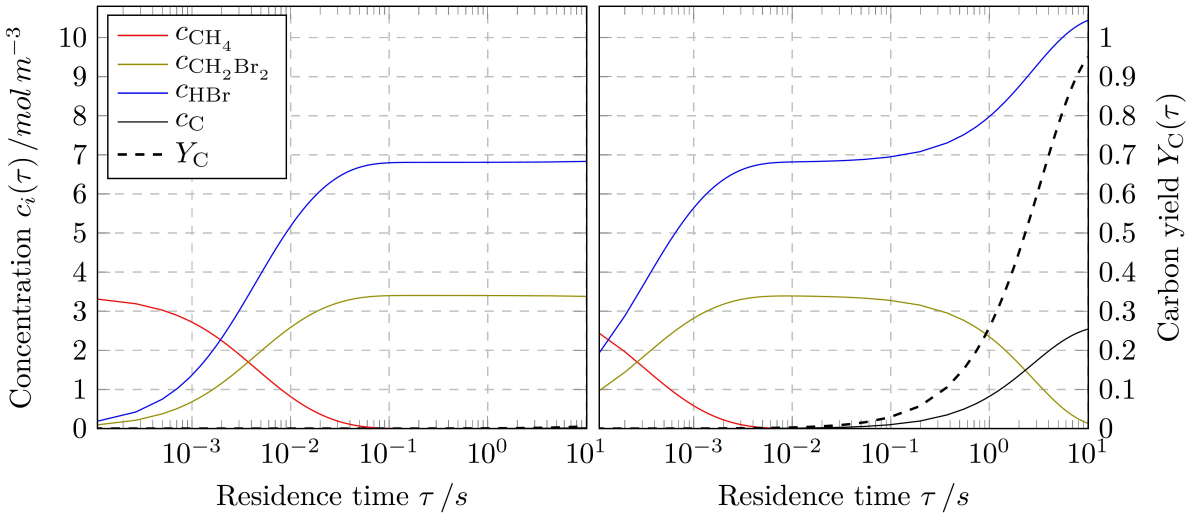


Figure 3.8.: Rate fitting (left: T=750°C, right: R=900°C

Although this mechanism is extremely simplified it describes the system very accurately and enables an implementation of methane bromination within the CFD simulation that otherwise would be extremely complicated.

### 3.4.2. Co-current vs. counter-current

The first aspect of the vortex reactor investigated was the geometry of the methane inlet. In order to avoid carbon deposition at the base of the cylindrical body an inlet dip-pipe was proposed and added to the geometry. Since the reaction is likely to start with the maximum reaction rate at (or very close to) the methane inlet, a pipe that penetrates the cylindrical body and ensures that methane is not introduced too close to the wall is expected to reduce noticeably carbon deposition.

Two geometries, with and without dip-pipe, have been used to simulate methane bromination and the results have been compared as can be seen in figure 3.9. The results show that the high reaction zone represented in red is close to the wall when no dip-pipe is used and that the use of the dip-pipe solves this problem.

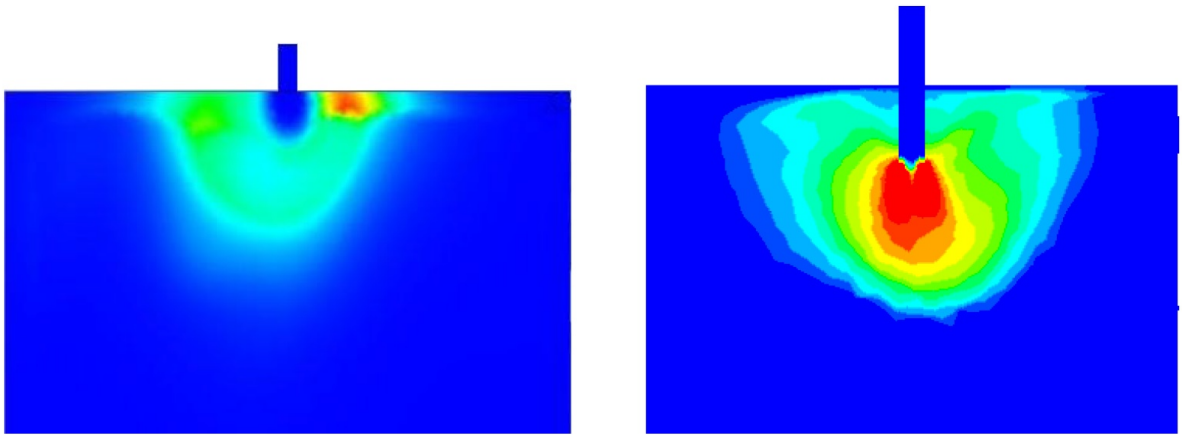

Figure 3.9.: Reaction rate fields at the methane inlet without (left) and with (right) dip-pipe

In the original concept of the vortex reactor methane is fed longitudinally while bromine is fed transversely in a co-current scheme. The expected result was a reaction zone that is stretched and constrained to the centre of the reactor so that solid carbon would be produced away from the walls. The simulation results are shown in figure 3.10.

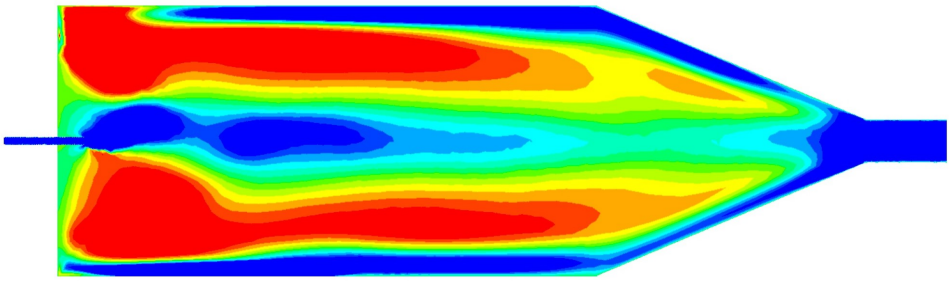

(a) Flow field in the co-current vortex reactor (red: movement to the left; blue: movement to the right)

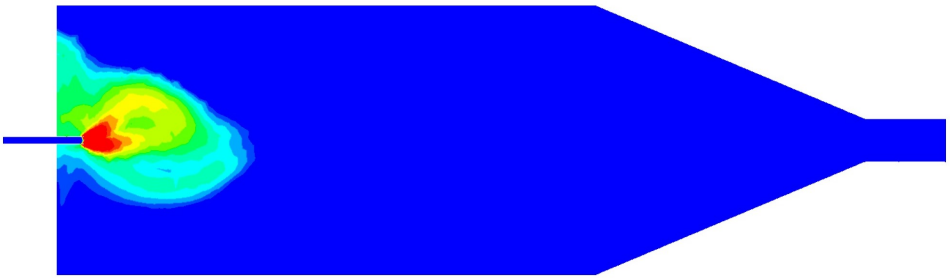

(b) Reaction rate field in the co-current vortex reactor (red: 50 $mol\frac{mol}{m^3 s}$; blue: $< 1 mol\frac{mol}{m^3 s}$)

Figure 3.10.: Simulation results of the co-current scheme

As can be seen in sub-figure 3.10b the reaction zone has a quasi-spherical form instead of the desired stretched one. In this case the reactor is over-dimensioned since reaction occurs just in a small zone near methane inlet but if higher flow rates or a smaller reactor were used, the reaction zone would be too close to the walls thus making it impossible to avoid carbon deposition. This behaviour can be explained when figure 3.10a is taken into consideration. It is clear that although both inlet feeds are fed in a co-current way the transversal flow builds an outer and inner swirl that opposes that of methane. As a result the reaction zone is pushed by these opposing flow towards the wall at the base of the cylindrical body and is thus constrained to a zone near the methane inlet (figure 3.11a).

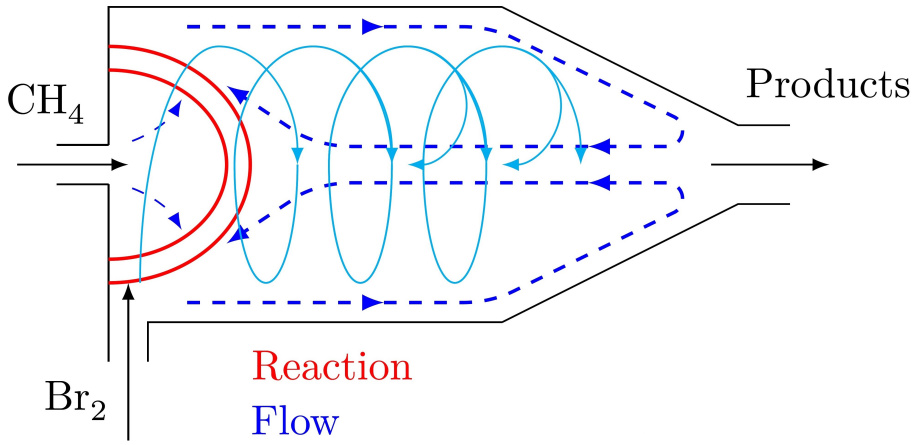


(a) Schematic representation of the co-current vortex reactor

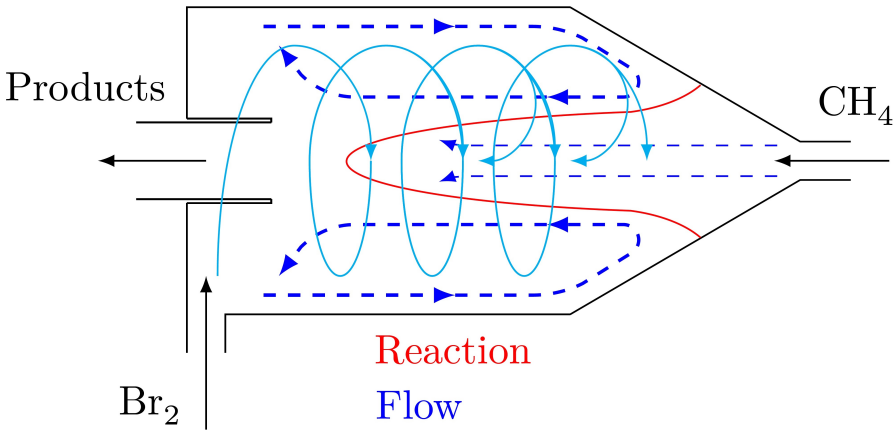


(b) Schematic representation of the counter-current vortex reactor

Figure 3.11.: Comparison between co-current and counter-current reactors

Since with this flow field carbon particles would form near the walls of the reactor and that no geometry modification is expected to solve this problem a new flow scheme has been developed in which the methane is fed longitudinally and in counter-current to the transverselly fed bromine. In this way, the former outlet is now the methane inlet and the previous methane inlet becomes the outlet, shifting as well the pipe diameters. In contrast with the previous flow field (figure 3.11a) the counter-current flow is expected to generate a protective layer of swirling bromine while at the same time stretching the reaction zone and keeping it at the reactor core as shown in figure 3.11b.

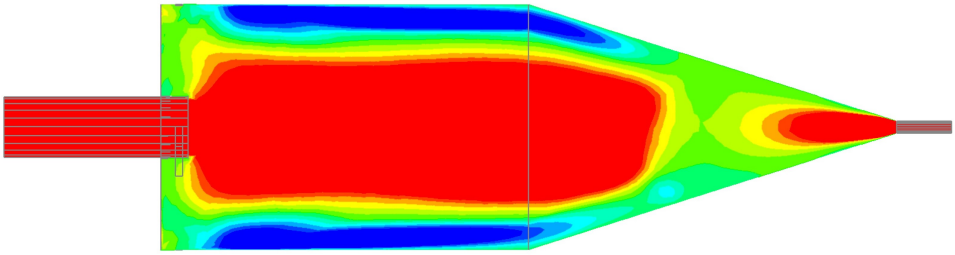

(a) Flow field in the counter-current vortex reactor (red: towards the left side; blue: towards the right side)

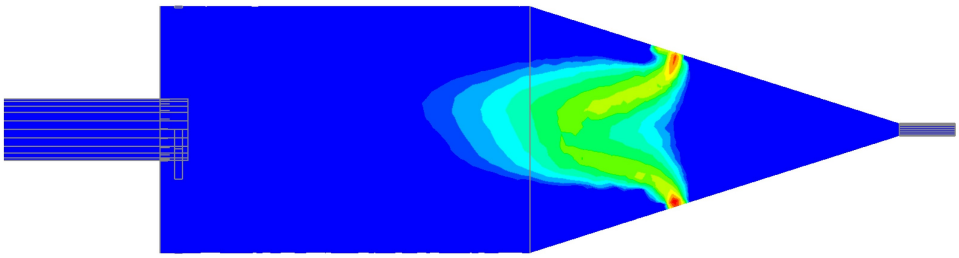

(b) Reaction rate field in the counter-current vortex reactor (red: 50 $mol\frac{mol}{m^3s}$; blue: $< 1mol\frac{mol}{m^3s}$)

Figure 3.12.: Simulation results of the counter-current scheme

A simulation performed with the counter-current flow scheme is shown in figure 3.12. Figure 3.12b shows that the reaction zone is now stretched and constrained to the centre of the reactor although the region with the higher reaction rate is close to the walls of the conical section. A modification of the grometry can nonetheless improve this feature. Moreover, figure 3.12a shows that counter-current feeding guarantees that only the protective swirling flow of bromine opposes methane flow close to the walls while the central flow is directed towards the outlet. Therefore counter-current scheme is selected as the option of choice and further optimisation of the geometry of the vortex has been conducted with counter-current feed of methane.

### 3.4.3. Improvement of the vortex reactor geometry

The results shown in figure 3.12, although promising, require further refinement since otherwise carbon deposition would occur. The first challenge that needs to be overcome is the position of the high intensity reaction zone. In figure 3.12b the high reaction rate (in red) is located at the walls of the conical section so that most of the carbon would form at the wall and deposit there making it impossible for the hydrodynamics of the system to carry it out of the reactor. The location of the reaction zone in this case is determined by the opposition of bromine and methane flows. Due to the conical geometry methane does not enter the reactor like a thin stream surrounded by swirling bromine but expands instead and faces the bromine flow. The reaction zone is located at the mixing point of both streams (Figure 3.13a).

As shown in figure 3.9 the use of a dip-pipe can help to introduce methane as a thin stream protected by a swirling bromine flow. Nevertheless, in this case the simple addition of a dip-pipe would also cause the presence of an undesired dead volume at the conical tip. The geometry of the reactor has been thus modified by cutting the cone tip so that it ensures that methane will enter the reactor via a nozzle-like structure as a thin stream reinforced by the bromine swirling flow. Figure 3.13 clearly shows the change in the reactor geometry and its remarkable effect in both the flow field and the location of the reaction zone. The high intensity reaction zone is now separated from the walls of the reactor and stretched along the longitudinal axis. Additionally, the bromine swirling flow is now able to move towards the methane inlet and bounce back accompanying the methane stream and acting as a protective layer.

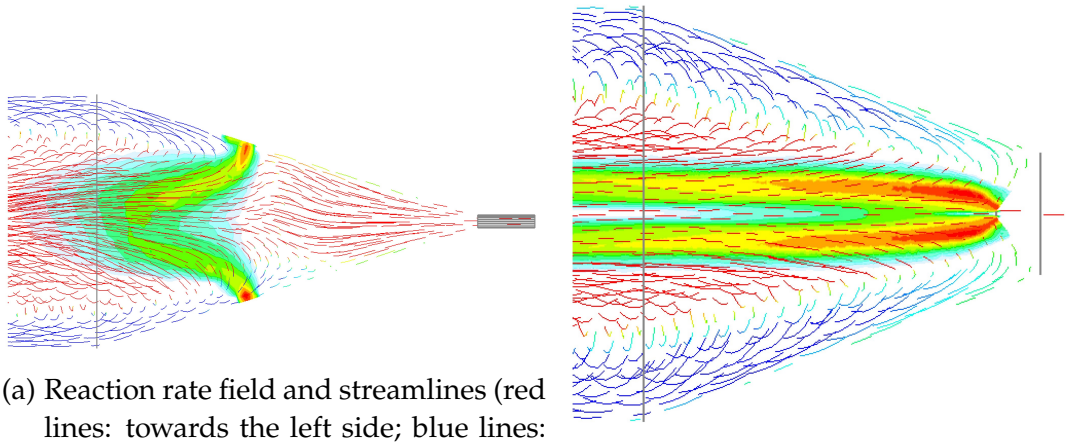

(a) Reaction rate field and streamlines (red lines: towards the left side; blue lines: towards the right side) at the conic methane inlet

(b) Reaction rate field and streamlines (red lines: towards the left side; blue lines: towards the right side) at the semi-conic methane inlet

Figure 3.13.: Comparisson between the original conic methane inlet and a modified semi-conic methane inlet

Simulations introducing carbon particles have been carried out with the new geometry and flow scheme. Despite a reaction zone with the desired location and shape and a favourable flow field, the results showed that carbon particles did not leave the system. The solid particles were carried by the flow through the longitudinal axis but they deviated before the outlet missing it and hitting the wall of the reactor instead. One possible explanation to this phenomenon is that the geometry is not entirely symmetrical since there is only one tangential inlet. This could cause that the particles are being pushed to one side of the reactor preferably. Therefore additional tangential bromine inlets have been added and their influence on the behaviour of carbon particles has been assessed.

Figure 3.14 shows the comparison between one geometry with two tangential inlets and another with 6 tangential inlets. The aforementioned behaviour can be easily

identified in figure 3.14b. The black lines describe the paths that the carbon particles follow, moving along the longitudinal axis until they deviate to miss the outlet and hit the wall. An explanation for this phenomenon can be found in the flow field of the cross-sectional area of the reactor (figure 3.14b) in which it is clear that, although the geometry has now symmetry, the flow field is not symmetrical. With six tangential inlets equidistantly distributed the flow field shown in figure 3.14d is symmetrical. In this case the particles are able to follow a straight line along the longitudinal axis of the reactor and abandon it, regardless of the size of the particle, as shown in figure 3.14c.

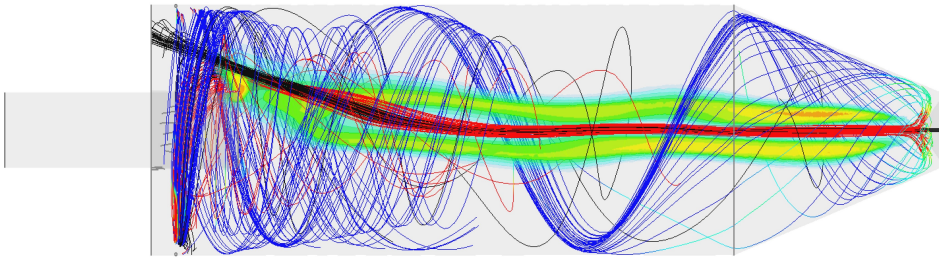

(a) Reaction zone, streamlines and particle path of a 2 inlet vortex reactor

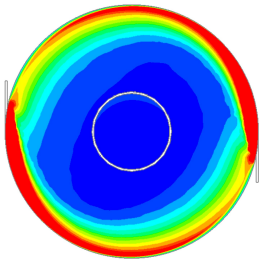

(b) Flow field at a cross-sectional area of a 2 inlet vortex reactor

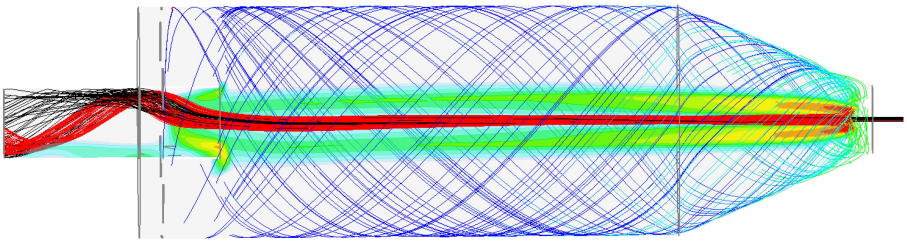

(c) Reaction zone, streamlines and particle path of a 6 inlet vortex reactor

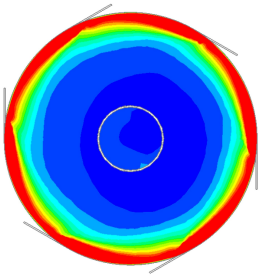

(d) Flow field at a cross-sectional area of a 6 inlet vortex reactor

Figure 3.14.: Flow fields, reaction zones and particle paths for vortex reactors with multiple tangential inlets

The final design of the reactor for methane brominaton combines all four design changes, namely counter-current feed of methane, use of a dip-pipe at the outlet, removal of the conic tip and multiple bromine inlets. This modified design produces an enhanced flow, reaction and particle behaviour. In order to test the new design of the reactor, a simulation has been performed in which the drag model trigger is deactivated, thus obtaining full particle behaviour, and new particle sources are placed. In this way the reactor performance on avoiding carbon deposition is tested under disadvantageous conditions.

The results of the simulation are shown in figure 3.15. As can be seen, the new design has some features that enhance the performance of the reactor:

- The reaction zone is now stretched along the longitudinal axis of the reactor (figure 3.15a) thus ensuring that carbon will be formed at its core and far from the walls.
- Distinct regions of axially and tangentially dominated flow can be observed (figure 3.15a). There is an upwards axial flow at the centre of the reactor and a swirling flow close to the walls.
- There is a reactant distribution (figure 3.15b). Bromine is located at the region close to the walls whereas methane is constrained to the inner axial flow core. The intermediate products are located in between the reactant transition area, where the reaction zone lies.
- Particle transport is now constrained to the reactor core, hence essentially avoiding carbon deposition. There is only minor deposition as a result of centrifugal forces, but the vast majority of particles are carried by the flow out of the system (figure3.15c).

As observed in figure 3.15b a secondary reaction zone is present at the outlet pipe. This feature is disadvantageous for the process since it could derive in carbon deposition at the outlet pipe. Nonetheless, the amount of carbon particles produced at this secondary reaction zone is much lower than that produced in the main reaction zone. Additionally, in case there is carbon deposition it would occur at the inner wall of the outlet pipe in a way that is more accessible for cleaning. In order to avoid this secondary reaction zone higher inlet temperature should be used since it would result in higher reaction rates so that all methane would be depleted within the main reaction zone.

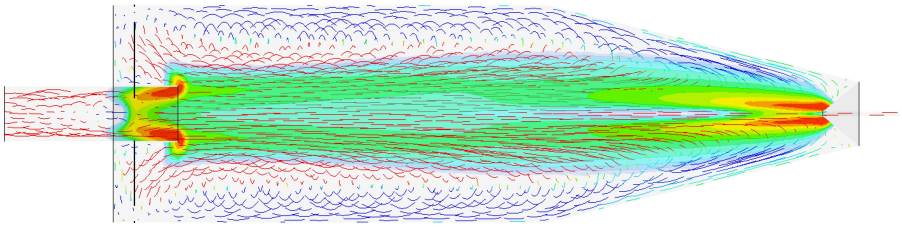

(a) Composition of methane (red from 0 to 0.5), bromine (green from 0 to 0.5) and dibromomethane (blue 0-0.03)

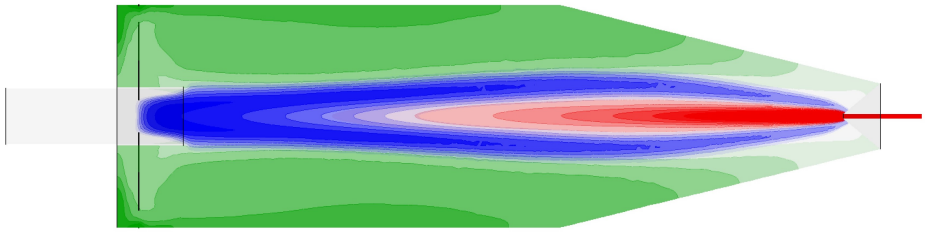

(b) Streamlines coloured according to flow direction (blue: towards methane inlet; red: towards the outlet) and reaction zone (red: 0.3 $mol\frac{mol}{m^3 s}$; blue: 0.3 $mol\frac{mol}{m^3 s}$

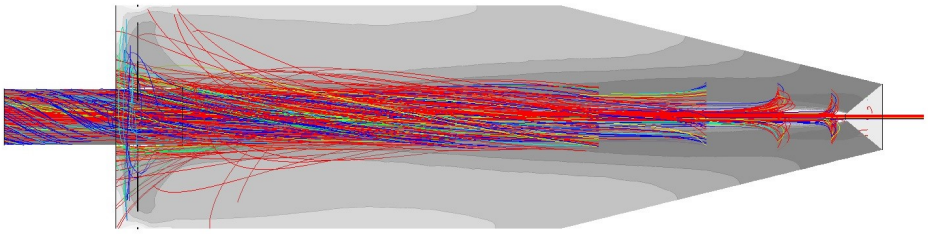

(c) Particle tracks coloured according to their diameter in a range going from 40 to 80 $\mu$m

Figure 3.15.: Final design of the reactor for methane bromination

A mesh independent study has been performed on the final geometry by carrying out three simulations with the same parameters and conditions but with meshes of $5 \cdot 10^5$, $8.5 \cdot 10^5$ and $15 \cdot 10^5$ elements. The results of the three simulations performed were virtually identical thus demonstrating that the results of the simulations are independent from the mesh.

## 3.5. Conclusion

A vortex reactor is proposed to avoid carbon deposition during methane bromination. CFD simulations have been performed with the commercial software ANSYS CFX on an initial geometry consisting of a transversal inlet for bromine, a longitudinal inlet for methane and a cylindrical reactor ending in a conical section. The model has been

successfully implemented and the first results showed that a spherical reaction zone close to the inlet wall appears, rather than the desired stretched reaction zone located at the centre of the reactor. The reason for such a behaviour is that the swirling bromine flow moves first towards the outlet to return after bouncing at the conical section and oppose methane flow. Feeding the methane counter-currently with a pipe located at the conical section has proved to succeed in generating a convenient reaction zone. Therefore the counter-current feeding scheme has been selected as optimal for the bromination reactor.

Further adjustments to the original geometry have been implemented. The addition of a dip pipe, although originally intended to detach the inlet methane flow in the co-current scheme, has proved to improve the creation of a swirling bromine layer at the wall in the counter-current scheme. Additionally, the use of a dip-pipe at the outlet prevents bromine from short-cutting the reaction zone, leaving the reactor immediately. One of the main drawbacks of the counter-current scheme is that the high intensity reaction zone is still located at the wall of the conical section due to the inability of methane to enter the reactor detaching from the wall. A simple modification of the geometry consisting in the removal of the cone tip has been carried out. As a result, methane enters the reactor via a nozzle-like inlet resulting in a stretched reaction zone located at the core.

When spherical carbon particles with diameters ranging 40-80 $\mu$m are introduced in the modified bromination reactor they follow a path trough the center of the reactor but they deviate before the outlet and therefore they hit the wall and deposit there. This behaviour is caused by the asymmetry of the flow field. The use of multiple transversal inlets to feed bromine results in an improvement on the reactor performance, avoiding carbon fouling completely with six transversal inlets.

The effect of boundary conditions on the performance of the reactor in avoiding carbon fouling has been assessed. In all simulations, a reactor of 500 ml and a residence time of 2 seconds have been used. Due to kinetic considerations, high inlet temperatures, of at least 1000 °C are recommended. Inlet velocities have a huge influence on the vortex reactor flow pattern. Low axial velocities ($<$5 m/s) fail to establish a long and stretched reaction zone because the methane flow tends to broaden towards the walls and loses overall momentum. As a consequence, carbon forms close to the wall and deposition occurs. Methane inlet velocities greater than 75 m/s result in very fast axial transport, moving the reaction zone towards the outlet and risking incomplete reaction. Tangential velocity has also a strong effect on the capacity of the reactor on avoiding carbon deposition. It has been found that the tangential velocity has to be high enough to ensure that the swirling flow is able to reach the conical tip of the reactor and flow back with the methane flow, since otherwise the reaction zone would be displaced towards the reactor wall.

## 3.6. Acknowledgments

Financial support from the Graduate School of Energy Efficient Production and Logistics (*Forschungsschule für Energieeffiziente Produktion und Logistik*) is gratefully acknowledged.

## Preamble

The following chapter has been submitted for publication as:

**González Rebordinos, J., Tian, R., Robert, N., Agar, D.W.**: "Carbon retrieval and purification in the BrOx cycle for $CO_2$-free energy" in *Chemical Engineering Research and Design*.

This work is partly based on the experimental work of Mr. Tian during his Master thesis: "Experimental study of high temperature methane bromination with sacrificial wall to avoid carbon deposition"; and on the experiments performed by Ms. Robert in her Master Thesis: "Experimentelle Untersuchung zur Debromierung der kohlenstoffhaltigen Nebenprodukte der Methanbromierung". Conceived, directed and supervised by myself and evaluated by Prof. Agar. Coating experiments and test of the coated reactor during methane bromination were carried out by Mr. Tian and carbon debromination experiments by Ms.Robert.

### 3.6.1. Table of contributions to chapter 3

Table 3.1.: Contributions to Chapter 3

| *Contributor* | *Contribution percentage* |
|---|---|
| Jesús González Rebordinos | 55 |
| Nicole Roberts | 20 |
| Ruozhong Tian | 20 |
| David W. Agar | 5 |

## Abstract

Current combustion of fossil fuels for energy production is the largest anthropogenic source of $CO_2$, a greenhouse gas that is regularly emitted into the atmosphere causing a steady increase in global average temperatures. The BrOx (bromination-oxidation) cycle is a process that enables $CO_2$-free energy generation from fossil fuels and whose major challenges are carbon deposition during the first reaction step, methane bromination, and presence of brominated compounds in the produced carbon.

An experimental study has been carried out on the use of sacrificial walls to avoid carbon deposition directly on the reactor walls and to facilitate its retrieval. The optimal parameters for the generation of a NaCl coating have been determined and used to successfully provide a tubular reactor with a sacrificial wall. Another method consisting on the solidification of a molten salt has been also implemented. Both methods have been tested during methane bromination enabling easy recovery of produced carbon.

Carbon samples containing brominated compounds have been analysed via EDX (Energy-dispersive X-ray spectroscopy) and treated by atmospheric hydrolysis, high temperature hydrolysis and Raney-nickel debromination. With hydrolysis methods debromination up to 99% has been achieved after 28 hours and higher than 90% with lower residence times. Raney-nickel debromination has been able to remove up to 60% of the bromine in the carbon due to mixing limitations.

# 4. Carbon retrieval and purification in the BrOx cycle for $CO_2$-free energy

## 4.1. Introduction

In the last century, the world has experienced a steady increase in energy consumption motivated by the increasing population and the constant improvement in the standard of living worldwide. As a result world energy demand has reached 500 EJ in 2014 [1]. Currently, the combustion of fossil fuels satisfies more than 80% [1] of the global energy demand and is the main responsible of anthropogenic $CO_2$ emissions [80]. In 2015, the countries member of the United Nations achieved an agreement at the Climate Change Conference held in Paris (COP21) in which the members commit themselves to apply the necessary policies to ensure that the increase in global average temperature compared to pre-industrial levels is kept below 2 °C [62] . In order to limit the temperature increase a reduction in greenhouse gas emissions derived from human activity is necessary. Since energy production from fossil fuels is the main contributor to anthropogenic $CO_2$ emissions, avoiding or reducing these emissions is the most direct strategy to achieve the objectives of the 2015 United Nations Climate Change Conference. Contrary to popular belief and despite an increase in their use, fossil fuel proven reserves have increased in the last decades driven by increasing fuel prices and the development of new extraction technologies [67]. The use of fossil fuels for energy production is thus more limited by the concomitant $CO_2$ emissions than by its availability.

A promising strategy to reduce $CO_2$ emissions comes from processes that allow the use of the relatively abundant and cheap fossil fuel reserves without emitting greenhouse gases thus benefiting from the existing fuel transportation and storage infrastructure. Two well-known processes that enable $CO_2$-free energy generation are carbon capture and storage (CCS) and methane pyrolysis. In CCS, the $CO_2$ present in the flue gases after fuel combustion is captured, concentrated and subsequently stored underground [81]. Methane pyrolysis directly avoids the formation of $CO_2$ by thermally decomposing methane at high temperatures in an inert atmosphere [47]. The decomposition results in a hydrogen stream that can be burned in an oxidant atmosphere to produce energy and a solid carbon by-product [45]. Both processes present disadvantages that have hindered their industrial implementation. CCS present uncertainties regarding storage capacity and long-term environmental effects, while methane pyrolysis presents unsolved technical problems regarding the introduction of heat in the reaction zone in large-scale plants [27, 88].

A novel process that enables $CO_2$-free energy production from natural gas, namely the BrOx (Bromination-Oxidation) cycle, has been proposed. This process circumvents the problem of adding heat at high temperatures experienced in methane bromination by carrying out the partial oxidation of methane in two exothermic reaction steps with an internal bromine recycle between them [95]. In a first reaction step methane reacts with bromine to yield solid carbon and hydrogen bromide [55]. After the separation of solid carbon with a cyclone, hydrogen bromide reacts with oxygen to produce water and regenerate the bromine. Following bromine separation from water it is recycled to the first reactor (methane bromination). In this way methane and oxygen yield solid carbon and water in two exothermic steps from which energy can be obtained. A simplified depiction of the BrOx cycle is presented on figure 6.1.

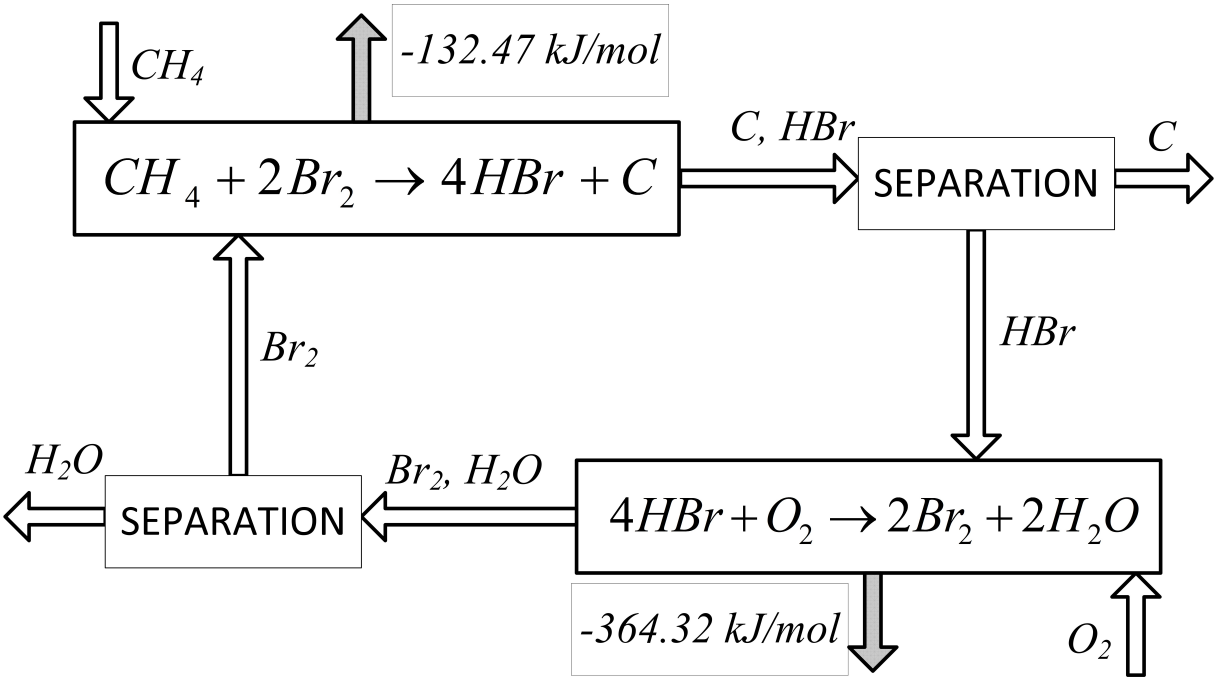


Figure 4.1.: Representation of the BrOx cycle

Although the feasibility of the process has already been demonstrated [96] and the experimental study shows promising results [95], there are two major challenges that need to be overcome in order to present the BrOx cycle as an alternative for $CO_2$-free energy generation from natural gas. Both challenges concern the first reaction step, namely methane bromination, and are carbon deposition and by-product formation.

During methane bromination solid carbon is formed from the gas phase. Solid carbon forms at the reaction front and has a tendency to deposit at the walls of the reactor as previous experiments show (figure 4.2) [95, 55]. This continuous coating of the reactor may cause obstructions in the reactor that would lead to a safety problem and thus need to be avoided. Moreover, the reactor maintenance and cleaning of the deposited carbon is a complex process that reduces the operation time of the bromination reactor. Carbon fouling is also common to methane pyrolysis and plenty of research has been carried out in order to solve the problem but a completely satisfac-

tory solution has not been found yet [47, 44]. One proposed solution to this problem is the use of a vortex solar reactor to carry out methane pyrolysis [90, 91]. Based on this concept a vortex reactor for methane bromination has been proposed that aims to minimise carbon deposition by constraining the reaction zone to the centrer of the reactor and removing carbon particles with the gas flow. The results from CFD simulations show that a major reduction in carbon fouling can be achieved at a small scale. Despite the good results obtained in steady-state simulations, there is still a low fraction of the carbon that deposits on the walls and so a strategy to avoid it, or at least facilitate its removal during maintenance, is required [92]. The present work proposes and investigates the use of sacrificial walls as a novel technique to improve the retrieval of the deposited solid carbon. The concept of sacrificial walls consists on coating the interior walls of the reactor with a material so that during reaction carbon particles cannot access the wall and deposit instead on the sacrificial wall. After reaction a solvent is introduced to wash out the sacrificial wall and the attached carbon thus facilitating the retrieval and cleaning of the reactor.

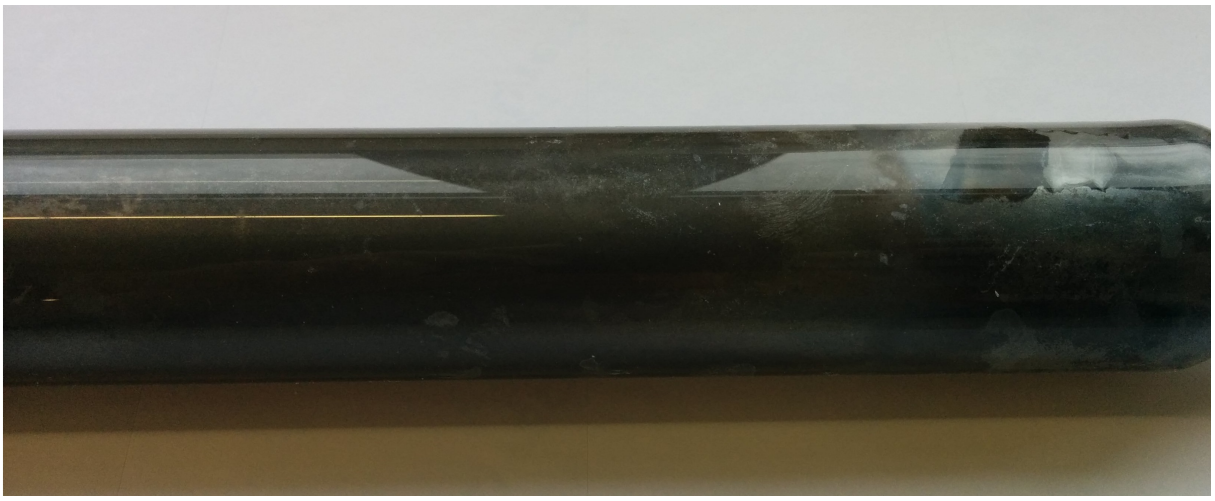

Figure 4.2.: Carbon deposition in a quartz glass tubular reactor after methane bromination

The second challenge involved in the BrOx cycle is the formation of by-products during methane bromination. Although thermodynamically the equilibrium composition of the products is mainly carbon, hydrogen bromide and traces of brominated hydrocarbons, there exists a kinetic limitation for brominated intermediates to react towards equilibrium and the experimental study of methane bromination shows that these brominated compounds are present in the solid carbon produced [95]. A previous work on methane bromination shows that the concentration of brominated compounds in the product streams radically decreases with reaction temperature but, given the potential hazard to the environment and human health that these compounds represent, a purification step is required. The problematic neutralisation of solid brominated hydrocarbons has not been treated before in the literature but there has been research on the destruction of chlorinated hydrocarbons. Given the similarities of chlorine and bromine and considering that the electronegativity of bromine is

lower than that of chlorine (and thus bromine bonds weaker than chlorine with other atoms) it is safe to assume that these techniques are appropriate for the treatment of bromination by-products.

One well known dehalogenation is the use of hydorxides (KOH, NaOH) with an organic solvent at high temperatures. Although this method is normally used to dehalogenate liquid effluents it has been successfully applied to the removal of chlorinated compounds from solids [83]. Another method has been widely used based on the use of metal catalysts such as Raney-nickel alloy for the reductive dehalogenation of organic halides [84, 85, 86, 87].

## 4.2. Materials and methods

Several experimental set-ups were used during the present work and will be described with detail in sections 4.2.1 and 4.2.2. An already constructed experimental bench-scale plant described in previous works [95, 96] was used to conduct tests with sacrificial wall reactors. Additionally, carbon samples collected in previous experiments where used for the carbon characterisation and purification investigation. A simplified schematic representation of the set-up is shown in figure 4.3. It consists of a stream containing methane, nitrogen, bromine and argon that is fed to a quartz glass tubular reactor housed in a high temperature ceramic oven. Two inert gases (nitrogen and argon) are used to dilute reactants and to sweep bromine vapour into the reactor. After reaction, the product stream is fed to a PTFE filter in which, all carbon particles that have not deposited in the reactor are collected. Subsequently the gaseous stream is send to an analysis and neutralisation section.

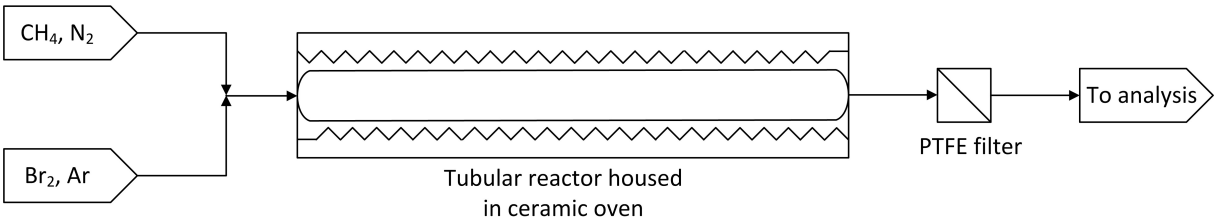


Figure 4.3.: Scheme of the bench-scale plant for the experimental study of methane bromination

### 4.2.1. Experimental study on sacrificial walls

NaCl has been selected as material for the generation of sacrificial walls due to its availability, low cost, its high solubility in water which makes it easy to remove and its high melting point (801 °C), high enough to endure methane bromination tests without melting. NaCl is also not subject to bromine corrosion because of its chlorine-sodium bond. The experimental study on sacrificial walls has been systematically carried out in four steps.

#### Determination of optimal parameters for reactor coating

During this step the influence of several parameters on the coating quality has been determined in order to find optimal coating conditions. A vacuum rotary evaporator has been used in which a transparent rounded flask with a solution of NaCl is heated while it rotates with a certain rotational speed. After all water from the solution has been evaporated the quality of the coating is visually determined by identifying holes and irregularities. The concentration of the solution, the rotational speed of the rounded flask and the evaporation time (by controlling bath temperature and vacuum) have been systematically varied to assess their impact on the coating quality.

#### Coating of a glass tubular reactor

A glass tubular reactor with the same dimensions as the quartz glass reactor used during methane bromination experiments has been constructed to carry out coating tests. The main reason for the construction of a new reactor is prevent the expensive quartz glass reactor from breaking during the coating tests. Since the diameter of the rounded flask is not the same as that of the tubular reactor the rotational speed is modified to achieve the same linear velocity at the wall of the reactor than that at the lateral wall of the rounded flask. Both temperature and NaCl concentration are kept at the optimal values determined during the previous phase. The set-up used to coat the reactor is shown in figure 4.4 In order to coat the reactor the aforementioned ceramic (C) oven is used. The reactor is introduced in the oven and its outlet (B) is connected to a laboratory rotary motor (A) that is able to rotate with speeds ranging from 200 rpm to 3000 rpm. The reactor is hold at the other extreme so that it can rotate without touching the oven ceramic heating element. After introducing the NaCl solution in the reactor via its inlet pipe, the temperature and the rotational speed are set in the oven and motor respectively. Once the water has evaporated the quality of the coating is assessed visually and imperfections are identified.

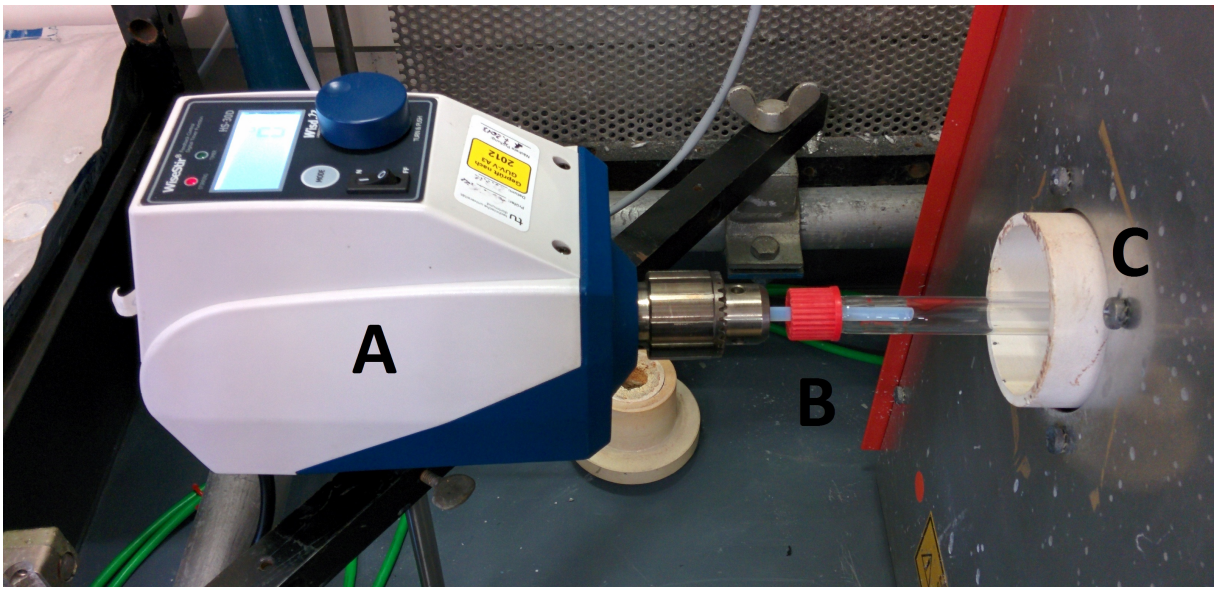


Figure 4.4.: Set-up for the coating of a glass tubular reactor

#### Coating of quartz tubular reactor and test during methane bromination

This step consists on the coating of the quartz glass tubular reactor according to the process described in section 4.2.1. After the reactor is coated with a NaCl sacrificial wall it is used in the experimental set-up for methane bromination and an experiment is carried out. Methane bromination is conducted at 600 °C (in order to ensure that the sacrificial wall does not melt) for 30 minutes with a flow rate of 150 ml/min of argon, 58 ml/min of methane and 59 ml/min of bromine. Once the experiment is finished and the reactor is cooled down to ambient temperature water is introduced in the reactor to dissolve the sacrificial wall. After removing the liquid carbon deposits in the reactor are identified.

#### Coating of quartz glass reactor with solidification method and test during methane bromination

In this step an alternative coating method is used that involves the solidification of a molten salt instead of the evaporation of a solution. In this method the quartz-glass reactor filled with NaCl rotates inside the oven 4.4 while the oven is set to 900 °C for 10 minutes to ensure that NaCl in the reactor is maintained at 810 °C. The reactor is then cooled down thus so that salt solidifies forming a sacrificial wall and it is used during methane bromination. After the experiment water is introduced to remove the sacrificial wall and carbon deposits are identified.

### 4.2.2. Carbon characterisation and purification

For the study of carbon purification methods, carbon samples from previous methane bromination experiments were used. Firstly, they were analysed to determine their elemental bromine content prior to dehalogenation treatment. Afterwards the samples were treated with varying parameters by means of three debromination methods, namely atmospheric alkali hydrolysis, high temperature alkali hydrolysis and Raney-Nickel alloy enhanced debromination. The treated samples were subsequently cleaned with distilled water, dried and analysed again. Since the initial bromine content of carbon samples varies from one experiment to another and depends on the reactor position at which they were collected a normalised parameter, the debromination degree (DBD), was established to enable the comparison between results. DBD is defined by equation 4.2.1. In order to ensure reproducibility, every measurement was repeated at least three times.

$$DBD = \frac{[Br]_{initial} - [Br]_{final}}{[Br]_{initial}}.100 \qquad [\%] \tag{4.2.1}$$

#### Atmospheric alkali hydrolysis

An experimental set-up was constructed for the study of carbon debromination by means of atmospheric alkali hydrolysis (figure 4.5). The rounded flask containing the carbon sample, 50 ml of NaOH aqueous solution and 50 ml of a solution containing an organic solvent is heated to the boiling point while stirred for a given time. NaOH acts as the hydrolysing agent while the organic solvent helps dissolve organobromine compounds present in the carbon sample. A condenser is placed at the top so that the set-up operates under reflux and no water is lost trough evaporation.

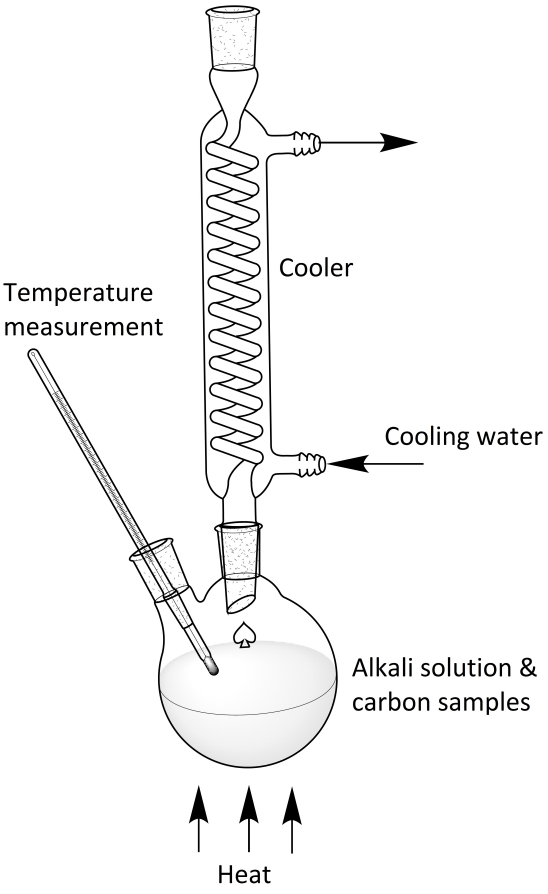


Figure 4.5.: Set-up for the coating of a glass tubular reactor

The influence parameters were varied in the following way:

- NaOH concentration: 0,5 M, 1 M, 2 M
- Organic solvent: Methanol, ethanol, iso-propanol, glicerine
- Concentration of organic solvent: 50 vol.-%, 75 vol.-%, 100 vol.-%
- Reaction time: 16 h, 24 h, 28 h

#### High temperature alkali hydrolysis

In order to carry out high temperature alkali hydrolysis of brominated compounds in the carbon samples a new set-up was used which consisted of a high pressure autoclave (Berghof BR-300) with a PTFE protection to avoid corrosion in the inner walls. The mixture of organic solvent, NaOH and carbon sample was introduced in the autoclave and pressurised with nitrogen. Afterwards it was heated to the desired temperature and maintained for a certain amount of time.

The influence parameters were varied in the following way:

- Temperature: 150 °C, 175 °C, 200 °C
- Reaction time: 1,5 h, 3 h, 6 h, 12 h

#### Raney-Ni alloy enhanced debromination

A stirred and heated rounded flask was used for the experimental study of carbon debromination enhanced with Raney Ni-Al alloy. A mixture containing water, NaOH, the carbon sample and a certain amount of particulate Raney-Ni alloy was introduced in the rounded flask and heated so that a certain temperature was achieved during a given time. The experiments were conducted at 90 °C and a Br/NaOH/Al ratio of 1/20/5 was used. Reaction times were 0.5, 1, 2, 3 and 5 hours.

#### Analysis of carbon samples

Carbon samples were analysed before and after dehalogenation treatment in order to quantitatively determine their elemental composition and so their bromine content by means of Energy-dispersive X-ray spectroscopy (EDX). This method consists on the analysis of peak areas in the emission spectre after the excitation of the sample with X-rays.

## 4.3. Results and discussion

### 4.3.1. Sacrificial walls

A total of 26 experiments have been carried out to determine the optimal parameters for reactor coating with NaCl. Results from preliminary experiments clearly established that an under-saturated solution of NaCl only had the effect of adding time to the evaporation process and thus during the experiments only saturated and over-saturated solutions were compared. Rotational speed was varied from 20 to 250 rpm and the evaporation time from 3 hours to 10 minutes (by using bath temperatures in the range from 50 to 95 °C).

Firstly the rotational speed influence was studied. The results obtained were reproducible and it was determined that rotational speeds inferior to 50 rpm resulted in coatings with poor quality that did not adhere properly to the glass surface. Figure 4.6 shows some coatings obtained at several rotational speeds.

(a) Rotational speed = 50 rpm

(b) Rotational speed = 150 rpm

(c) Rotational speed = 250 rpm

Figure 4.6.: NaCl coating at 50, 150 and 250 rpm

From the results it is clear that there is an optimum rotational speed at 150 rpm (for the rounded flask geometry). At 50 rpm (figure 4.6a) the coating is clearly inhomogeneous with lots of holes. At 250 rpm (figure 4.6c) The bottom of the flask is inhomogeneous and only a small amount of NaCl deposits there. Nonetheless, the bad quality of the coating is established due to the presence of holes in the coating along the laterals of the flask. At 150 rpm (figure 4.6b) the coating is homogeneous and no holes can be found at the bottom nor at the laterals of the flask. The laterals of the flask are of vital importance since they are parallel to the rotational axe (centrifugal force acts at the laterals forming a film of solution that evaporates leaving a coating) and the method is to be used in tubular reactors whose walls are also parallel to the rotational axe.

Several experiments were conducted to determine the influence of evaporation time on coating quality but no influence could be detected. Varying the bath temperature and vacuum in the flask while keeping constant the rest of parameters produced coating virtually identical. Changing NaCl concentration was found to have no influence neither on the coating quality. The only effect NaCl concentration presented on the coating layer was to increase its thickness when using an over-saturated solution since more NaCl was introduced.

According to the results obtained in the evaporation experiments, a saturated solution (approximately 400 g/l) was used to coat the glass tubular reactor. Temperature inside the oven was kept at 120 °C to ensure a fast evaporation and the rotational speed was set at 300 rpm. This value of rotational speed was obtained by acknowledging the difference in diameter and adjusting the optimal value of 150 rpm obtained in the rounded flask so that the centrifugal force at the walls of the tubular reactor walls was the same as that at the lateral walls of the rounded flask. Results of this experiments can be seen in figure 4.7.

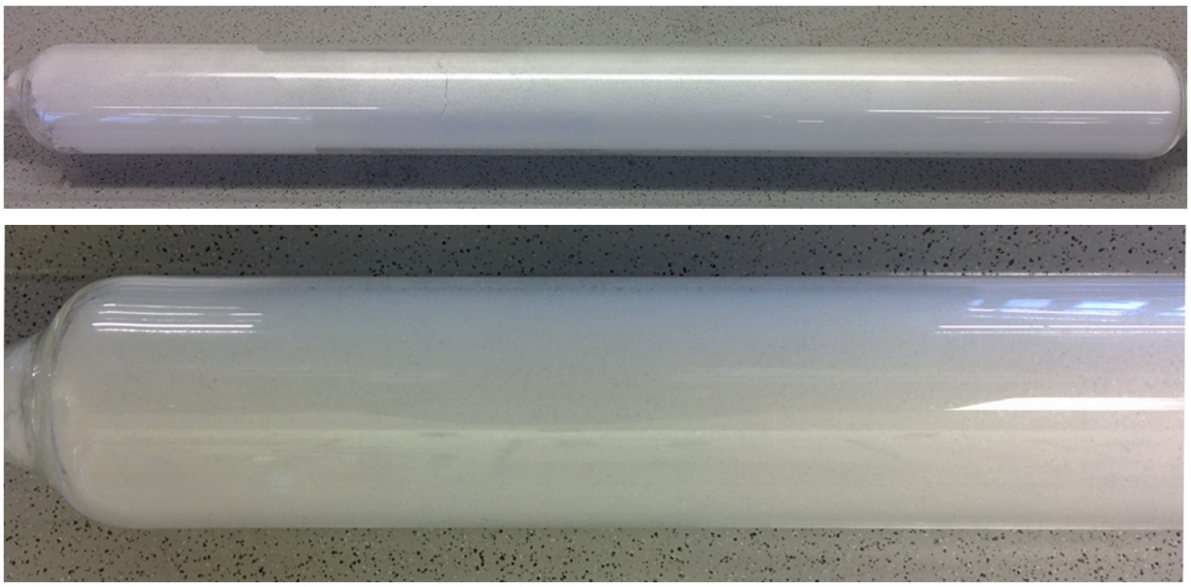

Figure 4.7.: Glass tubular reactor after coating experiment

The sacrificial wall obtained in experiments with the glass reactor was very homogeneous and it did not present holes. Nonetheless, all coatings presented a small fracture due to the differences in thermal expansion coefficients between the glass and the salt. Slower cooling diminished the size of the crack on the coating but it did not disappeared completely.

The same parameters and methodology were used to create a sacrificial wall in the quartz glass tubular reactor. The coating from one experiment is shown in figure 4.8. The results are quite different from those obtained with the glass reactor. The coating in the quartz glass reactor presents obvious inhomogeneities and holes along the length of the reactor. During the coating process of the quartz glass reactor it

was noticed that it did not rotate smoothly along the longitudinal axe. A careful examination of the reactor geometry shows that it is not perfectly symmetrical along the axe. This asymmetry causes that the mass is unbalanced and that the reactor vibrates during rotation. It was also noticed that these vibrations were stronger the further from the motor.

Figure 4.8.: Quartz glass tubular reactor after coating experiment

The resulting coating on the reactor shows two differentiated zones. The part of the reactor that was closer to the motor, and thus vibrated less, presents a relatively good coating (figure 4.8 right side) while the part further away from the motor presented holes in loose coating that fell off while handling the reactor. The reactor was nonetheless used during a methane bromination experiment to test its performance. Having a half with a good coating and one half practically without coating provided a good opportunity for comparison. This experiment was conducted in the aforementioned plant and after cooling the reactor was observed before and after introducing water to dissolve the sacrificial wall.

Figure 4.9.: Quartz glass tubular reactor with sacrificial wall after methane bromination experiment. Before (top) and after (bottom) dissolving sacrificial wall with water

As figure 4.9 shows, carbon was deposited during methane bromination experiment. After introducing water in the reactor to dissolve the sacrificial wall the reactor presented two differentiated halves. One, corresponding to the half with bad quality coating, presented carbon deposition while the half with better coating quality had no carbon deposits. The experiment shows that a sacrificial wall with good quality can avoid direct carbon deposition on the reactor walls and facilitate the retrieval of carbon from the reactor after methane bromination.

Additionally, another coating method was tested consisting of the solidification of molten NaCl in a rotating reactor. The reactor with the sacrificial wall was subse-

quently used during methane bromination reaction and, after cooling, the sacrificial wall was dissolved with water. The results are presented in figure 4.10.

(a) Quartz glass reactor with solidification sacrificial wall after methane bromination experiment

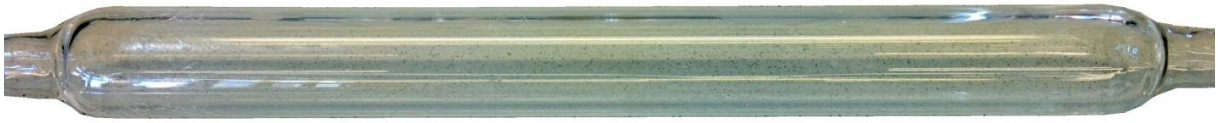

(b) Quartz glass reactor with solidification sacrificial wall after dissolving the coating

Figure 4.10.: Quartz glass reactor with solidification sacrificial

The coating obtained with this method is transparent and completely covers the wall with no holes in its structure. There were fractures in the surface of the coating due to thermal expansion which also caused damage to the reactor inner surface. Therefore the bromination test was conducted for 10 minutes, enough for carbon to form and deposit. As can be seen from the results, after introducing water the reactor presents no carbon on its surface. The solid carbon left the reactor with the water and dissolved NaCl.

### 4.3.2. Carbon debromination

The first experiments conducted on atmospheric carbon debromination were aimed at determining which organic solvent was more effective and thus experiments were conducted with methanol, ethanol, iso-propanol and glycerine. As shown in table 4.1 methanol and glycerine clearly present a lower performance while ethanol and iso-propanol present similar debromination efficiencies. Ethanol was selected as the organic solvent for following experiments given its slightly better performance and its availability.

Table 4.1.: Experimental results for carbon debromination using different organic solvents (NaOH concentration of 1 mol/l and 24 h reaction time)

| *Organic solvent* | *Methanol* | *Ethanol* | *iso-propanol* | *Glycerine* |
|---|---|---|---|---|
| Average DBD (Eq. 4.2.1) [%] | 87.9 | 93.6 | 93.1 | 77.3 |

Another series of experiments was conducted to assess the influence of the organic solvent concentration on the debromination efficiency. Carbon samples taken in

methane bromination experiments present different forms and bromine content depending on the position of the reactor at which they were taken [95]. Solid carbon can be obtained as flakes, powder and a form that lies in between them (here named mixed). Figure 4.11 shows the results of this experiments. It is clear that an increase in ethanol concentration involves a higher debromination degree achieving a maximum when using pure ethanol. Additionally, although at lower concentrations the debromination effect varies, when using pure ethanol the debromination degree is virtually the same for all kinds of carbon samples. Therefore pure ethanol was used in subsequent experiments.

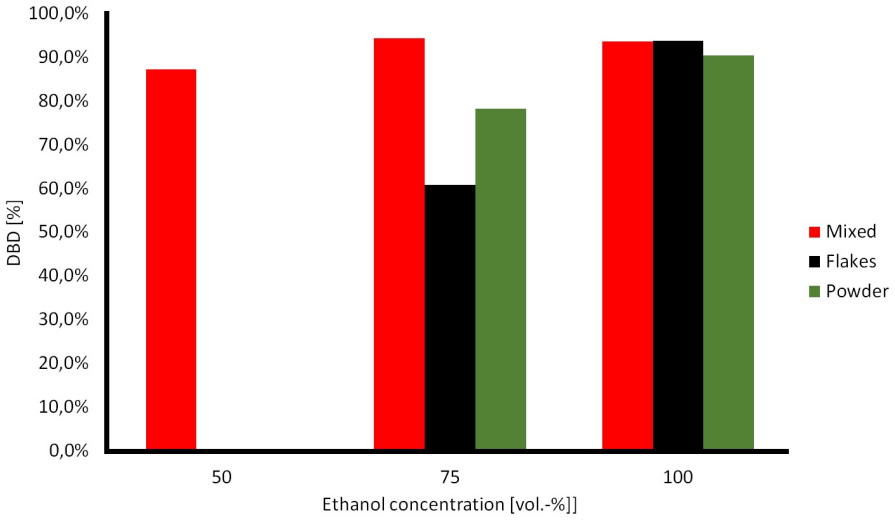


Figure 4.11.: Experimental results for carbon debromination with different carbon types and ethanol concentrations (NaOH concentration of 1 mol/l and 24 h reaction time)

The dependency of debromination efficiency with NaOH concentration was also studied, showing that high concentrations of NaOH favour dehalogenation. Table 4.2 shows that NaOH concentrations of 1 mol/l and 2 mol/l have a similar effect and thus a concentration of 1 mol/l was selected due to its slightly higher efficiency and the lower consumption of reactive.

Table 4.2.: Experimental results for carbon debromination with different NaOH concentrations (24 hours reaction time)

| *NaOH concentration [mol/l]* | *0.5* | *1* | *2* |
|---|---|---|---|
| Average DBD (Eq. 4.2.1) [%] | 87.3 | 94.4 | 93.6 |

Table 4.3 shows how increasing the reaction time from 16 hours to 24 has little effect on the debromination degree, but a very high debromination can be achieved when increasing reaction time to 28 hours. Experiments also show that that debromination degrees superior to 90% are achieved with residence times of 16 hours or more.

Table 4.3.: Experimental results for carbon debromination with different reaction times

| *Reaction time [h]* | *16* | *24* | *28* |
|---|---|---|---|
| Average DBD (Eq. 4.2.1) [%] | 93.7 | 93.6 | 98.6 |

The temperature at which atmospheric debromination can be carried out is limited to the boiling point of the solution. In order to test higher temperatures operation pressure was increased so that the process could be conducted at 150 °C and 175 °C. Figure 4.12 shows that the performance is better at 175 °C than at 150 °C. Moreover, the results show that an increase in time improves purification and that debromination degrees comparable to those obtained in 16 to 24 hours at atmospheric pressure can be achieved within 4 hours when operating at high pressure.

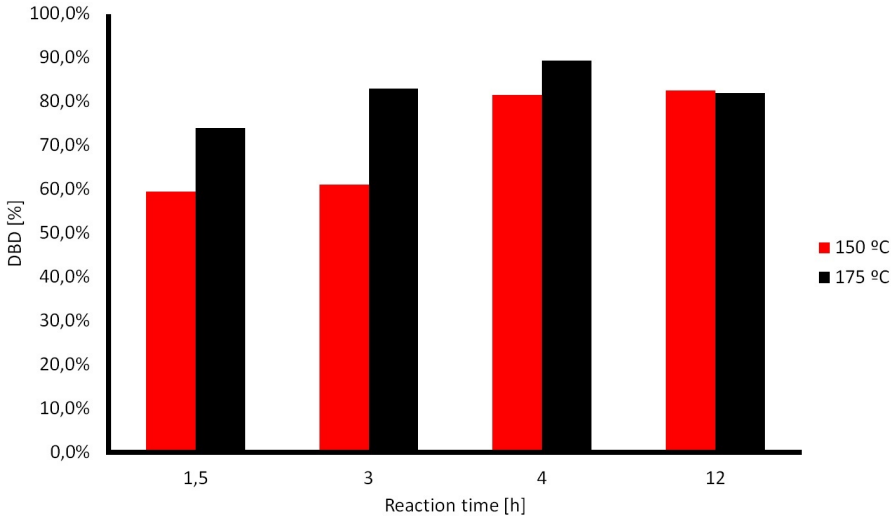


Figure 4.12.: Experimental results for high temperature carbon debromination with different temperatures and reaction times

Finally, the use of Raney-Ni alloy in debromination was tested. The experiments were conducted for a time ranging from 0.5 to 5 hours and showed that, although increasing time resulted in better debromination, the debromination degree was lower than expected being inferior to 60% after 5 hours reaction time.

Table 4.4.: Experimental results for Raney-Ni alloy enhanced carbon debromination at 90 °C

| *Reaction time [h]* | *0.5* | *1* | *2* | *3* | *5* |
|---|---|---|---|---|---|
| Average DBD (Eq. 4.2.1) [%] | 3.8 | 12.8 | 18.9 | 40.2 | 59.8 |

## 4.4. Conclusion

In this work two main challenges of the BrOx cycle were addressed, namely carbon deposition during methane bromination and presence of organobromine compounds due to kinetic limitations. A novel solution involving the use of sacrificial walls was proposed to minimise the negative consequences of carbon fouling and to facilitate its retrieval, and three methods to eliminate bromine from the carbon produced were tested.

Two methods to create a sacrificial wall of NaCl in a tubular reactor were used, evaporative and solidification coating. In a first step the optimum parameters for the evaporative coating process were established. The use of a saturated or oversaturated solution, as well as the evaporation rate, had no influence on the coating quality and therefore a saturated solution and a temperature at the oven superior to boiling point were used to reduce NaCl consumption and evaporation time. Rotational speed strongly influenced coating quality and an optimal value was found at 150 rpm for a rounded flask with 4.92 cm diameter (centrifugal force of 12.14 N/kg). This parameters were used in the coating of a tubular reactor resulting in a sacrificial wall of very good quality when applied to a glass tubular reactor. The coating process of the quartz glass reactor resulted in a sacrificial wall with good quality in one half of the reactor and another inhomogeneously coated half. This behaviour was consequence of a vibrations experienced while rotating due to a non symmetric geometry. When the quartz glass reactor was tested during methane bromination experiment the half with the homogeneous sacrificial wall was able to prevent carbon from reaching the reactor wall so that was easily retrieved by introducing water in the reactor. As shown by this experiment and by the sacrificial walls achieved in the glass reactor, evaporative method can avoid carbon deposition provided that the reactor is carefully constructed so that vibrations during the coating process are avoided.

The solidification method was used on a quartz glass reactor resulting in a transparent coating with very good quality. No holes were present on the coating although some fractures appeared in the coating as well as at the inner surface of the reactor due to differences in thermal expansion coefficients. Nonetheless, the performance of the reactor with sacrificial walls during methane bromination was excellent. No carbon deposit on the walls of the reactor and all was retrieved when water was used to dissolve the coating thus demonstrating that this method is able to avoid carbon fouling. In order to avoid fractures in the reactor that would hinder its long term usability, different materials such as silicon carbide should be explored in the future.

Three debromination methods were used to purify carbon samples from methane bromination experiments. An experimental study on atmospheric alkali hydrolysis showed that the choice of organic solvent had an influence on the debromination efficiency, being ethanol the solvent that offered the best performance. It was also established that the use of pure ethanol and a NaOH solution of 1 mol/l produced optimal results. The influence of reaction time on the process was also tested showing that higher reaction times favoured dehalogenation and that debromination degrees

of almost 99% can be achieved when running the process for 28 hours. Since the operation temperature is limited to the boiling point of the solution an autoclave was used to increase pressure and thus reaction temperature. The experiments at high pressure showed that increasing the temperature resulted in better debromination efficiencies and that results similar to those obtained at atmospheric pressure could be obtained with reaction times 80% lower.

Additionally, the use of Raney-Ni alloy for debromination was investigated. The results showed that reaction times of 5 hours resulted in low debromination degrees (lower than 60%). One likely explanation is that the mixing inside the flask was not sufficient and thus the reaction with brominated compounds in the carbon particles was limited.

The present work shows that the use of sacrificial walls on methane bromination reactions avoids direct contact between produced carbon particles and the reactor walls and facilitates the cleaning of the reactor and the retrieval of carbon particles. It is also demonstrated that bromine content in carbon particles can be reduced in 99% by means of alkali hydrolysis and it is therefore a promising strategy for carbon purification.

## 4.5. Acknowledgements

Financial support from the Graduate School of Energy Efficient Production and Logistics (*Forschungsschule für Energieeffiziente Produktion und Logistik*) is gratefully acknowledged.

The authors would also like to express their gratitude for the assistance of Ms. Meuris from the(*Lehrstuhl für Biomaterialien und Polymerwissenschaften*) in te SEM and EDX analysis of the carbon samples.

## Preamble

The following chapter has been submitted for publishing as:

**González Rebordinos, J., Saki, F., Matulla, F., Agar, D.W.**: "Experimental study on thermal and catalytic hydrogen bromide oxidation" in *International Journal of Hydrogen Energy*.

This work is partly based on the experimental work of Mr. Saki during his Master thesis: "Experimentelle Untersuchung und Simulation der thermischen Bromwasserstoffoxidation"; and on the work of Mr. Matulla in his Master thesis: "Experimental study of catalytic hydrogen bromide oxidation". Conceived, directed and supervised by myself and evaluated by Prof. Agar. Mr. Saki carried out the required modifications to the bench-scale plant and performed the experiments of thermal oxidation. Mr. Matulla synthesised the catalyst and carried out experiments of catalytic oxidation. The design of the plant modifications, experimental protocols and reactor simulations were performed by myself.

### 4.5.1. Table of contributions to chapter 4

Table 4.5.: Contributions to Chapter 4

| *Contributor* | *Contribution percentage* |
|---|---|
| Jesús González Rebordinos | 55 |
| Furkan Saki | 25 |
| Felix Matulla | 15 |
| David W. Agar | 5 |

## Abstract

Hydrogen bromide oxidation is one important part of the Bromination-Oxidation (BrOx) cycle for $CO_2$-free energy production, being the most exothermic reaction step. Although high temperatures favour reaction kinetics, the equilibrium conversion decreases and thus thermal HBr oxidation is limited. A catalyst may be used to overcome thermodynamic limitations while ensuring high reaction rates with the main drawback of an increase in the costs. An experimental study has been conducted that shows that high conversions can be achieved within residence times lower than 10 seconds at temperatures ranging 800 °C - 1000 °C. A $RuO_2/Al_2O_3$ catalyst has been synthesised and used for HBr oxidation showing that conversions superior to 90% are achievable at temperatures as low as 200 °C with residence times inferior to 1 seconds.

# 5. Experimental study on thermal and catalytic hydrogen bromide oxidation

## 5.1. Introduction

The growth in worldwide population and economy experienced in the last century has led to a significant increase in world energy demand, reaching more than 500 EJ in 2014 [93]. Currently, almost 85% of the total primary energy demand of the OECD (Organisation for Economic Co-operation and Development) members is satisfied by fossil fuels [1]. Energy is obtained from coal, oil and gas mainly through their combustion therefore resulting in the generation of $CO_2$, a greenhouse gas that is generally released into the atmosphere. Scientific consensus regards anthropogenic $CO_2$ emissions as the main cause of the increase in its atmospheric concentration, from 338.80 ppm in 1980 to 399.41 ppm in 2015, and consequently of global warming [93]. At the 2015 United Nations Climate Change Conference (COP21) an agreement was achieve, in which a limit of 2 °C (above pre-industrial levels) for the increase in the global average temperature was established, thus urging a dramatic decrease in the global $CO_2$ emissions [94].

Contrary to popular belief and in spite of the continuous increase in fossil fuel consumption, fossil fuel proven reserves have increased in the last decades. In the time from 1992 to 2012, natural gas proven reserves have gone from 117.6 $Tm^3$ to 187.8 $Tm^3$ while those of oil have experienced an increment from 1039.3 to 1689.9 thousand million barrels [1]. Additionally, there are unconventional resources such as shale gas, coal-bed methane, tight gas or methane hydrates whose availability is estimated in centuries of supply at the current consumption rate [66]. Although most unconventional resources are not economically or technically exploitable, the development of new extraction technologies as well as the change in fossil fuel prices could render its exploitation feasible as exemplified by the recent shale gas boom [67]. This figures show that the use of fossil fuels for energy production is more limited by the concomitant $CO_2$ emissions than by their availability.

Energy production is the largest single source of anthropogenic global greenhouse emissions and therefore a reduction in the $CO_2$ emissions associated to energy production will have the highest impact on global warming [62]. A promising strategy to achieve $CO_2$-free energy production is the decarbonisation of fossil fuels since it avoids greenhouse emissions while still retaining the advantages of fossil fuels, namely its relatively low price and the presence of an existing infrastructure for ex-

traction, transportation, processing and storage [41]. CCS and methane pyrolysis are the most well-known strategies for $CO_2$-free energy production from fossil fuels. The former consists on capturing the $CO_2$ after combustion and sequestering it either under the ocean or in underground geological formations while the latter consists on the thermal decomposition of methane in an endothermic reaction to yield solid carbon and hydrogen that can be used for net energy generation [47, 44]. CCS is nonetheless a controversial technology that lacks the acceptance of a large section of society and presents many uncertainties regarding long-term reliability and storage capacity [81]. Methane pyrolysis, although widely studied, is still technologically unfeasible since it involves the introduction of heat into the reaction zone at temperatures superior to 1200 °C [47, 44].

A novel process that enables $CO_2$-free energy production from natural gas is the Bromination-Oxidation (BrOx) cycle. In the first step of the process, methane bromination, methane and bromine react exothermically to yield solid carbon and hydrogen bromide. Following carbon separation the product stream, containing hydrogen bromide, and oxygen are fed to a second reactor to regenerate bromine and produce water in an exothermic reaction. After bromine-water separation, bromine is recycled to the methane bromination reactor so that the overall process is the partial oxidation of methane to solid carbon and water (figure refSchbrox). Thus the BrOx cycle can generate around 55% of the energy released from methane in its combustion without producing $CO_2$ [95]. The carbon produced is a potentially valuable by-product that can be sold or easily sequestered. Methane bromination has been already studied in previous works, showing that complete conversion of methane and carbon formation can be achieved within short residence times at temperatures ranging 900 °C - 1100 °C [96, 55, 56].

An additional advantage of the BrOx cycle is its flexibility, since it can either be set to produce $CO_2$-free hydrogen by substituting hydrogen bromide oxidation with hydrogen bromide electrolysis [97] or be used for methane functionalisation and production of chemicals [98].

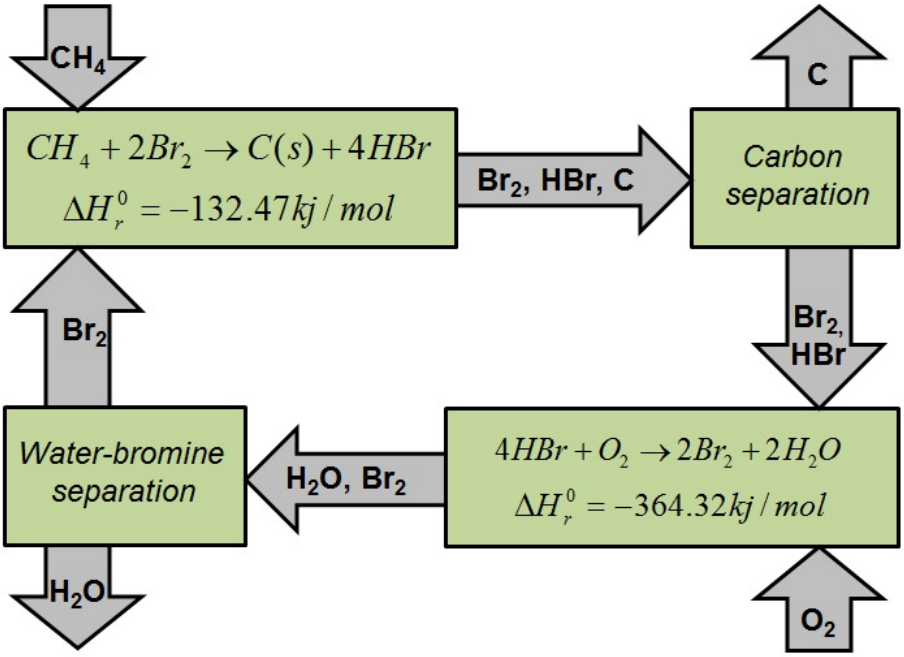


Figure 5.1.: Schematic representation of the BrOx cycle

Rosser et al suggest a reaction mechanism for thermal hydrogen bromide oxidation and present a kinetic expression with experimentally determined values for the pre-exponential factor and the activation energy. Nonetheless, the experiments have been performed at conditions of temperature and reactants ratio very different from those of the BrOx cycle [99]. Since hydrogen bromide oxidation is an exothermic reaction, the equilibrium conversion decreases with temperature so that high enough temperatures to ensure a realistic reaction rate could lead to incomplete conversions. Several patents suggest the possibility of using a catalyst ($CeO_2$, $RuO_2$, $TiO_2$...) that enables the reaction at lower temperatures [100, 101, 102, 103] although the amount of catalyst required has a high cost. A hybrid strategy is presented by Waycuilis et al. in which the hydrogen bromide oxidation is carried out in two steps. The first step is the thermal oxidation of hydrogen bromide at high temperatures followed by a catalytic oxidation using NiO/alumina or CuO/alumina as catalysts [104]. This method uses excess air to oxidise hydrogen bromide and the thermal oxidation is performed isothermally. The use of air implies a low concentration of oxygen and therefore diminished reaction rate during thermal oxidation, which is also reduced because of isothermal operation. Additionally, the presence of nitrogen complicates substantially the separation of the products following reaction.

The present study proposes a method that provides an optimal hydrogen bromide oxidation strategy within the BrOx cycle. In a first reactor, hydrogen bromide reacts with pure oxygen at high inlet temperatures. The operation can be carried out adiabatically with intermediate cooling or alternatively optimal operation can be achieved with a tailored temperature profile depending on the amount of heat that needs to be removed. After reaching high conversion through thermal oxidation, the product stream can be cooled down and a catalytic step carried out to achieve full conversion

(figure 5.2). $RuO_2/Al_2O_3$ has been selected as the catalyst for the catalytic step due to its high activity at low temperatures, thus ensuring high equilibrium conversions.

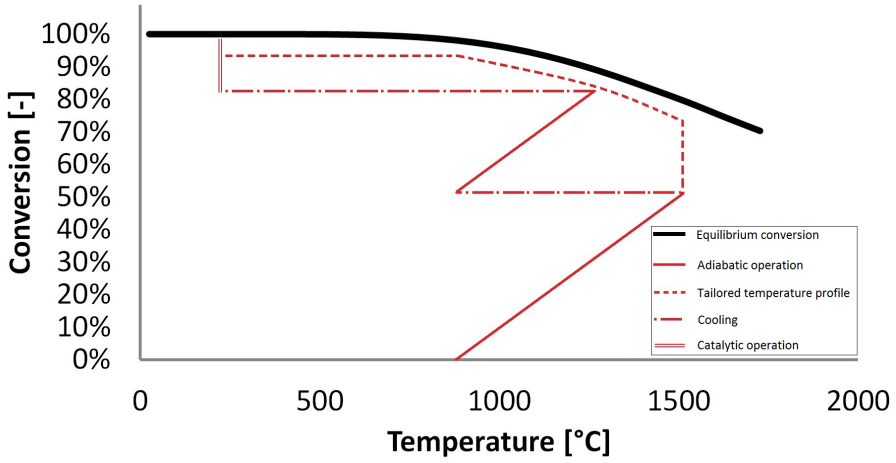


Figure 5.2.: Schematic representation for the hydrogen bromide oxidation strategy

## 5.2. Experimental methods

An experimental bench-scale plant has been constructed in order to perform experiments on both thermal and catalytic hydrogen bromide oxidation. As shown in the flowsheet of the experimental set-up (figure 5.3), gas bottles of hydrogen bromide (B-101), nitrogen (B-102) and oxygen (B-103) are used to supply the reactants. Nitrogen was used during catalytic oxidation experiments in order to dilute the reactants so that the mixture resembles a partially converted stream. The flow rate of hydrogen bromide and oxygen is controlled with mass flow controllers (V-102, V-103) while that of nitrogen is controlled with a rotameter (FIC-104). Nitrogen can be introduced to the reactor after the oxygen mass flow controller to dilute the mixture or through the hydrogen bromide pipe to flush the system after the experiment and during pre-heating. The reactants are fed to a quartz glass reactor (R-101). For the thermal oxidation experiments, a tubular reactor of approximately 500 ml housed in an oven is used while for catalytic oxidation experiments a smaller reactor with a frit at the end (to support the catalyst) and heated via heating bands is employed. The temperature in the reactor is monitored with a type K thermocouple (TIC-107). During normal operation, the analysis bottle containing a 1M KI solution (B-104) is by-passed and the product stream is bubbled through a first neutralisation bottle containing a 2M $NaOH$, 0.2M $Na_2S_2O_3$ solution (B-105) in order to neutralise both hydrogen bromide (equation 5.2.1) and bromine (equation 5.2.2).

$$NaOH + HBr \rightarrow NaBr + H_2O \tag{5.2.1}$$

$$Na_2S_2O_3 + 4Br_2 + 10NaOH \rightarrow 2Na_2SO_4 + 5H_2O + 8NaBr \quad (5.2.2)$$

A second neutralisation bottle (B-106) is subsequently placed to ensure complete neutralisation and afterwards a control bottle containing a 1M KI solution is placed for safety reasons. A colour change in this bottle would indicate that bromine is reacting with potassium iodide and releasing iodine, thus showing that the neutralisation section is not working properly so that the plant would have to be shut down.

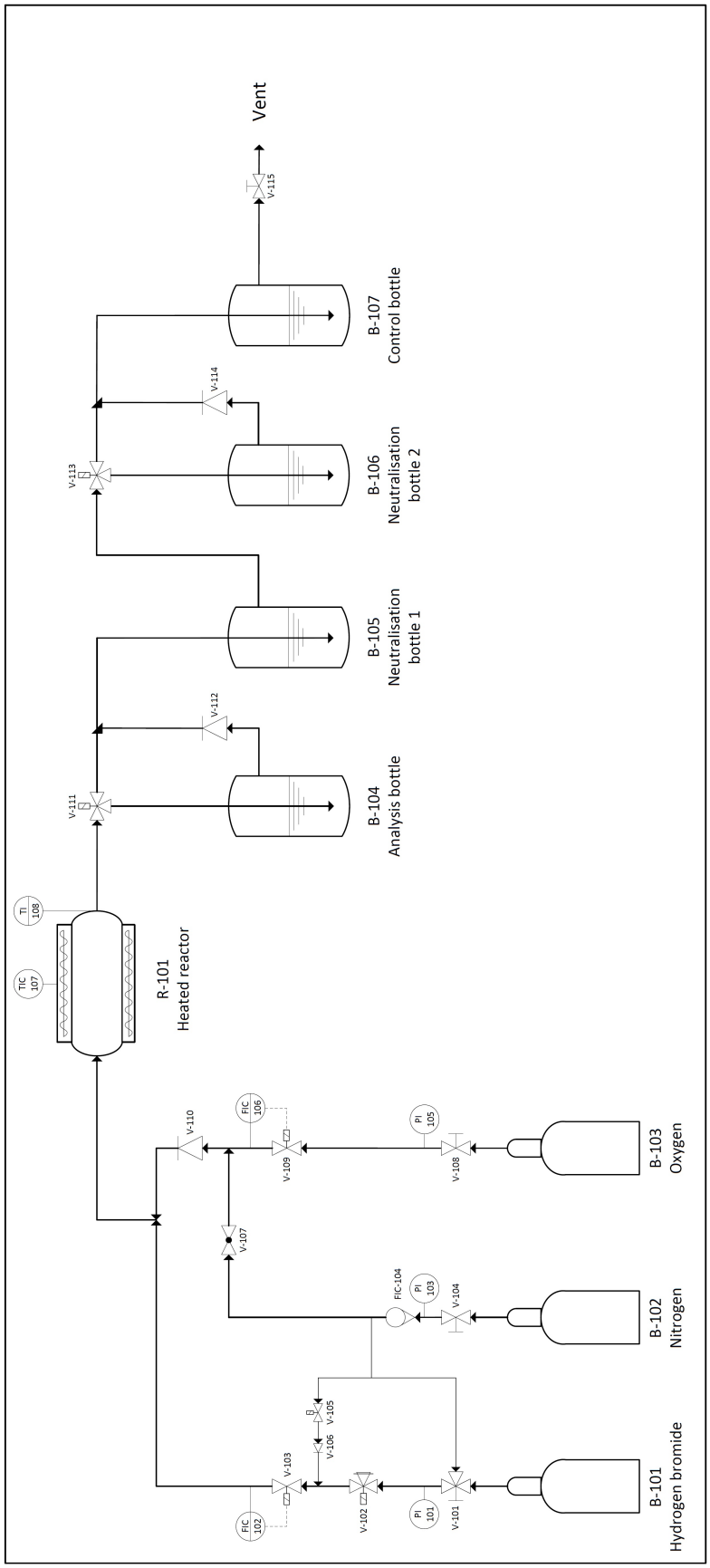


Figure 5.3.: Schematic representation for the hydrogen bromide oxidation strategy

A 3-way-valve (V-111) can be used to direct the product stream to the analysis bottle (B-104) prior to neutralisation once the system is in steady-state and the time that this valve is open is automatically recorded. Any bromine present in the product stream reacts immediately with potassium iodide releasing iodine (equation 5.2.3). After an experiment, three samples are taken from the bottle and they are titrated with a 0,1M $Na_2S_2O_3$ solution to determine the iodine content. Through simple calculations the flow rate of bromine being bubbled through the analysis bottle can be determined and thus the conversion of the oxidation reaction ascertained.

$$2KI + Br_2 \rightarrow 2KBr + I_2 \tag{5.2.3}$$

The preparation of the $RuO_2/Al_2O_3$ catalyst was carried out according to a Schubert et al. patent [104]. The raw materials used were a pulverulent gamma-aluminum oxide provided by Sasol (Puralox®SCCa-30/170) with $50.10^{-6}$ m particle size for the support material and soluble $RuCl_3$ provided by abcr GmbH (ruthenium (III) chloride hydrate (39-42% w/w Ru)). The synthesis of the catalyst was performed according to the following steps:

- Calcination of $Al_2O_3$: The support was heated under oxidant atmosphere at 1300 °C for 5 hours in order to achieve a phase change from gamma-alumina to alpha-alumina given the higher mechanical stability of the later over the former [104].
- An aqueous solution of $RuCl_3$ was prepared and poured over the support while ensuring mixing to impregnate it. The volume of the solution used was lower than the pore volume available at the support.
- Drying: The catalyst was dried at 120 °C for 6 hours to remove all water.
- Calcination of the catalyst: The dry catalyst is heated under oxidant atmosphere at 350 °C for 5 hours. During this time, $RuCl_3$ reacts with the oxygen in the air thus being transformed to $RuO_2$.

After synthesis of the catalyst it was used in hydrogen bromide oxidation experiments and it was analysed by using SEM (Scanning Electron Microscope) photography in order to qualitatively assess the distribution of $RuO_2$ in the support. Additionally, an EDX (Energy-dispersive X-ray Spectroscopy) analysis was performed before and after oxidation experiments to detect changes in the catalyst chemical composition.

Hydrogen bromide oxidation was simulated with Matlab and the results obtained were compared to the experimental results. A plug flow reactor model was implemented (equation 5.2.4) and the values of the kinetic constant were calculated with the pre-exponential factor and the activation energy provided by the literature (equation 5.2.5) [99]. The simulations were performed either assuming isothermal operation or by defining a temperature profile along the reactor T(V).

$$\frac{dX}{dV} = \frac{4}{\dot{n_0}} k C_{HBr} C_{O_2} \tag{5.2.4}$$

$$k = 10^{12.5} e^{\frac{-37000}{RT}} \qquad cm^3/mol.s \tag{5.2.5}$$

A hydrogen bromide-to-oxygen ratio of 4 was used in all thermal oxidation experiments to ensure stoichiometric feed of reactants. An initial experiment was carried out to determine at which temperature thermal hydrogen bromide oxidation starts. The experiment started at 300 °C and temperature was increased 100 °C until bromine was detected in the product stream. Bromine can be identified visually at concentrations as low as 0.1 ppm, so it was possible to determine its presence visually by looking at the outlet of the reactor for a red vapour. Additionally, for each temperature the product stream was directed to the analysis bottle to simplify bromine detection. At 500 °C bromine was found to be present in the product stream.

## 5.3. Results

### 5.3.1. Thermal oxidation of hydrogen bromide

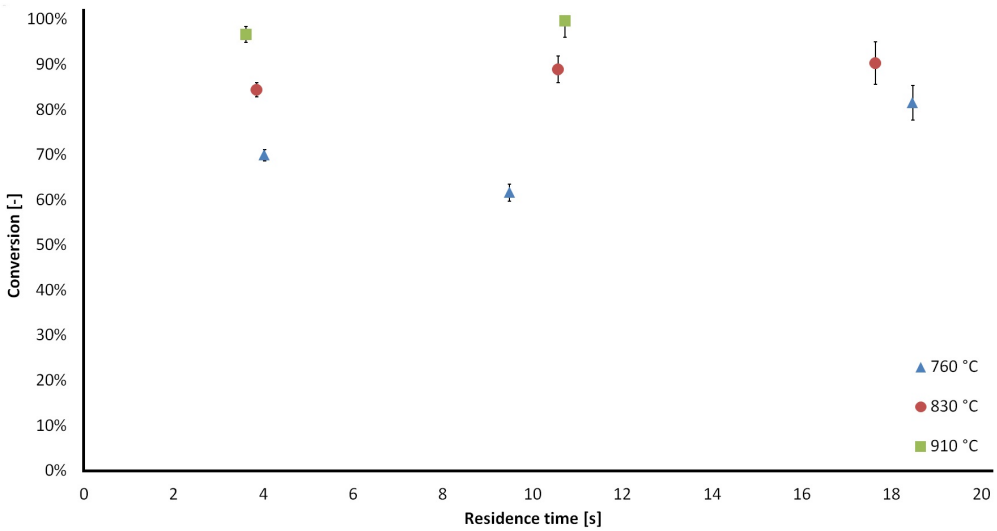


(a) Conversion versus residence time

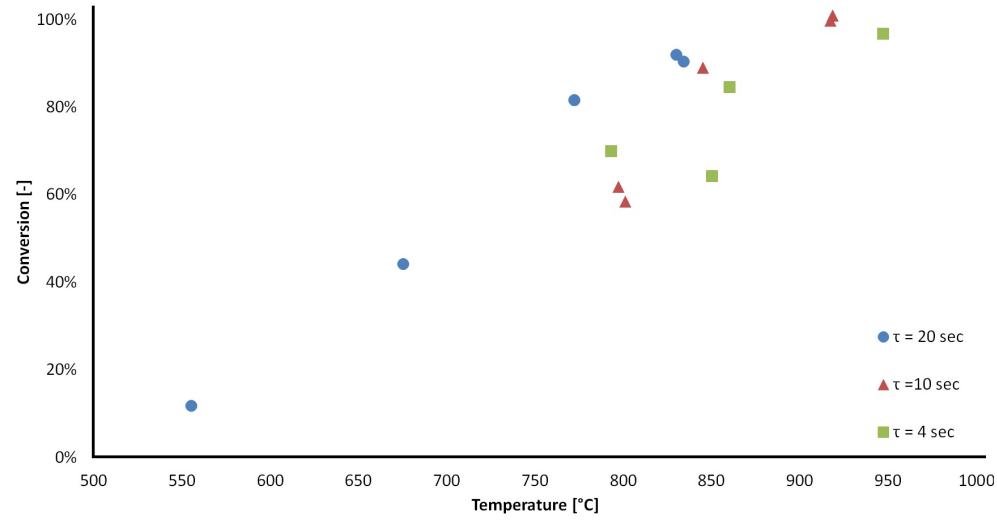


(b) Conversion versus temperature

Figure 5.4.: Experimental results of thermal hydrogen bromide oxidation

Figures 5.4a and 5.4b show the experimental results of thermal hydrogen bromide oxidation. As can be seen, experiments were conducted at temperatures from 550 °C to 950 °C with flow rates adjusted so that the residence time was in the range of 4 to 20 seconds. As expected, the experiments show that higher temperatures and

residence times enable higher conversions. This trend is only interrupted at 760 °C since the conversion achieved with a residence time of 10 seconds is lower than that after 4 seconds.

A reproducibility study was carried out by repeating experiments with the same temperature and flow rates. The results of these experiments at 800 °C, 830 °C and 920 °C are shown in table 15.1. The deviation in the conversion values obtained varies from 1% to 5%, which is attributable to experimental error, thus demonstrating that the bench-scale plant and the analysis system are able to provide reproducible results.

Table 5.1.: Experimental results of thermal hydrogen bromide oxidation and reproducibility

| **Temperature [°C]** | **Flow rate HBr [mol/min]** | **Flow rate $O_2$ [mol/min]** | **Conversion [%]** |
|---|---|---|---|
| 797 | 740 | 185 | 61.73 |
| 801 | 740 | 185 | 58.43 |
| 919 | 620 | 155 | 100.86 |
| 917 | 620 | 155 | 99.69 |
| 830 | 400 | 100 | 91.28 |
| 834 | 400 | 100 | 90.40 |

In order to validate the pre-exponential factor and the activation energy provided in the literature [99] a simulation was performed in Matlab. The flow rates, temperature and reactor volume were the same as those used in each experiment. Although for the first simulations an isothermal reactor was simulated, the actual reactor used in the experiments did not have a perfect isothermal behaviour. Therefore, the temperature profile of the reactor was measured and implemented in Matlab simulation. The temperature profile could not be measured while the reaction was taking place due to the high risk of leaks implied so it was measured with just nitrogen flowing (figure 5.5).

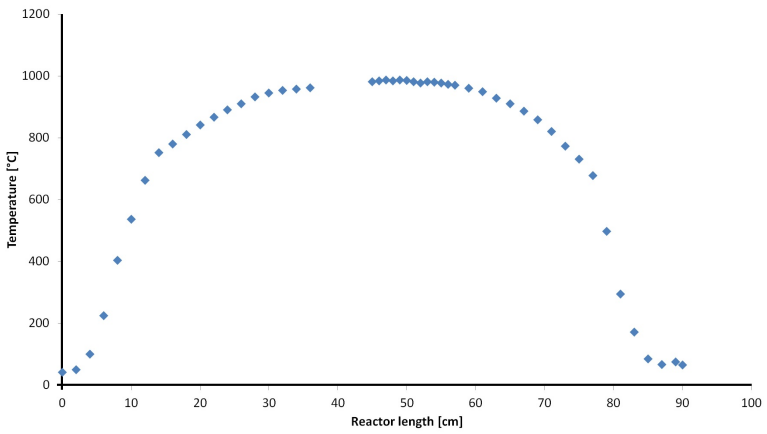


Figure 5.5.: Experimentally measured temperature profile of the reactor

The comparison between the experimental results and those produced with the simulation is shown in chart 6. For most reaction conditions the conversion value obtained experimentally lies within the value obtained from the isothermal simulation and that obtained when the experimentally measured temperature profile was implemented. Moreover, the experimental value for conversion is usually lower than that of the isothermal simulation and greater than that obtained when using the temperature profile. There are only 3 cases (550 °C, 925 °C and 960 °C) for which the experimental value is slightly higher than the simulation values. It can also be observed that the experimental conversion at 780 °C is inferior to simulation conversions. This value corresponds to the discrepancy observed in figure 5.4.

An increase in the temperature was observed during the experiments when the reactants were introduced in the reactor. This temperature increase is due to the exothermicity of the reaction and points at the presence of a hot spot located at the reaction zone, so that the temperature profile shown in figure 5.5 does not describe accurately the real temperature profile. Instead, it lacks this hot-spot. This explains why the conversions obtained in real operation are greater than those obtained using the temperature profile in the simulations. The discrepancy experienced at 760 °C can also be explained by the presence of the hot-spot. In the isothermal simulations, the temperature was fixed at the value measured in the experiments while for the simulations using a temperature profile the maximum temperature was fixed at the measured value. Temperature at the reactor is measured by means of a thermocouple and therefore is only known at one position so that if the thermocouple lies at the hot-spot the temperature measured would be much higher than the average temperature along the oven. During the experiment carried out at 760 °C with 10 seconds residence time the thermocouple was probably located at the hot-spot so that the average temperature in the oven was actually lower than 760 °C and thus a lower conversion was achieved than that obtained after 4 seconds. This would also explain why the experimental result for these conditions is lower than the simulation results (figure 5.6).

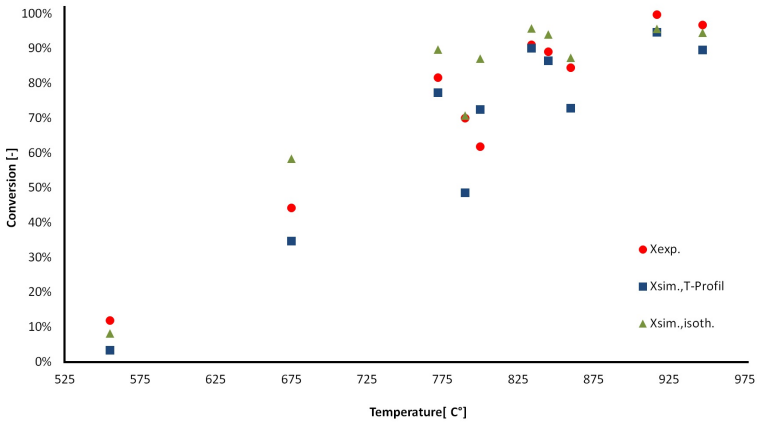


Figure 5.6.: Comparison between experimental results, simulation results assuming isothermal operation and simulation results with the reactor temperature profile

### 5.3.2. Cathalyst synthesis

After impregnation of the white powdery aluminium oxide with the black $RuCl_3$ aqueous solution the particles acquired a grey tonality that seemed homogeneous to the naked eye. Samples of the catalyst were taken and analysed with scanning electron microscopy. Figure 5.7 shows the images obtained at several magnifications (130x, 900x and 10000x). The particle size of the catalyst is in the range of $40.10^{-6}$ m to $60.10^{-6}$ m and, as can be seen under 10000x magnifications, $RuO_2$ is homogeneously distributed over the support surface. The whole process, including catalyst synthesis and characterisation was repeated producing virtually identical results.

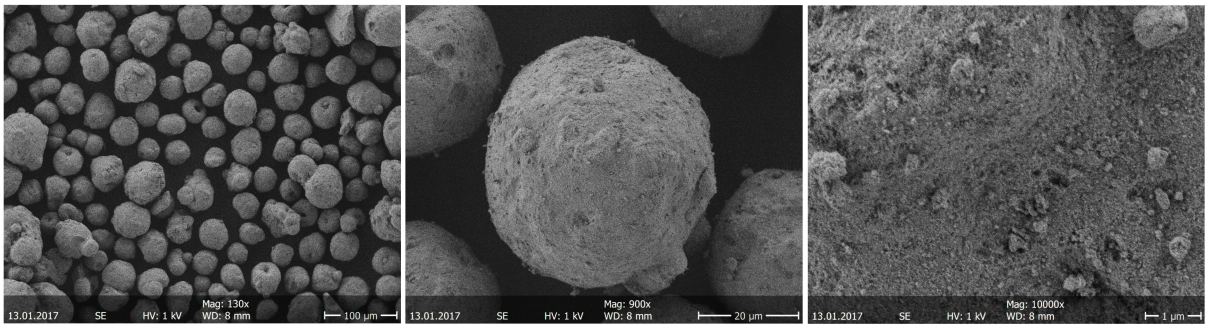


Figure 5.7.: $RuO_2/Al_2O_3$ catalyst viewed through a Scanning Electron Microscope (Left: 130x magnification; middle: 900x magnification; right: 10000x magnification)

### 5.3.3. Catalytic oxidation of hydrogen bromide

The aforementioned catalyst was used to fill a fixed bed reactor in order to perform an experimental study on catalytic hydrogen bromide oxidation. All experiments were carried out with feed flowrates of 300 ml/min of $N_2$, 80 ml/min of HBr and 20 ml/min of $O_2$, and thus stoichiometric amounts of reactants highly diluted with nitrogen. The amount of catalyst introduced in the reactor was varied so that experiments were carried out with residence times of 2.5 seconds and 0.95 seconds. The experiments with residence times of 2.5 seconds show that the catalyst is highly active at temperatures as low as 200 °C and that there is a substantial increase in the conversion with 50 °C increase temperature, reaching a conversion of 93% at 250 °C. Figure 5.8 also shows that the experiments conducted with 0.95 seconds residence time offer a strong increase in the conversion with temperature, reaching 93% at 315 °C, although at higher temperatures it drops to values around 80%. The experiments were performed two times with negligible deviation in the results. The use of stoichiometric amounts of reactants could lead to insufficient adsorption of oxygen at high temperatures, which would explain why at temperatures higher than 315 °C the conversion drops to 80%. An experiment at 350 °C with 25% excess oxygen in the feed was performed and, although no quantitative analysis was performed, it was qualitatively determined that the conversion achieved was much higher than 80% by comparing the colour of the

analysis bottle after the experiment with that of the analysis bottle from a previous experiment at 350 °C and stoichiometric conditions and noticing that it was much darker.

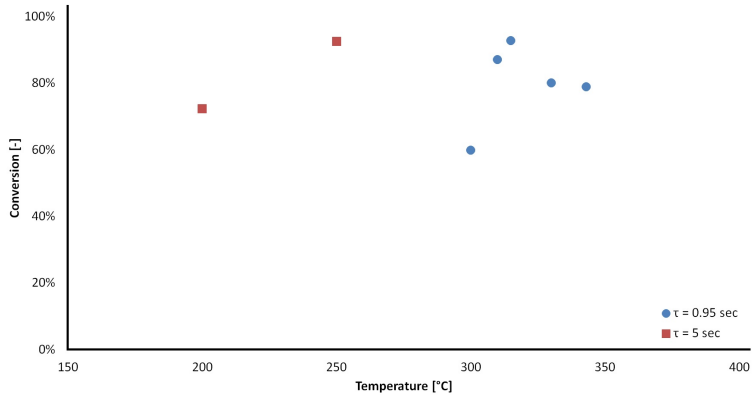


Figure 5.8.: Experimental results of catalytic hydrogen bromide oxidation

Figure 5.9 shows the qualitative results from the EDX analysis to the catalyst before and after oxidation experiments. The main objective of this analysis was to detect changes in the chemical composition with the reaction so that quantitative analysis was not required. The two main changes occurring between analyses are the decrease in size of the ruthenium peak after the experiment and the apparition of a new peak corresponding to bromine.

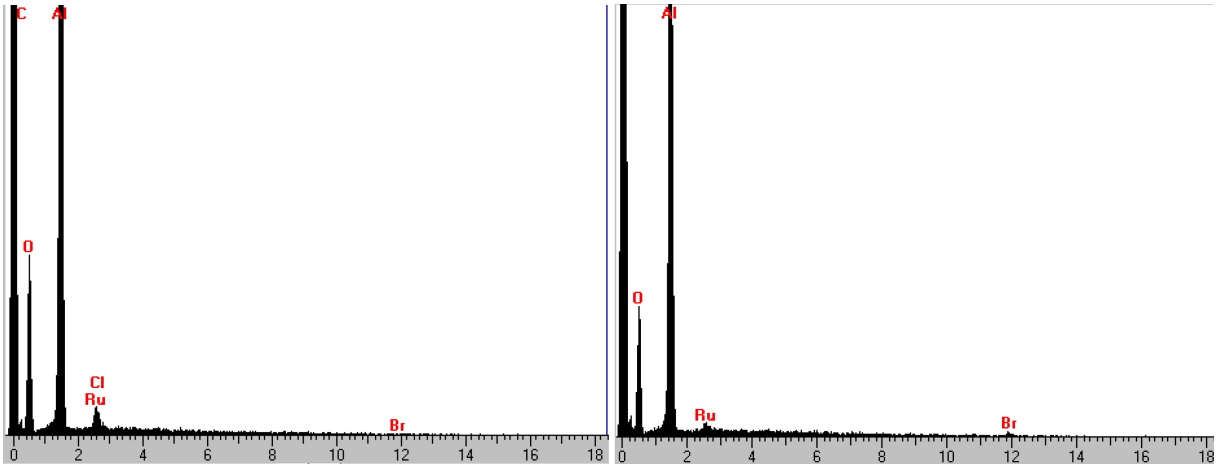


Figure 5.9.: EDX (Energy-dispersive X-ray Spectroscopy) analysis of the catalyst before reaction (left) and after reaction (right)

The position of the ruthenium peak coincides with that of a chlorine peak, so that a decrease in the peak after the experiment implies that the calcination of $RuCl_3$ was incomplete. After using the catalyst in hydrogen bromide oxidation experiments, chlorine is no longer detectable. The presence of a bromine peak after reaction indicates

that small amounts of bromine are added to the catalyst during operation and points to the presence of a bromine containing intermediate in the catalysis mechanism.

## 5.4. Conclusions

An experimental study of hydrogen bromide oxidation has been presented in this paper and an experimental bench-scale plant able to provide reproducible results has been constructed to perform the aforementioned study. The study includes thermal oxidation, the validation of the kinetic parameters presented by Rosser et al [99] under conditions similar to those of the BrOx cycle, the preparation and characterisation of a highly active $RuO_2/Al_2O_3$ catalyst and the study of its performance at the oxidation of hydrogen bromide.

Thermal oxidation of hydrogen bromide starts to occur at 500 °C achieving a conversion of 12% with a residence time of 25 seconds at 550 °C. Full conversion is virtually achieved at 920 °C within 10 seconds while at 950 °C a conversion of 96% is obtained after 4 seconds. This results show that thermal oxidation is a feasible strategy for achieving high conversions even with quasi-isothermal operation. A further reduction of the residence time can be achieved if either multi-stage operation with intermediate cooling is used or a tailored temperature profile is ensured. A simulation in Matlab of thermal hydrogen bromide oxidation shows that the kinetic parameters proposed by Rosser et al [99] describe the experimental results in a satisfactory manner. The deviations detected between experimental and simulation results have been found to be caused by the differences existing between the temperature profile implemented and the real one.

A catalyst consisting of $RuO_2$ supported on $\alpha$-Al2O3 was synthesised following the instructions found in the literature [104] and subsequently characterised by using scanning electron microscopy and energy-dispersive X-ray spectroscopy. The EDX results show that after synthesis, the catalyst still contains chlorine, thus indicating that the calcination time in which $RuCl_3$ is oxidised to $RuO_2$ is not sufficient and that after reaction a small amount of bromine is introduced in the catalyst. The catalyst particles have a size ranging 40.10-6 m to 60.10-6 m and $RuO_2$ is homogeneously distributed on the surface of the alumina support.

The $RuO_2/Al_2O_3$ catalyst previously synthesised was used hydrogen bromide oxidation experiments showing that is extremely active at low temperatures (72% at 200 °C after 2.5 seconds). A conversion of 93% can be achieved at 250 °C with residence times of 2.5 seconds whereas with residence times of 0.95 seconds it takes 315 °C to obtain the same conversion. Temperatures higher than 315 °C resulted in lower conversions (around 80%). This can be explained by the difficulty of adsorbing oxygen when stoichiometric amounts of reactants are fed to the reactor so that this problem can be easily circumvented by using excess oxygen in the feed.

With the kinetic parameters from Rosser et al [99] a simulation has been carried in Matlab of a plug flow reactor with a tailored temperature profile. The feed was

a stoichiometric mixture of hydrogen bromide and oxygen at 800 °C. The reaction proceeds adiabatically until a temperature of 1500 °C is reached. Then an isothermal step leads to a cooling step through an optimal temperature profile (figure 5.10). The simulation results show that residence times lower than 4 seconds lead to conversions higher than 90%.

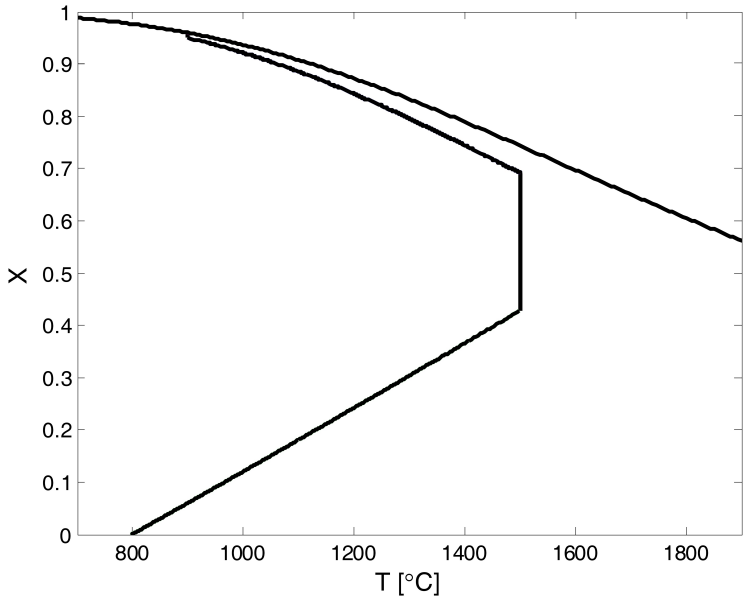


Figure 5.10.: Temperature profile of the simulated hydrogen bromide oxidation

This results together with those obtained experimentally for the catalytic step suggest that a strategy that combines a thermal oxidation followed by cooling and subsequent catalytic oxidation will ensure high conversions of hydrogen bromide (figure 5.11)). Low amounts of unreacted hydrogen bromide and oxygen will not generate any problems as they can be recycled with negligible consequences to the overall BrOx cycle [96].

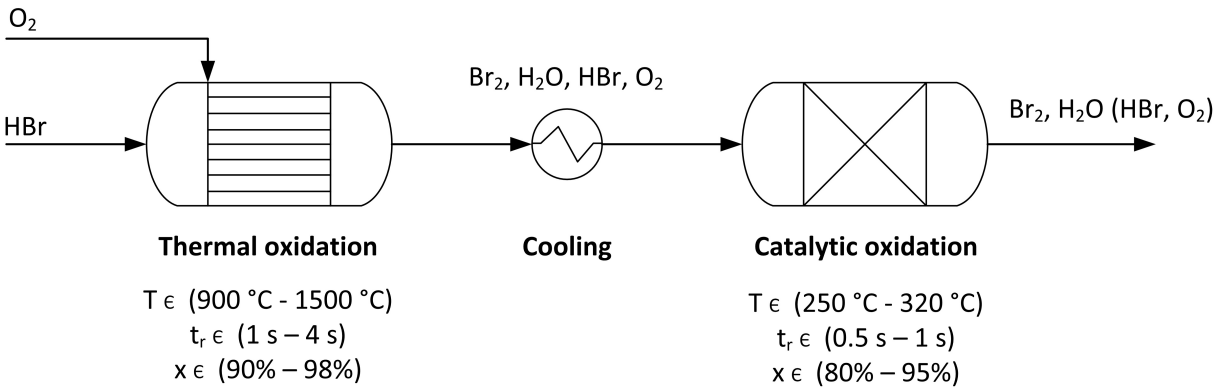


Figure 5.11.: Schematic representation of the strategy proposed for hydrogen bromide oxidation

## 5.5. Acknowledgments

Financial support from the Graduate School of Energy Efficient Production and Logistics (*Forschungsschule für Energieeffiziente Produktion und Logistik*) is gratefully acknowledged.

The authors would also like to express their gratitude to SASOL for providing the alumina support and their appreciation for the assistance of Ms. Meuris from the Lehrstuhl für Biomaterialien und Polymerwissenschaften in the SEM and EDX analysis of the catalyst.

## Preamble

The following chapter has been published as:

**González Rebordinos, Kampwerth, J., Agar, D.W.** (2017): "Flowsheeting and optimisation of the BrOx cycle for $CO_2$-free energy production from natural gas" in *Energy* 133, pp. 327 – 337.

This article is partly based on the calculations performed by Mr. Kampwerth during his Master thesis: "Detailed flowsheeting and heat integration of the BrOx cycle for $CO_2$-free energy production from natural gas". Conceived, directed and supervised by myself and evaluated by Prof. Agar. An initial working simulation of the plant was provided by myself.

### 5.5.1. Table of contributions to chapter 5

Table 5.2.: Contributions to Chapter 5

| *Contributor* | *Contribution percentage* |
|---|---|
| Jesús González Rebordinos | 60 |
| Jan Kampwerth | 35 |
| David W. Agar | 5 |

## Abstract

The BrOx (Bromination-Oxidation) cycle is a novel process that enables energy generation from natural gas without concomitant $CO_2$ emissions and thus a promising strategy against climate change. The cycle's main unit operations are two exothermic reactions, namely methane bromination and hydrogen bromide oxidation, a carbon separation unit, a water-bromine separation and a bromine recycle that result in an overall process in which methane and oxygen yield water, solid carbon and energy. The flowsheeting of the BrOx cycle has been carried out with Aspen Plus® and has been optimised. The results show that complete conversion during methane bromination can be achieved while ensuring that by-products are in trace amounts. Hydrogen bromide oxidation has been simulated with a first thermal step followed by a catalytic one obtaining high equilibrium conversions and the use of oxygen has been determined to be advantageous to the use of air. Chlorine has been considered as an alternative halogen although the comparison of the energy efficiencies and the number of equipments necessary in both processes show that bromine is the most suitable halogen for the process. The final flowsheet after heat integration results in a theoretical energy generation efficiency of 73.30% thus showing that the BrOx cycle is both a feasible and a promising strategy for $CO_2$-free energy generation from fossil fuels.

# 6. Flowsheeting and optimisation of the BrOx cycle for $CO_2$-free energy production from natural gas

## 6.1. Introduction

Energy consumption has increased substantially in the last century due to the steady growth of both the average standard of living and of world population. Currently, more than 80% of the world annual energy demand (ca. 500 EJ in 2014) is satisfied by the combustion of fossil fuels, a process that implies the formation of $CO_2$. The emissions of this greenhouse gas have lead to an unprecedented increase in its atmospheric concentration which scientific consensus considers to be the main cause of climate change [12]. An agreement as been recently achieved at the 2015 United Nations Climate Change Conference (COP21) that intends to limit the increase in the global average temperature to less than 2 °C above pre-industrial levels. Therefore a reduction in $CO_2$ emissions is mandatory [62]. Energy generation is the largest anthropogenic $CO_2$ source and therefore avoiding or minimising these emissions is the most direct strategy to accomplish COP21 agreement objectives [1].

Although the use of fossil fuels for energy generation has continually increased during the last century and contrary to popular belief, the proven reserves of fossil fuels have steadily increased as well during the last decades. Oil reserves have gone from 1039,3 thousand million barrels in 1992 to 1668,9 by the end of 2012 while natural gas reserves went from 117,6 trillion cubic meters in 1992 to 187,3 by the end of 2012 [1]. Additionally, there are big amounts of fossil fuel resources that are not yet either technically or economically exploitable, although this can soon change as demonstrated by the shale gas boom propitiated by the development of new technologies (horizontal drilling and hydraulic fracture) and by high oil and gas prices [67]. The resource potential of shale gas is estimated at 13903 EJ and that of methane hydrates is of 40274 EJ [66]. This demonstrates that the use of fossil fuels is less limited by their availability than by the $CO_2$ emissions associated to their combustion.

The strategies for reducing $CO_2$ emissions derived from energy production can be separated into two categories: use of non-fossil fuel energy sources or decarbonisation of fossil fuels. Alternatives to fossil fuels are renewable technologies (solar, wind, biomass) nuclear energy and hydroelectric among others. Renewable energies are experiencing a boom in the last years driven in part by a very favorable public

opinion and by the perspective of reducing the energy dependency on foreign countries. Nonetheless, the implementation of renewable energies for energy production is still very low and they supplied less than 2% of the total world energy production in 2012. Additionally, the price of renewable energies is still too high and the implementation of these technologies still requires technical advances to give a definitive solution at the challenging energy storage and to guarantee continuous energy supply from a fluctuating energy production. Nuclear energy is not affected by fluctuations but nuclear fission implies the production of radioactive wastes that last thousands of years and are thus problematic to store. Society is currently very critical towards nuclear energy as it is perceived by the public as a dangerous and environmentally unfriendly technology prone to accidents like those of Three Miles Island, Chernobyl and more recently Fukushima. Alternative technologies to fossil fuels, although important, still require decades of technical improvements and it is widely accepted that fossil fuels will remain the dominant energy source in the near future thus making decarbonisation of fossil fuels the most important strategy to reduce $CO_2$ emissions [65, 47, 44].

Well-known fossil decarbonisation techniques are carbon capture and storage (CCS) and methane pyrolysis. CCS consists on capturing $CO_2$ before or after combustion and sequestering it under the ocean or in an underground geological formation thus preventing it from entering the atmosphere. This technology lacks the acceptance of a large section of the public and aspects such as storage capacity and long-term reliability are not yet fully understood [81]. Methane pyrolysis is the decomposition of methane into hydrogen and solid carbon, so that the hydrogen can later react with oxygen to result in a net release of energy. The main drawback of this process is that it is an endothermic reaction that requires heat introduction at temperatures higher than 1200 °C. This involves electricity costs and leads to carbon deposition at the walls of the reactor, two problems that do not have yet a feasible technical solution [41, 47, 44].

The BrOx (bromination-oxidation) cycle is a novel process that enables the decarbonisation of energy generation from fossil fuels [105]. It consists of two exothermic reactions with a bromine recycle between them that result in a net reaction in which methane and oxygen yield solid carbon, water and energy, thus avoiding $CO_2$ production. An schematic view of the cycle is shown in figure 6.1.

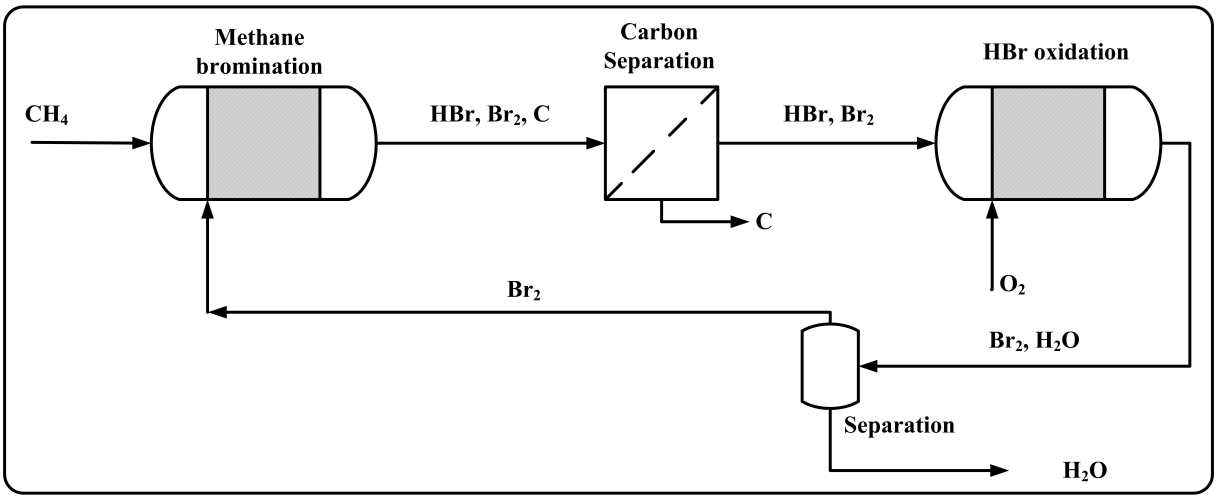


Figure 6.1.: Schematic representation of the BrOx cycle

In a first step, methane reacts exothermically with bromine (Equation 6.1.1) to yield solid carbon and hydrogen bromide. Excess bromine must be used in order to ensure full conversion of methane. Following separation of the solid carbon, the gas stream is oxidised in a second reactor yielding water and bromine in an exothermic reaction (Equation 6.1.2). The remaining gas stream is mainly water and bromine, and after separation, bromine can be recycled to the bromination reactor. Therefore the BrOx cycle results in a net reaction in which methane and oxygen yield solid carbon, water and energy without concomitant $CO_2$ emissions (Equation 6.1.3).

$$CH_4 + 2Br_2 \rightarrow C\,(s) + 4HBr \qquad \Delta H_r^o = -132.47kJ/mol \tag{6.1.1}$$

$$4HBr + O_2 \rightleftarrows 2Br_2 + 2H_2O \qquad \Delta H_r^o = -364.32kJ/mol \tag{6.1.2}$$

$$CH_4 + O_2 \rightleftarrows C\,(s) + 2H_2O \qquad \Delta H_r^o = -496.79kJ/mol \tag{6.1.3}$$

In the BrOx cycle the carbon is not fully oxidised and therefore the energy released is limited to a fraction of that released during conventional methane combustion. As shown in figure 6.2 the maximum energy that can be released in the BrOx cycle is slightly above 55% of the reaction enthalpy of methane combustion. Nonetheless, the remaining 45% is not lost as it is in CCS, but is stored in the solid carbon that can be sequestered safely and easily for future use. The solid carbon produced during the cycle is also a potentially valuable product that can be sold, although its price strongly depends on the type of carbon and its quality.

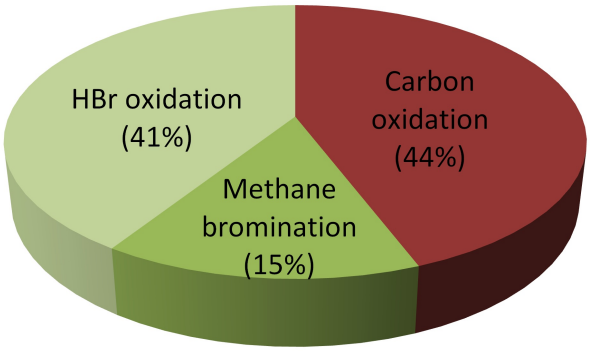


Figure 6.2.: Energy released in the BrOx cycle compared to methane combustion

## 6.2. Methodology

In the present work experimental data and theoretical models have been used to perform the steady-state simulation of the BrOx cycle. The simulation has been performed mainly with the software Aspen Plus® and several reaction and separation strategies as well as the effect of modifying critical parameters (inlet temperature, bromine to methane ratio,...) have been simulated and compared to ensure the optimal flowsheeting of the process. The use of chlorine as an alternative to bromine for the cycle has been considered by simulating the ClOx (Chlorination-oxidation) cycle and comparing its performance to that of the BrOx cycle. Additionally, the heat integration of the BrOx cycle has been performed.

### 6.2.1. Preconditions and properties of the steady-state simulation

The capacity of a medium size power plant (100 MW) has been used as a base of calculus for the simulation of the BrOx cycle. This base of calculus of 100 MW is referred to the maximum theoretical power that could be generated by the BrOx cycle assuming that the plant is perfectly efficient and that there are no energy losses. This means that a total of 496.8 kJ could be obtained per mol of methane and therefore 725 kmol/h of methane are used as the feed to the plant. In this way the energy outcome of the simulated BrOx cycle can be compared with the maximum 100 MW and provide a cycle efficiency value. For simplicity, the feed is considered to be 100% methane although typical compositions of natural gas should not pose a problem to the BrOx cycle plant since other hydrocarbons would react similarly to methane and $CO_2$ can be easily separated beforehand.

The species considered in the steady-state simulation of the BrOx cycle are shown in table 6.1.

Table 6.1.: Species considered in the steady-state simulation of the BrOx and ClOx cycle

| | | | | | | |
|---|---|---|---|---|---|---|
| $H_2$ | $C$ | $CH_4$ | $C_2H_2$ | $C_2H_4$ | $C_2H_6$ | $Br_2$ |
| $HBr$ | $CH_3Br$ | $C_2H_5Br$ | $C_2H_3Br$ | $CH_2Br_2$ | $CHBr_3$ | $CBr_4$ |
| $Cl_2$ | $HCl$ | $CH_3Cl$ | $C_2H_5Cl$ | $C_2H_3Cl$ | $CH_2Cl_2$ | $CHCl_3$ |
| $CCl_4$ | $O_2$ | $H_2O$ | $CO_2$ | $N_2$ | $H_2SO_4$ | $H_3O^+$ |
| $OH^-$ | $H_2SO_4^{2-}$ | $SO_4^{2-}$ | | | | |

Amongst the species considered are obviously methane, bromine, hydrogen bromide, oxygen, water and solid carbon together with brominated hydrocarbons that have been suggested as likely by-products in previous studies [55, 56]. Additionally, chlorine and chlorinated hydrocarbons have been added so that the simulation can deal with impurities of chlorine on the feed stream and to enable the flowsheeting of the ClOx cycle. Nitrogen is also considered so that air can be used as feed for the hydrogen bromide oxidation reactor and compared with the use of pure oxygen. Since it is possible that methane conversion is not complete, carbon dioxide has been introduced in the simulation. The reason for adding sulfuric acid and ions generated with *Elec Wizard* of Aspen Plus® ($H_3O^+$, $OH^-$, $H_2SO_4^-$ and $SO_4^{2-}$) is that one of the separation methods to be simulated is water absorption with sulfuric acid.

A fundamental decision in the process of implementing a simulation in Aspen Plus® is the selection of the property method. After testing all available property methods built-in the software, only four methods were able to predict the azeotrope that water and bromine form. This methods were PSRK, RKSMHV2, UNIF-LBY and UNIF-DMD. These methods are also able to offer liquid-liquid equilibrium (LLE) data for the bromine-water system although all methods were unsuccessful at showing LLE data consistent with experimental results found on the literature [106]. Therefore the regression mode was used to adapt the property methods to experimental LLE data showing that only PSRK (Predictive Soave-Redlich-Kwong) was able to achieve considerable improvements. This model uses the Redlich-Kwong-Soave equation of state for pure compounds (equation 6.2.1) combined with predictive rules.

$$P = \frac{RT}{v-b} - \frac{a\alpha\left(T\right)}{v\left(v+b\right)} \tag{6.2.1}$$

Figure 6.3 shows that the original PSRK presents noticeable deviations from experimental data. After applying the regression mode, these deviations disappear almost completely for liquid-liquid equilibrium (Figures 6.3a and 6.3b) and they are considerably reduced for vapour-liquid equilibrium (Figures 6.3c and 6.3d) proving that the PSRK successfully predicts the azeotrope and the miscibility gap between bromine and water. Furthermore, PSRK is appropriate for non-polar ($CH_4$, $Br_2$) and polar compounds ($H_2O$, $HBr$) in combination with light gases ($CH_4$) and for high temperatures such as those at which both methane bromination and hydrogen bromide oxidation are to be carried out. However it is not suitable for modeling electrolyte systems and therefore ELECNRTL was used for simulating drying with sulphuric acid.

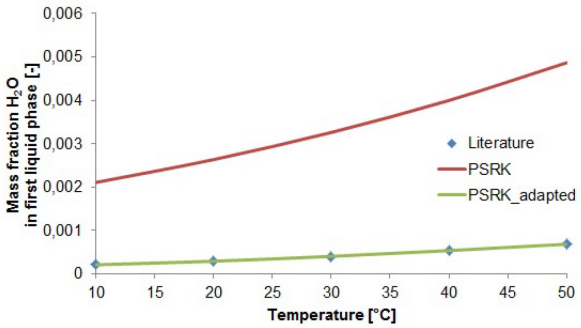


(a) Temperature dependency of the solubility of water in bromine according to literature [106] and simulation results

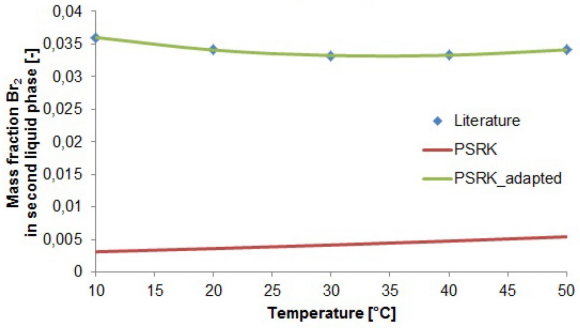


(b) Temperature dependency of the solubility of bromine in water according to literature [106] and simulation results

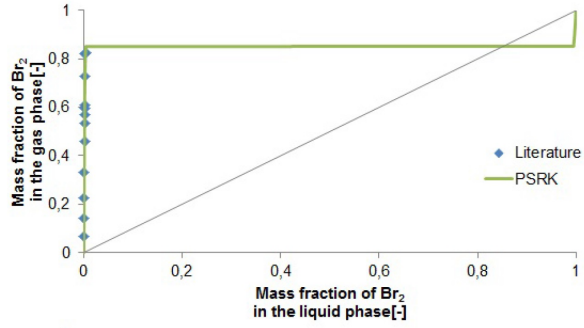


(c) Comparison between experimental vapor-liquid data [107] and simulation results with PSRK

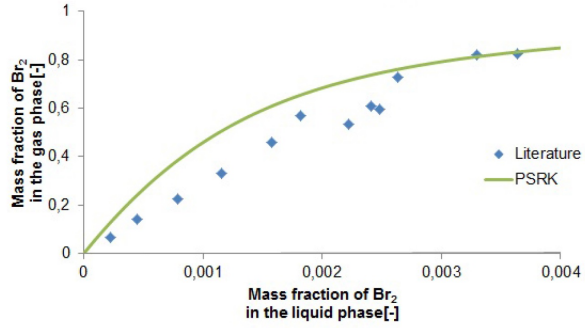


(d) Comparison between experimental vapor-liquid data [107] and simulation results with PSRK (enlarged)

Figure 6.3.: Comparison of LLE and VLE data from literature with PSRK predictions before and after application of regression mode

## 6.3. Steady-state simulation of the BrOx cycle

The steady-state simulation of the BrOx cycle and its optimisation has been divided in two main units: reaction section and separation section. The former includes methane bromination, carbon separation and hydrogen bromide oxidation whereas the later consists on the separation of bromine from water and the recycle of the halogen to the methane bromination reactor.

### 6.3.1. Reaction section

In this simulation no reaction kinetics are considered and therefore the *RGibbs*-block is used to calculate equilibrium compositions via minimisation of Gibbs energy constrained by an atomic balance. Thermodynamic calculations on methane bromination (6.4a) show that equilibrium conversions close to full conversion are possible for temperatures up to 1800 °C and thus methane conversion is only kinetically limited. Therefore, an inlet temperature of 800 °C is used as it has been experimentally de-

termined in a previous study to be kinetically feasible [105]. Inlet temperature has been set at the minimum feasible temperature to reduce energy demand during preheating but it could be increased with virtually no influence on the cycle should the residence time be lower. The reactor is operated adiabatically in order to reduce the residence time and to produce heat at the highest temperature possible. A sensitivity analysis applied to the bromination reactor shows that there is a slight increase of the equilibrium conversion with over-stoichiometric feed ratios as it is predicted by Le Chatelier's principle. For these reason and in order to ensure a complete conversion of methane, a conservative value for bromine excess of 10% is used.

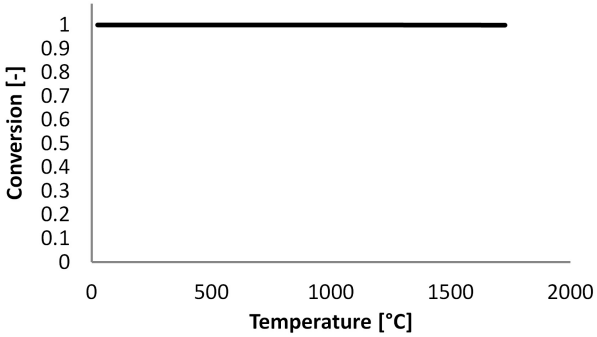


(a) Equilibrium conversion vs temperature at stoichiometric amounts and ambient pressure for methane bromination

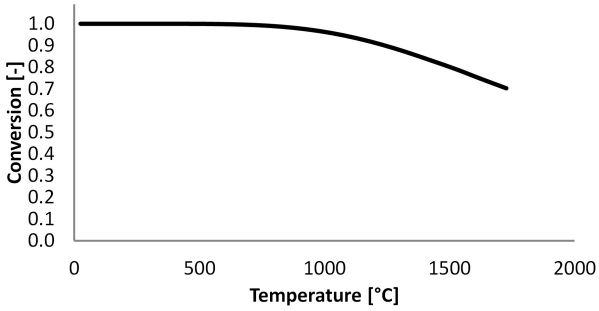


(b) Equilibrium conversion vs temperature at stoichiometric amounts and ambient pressure for hydrogen bromide oxidation

Figure 6.4.: Equilibrium conversion dependency with temperature

Subsequent to methane bromination, the solid carbon produced needs to be separated before feeding the stream to the oxidation reactor, in order to avoid its reaction with oxygen that would lead to $CO_2$ production. Carbon separation can be performed by means of an electro-filter or by combining a cyclone to separate the bigger particles with a bag filter that removes the finest. Since no information on the particle size is yet available, a *SSplit*-block was used assuming that all solid carbon is removed.

Thermodynamic calculations show that hydrogen bromide oxidation presents high equilibrium conversion up to approximately 700 °C and and that it drops noticeably with increasing temperatures (figure 6.4b). Kinetic simulations performed using a reaction rate expression expression found on the literature and supported by experimental data show that hydrogen bromide oxidation proceeds within residence times in the order of one second at temperatures of at least 750 °C [108]. Since temperatures higher than 700 °C would imply equilibrium conversions lower than unity and at temperatures inferior to 700 °C the reaction proceeds extremely slow so it can be concluded that complete conversion cannot be achieved solely with thermal oxidation. Therefore, a solution is proposed in which a first thermal oxidation reactor is used to convert most of the hydrogen bromide at high temperatures followed by cooling and a catalytic reactor operating at lower temperatures to. A temperature of 800°C was selected as the inlet temperature to the thermal oxidation reactor. This reactor is operated with a tailored temperature profile so that the outlet temperature is 950

°C thus ensuring a feasible reaction rate while guaranteeing high equilibrium conversion. The amount of heat that needs to be retired to achieve such a temperature profile was calculated to be 49.4 MW. After the oxidation reactor, the stream is cooled down to 350 °C and fed to a catalytic reactor operating isothermally. This temperature was selected because it is within the range in which the most common catalysts for hydrogen bromide oxidation ($CeO_2/ZrO_2$, $RuO_2/TiO_2$ and $TiO_2$) offer high activity [109, 110, 111]. Figure 6.5 shows the reaction section.

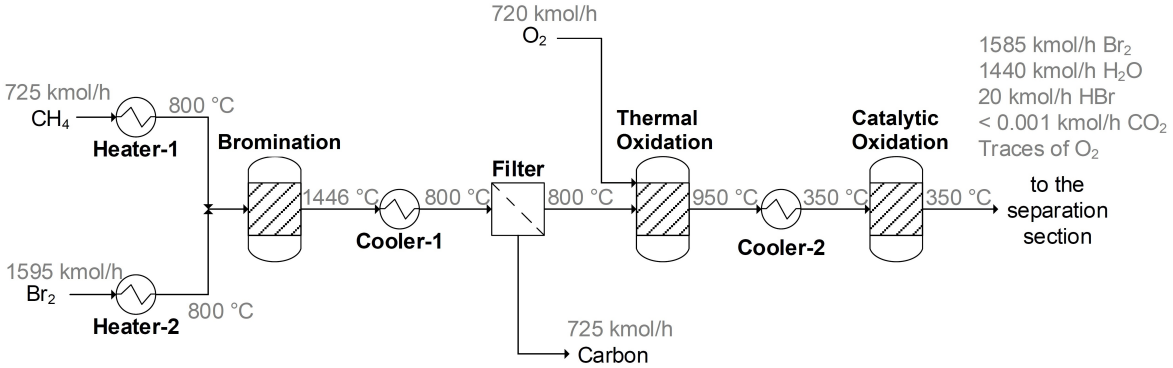


Figure 6.5.: Flowsheeting of the reaction section

As can be seen in the stream table of the final BrOx cycle (tables 6.2, 6.3), by-products are present only in trace amounts after methane bromination. The main products are carbon and water together with a small amount of hydrogen due to methane pyrolysis that, in case that the kinetics are fast enough to actually produce it, will either combine with the remaining bromine to yield hydrogen bromide at lower temperatures or will react to water in the oxidation reactor. A high conversion of hydrogen bromide is achieved in the first oxidation reactor and it is completed in the catalytic step. Naturally, the catalytic oxidation of hydrogen bromide is limited by the kinetics of the reaction and it could be that complete conversion of oxygen could not be achieved within feasible residence times. Should that be the case, an excess of hydrogen bromide could be used. An alternative solution would be the use of a third reactor in which hydrogen is used as an oxygen scavenger to regulate its final concentration to values acceptable within the cycle.

### 6.3.2. Separation section

The resulting stream of the reaction section is composed mainly of bromine and water and requires separation in order to recycle bromine to the first reaction step and to get the purified water out of the process. Given the miscibility gap existing between bromine and water, it seems logical to use a decanter to exploit it. The purity of both outlet streams is still inadequate and thus further separation is required but the decanter is a cost-efficient primary separator. The use of polyurethane membranes is a possible separation technique. However, these membranes are recommended for

small flow rates and for streams with low concentrations of bromine rendering them unfeasible for this process [112, 113].

Distillation is a promising alternative given the difference between bromine and water boiling points. It has to be considered that bromine-water system form an azeotrope with the following characteristics:

- Pressure: 1.01325 bar
- Temperature 48.41 °C
- Composition: 73.85 mol% $Br_2$, 25.15 mol% $H_2O$

Therefore, it can be concluded that a single column would not suffice to conduct the separation. Another strategy that deserves consideration is absorption with sulphuric acid since it is highly hygroscopic. High concentrated sulphuric acid (ca. 98%) is widely used in industrial processes as a drying agent for gaseous streams although a high water content would imply using big amounts of concentrated sulphuric acid and an energy-intensive regeneration.

For the separation section of the BrOx cycle four strategies have been selected as the most promising and they have been simulated and compared (figure 6.6). In the first separation train (figure 6.6a) a heat exchanger is used to cool the incoming stream to 25 °C condensing bromine and water followed by a decanter from which two liquid streams are obtained, a bromine-rich and a water-rich stream. The bromine-rich stream is fed to a distillation column with 9 stages, a reflux ratio of 3 and a distillate-to-feed ratio of 0.04 while the water-rich stream is fed to another column that consists of 7 stages, a reflux ratio of 0.79 and a distillate-to-feed ratio of 0.007. At the bottom of the bromine column a bromine stream containing traces of other compounds is obtained and recycle to the bromination reactor. At the bottom of the water column a stream composed mainly of water and around 20 kmol/h of hydrogen bromide is obtained and removed from the system. The streams at the top of both columns are recycle to the condenser at the beginning of the separation train.

The second separation train considered (figure 6.6b) is similar to the previous although the stream at the top of the bromine distillation column is taken to a flash prior to its recycle to the condenser. This enables the easy separation of any residual oxygen that can be recycled to the thermal oxidation reactor thus making possible to use a small excess of oxygen in hydrogen bromide oxidation. This improves equilibrium conversion and, what is more important, improves the reaction rate minimising kinetic limitations. A consequence of achieving a higher conversion is that water separation is less complex, requiring only 5 stages, a reflux ratio of 0.3 and a distillate-to-feed ratio of 0.006 and obtaining at the bottom a water stream that contains only 1.3 kmol/h of hydogen bromide. The only parameter changing in bromine distillation column is the distillation-to-feed ration that is now 0.022.

In the third separation strategy (figure 6.6c) the bromine distillation column is changed for an absorption column with 7 stages in which the bromine-rich stream is put in contact with a stream containing concentrated sulphuric acid (98%). As a result, a water stream containing 20 kmol/h of hydrogen bromide is obtained at the

bottom of the water distillation column and a diluted sulphuric acid stream containing 18.5 kmol/h is obtained at the bottom of the absorption column. Separation train 4 (figure 6.6d) is similar to 3 but with an additional reboiler at the bottom of the absorption column that reduces the amount of bromine leaving the system with the diluted sulphuric acid stream to 10.6 kmol/h.

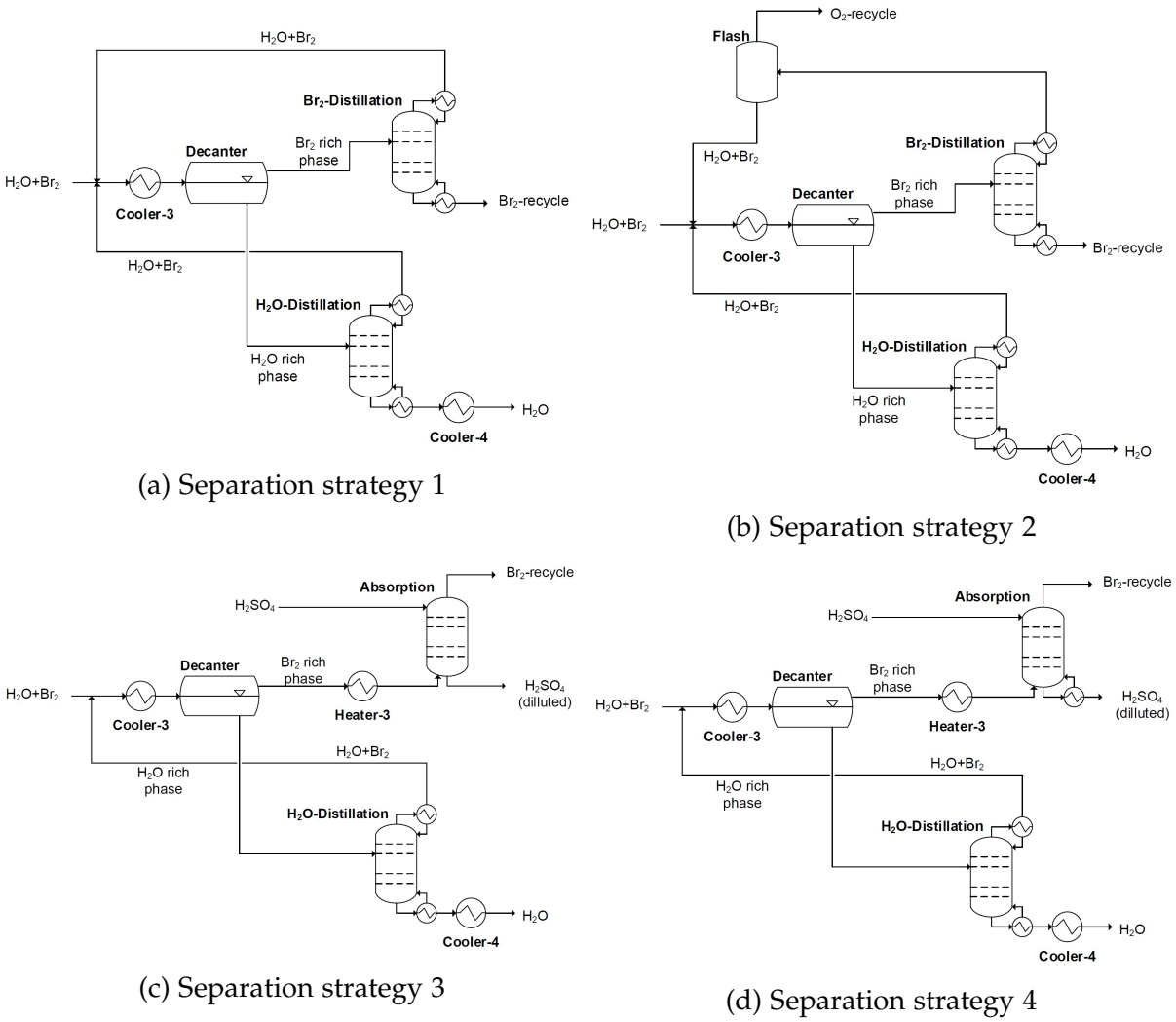


(a) Separation strategy 1

(b) Separation strategy 2

(c) Separation strategy 3

(d) Separation strategy 4

Figure 6.6.: Separation strategies

Comparing the four separation strategies, it can be easily seen that bromine losses, either in the form of hydrogen bromide or bromine, are lower when using separation train 2. Additionally, when comparing the overall energy gain of the cycle (energy production - energy consumption) the strategies involving absorption are clearly less efficient due to the high energy costs involved in sulphuric acid regeneration. Another issue that deserves consideration is that introducing a new substance such as sulphuric acid is that its accumulation in the cycle may lead to problems. Therefore, the second separation train (figure 6.6b) has been selected for the BrOx cycle. The final flowsheet of the cycle can be seen in figure 6.7 and the stream table with the most important parameters in tables 6.2 and 6.3. In the stream table the molar fraction of

all components is shown. Under by-products, all considered brominated compounds have been clumped together.

### 6.3.3. Flowsheet of the BrOx cycle

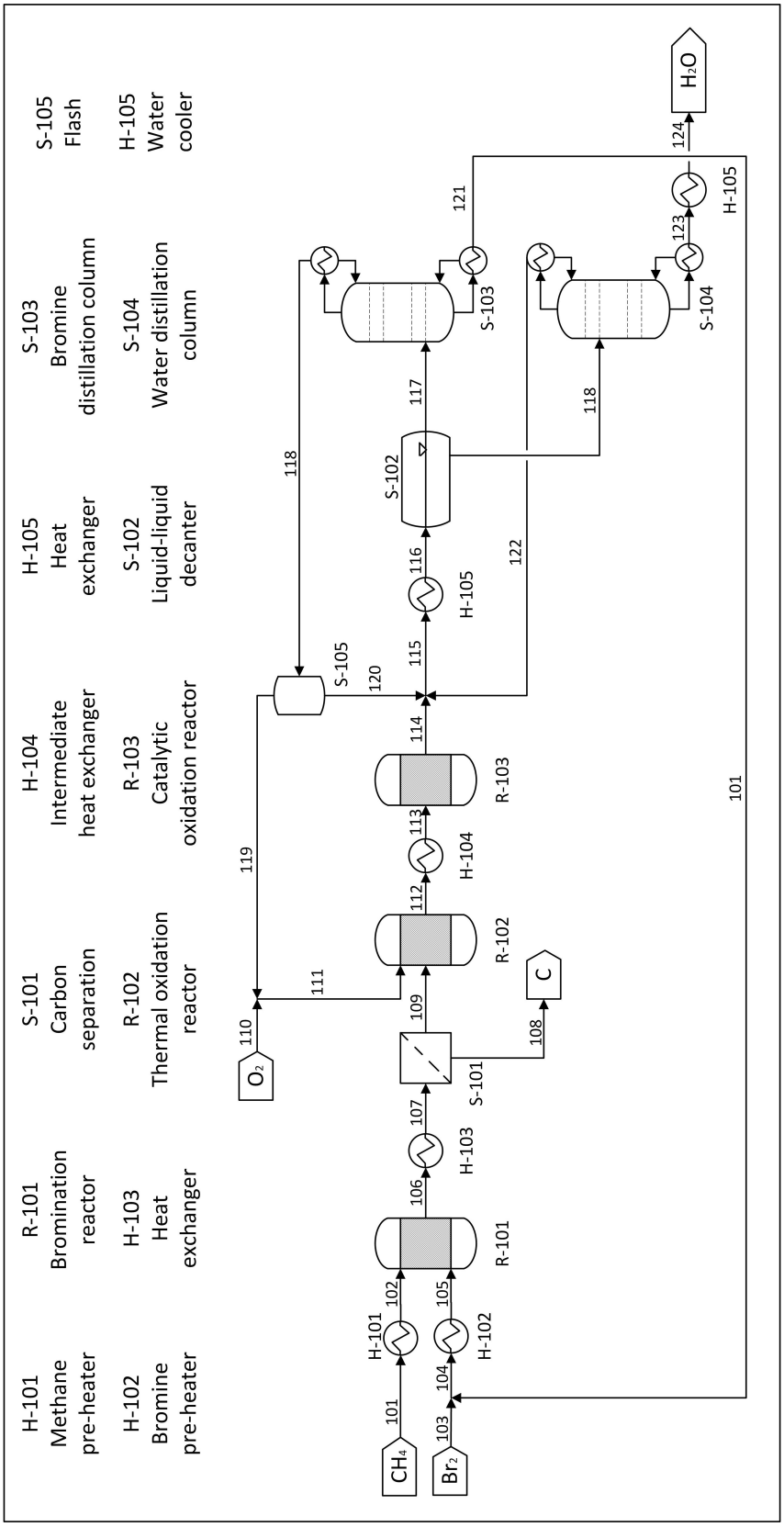


Figure 6.7.: Flowsheet of the BrOx cycle

| *Stream No.* | *101* | *102* | *103* | *104* | *105* | *106* | *107* | *108* | *109* | *110* | *111* | *112* |
|---|---|---|---|---|---|---|---|---|---|---|---|---|
| *Temperature [°C]* | 20 | 800 | 20 | 58 | 800 | 1446 | 800 | 800 | 800 | 20 | 20 | 950 |
| *Total flow rate [kmol/h]* | 725.000 | 725.000 | 0.700 | 1595.000 | 1595.000 | 3769.999 | 3769.999 | 725.000 | 3044.999 | 724.2670 | 725.177 | 3105.170 |
| *Molar fraction* | | | | | | | | | | | | |
| $CH_4$ | 1.000 | 1.000 | < 0.001 | < 0.001 | < 0.001 | < 0.001 | < 0.001 | < 0.001 | < 0.001 | < 0.001 | < 0.001 | < 0.001 |
| $Br_2$ | 0.000 | 0.000 | 1.000 | 1.000 | 1.000 | 0.040 | 0.040 | 0.000 | 0.050 | 0.000 | <0.001 | 0.475 |
| $C$ | 0.000 | 0.000 | 0.000 | 0.000 | 0.000 | 0.192 | 0.192 | 1.000 | 0.000 | 0.000 | 0.000 | 0.000 |
| $O_2$ | 0.000 | 0.000 | 0.000 | < 0.001 | < 0.001 | < 0.001 | < 0.001 | 0.000 | < 0.001 | 1.000 | 1.000 | 0.019 |
| $HBr$ | 0.000 | 0.000 | 0.000 | < 0.001 | < 0.001 | 0.766 | 0.766 | 0.000 | 0.984 | 0.000 | < 0.001 | 0.077 |
| $H_2O$ | 0.000 | 0.000 | 0.000 | < 0.001 | < 0.001 | < 0.001 | < 0.001 | 0.000 | < 0.001 | 0.000 | < 0.001 | 0.428 |
| $CO_2$ | 0.000 | 0.000 | 0.000 | < 0.001 | < 0.001 | < 0.001 | < 0.001 | 0.000 | < 0.001 | 0.000 | < 0.001 | < 0.001 |
| $H_2$ | 0.000 | 0.000 | 0.000 | < 0.001 | < 0.001 | 0.002 | 0.002 | 0.000 | 0.002 | 0.000 | 0.000 | < 0.001 |
| *By-products* | 0.000 | 0.000 | 0.000 | < 0.001 | < 0.001 | < 0.001 | < 0.001 | < 0.001 | < 0.001 | < 0.001 | < 0.001 | < 0.001 |

Table 6.2.: Stream table of the BrOx cycle (Part 1)

| *Stream No.* | *113* | *114* | *115* | *116* | *117* | *118* | *119* | *120* | *121* | *122* | *123* | *124* |
|---|---|---|---|---|---|---|---|---|---|---|---|---|
| *Temperature [°C]* | 350 | 350 | 335 | 25 | 25 | 53 | 25 | 25 | 58 | 66 | 100 | 25 |
| *Total flow rate [kmol/h]* | 3105.170 | 3045.410 | 3088.470 | 3088.470 | 1630.160 | 35.864 | 0.531 | 35.333 | 1594.300 | 7.718 | 1450.580 | 1450.580 |
| *Molar fraction* | | | | | | | | | | | | |
| $CH_4$ | < 0.001 | < 0.001 | < 0.001 | < 0.001 | < 0.001 | < 0.001 | < 0.001 | < 0.001 | < 0.001 | < 0.001 | < 0.001 | < 0.001 |
| $Br_2$ | 0.475 | 0.524 | 0.528 | 0.528 | 0.998 | 0.848 | 0.287 | 0.856 | 1.000 | 0.739 | < 0.001 | < 0.001 |
| $C$ | 0.000 | 0.000 | 0.000 | 0.000 | 0.000 | 0.000 | 0.000 | 0.000 | 0.000 | 0.000 | 0.000 | 0.000 |
| $O_2$ | 0.019 | < 0.001 | < 0.001 | < 0.001 | < 0.001 | 0.010 | 0.650 | < 0.001 | < 0.001 | < 0.001 | < 0.001 | < 0.001 |
| $HBr$ | 0.077 | < 0.001 | < 0.001 | < 0.001 | < 0.001 | < 0.001 | < 0.001 | < 0.001 | < 0.001 | < 0.001 | < 0.001 | < 0.001 |
| $H_2O$ | 0.428 | 0.476 | 0.472 | 0.472 | 0.002 | 0.141 | 0.032 | 0.143 | < 0.001 | 0.260 | 0.999 | 0.999 |
| $CO_2$ | < 0.001 | < 0.001 | < 0.001 | < 0.001 | < 0.001 | < 0.001 | < 0.001 | < 0.001 | < 0.001 | < 0.001 | < 0.001 | < 0.001 |
| $H_2$ | < 0.001 | < 0.001 | < 0.001 | < 0.001 | < 0.001 | < 0.001 | < 0.001 | < 0.001 | < 0.001 | < 0.001 | < 0.001 | < 0.001 |
| *By-products* | < 0.001 | < 0.001 | < 0.001 | < 0.001 | < 0.001 | < 0.001 | < 0.001 | < 0.001 | < 0.001 | < 0.001 | < 0.001 | < 0.001 |

Table 6.3.: Stream table of the BrOx cycle (Part 2)

Some alternative scenarios have been considered and simulated on the final flowsheet of the BrOx cycle (figure 6.7). These scenarios concern the effecto that the purity of the bromine feed may have on the cycle, how bromine losses due to the contamination of the solid carbon affect it and what is the effect of using air instead of pure oxygen during HBr oxydation.

Experimental data indicates that the carbon produced during methane bromination may contain solid brominated compounds reaching a bromine content lower than 2% w/w at 1070 °C. This bromine content decreases with increasing temperature and, by extrapolation from experimental data, at the final reaction temperature of 1450 °C a bromine content inferior to 0.04% w/w should be achieved. Nonetheless, a make-up stream of bromine is used to compensate for any bromine loss as shown in the flowsheet of the BrOx cycle.

Bromine usually contains impurities in the form of chlorine due to its production method. Therefore a chlorine content up to 1% has been simulated in the bromine stream, showing that the effect on the cycle is negligible since chlorine would react preferably with methane in the bromination reactor yielding carbon hydrogen chloride and traces of chlorinated hydrocarbons that eventually react with oxygen in the oxidation section. Nonetheless a low chlorine content is preferred. The effect of the presence of hydrogen bromide in the recycle stream has also been analysed showing that its content should be minimised in order to improve equilibrium conversion in the bromination step, however small amounts are acceptable since they will only shift the equilibrium slightly.

In the oxidation step pure oxygen is fed to the thermal oxidation reactor. Obviously, air is cheaper than pure oxygen and therefore its use has been simulated. The results show that despite the economical advantage of using air there are several drawbacks that make pure oxygen the best option. The use of air would increase the size of all equipments following carbon separation since approximately 79% of it is inert nitrogen. A decrease of 12.64% of the overall energy output has been calculated to be a consequence of using air instead of nitrogen. Additionally, the use of air entails the need of separating nitrogen and removing it from the system to prevent accumulation which would imply a substantial increase of the costs of the separation unit since either big bromine losses or the use of energy-extensive cryogenic separations will be required. Therefore, pure oxygen remains the option of choice for the BrOx cycle.

## 6.4. Is chlorine an alternative? ClOx vs. BrOx

Bromine acts as a catalyst in this process. It enables the reaction of methane with oxygen to yield solid carbon and water while avoiding $CO_2$ generation due to its high reactivity with methane and to the reactivity of hydrogen bromide with oxygen. Although other halogens like fluorine or iodine would not perform well in the cycle, chlorine remains a possibility. The use of chlorine has been simulated and the performance of the ClOx cycle has been compared with that of the previously simulated BrOx cycle. In order to do so, the Sumitomo process, which is the most up-to-date process for hydrogen chloride oxydation, has been adapted to the cycle and simulated [114].

An inlet temperature for chlorination reactor of 800 °C has been selected to overcome kinetic limitations and the reactor has been simulated isothermally since adiabatic operation would lead to an outlet temperature of 2286 °C although a tailored temperature profile could be used should the residence time resulting of isothermal operation be too long. The lower reactivity and the combination unfavourable thermodynamics at high temperature and low reaction rates at low temperatures renders unfeasible achieving complete conversion of hydrogen chloride making necessary the subsequent separation of the unreacted hydrogen chloride.

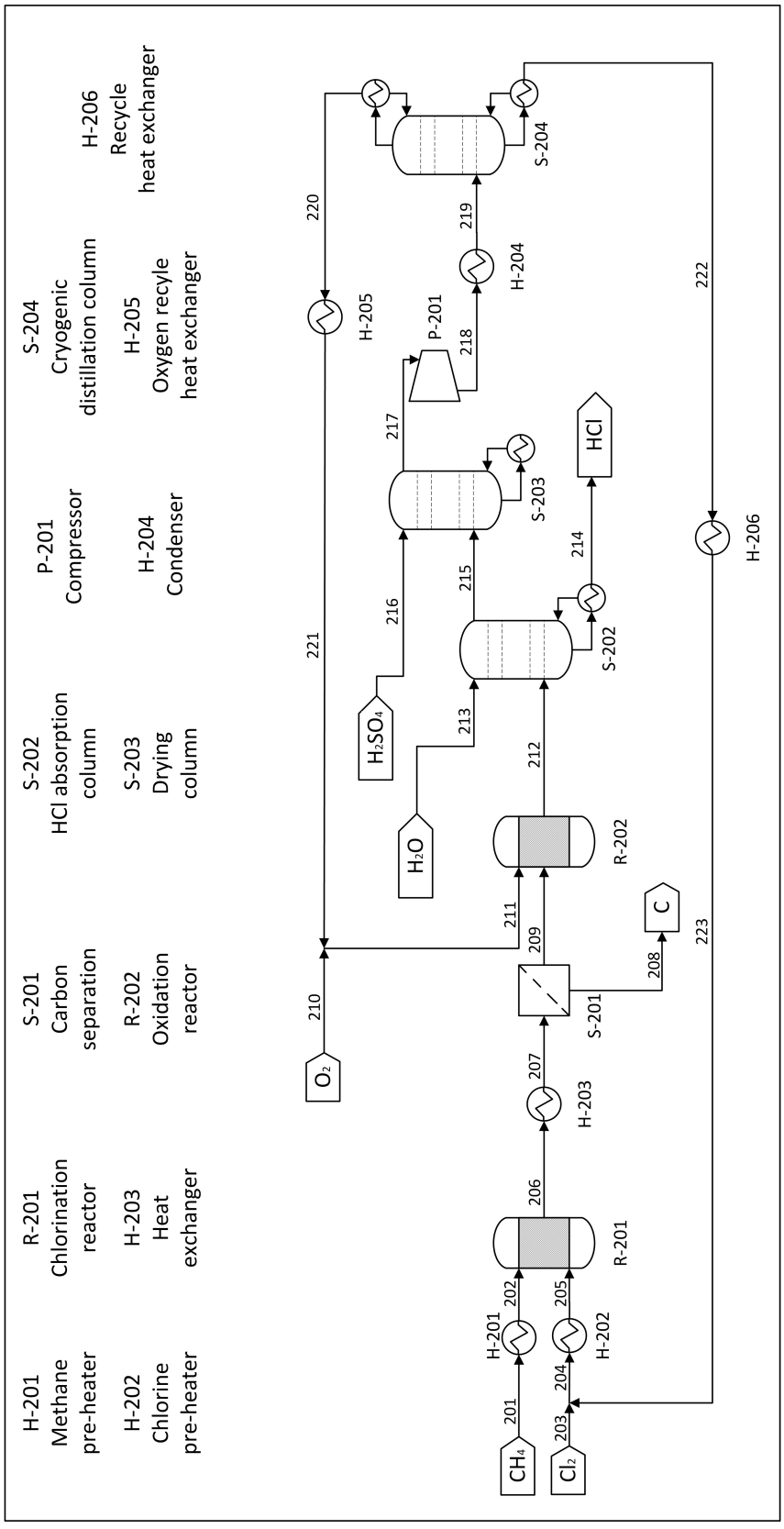


Figure 6.8.: Flowsheet of the ClOx cycle

Figure 6.8 shows the flowsheet of the proposed cycle. As can be seen, following catalytic oxidation at a temperature within 350 °C and 400 °C, an absorption column is used to remove hydrogen chloride from the system with a stream of water. A subsequent drying column is used to reduce the water content of the gas stream with a stream of concentrated sulphuric acid. Due to the incomplete conversion during the oxidation step, oxygen has to be separated from chlorine in order to recycle both streams to the oxidation and chlorination reactor respectively. This separation is carried out at high pressures (7 bar) and low temperatures (-26 °C) in a cryogenic distillation column.

The comparison between the ClOx and the BrOx cycle is done according to the overall energy gain since that is the final product of the process. ClOx cycle overall energy production is 95% of that of the BrOx cycle. This figure does not take into account the energy demand of the regeneration of sulphuric acid nor the energy demand of the separation of hydrogen chloride from water that should be performed to avoid chlorine loses. It is also clear that the number of apparatusses involved in the BrOx cycle is inferior to that of the ClOx cycle. This demonstrates the superior performance of bromine over that of chlorine for $CO_2$-free energy generation and thus bromine remains the halogen of choice for the cycle.

## 6.5. Heat integration of the BrOx cycle

In the BrOx cycle energy is released and consumed in several equipments making thus necessary the use of external utilities. In order to reduce the input of these utilities the heat integration of the cycle has been conducted by means of a Pinch analysis. A common minimum temperature difference of 10 K has been used within this analysis in which a hot composite and a cold composite curve have been created to determine the pinch point, which in this case lies at 805 °C (figure 6.9).

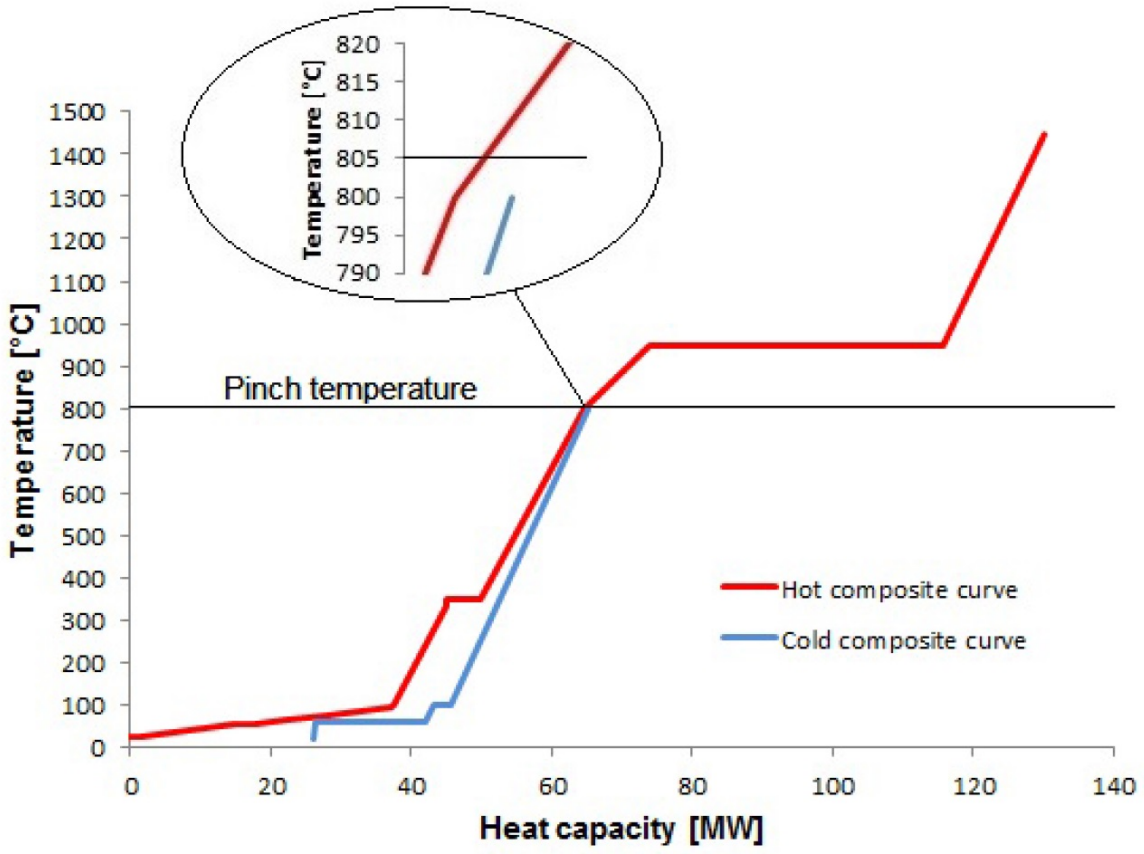


Figure 6.9.: Hot and cold composite curves of the BrOx cycle

The pinch analysis suggests building up a network of heat exchangers starting around the pinch point. Since in this case there are no cold streams available at temperatures higher than the pinch temperature there is at least one network of heat exchangers avoiding any external utilities for heating. Two promising strategies for heat integration have been found in this analysis which require three and four additional heat exchangers respectively. The results shown in table 6.4 show that both systems completely avoid the use of fired heat as well as low pressure steam (LPS) while considerably minimising the amount of cooling water.

Table 6.4.: Comparison of heat integration schemes for the BrOx cycle

| | *Number of additional heat exchangers* | *Use of LPS [t/h]* | *Use of fired heat [MW]* | *Production of HPS [t/h]* | *Use of cooling water [t/h]* | *Energy generation [MW]* | *Energy consumption [MW]* |
|---|---|---|---|---|---|---|---|
| *BrOx cycle* | 0 | 7.68 | 34.34 | 190.13 | 8,350 | 90.80 | 39.11 |
| *Heat integration 1* | 4 | 0 | 0 | 153.49 | 4550 | 73.30 | 0 |
| *Heat integration 2* | 3 | 0 | 0 | 151.58 | 4760 | 72.39 | 0 |

Although heat integration strategy 1 generates more energy than the second it also requires one additional heat exchanger and thus it has to be determined if it is advantageous from an economical point of view. In order to evaluate which option is more

beneficial, an average price for energy in the industry of 0.09 €/kWh was used, and the difference between the two heat integration options was calculated to be 230,000 €. The monetary savings due to the lower cooling water consumptions are calculated with a price of 0.06 €/t to be of 100,000 €. The difference in favour of the first heat integration option is 330,000 €, which taking into account an amortization time for equipments of three years leads to approximately 1,000,000 €, thus making beneficial the use of an additional heat exchanger. The flowsheet of the BrOx cycle with heat integration can be seen in figure 6.10.

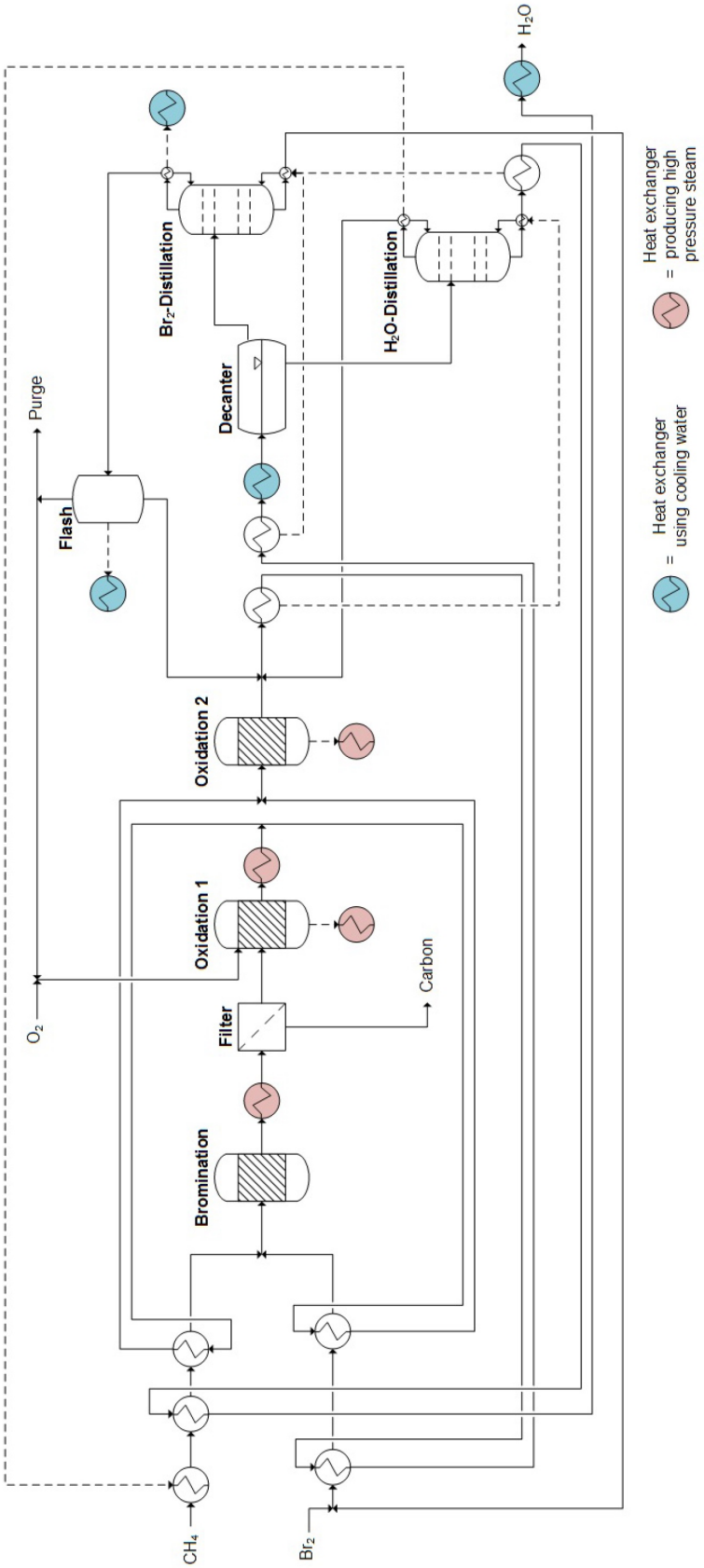


Figure 6.10.: Flowsheet of the BrOx cycle after heat integration

## 6.6. Conclusion

The flowsheeting of the BrOx cyle has been performed with Aspen Plus® and after heat integration it presents a theoretical energy production of 73.30 MW from a maximum of 100 MW. A 10% excess of bromine has been used during methane bromination to ensure good kinetics leading to conversions above 99.99% and to a negligible production of by-products. Following carbon separation a combination of thermal and catalytic oxidation have shown that conversions close to unity can be achieved in hydrogen bromide oxidation. In this section pure oxygen has been used instead of air because it results in a higher energy output and a much simpler separation. A separation strategy consisting of a first decanter, two small rectification columns and a flash has been proven to be optimal for the cycle.

The use of chlorine as an alternative halogen has been considered and the ClOx cycle has been simulated resulting in a lower energy production and a more complicated and likely expensive equipment mainly due to the more complex hydrogen chloride oxidation. Nonetheless, the presence of chlorine impurities in the bromine feed has been simulated. They lead to a tolerable decrease in the overall energy generation of the cycle since chlorine reacts readily with methane and small amounts of hydrogen chloride do not hurt noticeably the process. Nonetheless, a low chlorine content in the bromine feed is preferable.

Heat integration of the BrOx cycle has been carried out by means of a Pinch analysis resulting in the total avoidance of external heating of any sort and a reduction of approximately 50% of the required cooling water with the implementation of four additional heat exchangers. After heat integration of the process, it is able to generate energy with a theoretical energy efficiency of 73.30% thus showing that the BrOx cycle is a novel and feasible strategy for $CO_2$-free energy generation from natural gas that deserves to be considered and further studied.

An additional feature of the BrOx cycle that makes it more attractive is its flexibility. The cycle can be modified to obtain a different output than energy. One alternative scheme would be to carry out hydrogen bromide electrolyisis instead of its oxidation as the second step after methane bromination and its subsequent carbon separation. In this way the cycle would yield solid carbon and hydrogen although the overall process would consume energy. PEM electrolytic cells could be used to operate in the gas phase resulting in one stream composed mainly of bromine that is recycled to the bromination reactor and another stream of hydrogen that would require only drying and compression in order to be suitable for its use as chemical feedstock or as an energy carrier. Therefore a separation section would not be necessary in this configuration [115].

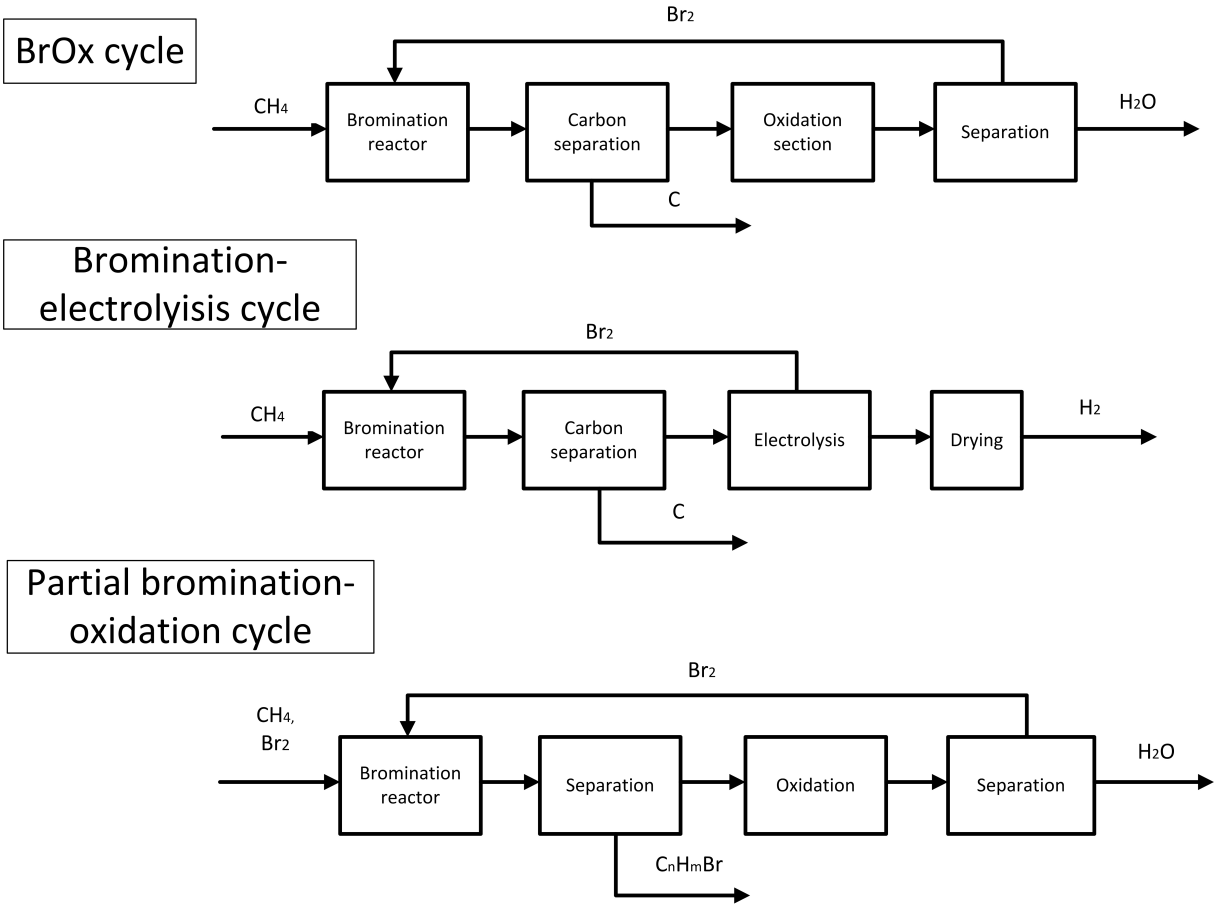


Figure 6.11.: Flexibility of the BrOx cycle

The plant can also be modified to produce brominated compounds such as bromomethane or dibromomethane that can be used as chemical intermediates. The modification of the plant would consist on reducing temperature and residence times during methane bromination so that a partial bromination of the methane is achieved that entails no carbon formation. It may be necessary the use of a catalyst to fine-tune the product distribution and a separation section should be used to achieve the required purities. The remaining hydrogen bromide can be taken to the oxidation section and proceed as in the normal BrOx cycle to ensure 100% halogen utilisation [116].

## 6.7. Acknowledgments

Financial support from the Graduate School of Energy Efficient Production and Logistics (*Forschungsschule für Energieeffiziente Produktion und Logistik*) is gratefully acknowledged.

# 7. Summary, Conclusions and Outlook

## 7.1. Summary

The present works presents an exhaustive research work on the BrOx (Bromination-Oxidation) cycle for the generation of energy from natural gas without concomitant $CO_2$ emissions. In a first step the BrOx cycle has been developed and bromine has been selected as the halogen of choice instead of chlorine and iodine due to thermodynamic advantages in both the halogenation and the halide oxidation step. The proposed method consists on the reaction of bromine with methane to yield solid carbon and hydrogen bromide while in an exothermic reaction. After separation of the carbon hydrogen bromide is further oxidised in another exothermic reaction in the presence of oxygen to regenerate bromine and produce water. Bromine is then recycled to the first reactor after separation from water thus resulting in a process in which approximately 500 $kJ/mol_{CH_4}$ while avoiding $CO_2$ emissions to the atmosphere.

Being a novel process for which only exists a very sparse literature concerning both reaction steps, a feasibility study was carried out in a first phase. Thermodynamic calculations showed that during methane bromination the equilibrium conversion is virtually complete for a wide range of temperatures and that brominated by-products are present only in trace amounts at equilibrium. Similarly, thermodynamics of hydrogen bromide oxidation have been considered resulting in high equilibrium conversions at low-medium temperatures. Nonetheless, equilibrium conversion drops above 900 °C so that reaction engineering might be required in order to achieve high enough conversions.

After proving the feasibility of the BrOx cycle from a purely thermodynamic point of view a kinetic study has been conducted for methane bromination in order to determine how fast equilibrium is reached and thus provide a suitable operation temperature range. The most comprehensive reaction mechanism for methane bromination provided by SANDIA laboratories [95] and consisting of 79 elementary reactions and 26 chemical species was used for the simulations. Nonetheless, this mechanism does no consider solid carbon and carbon formation and thus can only provide limited insights on the reaction. A simple plug flow reactor was simulated both isothermally and adiabatically. The results showed that methane reaction with bromine is very fast ($< 10^{-3}$ s) for a wide range of temperatures. This clearly indicates that, although total conversion of methane is expected for very short residence times, the determining step is not methane reaction but the transition of carbonaceous intermediates to solid carbon and hydrogen bromide. In order to determine valid operation conditions and

to assess the adequacy of residence times an experimental study of methane bromination is necessary.

In order to perform an experimental study on methane bromination a bench-scale plant was designed and constructed including safety measurements and control and instrumentation. In a preliminary step the plant consisted of a quartz glass reactor heated externally with heating bands which was later improved to a tubular reactor housed in a ceramic high temperature oven. The setup included a feeding system used to feed a controlled flow of methane and dilution nitrogen, and a mixture of bromine and argon, in which argon was used to carry vapour bromine. Additionally, a analysis and neutralisation step was placed downstream. The experiments showed that under excess methane conditions carbon forms at medium temperatures (above 500 °C). Although methane conversion is complete as predicted by kinetic simulations brominated by-products are present at relatively high concentrations in the obtained carbon. When working with excess bromine, as it is desired in the BrOx cycle, methane conversion is complete for the studied temperatures. Nonetheless, carbon formation starts to occur at temperatures above 750 °C. Further experiments at higher temperatures show that bromine content in the carbon (and thus by-product content) decreases with increasing temperature reaching a concentration below 2% in mass at 1070 °C with residence times in the order of 10 seconds. Additionally it was determined that both the carbon type (flakes, soot...) as well as bromine content greatly depends on the reactor region at which carbon is collected. The temperature profile in the reactor was measured and compared to the bromine content of the carbon showing that bromine content is minimum at the central region where temperature is the highest. Due to safety concerns experiments on methane bromination were conducted with small flow rates and thus the amount of heat produced was not enough to sustain the reaction so that the temperature was ultimately determined by the furnace. It is thus important to notice that the relatively high concentrations of bromine obtained are an artefact of the small scale, since if higher flow rates were used the exothermicity of the reaction would greatly increase reaction temperature and thus bromine content would drop significantly.

During methane bromnation carbon forms at the reactor walls and deposits. A novel reactor concept was developed aiming at the minimisation or avoidance of carbon deposition at the reactor walls. The vortex reactor concept consists of a cyclone-like geometry with separate inlets for bromine and methane so that the reaction zone is localised at the centre of the reactor and far from the walls. In this way carbon will form far from the walls and be carried out of the reactor by the system hydrodynamics. In a preliminary stage a CAD model for the reactor was created and discretised and a CFD model implemented including a simplified reaction mechanism.

CFD simulations were conducted to determine the effect of counter-current and co-current flow on the reactor performance resulting in a improved performance when counter-current feeding was used. Additionally, the reactor geometry has been modified and simulated resulting in the identification of reactor features that improve reaction performance. A final result shows that a counter-current reactor with modified geometry (several bromine inputs, addition of a dip pipe, removal of cone tip...)

virtually avoids carbon deposition when working with high methane inlet velocities (75 $m/s$) and inlet temperatures above 1000 °C.

Due to safety concerns the vortex reactor concept could not be tested experimentally since it heavily relies in the displacement of the reaction zone to the centre of the reactor and that can be only achieved with high flow rates sufficient to generate enough heat to sustain the reaction so that external heating is not necessary. A backup solution was developed with the concept of sacrificial walls consisting in coating the reactor with a salt both resistant to high temperatures and to bromine corrosion prior to reaction. In this way when the reaction takes place carbon cannot access the reactor walls and deposits instead at the sacrificial walls so that after a convenient reaction time carbon can be easily removed together with the sacrificial wall by dissolving it with water or another suitable solvent. The first method studied was coating by evaporation of a salt solution. An experimental set-up was designed to determine optimal coating conditions such as rotational speed and evaporation temperature and afterwards these parameters were applied to the coating of a tubular reactor. An additional method was tested consisting in melting salt in the reactor and slowly cooling it down while the reactor rotates. Coated reactors were later tested during methane bromination showing that when the reactor was correctly coated, carbon could be easily recovered after the experiment by dissolving the sacrificial wall with water.

As shown in the experimental study of methane bromination, the carbon formed might contain bromine in the form of brominated compounds. Although bromine content would significantly be reduced with higher temperatures a purifying step might be necessary in order to remove most of the bromine and thus obtain a carbon that can safely be disposed or sold as a potentially valuable by-product. Three debromination methods were proposed and studied experimentally, namely atmospheric alkali hydrolysis, high temperature alkali hydrolysis and Raney-Ni alloy enhanced debromination. An experimental set-up was constructed in order to test those methods. Carbon samples from methane bromination experiments were analysed via EDX (Energy-dispersive X-ray spectroscopy) before and after debromination so that a debromination degree could be obtained. The experiments determined that the most suitable solvent is ethanol and that NaOH concentrations of 1 mol/l resulted in bromine removal of nearly 99% could be achieved with residence times of 28 hours when working in atmospheric conditions. High temperature alkali debromination resulted in similar results with residence times 80% lower. Raney-Ni alloy method was only capable to achieve 60% removal due to poor mixing in the debromination flask.

The second reaction step, namely hydrogen bromide oxidation was also studied both experimentally and via simulation. In a first step thermal oxidation was studied and a laboratory bench-scale plant was designed and constructed. An already existing reaction rate expression for thermal hydrogen bromide oxidation was used in a plug flow reactor simulation and validated experimentally. The experiments showed that conversions between 90% and 100% were achieved when working isothermally at approximately 900 °C. The reaction was too slow and conversions below 60 % were achieved at temperatures lower than 800 °C. Since the reaction is highly exothermic adiabatic operation would lead in principle to improved kinetics while decreasing

conversion due to equilibrium limitations. In order to take advantage of the fast kinetics concomitant to high temperature operation while enabling high conversion resulting from lower temperatures catalytic operation might be required.

A catalyst of $RuO_2$ supported in alumina was synthesised and characterised resulting in catalyst particles with a diameter in the order of magnitude of $10^{-6}$ and homogeneously distributed ruthenium over the surface was obtained and tested during catalytic hydrogen bromide oxidation. The catalyst showed good activity reaching conversions around 70% at 200 °C with residence times of 2.5 seconds and conversions above 90% at 250 °C. In all cases stoichiometric amounts of reactants were used and thus higher conversions can be obtained when oxygen excess is used.

A reaction concept for hydrogen bromide oxidation was developed consisting of three reaction stages. The first part of the reactor operates adiabatically increasing the temperature and the reaction rate. Afterwards, heat is retired in order to achieved a tailored temperature profile and after cooling a catalytic stage is used in order to increase conversion. Thermal oxidation was simulated showing that a combination of adiabatic and tailored temperature profile operation leads to conversions higher than 90% with residence times below 4 seconds. Should higher conversions result in an advantage in the process that overcomes catalyst costs, a catalytic step could be used afterwards to further increase conversion.

The aforementioned work covers the exhaustive study of both reaction steps, methane bromination and hydrogen bromide oxidation, from an experimental and theoretical point of view. Additionally, the most challenging aspects involved in the process have been covered, including the development of solutions for carbon deposition during methane bromination, purification of the carbon produced during the first reaction step as well as reaction engineering for hydrogen bromide oxidation. Nonetheless, the process is aimed to the production of energy and thus intermediate steps such as carbon and bromine/water separation are required. In order to provide a concept that achieves this objective the flowsheeting of the entire process was carried out taking 100 MW as a base for calculations.

The flowsheeting of the process was carried out in several steps, following an approach that enable the study of the different sections and the selection of optimal reaction conditions as well as separation strategies. In a last step the recirculation was added and the mass and energy balances were closed. The flowsheeting of the process showed that inlet temperature to the first reaction step should be as high as possible and so 800 °C was selected as inlet temperature so that after adiabatic reaction an outlet temperature of ca. 1500 °C is reached. It was also established that hydrogen bromide oxidation should be carried in two steps, a thermal oxidation in which the feed is at 800 °C and a catalytic isothermal oxidation occurring at 350 °C.

Several strategies for water-bromine separation were considered in a preliminary stage and amongst them four candidates were selected as the best solutions considering energy efficiency, fixed costs associated to equipment and the requirements for external products. The four strategies selected for the separation step were the following:

- Use of a decanter followed by two distillation columns
- Use of a decanter followed by two distillation columns with the addition of a flash units for oxygen recycle
- Use of a decanter followed by a distillation unit and an absorption unit with sulphuric acid
- Use of a decanter followed by a distillation unit and an absorption unit with sulphuric acid with an aditional reboiler

The results showed that those strategies involving absorption with sulphuric acid were less advantageous from an energetic perspective due to the energy consumption during sulphuric acid regeneration. From the options based on distillation columns it was found that the option including a flash unit resulted in lower losses of bromine as well as an increased energy efficiency. A final simulation of the whole process after the selection of the appropriate conditions and unit operations was carried out producing an stream table and a solved energy balance. This simulation was also used to determine the effect of chlorine impurities in the bromine feed on the process showing little effect. Additionally it was determined that using air instead of oxygen leads to a decrease of 13% in the overall energy efficiency of the process.

The final simulation showed that the energy generation of the process was 90.80 MW whereas the energy consumed reached 39.11 MW. Heat integration of the process was performed by means of the well-known Pinch analysis. The results showed that by using four additional heat exchangers energy consumption of the process was completely avoided while energy production reached 73.30 MW. Since the maximum output of the plant was 100 MW the results indicate an energy efficiency increase from approximately 50% to 73.30%.

Although thermodynamic considerations taken into account at the very beginning of this work pointed out that bromine is the most suitable candidate from the halogen group an additional steady-state simulation of the process was performed in which bromine was substituted by chlorine. The operation units were modified based on the Sumitomo process. The results showed a decrease in energy efficiency as well as an increase in the number of equipments involved as well as in the complexity of the process thus demonstrating that bromine is indeed the best halogen for the cycle.

Finally, a preliminary economic analysis was carried out without. Since the size and materials of the equipments were not fully determined this analysis did not include investment costs and thus it was based on the cost of educts, utilities and labor costs. The result showed a levelised cost of electricity in the same order of magnitude of that associated to novel energy generation methods such as biogas and offshore wind energy but still high compared with fossil fuel direct combustion. The energy price for the BrOx cycle resulted in 0.2 €$//kW_h$, which doubles the cost of energy produced through combined cycle gas turbines. If investment costs are not considered for the established technologies the energy cost in the BrOx cycle is approximately three-to-four times higher than those associated with natural gas combustion. Nonetheless, it should be noticed that this analysis does not include the potential savings concomitant

to the avoidance of $CO_2$ emissions which could be translated into profit by means of carbon taxing or $CO_2$ certificates. Additionally, the carbon produced during methane bromination is considered a by-product and the possibility of selling it thus obtaining benefits is not considered.

## 7.2. Conclusions

In the present work a novel method has been proposed, namely the BrOx cycle. This method enables the generation of energy from relatively abundant fossil fuel resources without concomitant $CO_2$ emissions. The process has proved to be feasible from a thermodynamic perspective.

The two reaction steps involved in the process have been identified as the more challenging steps and thus have been studied experimentally. The results show that within reasonable residence times high enough conversions can be reached in both methane bromination and hydrogen bromide oxidation. Methane bromination has virtually no thermodynamic limitations and thus in order to achieve high kinetics high temperatures are desirable. On the other hand, hydrogen bromide oxidation is limited thermodynamically and high conversions can be reached at temperatures below 900 °C. Thermal hydrogen bromide oxidation is also limited kinetically since temperatures higher than 750 °C are required to achieve high conversions in reasonable residence times. Therefore the reaction has to be carried out isothermally or in a combination with a catalytic step.

Two challenges have been identified regarding methane bromination reaction. Those challenges are carbon deposition at the reactor walls during reaction and relatively high bromine content in the carbon produced.

A reactor concept has been proposed aiming to the avoidance or minimisation of carbon deposition during methane bromination. A CFD study has been conducted together with a geometry optimisation leading to a reactor geometry and inlet conditions that guarantee carbon retrieval at the outlet above 99%. The results show that a counter-current feeding of educts greatly improves reactor performance and that the addition of several bromine inlets leads to a more developed protection layer that results in lower carbon deposition.

Due to safety concerns the vortex reactor concept has not been experimentally validated. Therefore an alternative method involving the use of sacrificial walls has been proposed. The results during methane bromination experiments show that this method has the potential to fully avoid carbon deposition at the walls and make it easily retrievable instead.

Bromine content in the carbon has been linked to the temperature at which carbon forms. It has been determined that the higher the temperature the lower the bromine content. This experimental results are also supported by thermodynamic and kinetic considerations. Although thermodynamic calculations show that brominated com-

pounds are only present in trace amounts at equilibrium the transformation of this compounds into solid carbon and hydrogen bromide is limited kinetically and thus higher temperatures result in lower concentrations. Nonetheless, since the bromine content in the carbon should be as low as possible, three debromination methods have been suggested, optimised and tested. The results show that debromination degrees above 95% can be achieved with atmospheric alkali hydrolysis within residence times in the order of 24 hours. This time can be reduced in approximately 80% when the debromination is carried out at high pressure (and thus higher temperatures).

A complete BrOx cycle plant was simulated in steady-state showing that an efficiency of approximately 50% was achievable. This efficiency was boosted up to 73% after heat integration and adding four heat exchangers. This efficiency is expressed in terms of the output of the process, which in this case is heat at different temperature levels. Since the conversion of this heat to electricity was not studied nor simulated it cannot be compared to actual electricity generation technologies such as combined cycle gas plants.

The preliminary economic analysis of the BrOx cycle showed that this technology is in principle more expensive than current well-established energy generation technologies. Nonetheless, the economic analysis does not take into account the potential savings linked to avoiding $CO_2$ emissions nor the potential profit that can be obtained from the solid carbon produced. Carbon tax differs from country to country ranging from US\$0/$t_{CO_2}$ to US\$140/$t_{CO_2}$. Although in several countries this tax does not apply to energy generation more restrictive legislation is likely to arise in the near future in order to achieve an effective reduction of $CO_2$ emissions. Therefore, including carbon taxes in the economic analysis may reduce the gap between energy produced with the BrOx cycle and current technologies.

The BrOx cycle offers an additional advantage compared with traditional processes which is its high flexibility. By changing operation conditions or adding equipment the process can be tuned to production of high-added-value chemicals or to production of zero-emissions hydrogen that can later be used as an energy carrier.

Although BrOx cycle still requires further research to be fully developed, including the scale-up of the process, this work demonstrates that it is a feasible and promising strategy that can act as a bridge technology in the transition from fossil-fuel-derived technologies to renewable energy scenarios. This is mainly due to the fact that the process enables the use of abundant and cheap resources such as natural gas while avoiding the main drawback associated with them, namely $CO_2$ emissions.

## 7.3. Outlook

The present work presents a detailed study of the BrOx cycle as a means to enable $CO_2$-free energy generation from fossil fuels. Nonetheless, in order to fully develop this concept several steps should be followed. One of the weaknesses involved in the BrOx cycle concerns carbon formation and deposition during methane bromination.

In order to provide a suitable strategy to avoid carbon deposition and to assess realistic bromine content values of the carbon produced it would be advisable to scale-up methane bromination as well as the vortex reactor concept. In this way the reaction would release enough heat to make viable reactor insulation so that the reaction can be self-sustained in quasi-adiabatic operation. This will provide valuable information on the final bromine content of the carbon produced and make feasible experimental validation of the vortex reactor concept for avoiding carbon deposition. Additionally, it would be interesting to develop an experimental set-up in which the loop is closed so that continuous operation of the BrOx cycle can be demonstrated.

One of the advantages of the BrOx cycle is its flexibility. As it was briefly explained in the last chapter of this thesis reaction parameters such as temperature and residence time during methane bromination could be fine-tuned to produce valuable brominated compounds by conducting a partial bromination of methane instead of carrying it out until only solid carbon and hydrogen bromide remain. This affirmation is supported by literature sources and thus it would be interesting to conduct experiments to quantitatively determine reaction conditions and product stream composition. Similarly, hydrogen bromide oxidation could be substituted by hydrogen bromide electrolysis in order to produce $CO_2$-free hydrogen that can be used as a chemical or as an energy carrier. Although literature on hydrogen bromide electrolysis exists it would be advisable to carry out an experimental study that determines the feasibility of such a process with the stream resulting from methane bromination to assess the effect of the presence of other compounds in the feed stream.

Additionally, since the BrOx cycle successfully uses bromine as an intermediate compound in the partial oxidation of methane it would be interesting to assess the possibility of using it as an intermediate in other processes. One example could be its use to produce sulphur from hydrogen sulphide.

$$H_2S + Br_2 \rightarrow 2HBr + 1/xS_x \tag{7.3.1}$$

Further study could help identify other processes in which bromine could act as an intermediate while improving the overall process.

# A. Kinetic Simulation of Methane Bromination

This appendix contains additional information on kinetic simulations of methane bromination to support the material provided in Chapter 1 - BrOx cycle: a novel process for $CO_2$-free energy producton from Natural Gas.

## A.1. Species considered and NASA polynomials

For the kinetic simulations performed in Chapter 1, the following 26 chemical species have been considered:

- $H_2$
- $H$
- $C$
- $CH$
- $CH_2$
- $CH_2(s)$
- $CH_3$
- $CH_4$
- $C_2H$
- $C_2H_2$
- $C_2H_2$
- $C_2H_3$
- $C_2H_4$
- $C_2H_5$
- $C_2H_6$
- $Br$
- $Br_2$
- $HBr$

- $CH_2Br_2$
- $CHBr_3$
- $CHBr_2$
- $CBr_4$
- $CBr_3$

The thermodynamic properties of each chemical species have been calculated with the NASA polynomials:

$$\frac{c_p^0}{R} = a_1 + a_2T + a_3T^2 + a_4T^3 + a_5T^4 \tag{A.1.1}$$

$$\frac{h^0}{R} = a_1T + \frac{a_2T^2}{2} + \frac{a_3T^3}{3} + \frac{a_4T^4}{4} + \frac{a_5T^5}{5} + a_6 \tag{A.1.2}$$

$$\frac{s^0}{R} = a_1lnT + a_2T\frac{a_3T^2}{2} + \frac{a_4T^3}{3} + \frac{a_5T^4}{4} + a_7 \tag{A.1.3}$$

## A.2. Kinetic mechanism of methane bromination

A mechanism developed by SANDIA laboratories of methane bromination which considers 26 chemical species and consists of 79 elementary reactions has been used for the kinetic simulations of methane bromination. Following, the elementary reactions and parameters are displayed as portrayed in the literature [55]

```
!Reactions 79;  A-units (mol-cm-sec)  E-units (cal/mol)
REACTIONS     MOLES          CAL/MOLE
H + H + M <=> H2 + M                                1.00E+18        -1         0
    H2/0./ CH4/2./ C2H6/3./
H + H + H2 <=> H2 + H2                              9.00E+16      -0.6         0
H + CH <=> C + H2                                   1.10E+14         0         0
H + CH2 (+M) <=> CH3 (+M)                           2.50E+16      -0.8         0
    LOW / 3.20E+27      -3.14       1230 /
    TROE / 0.68         78       1995       5590 /
    H2/2./ CH4/2./ C2H6/3./
H + CH2(S) <=> CH + H2                              3.00E+13         0         0
H + CH3 (+M) <=> CH4 (+M)                           1.27E+16      -0.6       383
    LOW / 2.48E+33      -4.76       2440 /
    TROE / 0.783       74.6       2941       6964 /
    H2/2./ CH4/2./ C2H6/3./
H + CH4 <=> CH3 + H2                                6.60E+08       1.6     10840
H + C2H (+M) <=> C2H2 (+M)                          1.00E+17        -1         0
    LOW / 3.75E+33       -4.8       1900 /
    TROE / 0.6464        132       1315       5566 /
    H2/2./ CH4/2./ C2H6/3./
```

Figure A.1.: Reaction mechanism for methane bromination - Part 1

```
H + C2H2 (+M) <=> C2H3 (+M)                          5.60E+12         0       2400
     LOW / 3.80E+40      -7.27       7220 /
     TROE / 0.7507       98.5       1302       4167 /
     H2/2./ CH4/2./ C2H6/3./
H + C2H3 (+M) <=> C2H4 (+M)                          6.08E+12       0.3        280
     LOW / 1.40E+30      -3.86       3320 /
     TROE / 0.782        275       2663       6095 /
     H2/2./ CH4/2./ C2H6/3./
H + C2H3 <=> H2 + C2H2                               3.00E+13         0          0
H + C2H4 (+M) <=> C2H5 (+M)                          1.08E+12       0.5       1820
     LOW / 1.20E+42      -7.62       6970 /
     TROE / 0.9753        210        984       4374 /
     H2/2./ CH4/2./ C2H6/3./
H + C2H4 <=> C2H3 + H2                               1.32E+06       2.5      12240
H + C2H5 (+M) <=> C2H6 (+M)                          5.21E+17        -1       1580
     LOW / 1.99E+41      -7.08       6685 /
     TROE / 0.8422        125       2219       6882 /
     H2/2./ CH4/2./ C2H6/3./
H + C2H5 <=> H2 + C2H4                               2.00E+12         0          0
H + C2H6 <=> C2H5 + H2                               1.15E+08       1.9       7530
C + CH2 <=> H + C2H                                  5.00E+13         0          0
C + CH3 <=> H + C2H2                                 5.00E+13         0          0
CH + H2 <=> H + CH2                                  1.11E+08       1.8       1670
CH + CH2 <=> H + C2H2                                4.00E+13         0          0
CH + CH3 <=> H + C2H3                                3.00E+13         0          0
CH + CH4 <=> H + C2H4                                6.00E+13         0          0
CH2 + H2 <=> H + CH3                                 5.00E+05         2       7230
CH2 + CH2 <=> H2 + C2H2                              3.20E+13         0          0
CH2 + CH3 <=> H + C2H4                               4.00E+13         0          0
CH2 + CH4 <=> CH3 + CH3                              2.46E+06         2       8270
CH2(S) + H2 <=> CH3 + H                              7.00E+13         0          0
CH2(S) + CH3 <=> H + C2H4                            1.20E+13         0       -570
CH2(S) + CH4 <=> CH3 + CH3                           1.60E+13         0       -570
CH2(S) + C2H6 <=> CH3 + C2H5                         4.00E+13         0       -550
CH3 + CH3 (+M) <=> C2H6 (+M)                         2.12E+16        -1        620
     LOW / 1.77E+50      -9.67       6220 /
     TROE / 0.5325        151       1038       4970 /
CH3 + CH3 <=> H + C2H5                               4.99E+12       0.1      10600
CH3 + C2H4 <=> C2H3 + CH4                            2.27E+05         2       9200
CH3 + C2H6 <=> C2H5 + CH4                            6.14E+06       1.7      10450
C2H + H2 <=> H + C2H2                                4.07E+05       2.4        200
C2H4 (+M) <=> H2 + C2H2 (+M)                         8.00E+12       0.4      88770
     LOW / 7.00E+50      -9.31      99860 /
     TROE / 0.7345        180       1035       5417 /
     H2/2./ CH4/2./ C2H6/3./
BR + BR + M <=> BR2 + M                              1.92E+14         0      -1700
     BR2/14./ CH4/1.5/
BR + H + M <=> HBR + M                               4.78E+21        -2        511
HBR + H <=> BR + H2                                  1.26E+10       1.1        160
BR2 + H <=> BR + HBR                                 2.28E+11         1        440
CH3 + HBR <=> CH4 + BR                               9.46E+11         0       -380
C2H5 + HBR <=> C2H6 + BR                             1.02E+12         0      -1000
```

Figure A.2.: Reaction mechanism for methane bromination - Part 2

```
CH3BR + H <=> CH3 + HBR                          5.11E+13          0       5840
CH3BR + CH3 <=> CH4 + CH2BR                      1.26E+12          0      10100
CH3 + BR2 <=> CH3BR + BR                         1.21E+13          0       -390
CH3BR + BR <=> CH2BR + HBR                       1.00E+14          0      16310
CH3 + BR <=> CH2 + HBR                           1.10E+14          0      22968
CH2BR + BR <=> CH2 + BR2                         5.00E+09          0      10200
C2H5 + BR2 <=> C2H5BR + BR                       1.57E+13          0       -820
C2H5BR + H <=> C2H5 + HBR                        1.00E+14          0       5000
C2H3BR + H <=> C2H3 + HBR                        1.00E+14          0       6000
C2H3 + BR2 <=> C2H3BR + BR                       3.02E+13          0       -477
CH2BR + C2H6 <=> CH3BR + C2H5                    1.00E+12          0       8500
CH2BR + C2H4 <=> C2H3 + CH3BR                    2.00E+12          0      12000
CH2BR + CH3 <=> C2H5BR                           3.10E+11          0      -4300
CH2BR + CH3 <=> C2H4 + HBR                       5.40E+12          0       1400
CH2BR + CH3 <=> C2H5 + BR                        1.00E+13          0       7000
CH2BR + H2 <=> CH3BR + H                         2.00E+12          0      13100
C2H5 + BR <=> C2H5BR                             2.00E+13          0          0
C2H3 + BR <=> C2H3BR                             3.00E+13          0          0
BR + C2H4 <=> C2H3 + HBR                         5.00E+12          0      25000
C2H5BR + CH3 <=> C2H5 + CH3BR                    1.00E+13          0       6000
C2H3BR + CH3 <=> C2H3 + CH3BR                    1.00E+13          0      11000
CH3 + CBR4 <=> CH3BR + CBR3                      1.48E+14          0       7900
CH3BR <=> CH3 + BR                               1.58E+14          0      71700
CH2BR2 <=> CH2BR + BR                            1.00E+14          0      65600
CHBR3 <=> CHBR2 + BR                             1.58E+14          0      59000
CBR4 <=> CBR3 + BR                               2.00E+14          0      52400
CHBR3 + CH3 <=> CBR3 + CH4                       2.31E+13          0       7300
CH2BR2 + H <=> CH2BR + HBR                       5.11E+13          0       5840
CHBR3 + H <=> CHBR2 + HBR                        5.11E+13          0       5840
CBR4 + H <=> CBR3 + HBR                          5.11E+13          0       5840
CH2BR2 + BR <=> CH2BR + BR2                      1.82E+14          0      24513
CHBR3 + BR <=> CHBR2 + BR2                       1.82E+14          0      24513
CBR4 + BR <=> CBR3 + BR2                         1.82E+14          0      24513
CH2BR2 + BR <=> CHBR2 + HBR                      1.00E+14          0      16310
CHBR3 + BR <=> CBR3 + HBR                        1.00E+14          0      16310
CH2BR2 + H <=> CHBR2 + H2                        1.36E+14          0      11964
CHBR3 + H <=> CBR3 + H2                          1.36E+14          0      11964
END
```

Figure A.3.: Reaction mechanism for methane bromination - Part 3

## A.3. Rasmussen gas-phase mechanism

The mechanism developed by SANDIA laboratories does not include formation of solid carbon and thus all carbon present in the methane is present in brominated compounds after reaction. In order to try simulating carbon formation the Rasmussen mechanism was used (without reactions involving oxygen and nitrogen) combined with [117, 118, 119, 120, 121].

The elementary reactions used in this simulations are displayed in the following pages (figures A.4, A.5, A.6, A.7, A.8, A.9, A.10, A.11, A.12, A.13 and A.14)

```
! A-units (mol-cm-sec)  E-units (cal/mol)
REACTIONS     MOLES          CAL/MOLE
H + H + M <=> H2 + M                                1.00E+18        -1         0
    H2/0./
H + H2 + H <=> H2 + H2                              9.20E+16       -0.6         0
CH3 + CH3 (+M) <=> C2H6 (+M)                        6.77E+16      -1.18       654
    LOW / 3.40E+41      -7.03       2762 /
    TROE / 0.619       73.2       1180       9999 /
    H2/2./ CH4/2./ C2H6/3./ AR/0.7/
CH3 + H (+M) <=> CH4 (+M)                           1.39E+16      -0.63       383
    LOW / 2.62E+33      -4.76       2440 /
    TROE / 0.783         74       2941       6964 /
    H2/2./ CH4/2./ C2H6/3./ AR/0.7/
CH4 + H <=> CH3 + H2                                1.33E+04         3       8038
```

Figure A.4.: Elementary reactions for modified Rasmussen gas-phase mechanism - Part 1

```
CH3 + H <=> CH2 + H2                                  9.00E+13          0      15100
C + CH3 <=> C2H2 + H                                  5.00E+13          0          0
C + CH2 <=> C2H + H                                   5.00E+13          0          0
CH + H <=> C + H2                                     1.50E+14          0          0
CH + C2H2 <=> C3H2 + H                                1.00E+14          0          0
CH + CH2 <=> C2H2 + H                                 4.00E+13          0          0
CH + CH3 <=> C2H3 + H                                 3.00E+13          0          0
CH + CH4 <=> C2H4 + H                                 6.03E+13          0          0
CH2 + H <=> CH + H2                                   1.00E+18      -1.56          0
CH2 + CH4 <=> CH3 + CH3                               4.30E+12          0      10039
CH2 + CH2 <=> C2H2 + H + H                            4.00E+13          0          0
CH2 + CH3 <=> C2H4 + H                                4.00E+13          0          0
CH2 + C2H2 <=> H2CCCH + H                             1.20E+13          0       6621
CH2(S) + M <=> CH2 + M                                1.00E+13          0          0
    H/0./ C2H2/0./ AR/0./ C6H6/0./
CH2(S) + H <=> CH2 + H                                2.00E+14          0          0
CH2(S) + C2H2 <=> CH2 + C2H2                          4.00E+13          0          0
CH2(S) + AR <=> CH2 + AR                              1.45E+13          0        884
CH2(S) + C6H6 <=> CH2 + C6H6                          7.00E+13          0          0
CH2(S) + CH4 <=> CH3 + CH3                            4.30E+13          0          0
CH2(S) + H <=> CH + H2                                3.00E+13          0          0
CH2(S) + CH3 <=> C2H4 + H                             2.00E+13          0          0
CH2(S) + C2H2 <=> H2CCCH + H                          1.80E+14          0          0
CH2(S) + C6H6 <=> C6H5 + CH3                          1.70E+14          0          0
C2H6 + CH3 <=> C2H5 + CH4                             5.50E-01          4       8295
C2H6 + H <=> C2H5 + H2                                5.41E+02        3.5       5210
C2H5 + H <=> CH3 + CH3                                4.89E+12       0.35          0
C2H5 + H (+M) <=> C2H6 (+M)                           5.20E+17      -0.99       1580
    LOW / 2.00E+41      -7.08       6685 /
    TROE / 0.8422        125       2219       6882 /
    H2/2./
C2H5 + CH3 <=> C2H4 + CH4                             1.15E+12          0          0
C2H5 + C2H5 <=> C2H6 + C2H4                           1.45E+12          0          0
C2H4 + H <=> C2H3 + H2                                5.42E+14          0      14902
C2H4 + CH3 <=> C2H3 + CH4                             5.01E+11          0      15057
C2H4 + H (+M) <=> C2H5 (+M)                           1.08E+12      0.454       1822
    LOW / 1.11E+34         -5       4448 /
    TROE / 0.5         95         95        200 /
    H2/2./
C2H4 + M <=> C2H2 + H2 + M                            3.49E+16          0      71539
C2H3 + C2H3 <=> C2H4 + C2H2                           6.30E+13          0          0
C2H3 + H (+M) <=> C2H4 (+M)                           6.10E+12       0.27        280
    LOW / 9.80E+29      -3.86       3320 /
    TROE / 0.782      207.5       2663       6095 /
    H2/2.85/ CH4/2.85/ C2H6/4.29/
C2H3 + H <=> C2H2 + H2                                4.00E+13          0          0
C2H3 + CH2 <=> C3H4 + H                               3.00E+13          0          0
C2H3 + C2H <=> C2H2 + C2H2                            3.00E+13          0          0
C2H3 + C2H <=> H2CCCCH + H                            3.00E+13          0          0
C2H3 + CH3 <=> C2H2 + CH4                             2.05E+13          0          0
C2H3 + CH <=> CH2 + C2H2                              5.00E+13          0          0
```

Figure A.5.: Elementary reactions for modified Rasmussen gas-phase mechanism - Part 2

```
C2H3 + C2H3 <=> H2CCCH + CH3                          1.80E+13          0          0
C2H2 + H (+M) <=> C2H3 (+M)                           3.11E+11       0.58       2589
    LOW / 2.25E+40     -7.269       6577 /
    TROE / 0.5        675        675 /
    H2/2./
C2H + CH4 <=> CH3 + C2H2                              7.23E+12          0        976
H + C2H (+M) <=> C2H2 (+M)                            1.00E+17         -1          0
    LOW / 3.75E+33       -4.8       1900 /
    TROE / 0.6464        132       1315       5566 /
    H2/2./ CH4/2./ C2H6/3./ AR/0.7/
H2CC + C2H2 (+M) <=> CH2CHCCH (+M)                    3.50E+05      2.055      -2400
    LOW / 1.40E+60    -12.599       7417 /
    TROE / 0.98         56        580       4164 /
    H2/2./ CH4/2./ C2H2/3./ C2H4/3./ C2H6/3./
H2CC + C2H4 <=> CH2CHCHCH2                            1.00E+12          0          0
C2H + H2 <=> C2H2 + H                                 4.10E+05       2.39        864
C2H + C2H2 <=> C4H2 + H                               2.47E+12        0.5       -391
C2H3 + CH3 <=> C3H6                                   4.46E+56        -13      13865
C3H6 <=> C2H2 + CH4                                   2.50E+12          0      70000
C3H6 <=> C3H4 + H2                                    3.00E+13          0      80000
CH2CHCH2 + H <=> C3H6                                 1.88E+26       -3.6       5468
C3H6 + H <=> C2H4 + CH3                               7.23E+12          0       1302
C3H6 + H <=> CH2CHCH2 + H2                            1.73E+05        2.5       2492
C3H6 + H <=> CH3CCH2 + H2                             4.09E+05        2.5       9794
C3H6 + H <=> CH3CHCH + H2                             8.04E+05        2.5      12284
C3H6 + CH3 <=> CH2CHCH2 + CH4                         2.22E+00        3.5       5675
C3H6 + CH3 <=> CH3CCH2 + CH4                          8.43E-01        3.5      11656
C3H6 + CH3 <=> CH3CHCH + CH4                          1.35E+00        3.5      12848
C3H6 + C2H3 <=> CH2CHCHCH2 + CH3                      7.23E+11          0       5000
CH2(S) + C2H4 <=> CH2CHCH2 + H                        1.30E+14          0          0
C2H3 + CH3 <=> CH2CHCH2 + H                           4.73E+02        3.7       5677
CH3CHCH + H <=> C3H6                                  1.00E+14          0          0
CH3CHCH + H <=> C3H4P + H2                            2.00E+13          0          0
CH3CHCH + H <=> CH2CHCH2 + H                          1.00E+14          0          0
CH3CCH2 + H <=> C3H6                                  5.00E+13          0          0
CH3CCH2 + H <=> CH2CHCH2 + H                          1.00E+14          0          0
CH3CCH2 + H <=> C3H4P + H2                            4.00E+13          0          0
CH3CCH2 + CH3 <=> C3H4P + CH4                         1.00E+11          0          0
CH2CHCH2 + H <=> C3H4 + H2                            5.00E+13          0          0
CH2CHCH2 + CH3 <=> C3H4 + CH4                         3.02E+12       -0.3       -131
CH2CHCH2 + CH2CHCH2 <=> C3H6 + C3H4                   1.02E+13          0          0
CH3 + C2H2 <=> C3H4 + H                               5.14E+09       0.86      22153
C3H4 + H <=> C3H4P + H                                1.00E+13          0       5000
C3H4 + H <=> H2CCCH + H2                              3.00E+07          2       5000
C3H4P + H <=> H2CCCH + H2                             3.00E+07          2       5000
C3H4P + H <=> CH3 + C2H2                              1.00E+14          0       4000
C3H4P + H (+M) <=> CH3CCH2 (+M)                       6.50E+12          0       2000
    LOW / 8.45E+39      -7.27       6577 /
C3H4 + H (+M) <=> CH2CHCH2 (+M)                       1.20E+11        0.7       3007
    LOW / 5.56E+33         -5       4448 /
```

Figure A.6.: Elementary reactions for modified Rasmussen gas-phase mechanism - Part 3

```
H2CCCCH + C2H3 <=> CH2CHCCH + C2H2                  2.00E+12          0       5000
C2H4 + C2H <=> CH2CHCCH + H                         1.20E+13          0          0
C2H3 + C2H2 <=> CH2CHCCH + H                        2.00E+12          0       5000
CH2CHCCH + H <=> H2CCCCH + H2                       3.00E+07          2       5000
CH2CHCCH + H <=> HCCHCCH + H2                       2.00E+07          2      15000
CH2CHCCH + H2CCCH <=> C6H5CH2                       9.25E+11     -1.265     -14295
CH2CHCCH + CH2CHCCH <=> C6H5C2H3                    5.47E+40     -7.975      51241
CH2CHCCH2 + H <=> CH3 + H2CCCH                      1.00E+14          0          0
CH2CHCCH2 (+M) <=> CH2CHCCH + H (+M)                1.00E+14          0      50000
    LOW / 2.00E+15          0      42000 /
    H2/2./
CH2CHCCH2 + C2H <=> C5H4CH2                         1.00E+13          0          0
CH2CHCCH2 + C2H <=> C6H5 + H                        6.00E+12          0          0
CH2CHCCH2 + C2H <=> H2CCCH + H2CCCH                 4.00E+12          0          0
CH2CHCCH2 + C2H <=> CH2CHCCH + C2H2                 3.00E+12          0       5000
CH2CHCHCH + H <=> CH2CHCCH + H2                     3.00E+07          2       1000
CH2CHCHCH + H <=> CH2CHCCH2 + H                     1.00E+14          0          0
CH2CHCHCH (+M) <=> CH2CHCCH + H (+M)                1.00E+14          0      37000
    LOW / 1.00E+14          0      30000 /
    H2/2./
CH2CHCHCH + C2H2 <=> C6H6 + H                       8.21E+08      0.801       6348
CH2CHCHCH + C2H <=> C5H4CH2                         4.00E+12          0          0
CH2CHCHCH + C2H <=> C6H5 + H                        1.60E+13          0          0
CH2CHCHCH + C2H <=> CH2CHCCH + C2H2                 3.00E+12          0       5000
CH2CHCHCH + C2H2 <=> C6H7                           1.96E+19      -3.35       4910
CH2CHCHCH + C2H3 <=> C6H813                         5.50E+15      -1.67       1470
CH2CHCHCH + C4H2 <=> C6H5C2H + H                    3.16E+11          0       1800
CH2CHCHCH + C3H4 <=> C6H5CH3 + H                    2.00E+11          0       3700
CH2CHCHCH + C3H4P <=> C6H5CH3 + H                   3.16E+11          0       3700
CH2CHCHCH + CH2CHCCH <=> C6H5C2H3 + H               3.16E+11          0        600
CH3CCCH2 <=> CH2CHCCH2                              1.50E+67     -16.89      59100
C2H3 + C2H4 <=> CH2CHCHCH2 + H                      5.00E+11          0       7304
C2H3 + C2H3 <=> CH2CHCHCH2                          7.23E+13          0          0
CH2CHCHCH2 + H <=> C3H4P + CH3                      2.00E+12          0       7000
CH2CHCHCH2 + H <=> C3H4 + CH3                       2.00E+12          0       7000
CH2CHCHCH2 <=> CH2CHCCH2 + H                        5.70E+36      -6.27     112353
CH2CHCHCH2 + CH3 <=> CH2CHCCH2 + CH4                1.00E+14          0      19800
CH2CHCHCH2 + C2H3 <=> CH2CHCCH2 + C2H4              2.50E+13          0      19800
CH2CHCHCH2 + CH2CHCH2 <=> CH2CHCCH2 + C3H6          5.00E+12          0      19500
CH2CHCHCH2 + CH3 <=> CH2CHCHCH + CH4                2.00E+14          0      22800
CH2CHCHCH2 + C2H3 <=> CH2CHCHCH + C2H4              5.00E+13          0      22800
CH2CHCHCH2 + H2CCCH <=> CH2CHCHCH + C3H4            1.00E+13          0      22500
CH2CHCHCH2 + CH2CHCH2 <=> CH2CHCHCH + C3H6          1.00E+13          0      22500
CH2CHCHCH2 <=> CH2CHCCH + H2                        2.50E+15          0      94700
CH2CHCHCH2 + C2H3 <=> C6H813 + H                    1.14E+12      -0.24       9920
CH2CHCHCH2 + C2H3 <=> C6H814 + H                    1.14E+12      -0.24       9920
CH2CHCHCH2 + C2H2 <=> C6H814                        2.30E+12          0      35000
CH2CHCHCH2 + H <=> CH2CHCCH2 + H2                   5.00E+15          0      22800
CH2CHCHCH2 <=> CH2CHCHCH + H                        1.58E+16          0     110000
CH2CHCHCH2 + H <=> CH2CHCHCH + H2                   5.00E+15          0      22800
H2CCCH + CH3 (+M) <=> CH2CCHCH3 (+M)                1.50E+12          0          0
    LOW / 2.60E+57    -11.94      9770 /
```

Figure A.7.: Elementary reactions for modified Rasmussen gas-phase mechanism - Part 4

```
    TROE / 0.175    1340.6     60000    9769.8 /
    H2/2./ CH4/2./ C2H6/3./ AR/0.7/
CH2CCHCH3 + H <=> CH2CHCHCH2 + H                    2.00E+13         0      4000
CH2CCHCH3 + CH3 <=> CH2CHCCH2 + CH4                 7.00E+13         0     18500
CH2CCHCH3 <=> CH2CHCHCH2                            3.00E+13         0     65000
CH3CCCH3 + H <=> CH3 + C3H4P                        2.60E+05       2.5      1000
C5H6 + H <=> C5H5 + H2                              2.19E+08      1.77      3000
C5H6 + H <=> CH2CHCH2 + C2H2                        1.00E+13         0     12000
C5H5 + H <=> C5H6                                   2.92E+29      -4.7      6148
C5H5 <=> C5H5(L)                                    4.09E+47     -10.4     54874
C5H5 + CH3 <=> C6H7 + H                             2.44E+41    -7.989     39259
C5H5 + C2H2 <=> C6H5CH2                             1.73E+17    -1.885     10231
C5H5 + C5H5 <=> A2 + H + H                          2.00E+12         0      4000
H2CCCCCH + H <=> C5H2 + H2                          1.00E+13         0         0
H2CCCCCH + CH3 <=> C5H4CH2                          1.40E+13         0         0
H2CCCCCH + CH3 <=> C6H5 + H                         6.00E+12         0         0
H2CCCCCH + CH3 <=> C5H2 + CH4                       3.00E+12         0      5000
HCCCHCCH + H <=> C5H2 + H2                          1.00E+13         0         0
HCCCHCCH + H <=> H2CCCCCH + H                       1.00E+13         0         0
HCCCHCCH + CH3 <=> C5H4CH2                          1.00E+13         0         0
HCCCHCCH + CH3 <=> C6H5 + H                         1.00E+13         0         0
HCCCHCCH + CH3 <=> C5H2 + CH4                       3.00E+12         0      5000
C6H5 + H <=> C6H6                                   5.00E+13         0         0
C6H5 + H <=> C6H4 + H2                              2.00E+07         2      1000
C6H5 + C2H2 <=> C6H5C2H + H                         2.47E+06      1.77      2289
C6H5 + C2H <=> C6H5C2H                              2.54E+17    -1.489      1541
C6H5 + C4H2 <=> C6H5C2H + C2H                       2.00E+13         0         0
C6H5 + CH2CHCCH <=> C6H5C2H + C2H3                  3.20E+11         0      1350
C6H5 + CH3 <=> C6H5CH3                              2.00E+22    -3.045      2304
C6H5 + CH3 <=> C6H5CH2 + H                          5.00E+13         0         0
C6H5 + C2H3 <=> C6H5C2H3                            2.67E+19    -2.118      2187
C6H5 + CH2CHCCH <=> C6H5C2H3 + C2H                  3.20E+11         0      1900
C6H5 + CH2CHCHCH2 <=> C6H5C2H3 + C2H3               3.20E+11         0      1900
C6H5 + HCCHCCH <=> A2                               2.22E+43    -9.127     14810
C6H5 + HCCHCCH <=> PA2* + H                         1.36E+22    -2.304     18485
C6H6 + C2H <=> C6H5C2H + H                          1.00E+12         0         0
C5H4CH2 <=> C6H6                                    7.59E+13         0     73853
C5H4CH2 + H <=> C6H6 + H                            3.00E+12       0.5      2000
C6H7 <=> C6H6 + H                                   6.64E+46   -11.137     34478
C6H7 + H <=> C6H6 + H2                              1.00E+13         0         0
C6H7 + C6H5 <=> C6H6 + C6H6                         1.00E+12         0         0
C6H7 + C6H7 <=> C6H813 + C6H6                       2.82E+13         0         0
C6H7 + C6H7 <=> C6H814 + C6H6                       1.39E+13         0         0
C6H813 <=> C6H7 + H                                 2.42E+59   -13.316     96147
C6H813 <=> C6H6 + H2                                4.39E+37    -7.257     71949
C6H814 <=> C6H7 + H                                 1.21E+59   -13.316     96147
C6H814 + H <=> C6H7 + H2                            4.00E+13         0      3000
C6H814 <=> C6H6 + H2                                1.28E+28    -4.941     49309
C6H5C2H + H <=> C6H4C2H + H2                        2.50E+14         0     16000
C6H5C2H + CH3 <=> C6H4C2H + CH4                     1.67E+12         0     15057
C6H4C2H + C2H2 <=> SA2*                             3.98E+13         0     10100
C6H5CH2 + H <=> C6H5CH3                             4.81E+20    -2.124      1986
```

Figure A.8.: Elementary reactions for modified Rasmussen gas-phase mechanism - Part 5

| | | | |
|---|---|---|---|
| C6H5CH2 + CH3 <=> C6H5C2H5 | 2.10E+37 | -7.401 | 12269 |
| C6H5CH2 + CH3 <=> C6H5C2H3 + H2 | 4.68E+24 | -3.231 | 27018 |
| C6H5CH2 + C2H2 <=> INDENE + H | 3.20E+11 | 0 | 7000 |
| C6H5CH2 + H2CCCH <=> A2 + H + H | 6.03E+11 | 0 | 0 |
| C6H5CH3 + H <=> C6H5CH2 + H2 | 1.20E+14 | 0 | 8235 |
| C6H5CH3 + H <=> C6H6 + CH3 | 1.20E+13 | 0 | 5148 |
| C6H5CH3 + CH3 <=> C6H5CH2 + CH4 | 3.16E+11 | 0 | 9500 |
| C6H5CH3 + C2H3 <=> C6H5CH2 + C2H4 | 3.98E+12 | 0 | 8000 |
| C6H5CH3 + C6H5 <=> C6H5CH2 + C6H6 | 2.10E+12 | 0 | 4400 |
| C6H5C2H5 <=> C6H5C2H3 + H2 | 5.01E+12 | 0 | 64000 |
| C6H5C2H5 + H <=> C6H6 + C2H5 | 1.20E+13 | 0 | 5100 |
| C6H5C2H5 + H <=> C6H5C2H3 + H2 + H | 8.00E+13 | 0 | 8235 |
| C6H5C2H3 + H <=> C6H5C2H + H2 + H | 6.92E+14 | 0 | 14500 |
| SA2* + H <=> A2 | 1.00E+14 | 0 | 0 |
| PA2* + H <=> A2 | 1.00E+14 | 0 | 0 |
| INDENE + H <=> INDENYL + H2 | 2.19E+08 | 1.77 | 3000 |
| INDENYL + H <=> INDENE | 2.00E+14 | 0 | 0 |
| A2 + H <=> PA2* + H2 | 2.50E+14 | 0 | 16000 |
| A2 + H <=> SA2* + H2 | 2.50E+14 | 0 | 16000 |
| A2 + C2H <=> PA2* + C2H2 | 5.00E+13 | 0 | 16000 |
| A2 + C2H <=> SA2* + C2H2 | 5.00E+13 | 0 | 16000 |
| A2 + C2H3 <=> PA2* + C2H4 | 5.00E+13 | 0 | 16000 |
| A2 + C2H3 <=> SA2* + C2H4 | 5.00E+13 | 0 | 16000 |
| CH3CCCH2 + CH3CCCH2 <=> CH3C6H4CH2 + H | 1.00E+08 | 0 | 0 |
| CH3C6H4CH3 + H <=> CH3C6H4CH2 + H2 | 3.98E+02 | 3.44 | 3120 |
| CH3C6H4CH2 + C2H2 <=> H2A2 + H | 3.20E+11 | 0 | 7000 |
| CH3C6H4CH2 + C2H2 <=> INDENECH3 + H | 3.20E+11 | 0 | 7000 |
| CH3C6H4CH2 + H <=> CH3C6H4CH3 | 7.46E+13 | 0 | 78 |
| CH3C6H4CH2 + CH3 <=> CH3C6H4C2H5 | 6.00E+12 | 0 | 221 |
| CH3C6H4C2H5 + H <=> CH3C6H4C2H3 + H2 + H | 8.00E+13 | 0 | 8235 |
| CH3C6H4C2H3 + H <=> INDENE + H + H2 | 3.98E+02 | 3.44 | 3120 |
| C6H5CH2 + H2CCCH <=> C6H5C4H4 + H | 2.00E+12 | 0 | 0 |
| C6H5C4H5 + H <=> C6H5C4H4 + H2 | 2.00E+05 | 2.5 | 2500 |
| C6H5C4H4 + H <=> C6H5C4H5 | 1.00E+14 | 0 | 0 |
| C6H4C4H4 + H <=> C6H5C4H4 | 2.00E+13 | 0 | 1500 |
| C6H4C4H4 + H <=> A2 + H | 3.00E+12 | 0.5 | 0 |
| C6H4C4H4 <=> A2 | 5.00E+37 | -7.4 | 76979 |
| H2A2 + H <=> H2A2* + H2 | 2.00E+05 | 2.5 | 2500 |
| H2A2* + H <=> H2A2 | 1.00E+14 | 0 | 0 |
| A2 + H <=> H2A2* | 5.00E+14 | 0 | 5000 |
| INDENECH3 + H <=> INDENYLCH3 + H2 | 2.19E+08 | 1.77 | 3000 |
| INDENECH3 + H <=> INDENE + CH3 | 1.20E+13 | 0 | 5200 |
| INDENYLCH3 + H <=> INDENECH3 | 2.00E+14 | 0 | 0 |
| INDENYLCH3 + C5H5 <=> A3CH3 + H + H | 1.00E+13 | 0 | 8000 |
| PA2* + CH3 <=> A2CH3 | 5.00E+12 | 0 | 0 |
| PA2* + CH3 <=> A2CH2 + H | 5.00E+12 | 0 | 0 |
| SA2* + CH3 <=> A2CH3 | 5.00E+12 | 0 | 0 |
| SA2* + CH3 <=> A2CH2 + H | 5.00E+12 | 0 | 0 |
| A2CH3 + H <=> A2CH2 + H2 | 3.98E+02 | 3.44 | 3120 |
| A2CH3 + H <=> A2 + CH3 | 1.20E+13 | 0 | 5148 |
| A2CH2 + CH3 <=> A2C2H5 | 1.19E+13 | 0 | 221 |
| A2CH2 + H <=> A2CH3 | 1.00E+14 | 0 | 0 |

Figure A.9.: Elementary reactions for modified Rasmussen gas-phase mechanism - Part 6

```
SA2* + C2H2 <=> A2R5 + H                          3.98E+13         0      10100
A2R5 + H <=> A2R5* + H2                           2.50E+14         0      16000
A2R5* + CH3 <=> A2R5CH2 + H                       5.00E+13         0          0
A2R5CH2 + H <=> A2R5CH3                           1.00E+14         0          0
A2R5CH3 + H <=> A2R5 + CH3                        1.20E+13         0       5148
A2R5* + H (+M) <=> A2R5 (+M)                      1.00E+14         0          0
    LOW / 6.60E+75      -16.3       7000 /
    TROE / 1        0.1      584.9       6113 /
    H2/2./ CH4/2./ C2H6/3./
A2C2H3 + H <=> A2C2H + H2                         2.00E+07         2       6000
A2C2H5 + H <=> A2C2H3 + H2 + H                    8.00E+13         0       8235
PA2* + C2H2 <=> PA2*C2H + H                       3.98E+13         0      10100
PA2*C2H + H <=> SA2*C2H* + H2                     2.50E+14         0      16000
PA2*C2H + H <=> PA2*C2H* + H2                     2.50E+14         0      16000
A2 + C2H <=> PA2*C2H + H                          5.00E+13         0          0
A2 + C2H <=> SA2*C2H + H                          5.00E+13         0          0
PA2* + C2H2 <=> A2C2H                             1.70E+43     -9.12      21100
PA2*C2H + H <=> A2C2H                             5.90E+46    -10.03      19100
A2C2H + H <=> PA2*C2H + H2                        1.50E+13         0          0
SA2*C2H + H <=> SA2*C2H* + H2                     2.50E+14         0      16000
SA2*C2H* + H (+M) <=> SA2*C2H (+M)                1.00E+14         0          0
    LOW /3.80E+127    -31.434      18676 /
    TROE / 0.2      122.8      478.4     5411.9 /
    H2/2./ CH4/2./ C2H6/3./
PA2*C2H* + H (+M) <=> PA2*C2H (+M)                1.00E+14         0          0
    LOW /9.50E+129    -32.132      18782 /
    TROE / 0.87      492.7      117.9       5652 /
    H2/2./ CH4/2./ C2H6/3./
PA2*C2H* + C2H2 <=> S1A3*                         5.50E+61    -14.56      33100
PA2*C2H* + C2H2 <=> S2A3*                         5.50E+61    -14.56      33100
C6H5 + C6H5 <=> C6H5C6H5                          5.00E+12         0          0
C6H5 + C6H6 <=> C6H5C6H5 + H                      4.00E+11         0       4000
C6H6 + C6H5 <=> HC6H5C6H5                         3.70E+32     -6.74       9870
C6H5 + C6H5 <=> C6H5C6H4 + H                      2.30E-01      4.62      28950
C6H5C6H5 + H <=> C6H5C6H4 + H2                    2.50E+14         0      16000
C6H5C6H4 + C2H2 <=> A3 + H                        3.98E+13         0      10100
HC6H5C6H5 <=> C6H5C6H5 + H                        3.80E+37     -7.96      27880
C6H5C6H5 <=> C6H5C6H4 + H                         1.10E+25     -2.72     114270
C6H6 + C6H5CH2 <=> C6H5CH2C6H5 + H                1.20E+12         0      15940
C6H5 + C6H5CH2 <=> C6H5CH2C6H5                    2.00E+22    -3.045       2304
C6H5CH2C6H5 + H <=> C6H5CHC6H5 + H2               2.50E+14         0      16000
A2CH2 + C2H2 <=> A2R23 + H                        3.20E+11         0       7000
A2R23* + H <=> A2R23                              2.00E+14         0          0
A2R23 + H <=> A2R23* + H2                         2.19E+08      1.77       3000
C6H5CHC6H5 <=> A1L2A1 + H                         4.00E+11         0       4000
A1L2A1 + H <=> A1L2A1* + H2                       2.19E+08      1.77       3000
A1L2A1* + H <=> A1L2A1                            2.00E+14         0          0
PA2*C2H* + C2H2 <=> (C2H)A2(C2H) + H              1.80E+19     -1.67      18800
SA2*C2H* + C2H2 <=> (C2H)A2(C2H) + H              1.80E+19     -1.67      18800
(C2H)A2(C2H) + H <=> PA3*                         6.90E+63    -14.57      29900
(C2H)A2(C2H) + H <=> S1A3*                        6.90E+63    -14.57      29900
PA2*C2H + C2H <=> (C2H)A2(C2H) + H                5.00E+13         0          0
```

Figure A.10.: Elementary reactions for modified Rasmussen gas-phase mechanism - Part 7

```
SA2*C2H + C2H <=> (C2H)A2(C2H) + H                    5.00E+13         0         0
AL3 <=> A3                                           8.00E+12         0     65000
PA2*C2H* + C2H2 <=> S1AL3*                           3.98E+13         0     10100
S1AL3* + H <=> AL3                                   5.00E+13         0         0
AL3 + H <=> S1AL3* + H2                              2.50E+14         0     16000
AL3 + H <=> PAL3* + H2                               2.50E+14         0     16000
PAL3* + H <=> AL3                                    5.00E+13         0         0
INDENYL + C5H5 <=> A3 + H + H                        1.00E+13         0      8000
SA2*C2H* + C2H2 <=> S1A3*                            3.98E+13         0     10100
S1A3* + H <=> A3                                     5.00E+13         0         0
A3 + H <=> PA3* + H2                                 2.50E+14         0     16000
A3 + H <=> S1A3* + H2                                2.50E+14         0     16000
A3 + H <=> S2A3* + H2                                2.50E+14         0     16000
PA3* + H (+M) <=> A3 (+M)                            1.00E+14         0         0
    LOW /4.00E+148   -37.505     20551 /
    TROE / 1     536.3     144.9     5632.8 /
    H2/2./ CH4/2./ C2H6/3./
S1A3* + H (+M) <=> A3 (+M)                           1.00E+14         0         0
    LOW /2.10E+139   -34.803     18378 /
    TROE / 0.001     171.4     171.4     4992.8 /
    H2/2./ CH4/2./ C2H6/3./
S2A3* + H (+M) <=> A3 (+M)                           1.00E+14         0         0
    LOW /2.10E+139   -34.803     18378 /
    TROE / 0.001     171.4     171.4     4992.8 /
    H2/2./ CH4/2./ C2H6/3./
PA2* + CH2CHCCH <=> A3 + H                           3.30E+33      -5.7     25500
SA2* + CH2CHCCH <=> A3 + H                           3.30E+33      -5.7     25500
C6H4C2H + C6H6 <=> A3 + H                            1.10E+23     -2.92     15890
C6H5 + C6H5C2H <=> A3 + H                            1.10E+23     -2.92     15890
PA3* + CH3 <=> A3C5 + H + H                          5.00E+13         0         0
A3CH3 + H <=> A3C5 + H2 + H                          3.98E+02      3.44      3120
A3C5 + H <=> A3C5* + H2                              2.19E+08      1.77      3000
A3C5* + H <=> A3C5                                   2.00E+14         0         0
S2A3* + CH3 <=> A3CH2 + H                            5.00E+13         0         0
A3CH2 + H <=> A3CH3                                  1.00E+14         0         0
A3CH3 + H <=> A3CH2 + H2                             1.20E+14         0      8235
A3CH3 + H <=> A3 + CH3                               1.20E+13         0      5148
A3CH2 <=> A3C5 + H                                   1.20E+12         0     15940
PA3* + C2H2 <=> A3C2H + H                            3.98E+13         0     10100
A3C2H + H <=> A3C2H* + H2                            2.50E+14         0     16000
PAL3* + C2H2 <=> AL3C2H + H                          3.98E+13         0     10100
AL3C2H + H <=> AL3C2H* + H2                          2.50E+14         0     16000
A3 + C2H <=> A3C2H + H                               5.00E+13         0         0
S2A3* + C2H2 <=> A3C2H2                              8.00E+61     -14.5     34800
S2A3* + C2H2 <=> A3C2H + H                           1.20E+26     -3.44     30200
A3C2H + H <=> A3C2H2                                 1.90E+64    -15.12     29300
SA2* + C6H5 <=> A2L2A1 + H + H                       5.00E+12         0         0
SA2* + C6H6 <=> A2L2A1 + H + H2                      4.00E+11         0      4000
A2L2A1 + H <=> A2L2A1* + H2                          2.50E+14         0     16000
S1A3* + C2H2 <=> A3R5 + H                            3.98E+13         0     10100
A3R5 <=> A2L2A1                                      8.51E+12         0     62860
S2A3* + C2H2 <=> A4 + H                              3.98E+13         0     10100
```

Figure A.11.: Elementary reactions for modified Rasmussen gas-phase mechanism - Part 8

```
A4 + H <=> PA4* + H2                          2.50E+14          0      16000
A4 + H <=> S1A4* + H2                         2.50E+14          0      16000
A4 + H <=> S2A4* + H2                         2.50E+14          0      16000
A3C2H + H <=> A4 + H                          9.00E+38      -7.39      20700
A3C2H2 <=> A4 + H                             2.00E+63     -15.28      43200
C6H5C2H + C6H4C2H <=> A4 + H                  1.10E+23      -2.92      15890
A4 + A4 => SOOT                               1.00E+10        0.5          0
BR + BR + M <=> BR2 + M                       1.92E+14          0      -1700
    BR2/14./ CH4/1.5/
BR + H + M <=> HBR + M                        4.78E+21         -2        511
HBR + H <=> BR + H2                           1.26E+10        1.1        160
BR2 + H <=> BR + HBR                          2.28E+11          1        440
CH3 + HBR <=> CH4 + BR                        9.46E+11          0       -380
C2H5 + HBR <=> C2H6 + BR                      1.02E+12          0      -1000
CH3BR + H <=> CH3 + HBR                       5.11E+13          0       5840
CH3BR + CH3 <=> CH4 + CH2BR                   1.26E+12          0      10100
CH3 + BR2 <=> CH3BR + BR                      1.21E+13          0       -390
CH3BR + BR <=> CH2BR + HBR                    1.00E+14          0      16310
CH3 + BR <=> CH2 + HBR                        1.10E+14          0      22968
CH2BR + BR <=> CH2 + BR2                      5.00E+09          0      10200
C2H5 + BR2 <=> C2H5BR + BR                    1.57E+13          0       -820
C2H5BR + H <=> C2H5 + HBR                     1.00E+14          0       5000
C2H3BR + H <=> C2H3 + HBR                     1.00E+14          0       6000
C2H3 + BR2 <=> C2H3BR + BR                    3.02E+13          0       -477
CH2BR + C2H6 <=> CH3BR + C2H5                 1.00E+12          0       8500
CH2BR + C2H4 <=> C2H3 + CH3BR                 2.00E+12          0      12000
CH2BR + CH3 <=> C2H5BR                        3.10E+11          0      -4300
CH2BR + CH3 <=> C2H4 + HBR                    5.40E+12          0       1400
CH2BR + CH3 <=> C2H5 + BR                     1.00E+13          0       7000
CH2BR + H2 <=> CH3BR + H                      2.00E+12          0      13100
C2H5 + BR <=> C2H5BR                          2.00E+13          0          0
C2H3 + BR <=> C2H3BR                          3.00E+13          0          0
BR + C2H4 <=> C2H3 + HBR                      5.00E+12          0      25000
C2H5BR + CH3 <=> C2H5 + CH3BR                 1.00E+13          0       6000
C2H3BR + CH3 <=> C2H3 + CH3BR                 1.00E+13          0      11000
CH3 + CBR4 <=> CH3BR + CBR3                   1.48E+14          0       7900
CH3BR <=> CH3 + BR                            1.58E+14          0      71700
CH2BR2 <=> CH2BR + BR                         1.00E+14          0      65600
CHBR3 <=> CHBR2 + BR                          1.58E+14          0      59000
CBR4 <=> CBR3 + BR                            2.00E+14          0      52400
CHBR3 + CH3 <=> CBR3 + CH4                    2.31E+13          0       7300
CH2BR2 + H <=> CH2BR + HBR                    5.11E+13          0       5840
CHBR3 + H <=> CHBR2 + HBR                     5.11E+13          0       5840
CBR4 + H <=> CBR3 + HBR                       5.11E+13          0       5840
CH2BR2 + BR <=> CH2BR + BR2                   1.82E+14          0      24513
CHBR3 + BR <=> CHBR2 + BR2                    1.82E+14          0      24513
CBR4 + BR <=> CBR3 + BR2                      1.82E+14          0      24513
CH2BR2 + BR <=> CHBR2 + HBR                   1.00E+14          0      16310
CHBR3 + BR <=> CBR3 + HBR                     1.00E+14          0      16310
CH2BR2 + H <=> CHBR2 + H2                     1.36E+14          0      11964
CHBR3 + H <=> CBR3 + H2                       1.36E+14          0      11964
CH + BR <=> C + HBR                           3.00E+11       0.64       1900
```

Figure A.12.: Elementary reactions for modified Rasmussen gas-phase mechanism - Part 9

```
BR + CH2 <=> CH + HBR                          1.10E+14      0     23040
H2 + BR + BR <=> HBR + HBR                     4.79E+11      0         0
H2 + BR2 <=> HBR + HBR                         6.50E+14      0     40631
CH3BR + BR2 <=> CH2BR2 + HBR                   1.00E+11      0     24140
```

Figure A.13.: Elementary reactions for modified Rasmussen gas-phase mechanism - Part 10

```
REACTIONS      MOLES          CAL/MOLE
C => C(GR)                                     1.00E+10      0         0
CH + CH <=> C(GR) + C(GR) + H2                 1.00E+10      0         0
CH2 <=> C(GR) + H2                             1.00E+10      0         0
CH2(S) <=> C(GR) + H2                          1.00E+10      0         0
CH3 + CH3 <=> C(GR) + C(GR) + H2 + H2 + H2     1.00E+10      0         0
C2H + C2H <=> C(GR) + C(GR) + C(GR) + C(GR) + H2   1.00E+10      0         0
CH2BR + CH2BR <=> C(GR) + C(GR) + HBR + HBR + H2   1.00E+10      0         0
CHBR2 + CHBR2 <=> HBR + HBR + BR2 + C(GR) + C(GR)  1.00E+10      0         0
CBR3 + CBR3 <=> C(GR) + C(GR) + BR2 + BR2 + BR2    1.00E+10      0         0
```

Figure A.14.: Solid carbon formation reactions

These simulations were carried out in order to provide an idea of the kinetics of formation of soot precursors with the kinetics involving polyciclic aromatic hydrocarbons. Those molecules containing more than four benzene rings are lumped into shoot precursors. Additionally, the bromocarbon molecules have been lumped together for the representation of the results.

The results obtained from the kinetic simulations with the modified Rasmussen mechanism (figures A.15 and A.15) show that the formation of soot precursors occur at residence times below 0.1 seconds while bromocarbon depletion starts at residence times above 100 seconds. Due to the experimental results it is clear that the mechanisms for bromocaron depletion do not characterise the reaction behaviour accurately.

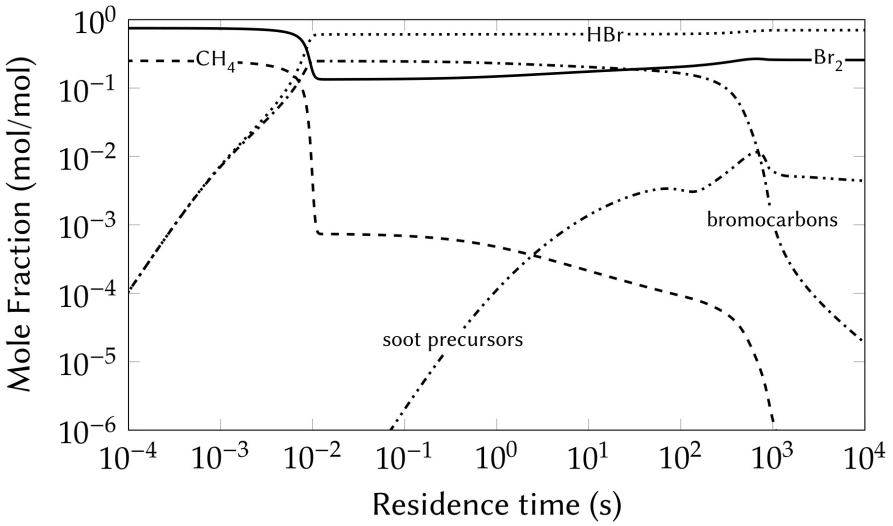


Figure A.15.: Results of simulation conducted with modified Rasmussen mechanism at 600 °C

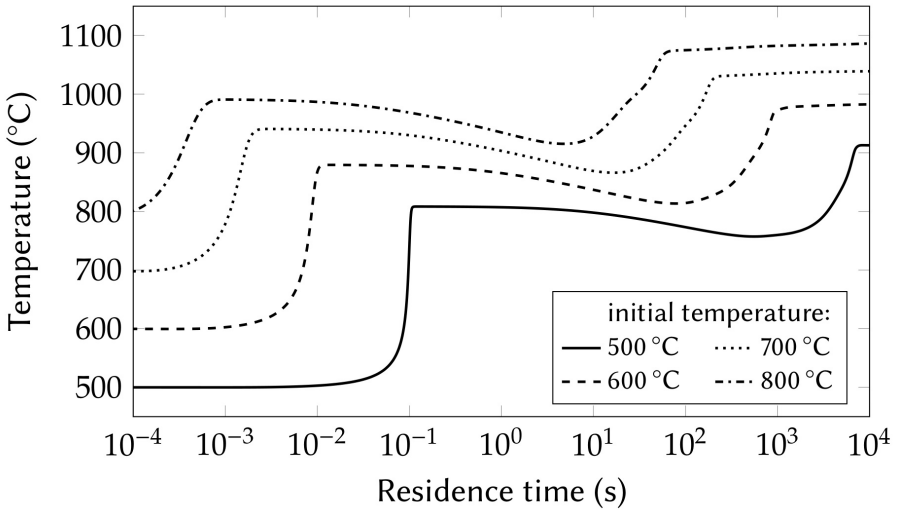


Figure A.16.: Adiabatic temperature profiles from simulation conducted with modified Rasmussen mechanism atseveral temperatures

Solid carbon formation reactions where included with arbitrary reaction parameters (preexponential factor, exponent and activation energy) in simulations showing that when an instantaneous rate is used bromocarbons readily evolve towards solid carbon A.17. This of course is an assumption that does not necessarily depict reality and thus it is not possible to determine via simulation the effect of residence time and temperature on carbon formation and bromocarbon depletion.

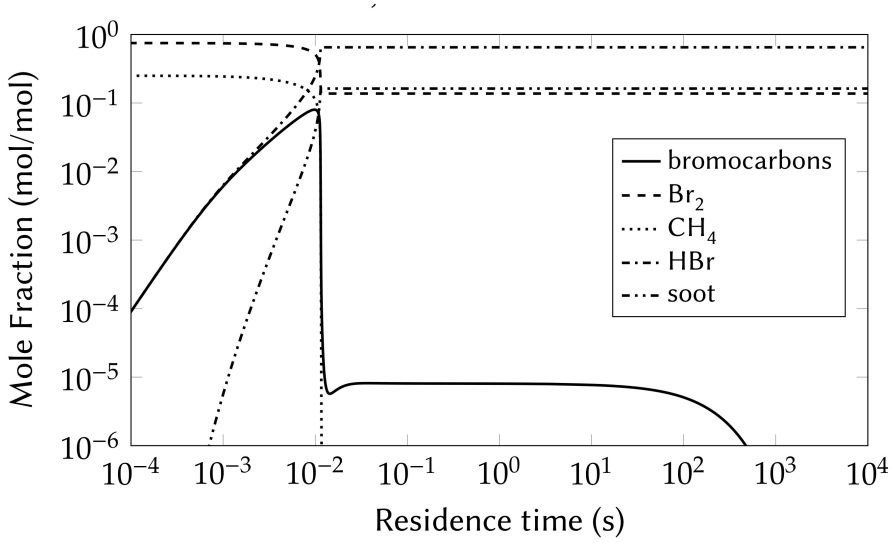


Figure A.17.: Results of simulations including soot formation from bromocarbons

Therefore it is necessary to develop an understanding on the kinetics and detailed mechanisms of solid carbon formation to enable accurate simulation of complete methane bromination. Since it is a task out of the scope of this work experimental work has been conducted in Chapter 1 to assess the viability of methane bromination reaction.

# B. CFD Simulations of Methane Bromination Reactor

This appendix contains additional information on computational fluid dynamics simulations of a vortex flow reactor for the avoidance or minimisation of carbon deposition during methane bromination. This information is a support to the material provided in Chapter 2 - Numerical simulation of a vortex reactor for avoiding carbon deposition during methane bromination.

## B.1. Hardware specifications

The hardware used for the discretisation of the geometries simulated in Chapter 2 has the following specifications:

- Local PC
- Architecture - Win7 SP1, 64-bit
- Processor - 1 Intel Core i5-4690, 3.5 GHz
- Cores - 4
- RAM - 8 GB

Simulations were conducted with LiDO high performance supercomputer of the Technical University Dortmund due to the complexity of the calculations involved. Request for each simulation were submitted as needed.

## B.2. Improvement of simulation behaviour

The use of an unstructured tetrahedron-dominated mesh has proven more appropriate to obtain a convergent solution although the simulation behaviour has been insufficient. In order to improve simulation behaviour several measurements were implemented including the addition of inflation layers to all surfaces with a wall boundary condition and the decrease, local refinement to the inlet regions and the reactor core, and fine-tuning of time scales. This approach significantly increased simulation times and the evolution of the simulation within reasonable simulation times is presented in figure B.1.

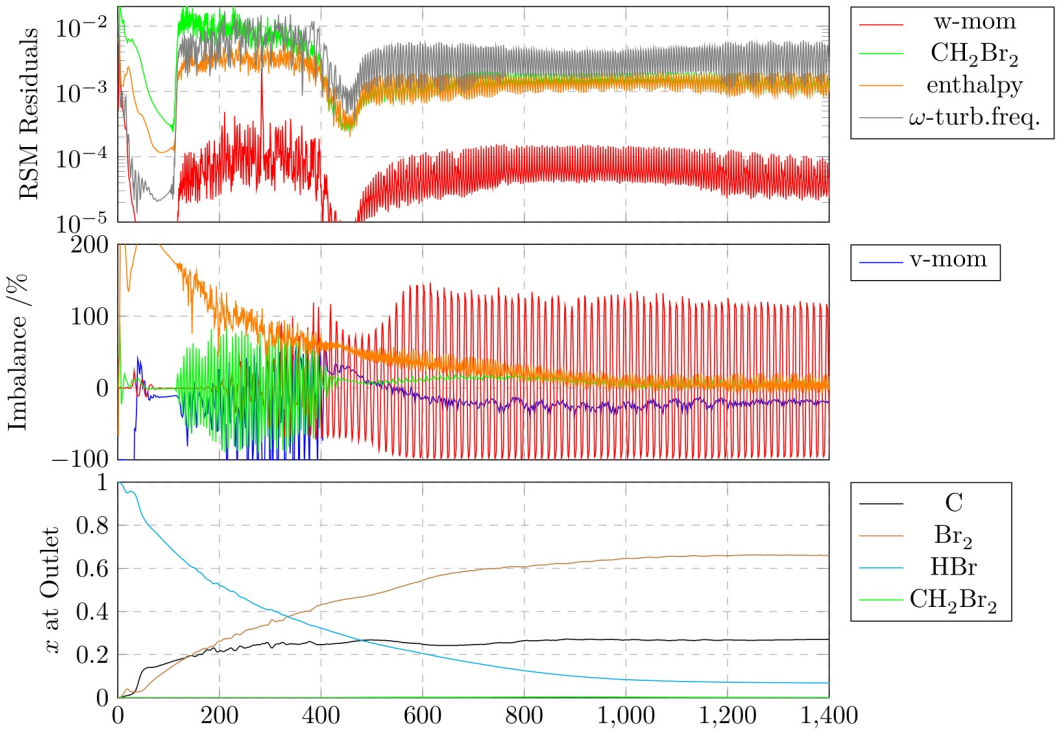


Figure B.1.: Evolution of residuals, imbalances and monitor variables with a a single step approach applied to a coarse mesh

The results show that although the values of the monitored variables achieved constant values within 1400 iterations the imbalances fluctuate in a range from -150% to 150%. Additionally, fluctuations also appear at the residuals. Therefore, this methodology is render unsuccessful for the simulation of the vortex reactor.

In order to improve simulation behaviour a multi-staged procedure was implemented. This methodology consists on starting the simulation with a coarse mesh, weak boundary conditions an the use of high time scales in order to obtain an approximated solution with few iterations. Following this starting step, the mesh is further refined and the time scales are reduced in each simulation step. Additionally, the boundary conditions are gradually changed towards the final state.

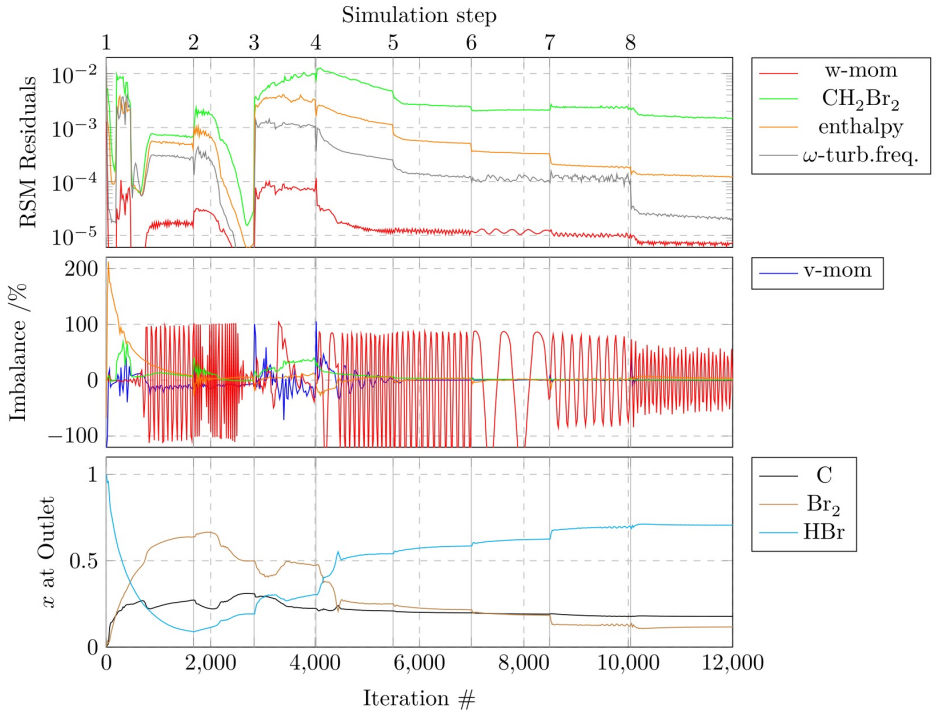


Figure B.2.: Evolution of residuals, imbalances and monitor variables with multi-step procedure applied to a coarse mesh

The results shown in figure B.2 show that still a constant value of the monitored variables is achieved. An improvement in the behaviour of the residuals is observed as they achieve a sufficiently low value and their oscillations are significantly reduced. Regarding the imbalances, most of them reach a value close to zero but there is still some fluctuation present in the w-momentum imbalance.

The simulation methodology was further improved by ignoring the gradual modification of the boundary conditions while being careful with the definition of time-scales. The simulations were performed so that for each step the time-scales were gradually reduced within each step. Once a convergent solution was found the mesh was refined and a new simulation step was carried out.

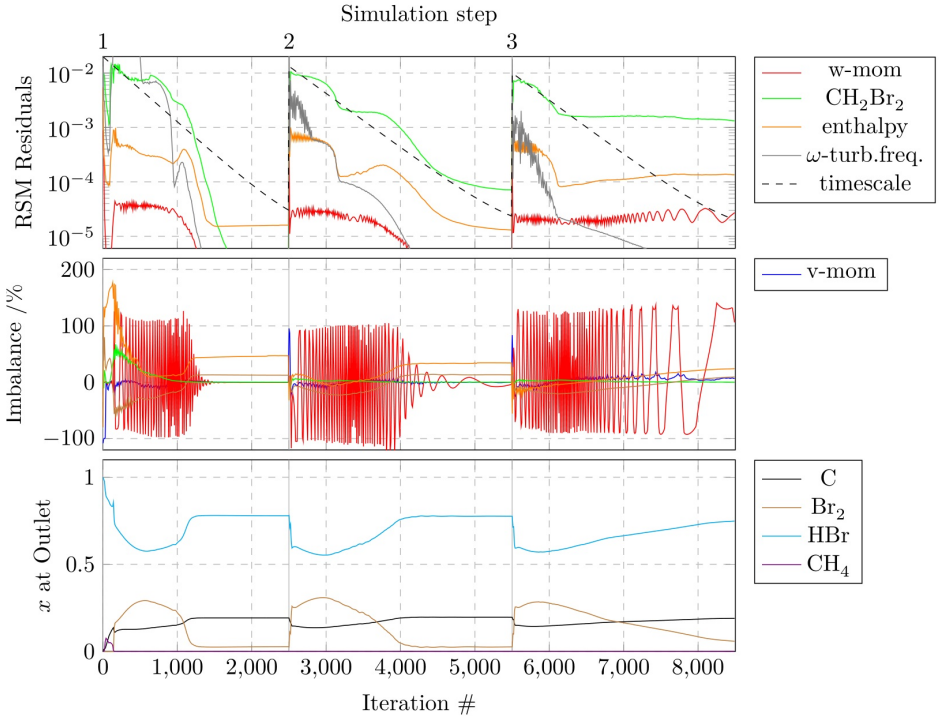


Figure B.3.: Evolution of residuals, imbalances and monitor variables gradual approach applied to a coarse mes

As can be seen in figure B.3 the simulation behaviour with this gradual approach is greatly improved. This techique results in a converged simulation in which the monitored variables achieve constant values while the residuals reach a low enough value (under $10^{-3}$). Additionally, all fluctuations previously present in the inbalances and the residuals is suppressed.

## B.3. Quality of the final mesh and mesh independent study

The mesh used for the final simulations of the vortex reactor is shown in figure B.4. As seen in the figure it is an unstructured tetrahedron-dominant mesh with inflation layers implemented at all wall boundaries and with a very refined mesh at the inputs as well as at the centre of the reactor. This is due to the results obtained in simulations with coarser meshes in which it was evident that the stronger gradients were present at those locations.

In order to characterise the quality of the mesh several techniques were carried out. An a priori analysis of the final mesh showed that the cell-average orthogonal quality value of the whole mesh was 0.87 with deviations within plus minus 0.13. According to Ansys CFX documentation this value accounts for a very good mesh. The worst orthogonal quality values were found at the tangential inlets with values of 0.23 plus minus 0.11 which is within an acceptable range. The most important part

of the reactor is its core because the reaction zone is located there and thus the stiffest gradients are present at this location. At the centre of the reactor an excellent mesh was achieved according to orthogonal quality criteria with a value of 0.97 plus minus 0.03. Moreover, the mesh at the cylindrical outer part of the reactor got orthogonal quality values of 0.90 plus minus 0.09.

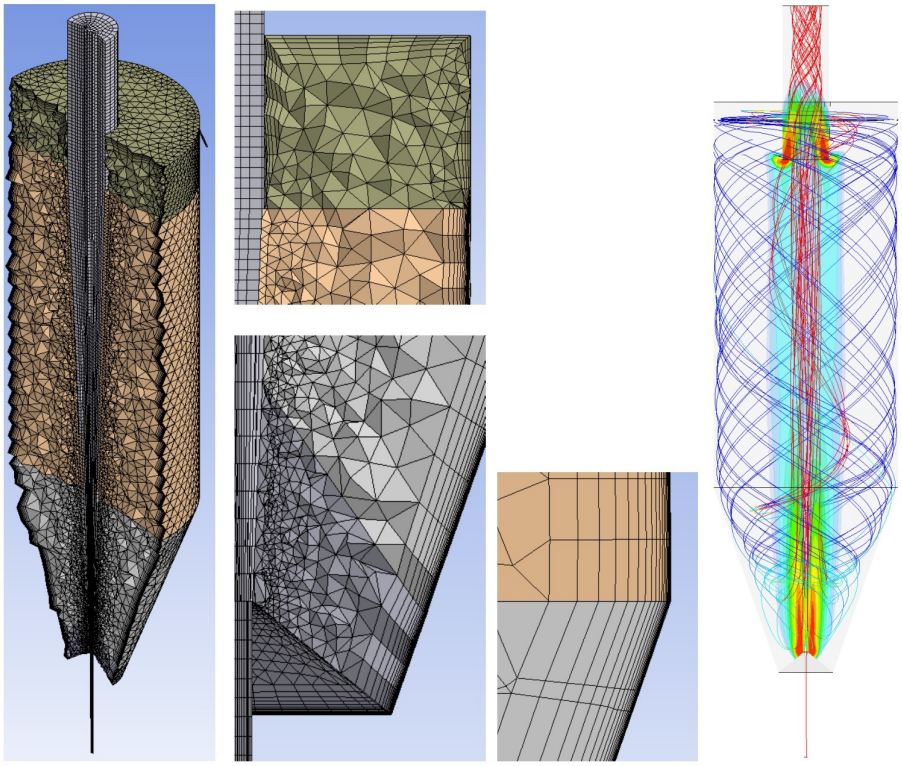

Figure B.4.: (a) Isometric view of a half-cut of the meshed geometry. (b) Detailed view of characteristic refinement zones. (c) Detailed view of inflation layers. (d) Flow and reaction phenomena

In order to perform an a posteriori analysis of the mesh a simulation was carried out with a residence time of 2.5 s, inlet temperature of 1323 K and a molar inlet ration of 1 (methane) to 2.5 (bromine). The results shown in figure B.5 show that the residuals achieve values below $10^{-4}$ and do not oscillate. Regarding imbalances, the values approach 0 and present no fluctuations. The monitored variables achieve constant values that do not vary as the simulation iterates.

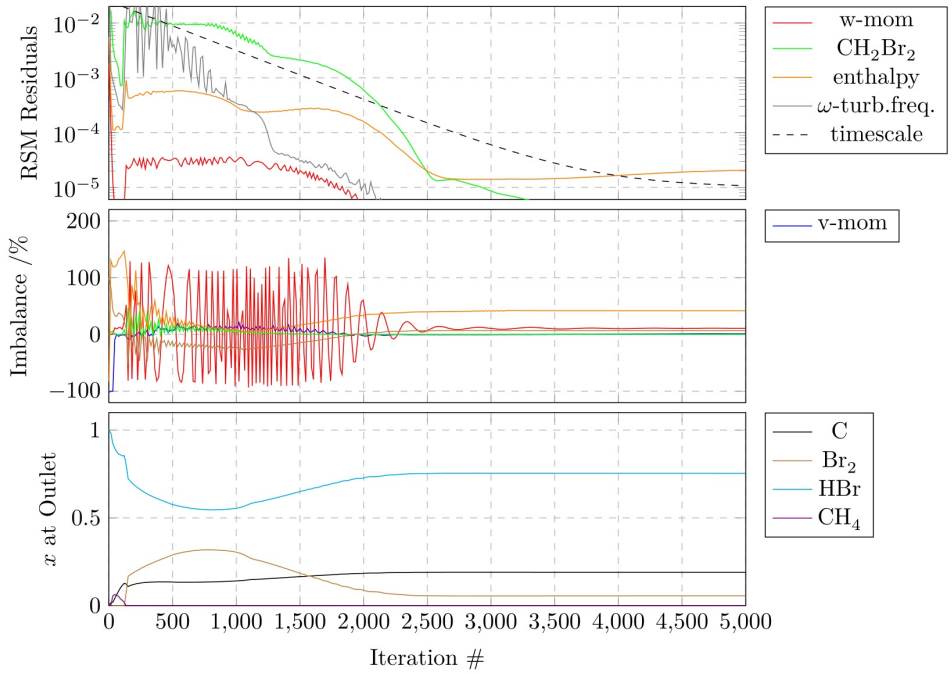


Figure B.5.: Convergence behaviour of a simulation with the final mesh

Due to the results of the a priori and a posteriori analysis it is clear that the mesh produces convergence and that it has a very good quality.

Additionally, a mesh independent study was carried out in order to ascertain whether the results obtained from the simulations have any dependency on the mesh and thus were unacceptable or they were independent from the number of elements in the mesh.

The mesh independent study was performed by carrying out simulations including flow behaviour, reaction and particle tracking for the same geometry and mesh layout. Three meshes with a number of elements of $5 \cdot 10^5$, $8.5 \cdot 10^5$ and $15 \cdot 10^5$ were used and the values of the monitored variables was compared without finding any significant deviations. Figure B.6 shows the simulation results including flow fields and particle trajectories. These results are virtually identical and thus it can be stated that the simulation results are independent of the mesh.

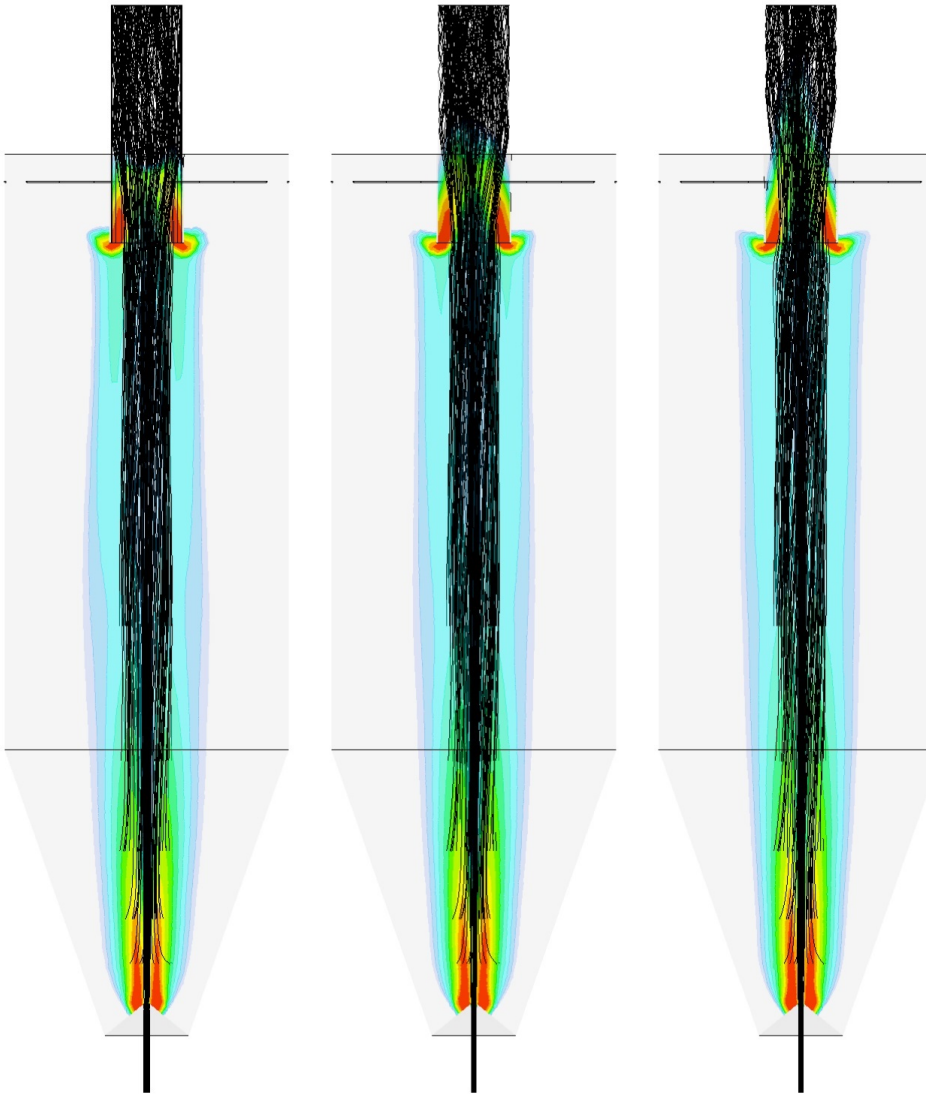

Figure B.6.: Results of mesh independence study. (a) $5 \cdot 10^5$ elements. (b) $8.5 \cdot 10^5$ elements. (c) $15 \cdot 10^5$ elements

## B.4. Experimental qualitative study on the performance of the Vortex Flow Reactor on avoiding carbon deposition

Due to the fact that an experimental set-up able to validate the CFD simulations would require larger flow rates of bromine and methane than those that can be safely handled in the facilities of the Chair of Chemical Reaction Engineering at the time at which the present work was carried out an alternative to gain experimental insight was developed. The use of small flow rates of bromine and methane would result in low release of energy so that the reaction would not be able to self-sustain itself thus producing no carbon. Therefore an experimental set-up has been constructed to

give validation to the simulations regarding hydrodynamics and particle behaviour. Figure B.7 shows a simplified P&ID diagram of such set-up.

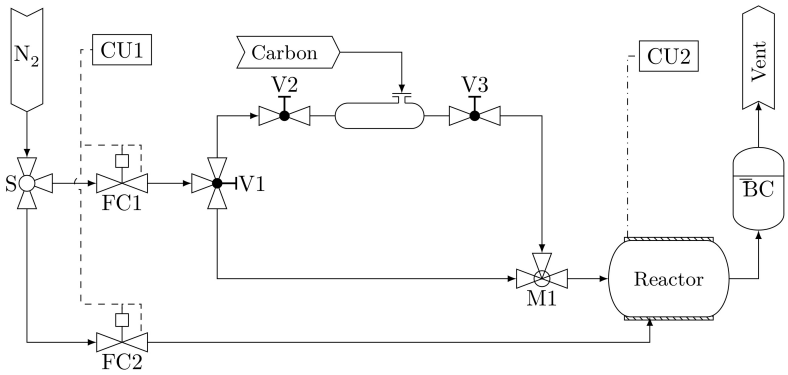


Figure 2.11: Basic PID flowsheet of experimental setup. CU: Controller unit – BC: Bubble column – S: Splitter – FC: Flow controller – V: Valve – M: Mixer

Figure B.7.: Simplified P&ID of the experimental set-up (CU:Controller; BC: Bubble column; S: Three-way joint; FC: Mass flow controller; V: Valve; M: Mixing three-way joint)

For the experiments with this set-up nitrogen was used as the gas phase and carbon particles provided by BASF were used to determine particle behaviour. Carbon particles were injected in the reactor via the axial inlet to closely resemble real operation. Figure B.8shows the quartz glass reactor used in these experiments. The reactor has an axial and a transversal inlet and can be operated with both counter- and co-current feed schemes.

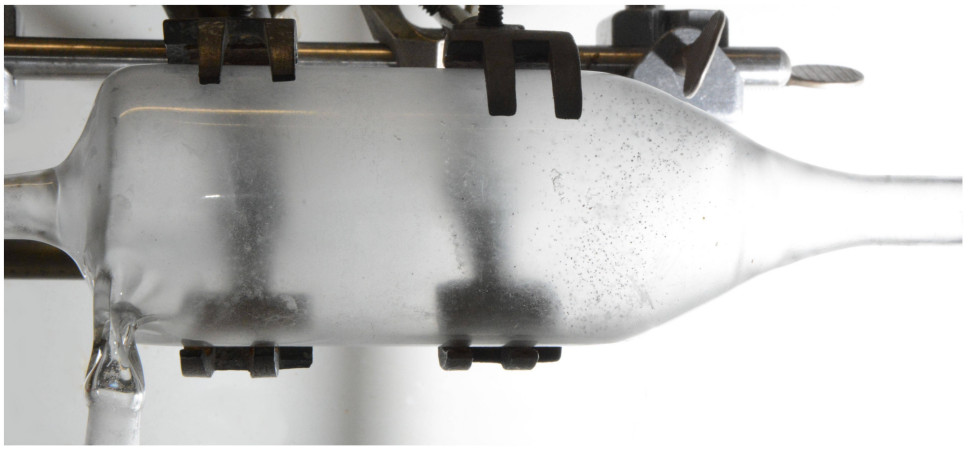

Figure B.8.: Quartz glass reactor

Figure B.9 shows the dimensions of the experimental quartz glass reactor.

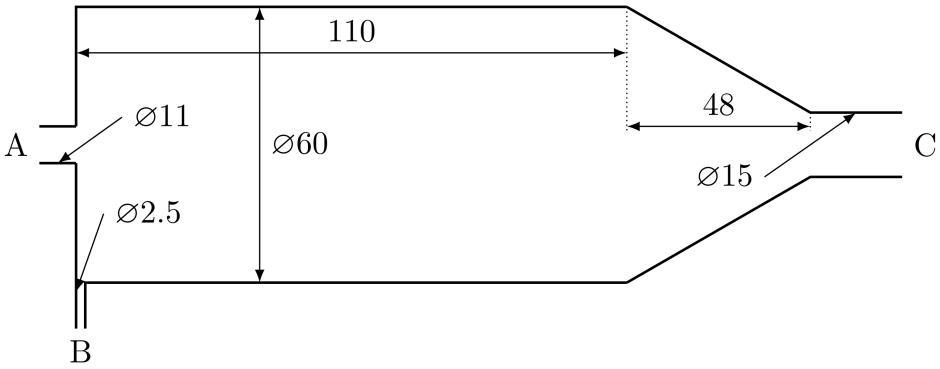


Figure B.9.: Dimensions of the vortex flow reactor

The particulate carbon provided by BASF was specified to have particle sizes within 300 $\mu m$ and 500 $mum$. In order to obtain smaller particles which were more representative of those obtained in the methane bromination experiments the material was mechanically ground. Figure B.10 shows the particle size distribution of the carbon material.

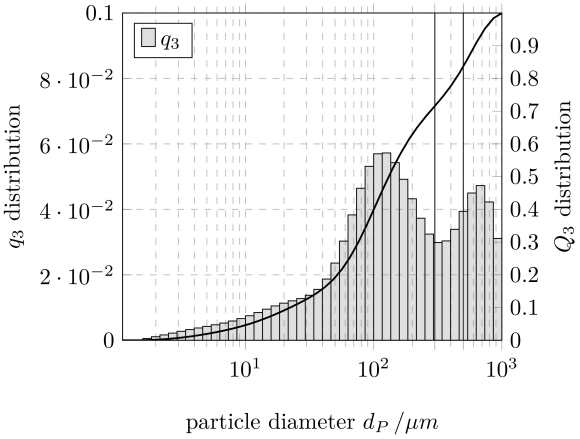


Figure 2.14: Particle size distribution of used raw material, that had been grinded before use. Originial material before grinding was specified with particle diameters between $300 \ldots 500\,\mu m$.

Figure B.10.: Particle size distribution of grinded carbon particles

Due to the fact that the experiments only pretend to qualitatively assess the performance of the vortex reactor regarding the capability of hydrodynamics to transport particles to the outlet.

Figure B.11 shows the particle size distribution of the particles introduced in the reactor and those that were collected at the outlet for several flow rates with co-current configuration.

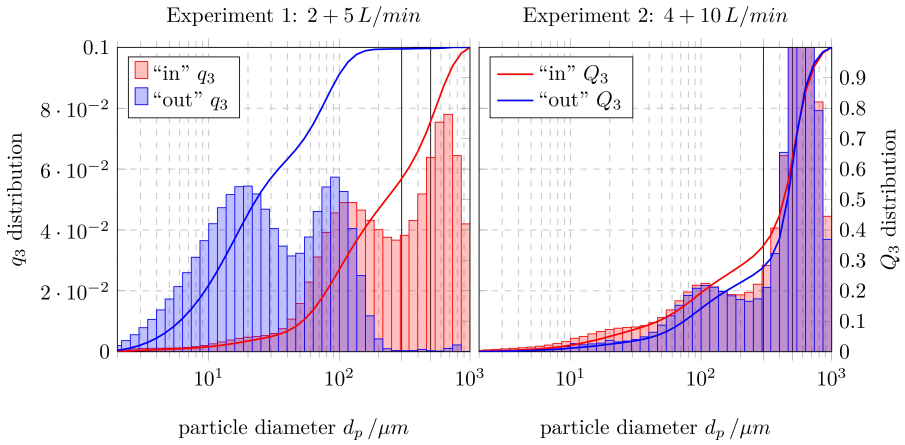


Figure 3.24: Particle size distribution for the change of flow rates

Figure B.11.: Input and output particle size distribution for several flow rates (counter-current)

Figure B.12 shows the status of the reactor after co-current experiments. It is noticeable that some particles were collected at the reactor wall whilst most of them were able to leave the system.

Figure B.12.: Carbon deposition on vortex flow reactor (co-current)

Figure B.13 shows the particle size distribution of the particles introduced in the reactor and those that were collected at the outlet for co- and counter-current flow schemes.

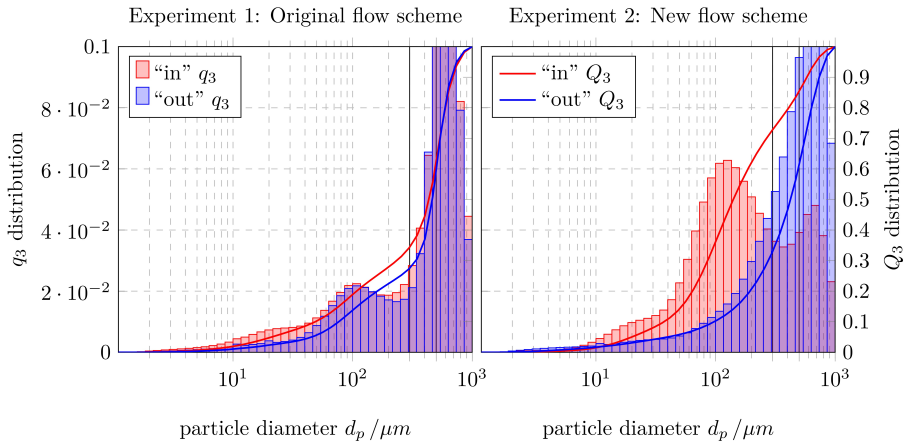


Figure 3.26: Particle size distribution for change of flow scheme. Flow rates are $4 + 10\,L/min$.

Figure B.13.: Input and output particle size distribution for several flow schemes

Figure B.14 shows the status of the reactor after counter-current experiments. It is noticeable that some particles were collected at the reactor wall whilst most of them were able to leave the system. Nonetheless, it is noted that for both co- and counter-current operations particles tend to hit the wall at the transition from the cylindrical to the conical section.

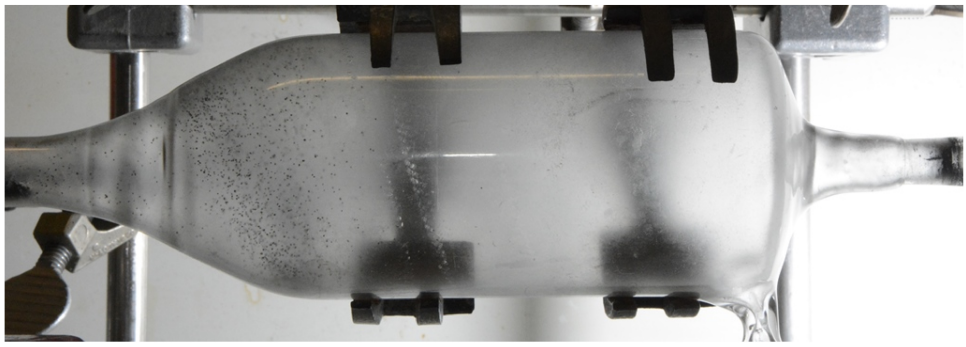

Figure B.14.: Carbon deposition on vortex flow reactor (counter-current)

# C. Experimental tuning of sacrificial wall coating parameter

Table C.1 lists the experiments performed with a rounded flask in an evaporator to determine the best parameters for coating the walls of the reactor with a NaCl sacrificial wall.

Table C.1.: Coating experiments with NaCl for different rotational speeds

| *No* | *NaCl concentration [g/ml]* | *Rotational speed [rpm]* | *Bath temperature [°C]* |
|---|---|---|---|
| 1 | 0.45 | 20 | 50 |
| 2 | 0.45 | 20 | 75 |
| 3 | 0.45 | 20 | 85 |
| 4 | 0.45 | 50 | 75 |
| 5 | 0.45 | 50 | 85 |
| 6 | 0.45 | 100 | 75 |
| 7 | 0.45 | 100 | 85 |
| 8 | 0.45 | 100 | 85 |
| 9 | 0.45 | 125 | 75 |
| 10 | 0.45 | 125 | 80 |
| 11 | 0.45 | 150 | 75 |
| 12 | 0.45 | 150 | 80 |
| 13 | 0.45 | 175 | 75 |
| 14 | 0.45 | 175 | 80 |
| 15 | 0.45 | 200 | 70 |
| 16 | 0.45 | 200 | 75 |
| 17 | 0.45 | 200 | 80 |
| 18 | 0.45 | 225 | 75 |
| 19 | 0.45 | 225 | 80 |
| 20 | 0.45 | 250 | 75 |
| 21 | 0.45 | 250 | 80 |
| 22 | 0.50 | 50 | 80 |
| 23 | 0.50 | 100 | 85 |
| 24 | 0.50 | 150 | 85 |
| 25 | 0.50 | 200 | 80 |
| 26 | 0.50 | 250 | 80 |

The results of the coating experiments with a rounded flask can be seen in figures C.1, C.2, C.3, C.4, C.5, C.6, C.7, C.8, C.9, C.10, C.11, C.12, C.13, C.14, C.15, C.16, C.17, C.18, C.19, C.20, C.21, C.22, C.23, C.24 and C.25.

Figure C.1.: Coating results of experiment number 2

Figure C.2.: Coating results of experiment number 3

Figure C.3.: Coating results of experiment number 4

Figure C.4.: Coating results of experiment number 5

Figure C.5.: Coating results of experiment number 6

Figure C.6.: Coating results of experiment number 7

Figure C.7.: Coating results of experiment number 8

Figure C.8.: Coating results of experiment number 9

Figure C.9.: Coating results of experiment number 10

Figure C.10.: Coating results of experiment number 11

Figure C.11.: Coating results of experiment number 12

Figure C.12.: Coating results of experiment number 13

Figure C.13.: Coating results of experiment number 14

Figure C.14.: Coating results of experiment number 15

Figure C.15.: Coating results of experiment number 16

Figure C.16.: Coating results of experiment number 17

Figure C.17.: Coating results of experiment number 18

Figure C.18.: Coating results of experiment number 19

Figure C.19.: Coating results of experiment number 20

Figure C.20.: Coating results of experiment number 21

Figure C.21.: Coating results of experiment number 22

Figure C.22.: Coating results of experiment number 23

Figure C.23.: Coating results of experiment number 24

Figure C.24.: Coating results of experiment number 25

Figure C.25.: Coating results of experiment number 26

# Bibliography

# Bibliography


[1] **BP,** *"BP statistical review of world energy 2015"*, BP, London, 2013

[2] **International Energy Agency,** *"$CO_2$ emissions from fuel combustion highlights"*, OECD/IEA, 2017

[3] **BP,** *"BP statistical review of world energy 2017"*, BP, London, 2017

[4] **United Nations Population Division** *"World population prospects 2017"*, https://esa.un.org/unpd/wpp/ (Accessed on February 2018)

[5] **The World Bank** *"World Bank national accounts data, and OECD National Accounts data files"* https://data.worldbank.org/indicator/NY.GDP.MKTP.CD?end=2016&start=1961&view=chart (Accessed on February 2018)

[6] **Smil, V.,** *"Energy transitions – History, requirements, prospects"* ABC-CLIO, LLC., California, isbn: 978-0-313-38177-5, 2010.

[7] **SPE, AAPG, WPC, SPEE,** *"Petroleum resources management system"*, 2007

[8] **Reuters** *"Japan reports successful gas output test from methane hydrates"*, May 8, 2017, https://www.reuters.com/article/japan-methane-hydrate/japan-reports-successful-gas-output-test-from-methane-hydrate-idUSL4N1IA35A (Accesed on November 2017).

[9] **US Department of Energy** *"2017 Gulf of Mexico drilling and coring expedition"*, https://www.netl.doe.gov/research/oil-and-gas/methane-hydrates/2017-gulf-of-mexico-drilling-and-coring-expedition (Accessed on January 2018).

[10] **Reuters** *"China produces gas from flammable ice under South China Sea"*, July 29, 2017 https://www.reuters.com/article/china-energy-gas/china-produces-gas-from-flammable-ice-under-south-china-sea-idUSL3N1KK076 (Accessed on February 2018).

[11] **Barnola, J.M., Raynaud, D., Lorius, C.,** *"Historical $CO_2$ record from the Vostok ice core"*, Trends Online: A Compendium of Data on Global Change, Carbon Dioxide, Information Amnalysis Center, 1999.

[12] **IPCC,** *"Climate Change 2014: mitigation of climate change. In: Edenhofery O., Pichs-Madruga R., Sokona, Y., Farahni, E., Kadner, S., Seyboth, K., et al., editors. Contributing Group III to the fifth assessment report of the intergovernmental panel on climate change"*, Cambridge University Press,Cambridge and New York NY, 2014.

[13] **IPCC,** *"Climate Change 1994: Radiative Forming of Climate Change and an Evaluation of the TPCC IS92 Emission Scenarios"*, Intergovernmental Panel on Climate Change, Cambridge University Press, 1994.

[14] **IPCC,** *"Climate Change 2001: the scientific basis, summary for policymakers and technical summary on the working group I report"*, Intergovernmental Panel on Climate Change, Geneva, 2001.

[15] **International Energy Agency,** *"$CO_2$ emissions from fossil fuel combustion 1971-1998"*, OECF/IEA, Paris, 2000.

[16] **Lewis, N.S., Nocera, D.G.,** *"Powering the planet: Chemical challenges in solar energy utilization"*, Proceedings of the National Academy of Sciences of the United States of America 2006 103 (43), pp. 15729 – 15735, https://doi.org/10.1073/pnas.0603395103, 2006.

[17] **Kousksou, T., Bruel, P., Jamil, A., El Rhafiki, T., Zeraouli, Y.,** *"Energy storage: applications and challenges"*, Solar Energy Materials and Solar Cells 120 (Part A), pp. 59 – 80, https://doi.org/10.1016/j.solmat.2013.08.015, 2014.

[18] **Stram, B.N.,** *"Key challenges to expanding renewable energy"*, Energy Policy, 96, pp. 728 – 734, https://doi.org/10.1016/j.enpol.2016.05.034, 2016.

[19] **Georgilakis, P.S.,** *"Technical challenges associated with the integration of wind power into power systems"*, Renewable and Sustainable Energy Reviews 12 (3), pp. 852 – 863, https://doi.org/10.1016/j.rser.2006.10.007, 2008.

[20] **Yang, W., Tavner, P.J., Crabtree, C.J., Feng, Y., Qiu, Y.,** *"Wind turbine condition monitoring: technical and commercial challenges"*, Wind Ennergy 17 (5), pp. 672 – 692, DOI: 10.1002/we.1508, 2014.

[21] **Leitner, W., Quadrelli, E.A., Sclögl, R.,** *"Harvesting renewable energy with chemistry"*, Green Chemistry 19, pp. 2307 – 2308, 10.1039/C7GC90045G , 2017.

[22] **Muruganatham, B., Gnanadass, R., Padhy, N.P.,** *"Challenges with renewable energy sources and storage in practical distribution systems"*, Renewable and Sustainable Energy Reviews 73, pp. 125 – 134, https://doi.org/10.1016/j.rser.2017.01.089 2017.

[23] **Verzijbergh, R.A., de Vries, L.J., Dijkema, G.P.J., Herder, P.M.,** *"Institutional challenges caused by the integration of renewable energy sources in the European electricity sector"*, Renewable and Sustainable Energy Reviews 75, pp. 660 – 667, https://doi.org/10.1016/j.rser.2016.11.039, 2017.

[24] **Leung, D.Y.C., Caramanna, G., Maroto-Valer, M.M.,** *"An overview of current status of carbon dioxide capture and storage technologies"*, Renewable and Sustainable Energy Reviews 39, pp. 426 – 443, https://doi.org/10.1016/j.rser.2014.07.093, 2014.

[25] **Boot-Handford, M.E., Abanades, J.C., Anthony, E.J., Blunt, M.J., Brandani, S., Mac Dowell, N., Fernández, J.R., Ferrari, M.-C., Gross, R., Hallet, J.P., Haszeldine, R.S., Heptonstall, P., Lyngfelt, A., Makuch, Z., Mangano, E., Porter, R.T.J., Pourkashian, M., Rochelle, G.T., Shah, N., Yao, J.G., Fennell, P.S.,** *"Carbon capture and storage update"*, Renewable and Sustainable Energy Reviews 7, pp. 130 –

189, DOI: 10.1039/C3EE42350F, 2014.

[26] **Haszeldine, R.S.,** *"Carbon capture and storage: how green can black be?"*, Science 352 (5948), pp. 1647 – 1652, DOI: 10.1126/science.1172246, 2009.

[27] **Global CCS Institute,** *"The global status of CCS: 2017"*, Global Carbon Capture and Storage Institute Ltd, Australia, 2017.

[28] **Gibbins, J., Chalmers, H.,** *"Carbon capture and storage"*, Energy Policy 36, pp. 4317 – 4322, https://doi.org/10.1016/j.enpol.2008.09.058, 2008.

[29] **Rao, A.B., Rubin, E.S.,** *"A technical, economic, and environmental assessment of amine-based $CO_2$ capture technology for power plant greenhouse gas control"*, Environmental Science Technology 36 (20), pp. 4467 – 4475, DOI: 10.1021/es0158861, 2002.

[30] **Davidson, J.,** *"Performance and costs of power plants with capture and storage of $CO_2$"*, Energy 32 (7), pp. 1163 – 1176, https://doi.org/10.1016/j.energy.2006.07.039, 2007.

[31] **House, K.Z., Harvey, C.F., Aziz, M.J., Schrag, D.P.,** *"The energy penalty of post-combustion $CO_2$ capture & storage and its implications for retrofitting the U.S. installed base"*, Energy & Environmental Science 2, pp. 193 – 205, DOI: 10.1039/B811608C , 2009.

[32] **Keating, G.N., Middleton, R.S., Viswanathan, H.S., Stauffer, P.H., Pawar, R.J.,** *"How storage uncertainty will drive CCS infrastructure"*, Energy Procedia 4, pp. 2393 – 2400, https://doi.org/10.1016/j.egypro.2011.02.132 2011.

[33] **Jouvet, P-.A., Renner, M.,** *"Social Acceptance and Optimal Pollution: CCS or tax?"*, Environmental Modelling & Assessment 20 (4), pp. 285 – 302, DOI 10.1007/s10666-014-9438-y 2015.

[34] **Veziroglu, T.,** *"Hydrogen technology for energy needs of human settlements"*, International Journal of Hydrogen Energy 12 (2), pp. 99 – 129, DOI:10.1016/0360-3199(87)90086-3, 1987.

[35] **Steinberg, M.,** *"Fossil fuel decarbonization technology for mitigating global warming"*, International Journal of Hydrogen Energy 24 (8), pp. 771 – 777, DOI: 10.1016/S0360-3199(98)00128-1, 1999.

[36] **Ausubel, J.H.,** *"Where is energy going"*, The Industrial Physicist, pp. 16 – 19, 2000.

[37] **Muradov, N.,** *"Thermocatalytic $CO_2$-free production of hydrogen from hydrocarbon fuels"*, Proceedings of the 2000 Hydrogen Program Review, pp. 1 – 29, 2000.

[38] **Muradov, N.,** *"Catalysis of methane decomposition over elemental carbon"*, Catalysis Communications 2 (3-4), pp. 89 – 94, DOI: 10.1016/S1566-7367(01)00013-9, 2001.

[39] **Barreto, L., Makihira, A., Riahi, K.,** *"The hydrogen economy in the first century: a sustainable development scenario"*, International Journal of Hydrogen Energy 28 (3), pp. 267 – 284, 2003.

[40] **Marbán, G., Valdés-Solís, T.,** *"Towards the hydrogen economy?"*, International Journal of Hydrogen Energy 32 (12), pp. 1625 – 1637, 2007.

[41] **Kreysa, G.,** *"Climate protection by an alternative use of methane – The carbon moratorium"*, ChemSusChem 2 (1), pp. 49 – 55, DOI: 10.1002/cssc.200800232, 2009.

[42] **Machhammer, O., Bode, A., Hormuth, W.,** *"Financial and Ecological Evaluation of Hydrogen Production Processes on Large Scale"*, Chemical Engineering & Technology 36 (6), pp. 1185 – 1193, DOI:10.1002/ceat.201600023, 2016.

[43] **Muradov, N.,** *"Low to near-zero $CO_2$ production of hydrogen from fossil fuels: Status and perspectives"*, International Journal of Hydrogen Energy 42 (20), pp. 14058 – 14088, DOI: 10.1016/j.ijhydene.2017.04.101, 2017.

[44] **Munera Parra, A.A., Agar, D.W.,** *"Molten metal capillary reactor for the high–temperature pyrolysis of methane"*, International Journal of Hydrogen Energy 42 (19), pp. 13641 – 13648, DOI: 10.1016/j.ijhydene.2016.12.044, 20117.

[45] **Muradov, N., Smith, F., Huang, C., T-Raissi, A.,** *"Autothermal catalytic pyrolysis of methane as a new route to hydrogen production with reduced $CO_2$ emissions"*, Catalysis Today, 116 (3), pp. 281 – 288, DOI: 10.1016/j.cattod.2006.05.070, 2006.

[46] **Serrano, D.P., Botas, J.A., Guil-López, R.,** *"$H_2$ production from methane pyrolysis over commercial carbon catalysts: Kinetic and deactivation study"*, International Journal of Hydrogen Energy 34 (10), pp. 4488 – 4494, DOI: 10.1016/j.ijhydene.2008.07.079, 2009.

[47] **Schultz, i., Agar, D.W.,** *"Decarbonisation of fossil energy via methane pyrolysis using two reactor concepts: Fluid wall flow reactor and molten metal capillary reactor"*, International Journal of Hydrogen Energy 40 (35), pp. 11422 – 11427, DOI: 10.1016/j.ijhydene.2015.03.126, 2015.

[48] **Pinilla, J., Moliner, R., Suelves, I., Lazaro, M., Echegoyen, Y., Palacios, J.,** *"Production of hydrogen and carbon nanofibers by thermal decomposition of methane using metal catalysts in a fluidized bed reactor"*, International Journal of Hydrogen Energy 32 (18), pp. 4821 – 4829, DOI: 10.1016/j.ijhydene.2007.08.013, 2007.

[49] **Domínguez, A., Fidalgo, B., Fernńdez, Y., Pis, J.J., Menéndez, J.,** *"Microwave-assisted catalytic decomposition of methane over activated carbon for $CO_2$-free hydrogen production"*, International Journal of Hydrogen Energy 32 (18), pp. 4792 – 4799, DOI: 10.1016/j.ijhydene.2007.07.041., 2007.

[50] **Czernichowski, A., Czernichowski, P.,** *"Pyrolysis of natural gas in the gliding electric discharges"*, $10^{th}$ Canadian Hydrogen Conference, Quebec, 2000.

[51] **Kugler, H.K., Keller, K.,** *"Gmelin Handbook of inorganic and organometallic chemistry - $8^{th}$ edition - Chapter At Astatine"*, Springer, 1985.

[52] **Schmittinger, P., Florkiewicz, T., Curlin, L. C., Lüke, B., Scannell, R., Navin, T., Zelfel, E., Bartsch, R.,** *"Ullmann's Encyclopedia of Industrial Chemistry - Chlorine"*, Ullmann's Encyclopedia of Industrial Chemistry, Wiley-VCH Verlag GmbH & Co. KGaA,m, isbn: 3527306730, 2000.

[53] **Schlief, R.A., Stoy, M.A., Heaton, H.LL., Hanrahan, R.J.,** *"Production of HBr from the bromine-steam and bromine-steam-methane reactions for electrolytic hydrogen*

*production"*, SRT Group, Inc., Miami, 1997

[54] **SRT Group, Inc.,** *"Production of hydrobromic acid from bromine, methane and steam for hydrogen production"*, SRT Group, Inc., Miami, 1998.

[55] **Bradshaw, R. W., Larson, R. S.,** *"Production of hydrobromic acid from bromine and methane for hydrogen production"*, 2001 U.S. DOE Hydrogen Program Review, Baltimore, April 17–19, 2001.

[56] **Bradshaw, R. W., Larson, R. S.,** *"Production of hydrogen bromide by bromine-methane reactions at elevated temperature"*, SANDIA Report, Sandia National Laboratories, Livermore, 2003.

[57] **Hall, T.J., McKinnie, B.G.,** *"Process for oxidizing hydrogen bromide to produce elemental bromine"*, US Patent: US2010/0015034A1, 2010.

[58] **Louvar, C.J.,de Rosset, E., de Rosset, A.J.,** *"Production of bromine by oxidation of hydrogen bromide"*, US Patent: US3346340, 1967.

[59] **Moser, M., Czekaj, I., López, N., Pérez-Ramírez J.,** *"The virtue of defects: Stable bromine production by catalytic oxidation on titanium oxide"*, Angewandte Chemie International Edition 52 (33), pp. 8628 – 8633, DOI: 10.1002/annie.201404022, 2014.

[60] **Waycuilis, J.J., Moore, P.K., Lisewsky, G.A.,** *"Conversion of hydrogen bromide to elemental bromine"*, US Patent: US2011/0015458A1, 2011.

[61] **Rosser, W.A.JR., Wise, H.,** *"The kinetics of oxidation of HBr"*, Division of Physical Sciences, Standford Research Institute, California, 1959.

[62] **IPCC,** *"Climate Change 2014: Synthesis Report. Contribution of Working Groups I, II and III to the Fifth Assessment Report of the Intergovernmental Panel on Climate Change [Core Writing Team, Pachauri, R.K. and Meyer, L.A. (eds.)]"*, Geneva, 2014

[63] **Sustainable Energy System 2050 expert committee of the ForschungsVerbund Erneubare Energien,** *"Energy Concept 2050 for Germany with a European and global perspective. A vision for sustainable Energy Concept based on energy efficiency and 100% renewable energy. Contribution by the following Institutes: Fraunhofer IBP, Fraunhofer ISE, Fraunhofer IWES, ISFH, IZES gGmbH, ZAE Bayern and ZSW, who have combined in the ForschungsVerbund Erneubare Energien (FVEE) [Renewable Energy Research Association] for the Federal Government Energy Concept"*, FVEE, Berlin, 2010

[64] **Burger, B.,** *"Power generation from renewable energy in Germany — assessment of first half of 2015"*, Fraunhofer Institute for Solar Energy Systems ISE, Freiburg, 2015, July 1

[65] **U.S. Energy Information Administration,** *"Annual energy outlook 2015 with projections to 2040"*, U.S. Energy Information Administration, Washington DC, 2015

[66] **Rogner, H.-H., R. F. Aguilera, C. Archer, R. Bertani, S. C. Bhattacharya, M. B. Dusseault, L. Gagnon, H. Haberl, M. Hoogwijk, A. Johnson, M. L. Rogner, H. Wagner and V. Yakushev,** *"Chapter 7 - Energy Resources and Potentials. In Global Energy Assessment - Toward a Sustainable Future"*, Cambridge University Press, Cambridge and New York NY, and the International Institute for Applied Systems

Analysis, Laxenburg, 2012, pp. 423–512.

[67] **Soeder, D. J.,** *"Shale Gas Development in the United States, Advances in Natural Gas Technology, Dr. Hamid Al-Megren (Ed.)"*, InTech, 2012, pp. 423–512. isbn 9789535105077. DOI: 10.5772/37430

[68] **Hanson, A., Bryngelsson, M.,** *"Expert opinions on carbon dioxide capture and storage — A framing of uncertainties and possibilities"*, Energy Policy 37 (6), Elsevier, Amsterdam 2009, pp. 2273–2282. isbn 03014215. DOI: 10.1016/j.enpol.2009.02.018

[69] **Muradov, N.,** *"Hydrogen via methane decomposition: an application for decarbonization of fossil fuels"*, International Journal of Hydrogen Energy 26 (3), Elsevier, Amsterdam, 2001, pp. 1165–1175. issn 03603199. DOI: 10.1016/S0360-3199(01)00073-8

[70] **McBride, B. J., Zehe, M. J., Gordon, S.** *"NASA Glenn coefficients for calculating thermodynamic properties of individual species"*, National Aeronautics and Space Administration, Glenn Research Center, Cleveland, 2002,

[71] **Schmittinger, P., Florkiewicz, T., Curlin, L. C., Lüke, B., Scannell, R., Navin, T., Zelfel, E., Bartsch, R.,** *"Chlorine"*, Ullmann's Encyclopedia of Industrial Chemistry, Wiley-VCH Verlag GmbH & Co. KGaA, Weinheim, 2000, isbn 3527306730. DOI: 10.1002/14356007.a06_399.pub3

[72] **Waycuilis, J. J., Moore, P. K., Lisewsky, G. A.,** *"US2011/0015458 A1: Conversion of hydrogen bromide to elemental bromine"*, United States Patent Application Publication, 2011,

[73] **Moser, M. Rodríguez García, L., Pérez Ramírez, J.,** *"Catalyst distribution strategies in fixed-bed reactors for bromine production"*, Industrial & Engineering Chemistry Research 53 (22), American Chemical Society, Washington D.C., 2014, pp. 9067–9075. issn 0888-5885-1520-5045. DOI: 10.1021/ie4036675

[74] **Moser, M., Czekaj, I., López, N., Pérez Ramírez, J.,** *"The virtue of defects: stable bromine production by catalytic oxidation of hydrogen bromide on titatnium oxide"*, Angewandte Chemie International Edition 53 (33), Wiley online Library, Weinheim, 2014, pp. 8628–8633. issn 1433-7851 0570-0833 1521-3773. DOI: 10.1002/anie.201404022

[75] **Soeder, D. J.,** *"Shale Gas Development in the United States, Advances in Natural Gas Technology, Dr. Hamid Al-Megren (Ed.)"*, InTech, 2012, pp. 423–512. isbn 9789535105077. DOI: 10.5772/37430

[76] **González Rebordinos, J., Salten, A.H.J., Agar, D.W.,** *"BrOx cycle: A novel process for $CO_2$-free energy production from natural gas,* International Journal of Hydrogen Energy, Elsevier, Amsterdam 2017 DOI: http:10.1016/j.ijhydene.2016.09.071

[77] **Hirsch, D., Steinfeld, A.,** *"Solar hydrogen production by thermal decomposition of natural gas using a vortex-flow reactor"*, International Journal of Hydrogen Energy, 29 (1), Elsevier, Amsterdam, 2012, pp. 47-55.

[78] **Yu, J., Cao, Y., Tian, Z., Xue, Y., Nathan, G.,** *"CFD modelling of aerodynamics in a solar - enhanced vortex gasifier (SVG): Part II. A preliminary study of the locations of*

*seal gas inlets"*, $9^{th}$ International Conference on CFD in the Minerals and Process Industries, Melbourne, 10-12 December, 2012

[79] **McBride, B. J., Zehe, M. J., Gordon, S.** *"NASA Glenn coefficients for calculating thermodynamic properties of individual species"*, National Aeronautics and Space Administration, Glenn Research Center, Cleveland, 2002,

[80] **United States Environmental Protection Agency,** *"Global greenhouse gas emissions data"*, https://www.epa.gov/ghgemissions/global-greenhouse-gas-emissions-data (Accessed October 2017)

[81] **Leung, D.Y.C., Caramanna, G., M. Mercedes, M-V.,** *"An overview of current status of carbon dioxide capture and storage technologies"*, Renewable and Sustainable Energy Reviews 39, Elsevier, Amsterdam 2014, pp. 426–443. DOI: https://doi.org/10.1016/j.rser.2014.07.093

[82] **González Rebordinos, J., Salten, A.H.J., Agar, D.W.,** *"BrOx cycle: A novel process for $CO_2$-free energy production from natural gas*, International Journal of Hydrogen Energy 42, Elsevier, Amsterdam 2017, pp. 4710–4720 DOI: http:10.1016/j.ijhydene.2016.09.071

[83] **Yoshioka, T., Kameda, T., Imai, S., Okuwaki, A.,** *"Dechlorination of poly(vinyl chloride) using NaOH in ethylene glycol under atmospheric pressure"*, Polymer Degradation and Stability 93 (6), Elsevier, Amsterdam 2008, pp 1138–1141 DOI: https://doi.org/10.1016/j.polymdegradstab.2008.03.007

[84] **Winans, C.F.,** *"Nickel as a catalyst for the hydrogenation of aromatic halogen compounds"*, Journal of the American Chemical Society 61 (12), American Chemical Society, Washington DC 1939, pp 3564–3565 DOI: 10.1021/ja01267a101

[85] **Barrero, A.F., Alvarez-Manzaneda, E.J., Chahbon, R., Romera, J.L.,** *"Raney Nockel: an effective reagent for reductive dehalogenation of organic halides"*, Synlett 2001 (4), Georg Thieme Verlag, Stuttgart 2001, pp 485–488 DOI: 10.1055/s-2001-12325

[86] **Weidlich, T., Krejcova, A., Prokes, L.,** *"Study of dehalogenation of halogenoanilines using Raney Al-Ni alloy in aqueous medium at room temperature"*, Monatshefte fuer Chemie 141, Springer, Berlin 2010, pp 1015–1020 DOI 10.1007/s00706-010-0362-9

[87] **Alonso, F., Beletskaya, I.P., Yus, M.,** *"Metal-mediated reductive hydrodehalogenation of organic halides"*, Chemical Reviews 102 (11), American Chemical Society, Washington DC 2002, pp 4009–4092 DOI: 10.1021/cr0102967

[88] **Abánades, A., Ruiz, E., Ferruelo, E.M., Hernández, F., Cabanillas, A., Martínez-Val, J.M., Rubio, J.A., López, C., Gavela, R., Barrera, G., Rubbia, C., Salmieri, D., Rodilla, E., Gutiérrez, D.,** *"Experimental analysis of direct thermal cracking"*, International Journal of Hydrogen Energy 36 (20), Elsevier, Amsterdam 2011, pp. 12877–12886. DOI: https://doi.org/10.1016/j.ijhydene.2011.07.081

[89] **González Rebordinos, J., Kampwerth, J., Agar, D.W.,** *"Flowsheeting and optimisation of the BrOx çycle for CO2-free energy production from natural gas"*, Energy 133, Elsevier, Amsterdam 2017, pp 327–337 DOI: hhttps://doi.org/10.1016/j.energy.2017.05.085

[90] **Hirsch, D., Steinfeld, A.,** *"Solar hydrogen production by thermal decomposition of natural gas using a vortex-flow reactor"*, International Journal of Hydrogen Energy, 29 (1), Elsevier, Amsterdam, 2012, pp. 47-55.

[91] **Yu, J., Cao, Y., Tian, Z., Xue, Y., Nathan, G.,** *"CFD modelling of aerodynamics in a solar - enhanced vortex gasifier (SVG): Part II. A preliminary study of the locations of seal gas inlets"*, $9^{th}$ International Conference on CFD in the Minerals and Process Industries, Melbourne, 10-12 December, 2012

[92] **González Rebordinos, J., Kurrat, E., Agar, D.W.,** *"Numerical simulation of a vortex reactor for avoiding carbon deposition during methane bromination"*, Submitted to Chemical Engineering Journal (2017)

[93] **Earth System Research Laboratory,** *"Atmospheric $CO_2$ at Mauna Loa Observatory"*, http://www.esrl.noaa.gov/gmd/ccgg/trends/full.html (Accessed on February, 2017)

[94] **United Nations,** *"Framework Convention on Climate Change – Conference of the Parties* $21^{st}$ *session"*, Paris, 11/30/2015 – 12/11/2015.

[95] **González Rebordinos, J., Salten, A.H.J., Agar, D.W.,** *"BrOx cycle: a novel process for $CO_2$-free energy production from natural gas"*, International Journal of Hydrogen Energy (accepted for publication), Elsevier, Amsterdam, 2016 DOI: 10.1016/j.ijhydene.2016.09.071

[96] **González Rebordinos, J., Kampwerth, J., Agar, D.W.,** *"Flowsheeting and optimisation of the BrOx çycle for CO2-free energy production from natural gas"*, Energy 133, Elsevier, Amsterdam 2017, pp 327–337 DOI: hhttps://doi.org/10.1016/j.energy.2017.05.085

[97] **DiPietro, J.P., Skolnik, E.G.,** *"Process Study: Analysis of the HBr-based hydrogen production process"*, The SRT Group Inc., 1997.

[98] **McFarland, E.,** *"Unconventional chemistry for unconventional natural gas"*, Science 338 (6105), pp. 340 – 342, DOI: 10.1126/science.1226840, 2012.

[99] **Rosser, W.A.JR., Wise, H.,** *"The kinetics of oxidation of HBr"*, Division of Physical Sciences, Standford Research Institute, California, 1959.

[100] **Hall, T.J., McKinnie, B.G.,** *"Process for oxidizing hydrogen bromide to produce elemental bromine"*, US Patent: US2010/0015034A1, 2010.

[101] **Louvar, C.J.,de Rosset, E., de Rosset, A.J.,** *"Production of bromine by oxidation of hydrogen bromide"*, US Patent: US3346340, 1967.

[102] **Moser, M., Czekaj, I., López, N., Pérez-Ramírez J.,** *"The virtue of defects: Stable bromine production by catalytic oxidation on titanium oxide"*, Angewandte Chemie International Edition 52 (33), pp. 8628 – 8633, DOI: 10.1002/annie.201404022, 2014.

[103] **Waycuilis, J.J., Moore, P.K., Lisewsky, G.A.,** *"Conversion of hydrogen bromide to elemental bromine"*, US Patent: US2011/0015458A1, 2011.

[104] **Schubert, O., Sesing, M., Seidemann, L., Karches, M., Grassler, T., Sohn, M.,** *"Mechanically stable catalyst based on alpha-alumina"*, US Patent: US8163265B2, 2012.

[105] **González Rebordinos, J., Salten, A.H.J., Agar, D.W.,** *"BrOx cycle: a novel process for $CO_2$-free energy production from natural gas"*, International Journal of Hydrogen Energy (accepted for publication), Elsevier, Amsterdam, 2016 DOI: 10.1016/j.ijhydene.2016.09.071

[106] **Seddon, K.R.,** *"Gmelin Handbook of Inorganic Chemistry"*, 8th Edition, Springer, Berlin, 1985

[107] **Brown, F.D.,** *"The comparative value of different methods of fractionl distillation"*, Journal of Chemical Society 37, London, 1880, pp. 49-60.

[108] **Rosser, W.R., Wise, H.,** *"The Kinetics of oxidation of HBr"*, Journal of Physical Chemistry 63 (10), ACS Publications, Whasington D.C., 1959, pp. 1753 - 1755 DOI: 10.1021/j150580a044

[109] **Waycuilis, J. J., Moore, P. K., Lisewsky, G. A.,** *"US2011/0015458 A1: Conversion of hydrogen bromide to elemental bromine"*, United States Patent Application Publication, 2011,

[110] **Moser, M. Rodríguez García, L., Pérez Ramírez, J.,** *"Catalyst distribution strategies in fixed-bed reactors for bromine production"*, Industrial & Engineering Chemistry Research 53 (22), American Chemical Society, Washington D.C., 2014, pp. 9067–9075. issn 0888-5885-1520-5045. DOI: 10.1021/ie4036675

[111] **Moser, M., Czekaj, I., López, N., Pérez Ramírez, J.,** *"The virtue of defects: stable bromine production by catalytic oxidation of hydrogen bromide on titatnium oxide"*, Angewandte Chemie International Edition 53 (33), Wiley online Library, Weinheim, 2014, pp. 8628–8633. issn 1433-7851 0570-0833 1521-3773. DOI: 10.1002/anie.201404022

[112] **Huaiyuan, H., Chengfei, X., Lei, T., Na, T., Xueki, W.,** *"Study on the separation of bromine-water by membrane pervaporation technology"*, Acta Geologica Sinica 88 (s1), Zhongguo di zhi xue hui, Beijing, 2014, pp. 328-330 DOI: 10.1111/1755-6724.12279_11

[113] **Tang, N., Wang, F., Zhang, L., Wang, X.,** *"Separation of bromine and water using polyurethane membranes with pervaporation technology"*, Material Research Innovations 619 (s5), Taylor and Francis, London, 2015, pp. 398 - 404 http://dx.doi.org/10.1179/1432891714Z.0000000001118

[114] **Iwanaga, K., Koushei, S., Hibi, T., Issoh, K., Suzuta, T., Nakada, M., Mori, Y., Abe, T.,** *"The development of improved hydrogen chloride oxidation process"*, Sumitomo Chemical (2004-I), Tokio, 2004

[115] **Parker, R., Clapper, W.L.,** *"Hydrogen-based utility energy storage system"*, Proceedings of the 2001 DOE Hydrogen program review, 2001

[116] **Paunović, V., Zichittella, G., Moser, M., Amrute, A.P., Pérez Ramírez, J.,** *"Catalyst design for natural-gas upgrading through oxybromination chemistry"*,

Nature Chemistry 8, Nature Publishing Group, London, 2016, pp. 803-809 DOI:10.1038/NCHEM.2522

[117] **Benson, S.W., Buss, J.H.,** *"Kinetics of gas phase halogenation reactions"*, The Journal of Chemical Physics 28 (2), 1958, pp. 301-309 DOI:10.163/1.1744111

[118] **Levy, A.,** *"The high temperature kinetics of the hydrogen-bromide"*, The Journal of Physical Chemistry 62 (5), 1958, pp. 570-574 DOI:10.1021/j150563a013

[119] **Mayer, S.W., Schieler, L., Johnston, H.S.,** *"Computed high-temperature rate constants for hydrogen-atom transfers involving light atoms"*, The Journal of Chemical Physics 45 (1), 1966, pp. 385-391 DOI:10.1063/1.1727340

[120] **Skjøth-Rasmussen, M. Glarbourg, P., Østberg, M., Johannessen, J.T., Livbjerg, H., Jensen, A.D., Christensen, T.S.,** *"Formation of polycyclic aromatic hydrocarbons and soot in fuel-rich oxidation of methane in a laminar flow reactor"*, Combustion and Flame 136 (1-2), 2004, pp. 91-128 DOI:10.1016/j.combustflame.2003.09.011

[121] **Yu, H., Kennedy, E.N., Uddin, M.A., Sullivan, D.P., Dlugogorski, B.Z.,** *"Experimental and computational studies of the gas-phase reaction of halon 1211 with hydrogen"*, Environmental Science and Technology 39 (9), 2005, pp. 3020-3028 DOI:10.1021/es049372o

# Supervised Theses

## Master Theses

- **Mahmood, H.**, *"CFD simulation of a vortex-flow reactor"*, Month (2014), Technische Universität Dortmund
- **Baith, S.**, *"Simulation and optimisation of a methane bromination-oxidation cycle"*, December(2014), Technische Universität Dortmund
- **Salten, A.H.J.**, *"Experimental measurements and CFD – simulations of methane – bromination"*, May (2015), Technische Universität Dortmund
- **Chakir, H.**, *"CFD simulations of a vortex reactor"*, Month (2015), Technische Universität Dortmund
- **Żołyniak, P.**, *"Design and optimisation of a temperature tailored reactor for $CO_2$-free energy production through hydrogen bromide oxidation"*, September (2015), Technische Universität Dortmund
- **Tian, R.**, *"Experimental study of high temperature methane bromination with sacrificial wall to avoid carbon deposition"*, March(2016), Technische Universität Dortmund
- **Kampwerth, J.**, *"Detailed flowsheeting and heat integration of the BrOx cycle for$CO_2$-free energy production"*, April (2016), Technische Universität Dortmund
- **Robert, N.**, *"Experimentelle Untersuchung zur Debromierung der kohlenstoffhaltigen Nebenprodukte der Methanbromierung"*, September (2016), Technische Universität Dortmund
- **Kurrat, E.**, *"CFD simulation and optimisation of a vortex reactor geometry for methane bromination"*, September (2016), Technische Universität Dortmund

## Bachelor Theses


- **Saki, F.**, *"Experimentelle Untersuchun und Simulation der thermischen Bromwasserstoffoxidation"*, January (2017), Technische Universität Dortmund
- **Matulla, F.**, *"Experimental study of catalytic hydrogen bromide oxidation"*, February (2017), Technische Universität Dortmund